EXPLORATION OF THE CLINICAL INTERACTION BETWEEN VASCULAR TARGETING AGENTS AND RADIOTHERAPY

A thesis submitted to University College London

for the degree of MD (Res)

Henry Campbell Mandeville

University College London

Marie Curie Research Wing

Mount Vernon Hospital

Rickmansworth Road

Middlesex

HA6 2RN

UK

This thesis is dedicated to my wife, Sugi, and my children, Thomas and Sarasa. For their endless encouragement, patience, understanding and laughter, throughout my experiments and write up.

Declaration

I, Henry Campbell Mandeville confirm that the work presented in this thesis is my own. Where information has been derived from other sources, I confirm that this has been indicated in the thesis.

Signed _____ Date _____

Abstract

Preclinical studies of vascular disruptive and anti-angiogenic agents, combined with radiation, have demonstrated the potential for enhanced anti-tumour activity. However, the optimal strategy and scheduling for combining these treatments with radiotherapy remains uncertain. In this thesis, combretastatin-A4-phosphate (CA4P) given concurrently with fractionated radiotherapy has been studied using preclinical models, in addition to assessing the impacts of adding the nitric oxide synthase inhibitor, N(omega)-nitro-L-arginine (L-NNA), or the anti-EGFR monoclonal antibody, cetuximab, to this combination. As part of an ongoing phase Ib clinical trial, the combination of CA4P and radiotherapy was investigated in patients with non-small cell lung cancer (NSCLC) and head and neck squamous cell carcinoma (HNSCC), where concurrent cetuximab was also given.

Functional imaging techniques, such as dynamic contrast enhanced (DCE)-CT and positron emission tomography (PET), provide non-invasive biomarkers, which can be harnessed to aid diagnosis, determine response to treatment and also offer prognostic information. The use of volumetric DCE-CT parameters as biomarkers of tumour hypoxia and angiogenesis in NSCLC has been explored here, with significant negative correlations demonstrated between DCE-CT parameters and immunohistochemical staining of intra-tumoural hypoxia. This illustrates the potential ability of volumetric DCE-CT to quantify whole tumour hypoxia in NSCLC.

The translational research described in this thesis, has established that the vascular disruptive effects of CA4P can be safely used in combination with fractionated radiotherapy in the clinical setting, producing demonstrable tumour vascular effects. However, despite promising preclinical tumour growth delay effects, the addition of cetuximab produced dose-limiting cardiotoxicity. In patients receiving CA4P and

radiotherapy, DCE-CT and circulatory biomarkers, including cytokines (VEGF, VEGFR-1, G-CSF and SDF-1), were utilised to assess treatment-induced changes in tumour vascularity and vasculogenesis. The findings in this thesis provide further information to guide future studies combining vascular targeted therapies and radiation, highlighting the role of DCE-CT and functional imaging in such work.

Acknowledgements

Professor Peter Hoskin, who provided me with the opportunity to undertake this research and who, as my supervisor, has supported and guided me in my efforts.

Dr Vicky Goh, who supervised all of the experiments using DCE-CT and has provided constant encouragement, advice and critical appraisal.

Dr Sally Hill, who supervised and facilitated all the laboratory work in this thesis.

Without the contributions of the following people, the work described in this thesis would not have been possible.

Marie Curie Research Wing

Prof Michele Saunders, Dr Roberto Alonzi, Mrs Jessica Finch, Dr Quan Ng, Ms Jackie Anderson

Paul Strickland Scanner Centre

Dr Anwar Padhani, Dr Wai-lep Wong, Dr Jane Chambers, Dr Jayne Taylor

Gray Cancer Institute

Mrs Frances Daley, Mrs Vivien Prise, Miss Gemma Lewis, Dr Paul Barber, Mr Glenn Pierce, Dr Michael Stratford, Ms Lisa Folkes

University of Sheffield

Prof Gillian Tozer

Harefield Hospital

Dr Margaret Burke, Dr Alex Bell, Mr Edward Townsend

University of Hertfordshire

Mr Robert Kozarski

University of Oxford/ NHSBT Oxford

Prof Adrian Harris, Dr Jon Smythe, Ms Nita Fisher, Dr Lisa McRae

In addition to the experiments and analysis undertaken by myself, other individuals have assisted in the work presented in this thesis. Dr Michael Stratford and Ms Lisa Folkes performed the preclinical pharmacokinetic specimen analysis presented in Chapters 3 and 4. Mrs Frances Daley taught me the principles for the immunohistochemical staining, assisting me in performing this and also performing the majority of the staining presented in Chapter 5. Dr Quan Ng performed the DCE-CT and FDG-PET image analysis and Dr Robert Kozarkski assisted in the statistical analysis, presented in Chapter 5. Finally, Dr Jon Smythe, Ms Nita Fisher and Dr Lisa McRae performed the cytokine testing presented in Chapter 7 at NHSBT in Oxford.

Table of Contents

List of Tables

List of Figures

Publications arising from this research

Original research

QS Ng, H Mandeville, V Goh, R Alonzi, J Milner, D Carnell, K Meer, MI Saunders, AR Padhani, PJ Hoskin (2011). A phase Ib trial of radiotherapy in combination with combretastatin-A4-phosphate in patients with non-small cell lung cancer, prostate adenocarcinoma, and squamous cell carcinoma of the head and neck. Ann Oncol. 2011 Jul 15. [Epub ahead of print]

Book Chapters

H.C. Mandeville and P.J. Hoskin. Vascular disruptive agents in combination with radiotherapy. In Vascular Disruptive Agents for the Treatment of Cancer. 1st Edition, T. Meyer (Ed.), New York: Springer, 2010. pp231- 250.

Abstracts

H. C. Mandeville, V. Goh, Q. S. Ng, J. Milner, M. I. Saunders, P. J. Hoskin. Volumetric perfusion CT assessment of concurrent combretastatin-A4-phosphate (CA4P) and radiotherapy (RT) in non-small cell lung cancer. J Clin Oncol 26: 2008 (May 20 suppl; abstr 14584). ASCO 2008

H.C. Mandeville, P. J. Hoskin, G. Lewis, V.E. Prise, M I Saunders, G.M. Tozer, S.A. Hill. Nitric oxide synthase inhibition and the effects combination with combretastatin-A4-phosphate and radiotherapy. Radiotherapy & Oncology, Vol 90 Suppl. 3 (2009), S54, Abstract number 133. ESTRO September 2008

H. C. Mandeville, P. J. Hoskin, G. Lewis, V. E Prise, M. I. Saunders, G. M. Tozer, S. A. Hill. N(omega)-nitro-L-arginine (L-NNA) and the effects of its combination with combretastatin-A4-phosphate and radiotherapy. CRUK Clinical Fellows Meeting Nov 2008.

H. Mandeville, V.J. Goh, Q. Ng, J. Milner, M. Saunders, P. Hoskin. Volumetric helical perfusion CT assessment of concurrent combretastatin-A4-phosphate and radiotherapy in non-small cell lung cancer. ECR March 2009

Mandeville HC, Hill SA, Goh VJ, Milner J, Lewis G, Saunders MI, Tozer GM, Hoskin PJ. Preclinical and clinical investigation of combretastatin-A4-phosphate induced vascular disruption in combination with the EGFR inhibitor cetuximab and fractionated radiotherapy in HNSCC. Radiotherapy & Oncology, Vol Suppl. 2 (2008), S156, Abstract number 471. ICTR March 2009

Q.S. Ng, H. Mandeville, W.L. Wong, J. Chambers, M.M. Burke, A. Bell, E. Townsend, M.I. Saunders, P.J. Hoskin, V. Goh. Volumetric helical perfusion CT and FDG-PET/CT as prognostic biomarkers in operable non-small cell lung cancer: correlation with clinico-pathological parameters. ECCO - ESMO September 2009.

Q.S. Ng, H. Mandeville, W.L. Wong, J. Chambers, M.M. Burke, A. Bell, E. Townsend, M.I. Saunders, P.J. Hoskin, V. Goh. Volumetric helical perfusion CT and FDG-PET/CT as prognostic biomarkers in operable non-small cell lung cancer: correlation with clinico-pathological parameters. RSNA December 2009.

H.C. Mandeville, V. Goh, F. Daley, P. Barber, Q.S. Ng, M. Burke, R.Kozarski, G. Pierce, A Bell, E. Townsend, M. I. Saunders, P. J. Hoskin. Validation of volumetric DCE-CT as a biomarker of tumour hypoxia and vascularity in NSCLC. Radiotherapy & Oncology, Vol 96 Suppl. 1 (2010), S82, Abstract number 222. ESTRO September 2010. Selected for oral presentation in Young Scientist Poster Session.

CHAPTER 1

Introduction

1.1 Targeting tumour vasculature to enhance the efficacy of radiotherapy

Recent advances have facilitated detailed genetic and molecular analysis of the key pathways involved in tumour growth, invasion and metastasis. This has enabled the identification of specific molecules, with functions critical to tumour growth and survival that can be targeted. A wide range of potential targeted therapies have now been identified including derivatives of natural compounds, monoclonal antibodies, small molecule tyrosine kinase inhibitors and even older drugs previously used for different indications. For more than 150 years the differences in the vasculature of tumours compared to normal tissues has been studied and tumour vasculature is known to play a key role in the processes of growth, invasion and metastasis. Novel vascular directed therapies allow the therapeutic targeting of tumour vasculature and the processes involved in its development, yet the optimal strategy for the deployment of these treatments remains uncertain.

The pathologist Rudolf Virchow, in the mid 19th century, documented the abnormal appearance of tumour vessels and the increase in vascularity associated with tumour growth (Virchow, 1863). At the start of the 20th century Goldman described tumour vascularisation and the angiogenic response, seen in the surrounding tissue of the organ in which the tumour develops (Goldman, 1907). By 1927 the

heterogeneity of tumour vasculatures had been determined, with the comparison of the vasculatures of several rodent tumours and the observation that each was different (Lewis, 1927). The subsequent development of a transparent chamber inserted into a rabbit's ear enabled microscopic analysis of tumour neovascularisation, with experiments demonstrating the rapid and extensive formation of new vessels accompanying tumour growth ([Sandison, 1928], [Ide, 1939]).

As early as the first half of the 19th century, Walshe reported that some solid tumours could be eradicated when their circulation is interrupted (Walshe, 1844). The key turning point, leading to the development of current vascular directed treatments, was in 1971 when Folkman proposed tumour growth to be angiogenesis dependant and the inhibition of angiogenesis as a treatment for cancer (Folkman, 1971). His paper resulted in intensification of work exploring this concept and other strategies for vascular directed therapies. The concept of vascular disruptive therapies arose following the discovery that endothelial cells in tumours rapidly proliferate, a finding that has now been demonstrated in both rodent and human tumour blood vessels ([Denekamp and Hobson, 1982], [Eberhard et al., 2000]). It was this finding that led Denekamp to propose the exploitation of the functional and morphological differences between tumour and normal blood vessels through the selective targeting of tumour blood supply (Denekamp, 1982). Early work exploring this concept demonstrated tumour regression, growth delay and long term tumour control as a result of compromised tumour blood flow (Denekamp et al., 1983). Over the last 25 years this concept has been extensively studied, and has resulted in the development of potent new vascular disruptive agents including the tubulin-binding agent combretastatin A4 phosphate (CA4P), the effects of which are being examined in this work.

Efforts to improve the efficacy of radiotherapy have led to the widespread adoption of combination schedules with chemotherapeutic and hormonal agents in a variety of cancers. As knowledge of molecular and cellular targets increases, this has resulted in the instigation of trials to explore the optimal therapeutic deployment of targeted agents and to determine whether they can enhance the effects of conventional chemotherapy or radiotherapy. Tumour hypoxia is an important radiobiological factor causing radioresistance and it had been assumed that combining vascular directed therapies with radiotherapy would increase tumour hypoxia, therefore negatively impacting the anti-tumour effect of ionising radiation (O'Reilly, 2006). Contrary to this hypothesis, preclinical studies of antivascular agents, both vascular disruptive and anti-angiogenic, combined with radiation have, in fact, demonstrated the potential for enhanced anti-tumour activity. Despite these findings and a number of early phase clinical trials, the optimal strategy and scheduling for vascular directed therapies in combination with radiotherapy remains uncertain. In this thesis further study of vascular targeting agents combined with radiotherapy has been undertaken in preclinical models and as part of an ongoing phase 1b clinical trial.

1.2 Tumour Microenvironment

1.2.1 Tumour vascular architecture and function

The vasculature in normal tissues with normal microvessels, consisting of arterioles, capillaries and venules, form a well-organised, regulated and functional architecture (Jain 2003). Normal vasculature is characterised by dichotomous branching. The key function of vasculature is to provide adequate levels of nutrients and oxygen to parenchymal cells and to remove waste products. Tumour vascular abnormalities cause disturbance in blood supply, permanent or temporary shutdown of vessels,

gradients in oxygen and nutrients along vessels and even reversal of flow ([Dewhirst et al., 1999], [Jain, 1988], [Walenta et al., 2001]).

The blood vessels in tumours are dilated, saccular, tortuous and heterogeneous in their spatial distribution, markedly different to those seen in normal tissues (Jain, 1988). Features such as compressed vessels, outpouchings, tortuous sinusoids, arteriovenous junctions and plasma channels are commonly seen ([Dewhirst, 1998], [Konerding et al., 1999]). Tumour vasculature is unorganised with trifurcations and branches with uneven diameters. Vessel wall structure is abnormal with large interendothelial junctions, increased number of fenestrations, vesicles, vesico-vacuolar channels and lack of normal basement membrane ([Chang et al., 2000], [di Tomaso et al., 2005], [McDonald and Choyke 2003]). Perivascular cells have abnormal morphology and heterogenous association with tumour vessels. Solid (mechanical) stress generated by proliferating tumour cells also compresses tumour blood vessels, which combined with molecular factors may render the tumour vasculature abnormal ([Padera et al., 2004], [Roose et al., 2003]).

Functional differences are also a feature of tumour vasculature. With the ultrastructural alterations in tumour vessel wall, permeability is generally higher than in normal tissues. The extravasation of molecules from the vasculature occurs by diffusion, convection and, to some extent, trancytosis in an exchange vessel. Diffusion is thought to be the major form of transvascular transport in tumours (Jain, 1987). Elevation of interstitial fluid pressure occurs in solid tumours as a result of tumour vessel hyperpermeability and the lack of functional intratumoural lymphatics (Fukumura and Jain 2008). Arterovenous pressure differences and flow resistance (combination of geometric and viscous resistances) govern blood flow in a vascular network; these factors producing increased resistance to blood flow in tumours (Jain, 1988). Focal leaks, commonly seen in tumours, may also compromise

downstream flow and both overall perfusion rates (blood flow rate per unit volume) and average red blood cell velocity are lower in tumours than in normal tissues.

1.2.2 Angiogenesis

New blood vessel growth, commonly termed angiogenesis, or alternatively neovascularisation, in tumours is an independent event that can occur prior to, coincidently or even after neoplasia. In 1971 the concept that tumour growth is dependent on angiogenesis was introduced (Folkman, 1971). Functional new vessels have been demonstrated at a tumour mass of only 100- 300 cells, an approximate size of 0.1- 0.3mm (Li et al., 2000). Only a few exceptions to this rule have been discovered, including the early phase of solid tumour growth, such as early in-situ carcinomas, when tumours can exist in a “prevascular” phase, and also the growth of tumour cells in ascites (Folkman, 1990). In the absence of neovascularisation, tumour growth is limited to 1- 2 mm^3, but after vascularisation rapid tumour growth is seen ([Folkman et al., 1966], [Gimbrone et al., 1974]). Continued tumour growth and the ability to metastasise depend on this production of new vessels from the pre-existing ‘host’ vasculature. However, the level of angiogenesis is not necessarily a measure of malignancy as even benign tumours, such as adrenal adenomas, may be highly angiogenic (Folkman, 1990). In addition to being integral to the growth and metastasis of tumours, angiogenesis is also a feature of non-malignant diseases including rheumatoid disease, age related macular degeneration, proliferative retinopathy and psoriasis (Folkman, 1995).

The signalling pathways that regulate the development of tumour vasculature, cell cycle control and cell survival are closely related to each other. Tumour angiogenesis occurs as a result of the imbalance between pro-angiogenic and anti-angiogenic factors, a process termed the angiogenic switch ([Jain, 2005], [Hanahan

and Folkman, 1996]). The upregulation of tumour oncogenes leads to increased expression of proangiogenic proteins including vascular endothelial growth factor (VEGF), basic fibroblast growth factor (bFGF), interleukin-8 (IL-8), placenta growth factor (PlGF), transforming growth factor-β (TGF-β), platelet derived endothelial growth factor (PD-ECGF) and many others (Relf et al., 1997). Down regulation or inhibition of endogenous anti-angiogenic proteins such as thrombospondin-1 (TSP-1), endostatin, angiostatin, 16kD prolactin, platelet factor-4 or others can similarly create an imbalance resulting in the promotion of angiogenesis. Bouck introduced the concept that oncogenes and tumour suppressor genes play an important role in tumour angiogenesis (Bouck, 1990). Oncogenes implicated in the regulation of tumour angiogenesis include RAS, MYC, ERBB2, EGFR, BCL2 and SRC (Kerbel and Folkman 2002). There are numerous pro- and anti-angiogenic factors involved in the formation of blood vessels and in their function, with new factors continuing to be discovered, the most significant of which are listed in Table 1.1. These molecules are released from tumour cells, intra-tumoural entrapped bone marrow-derived haematopoietic cells, cancer associated fibroblasts (CAF) and host cells including inflammatory cells, endothelial cells, epithelial cells, mesothelial cells and leucocytes.

VEGF is the main pro-angiogenic factor involved in tumour vessel formation. The expression of VEGF is upregulated in a large number of human tumours. Initially discovered in the early 1980s, when it was called tumour vascular permeability factor (Senger et al., 1983). It is secreted by tumour cells and also by fibroblasts and inflammatory cells in the stroma (Li et al., 2007). The VEGF family, including PlGF, is composed of dimeric glycoproteins that display a high amino acid similarity in the platelet-derived growth factor-like domain ([Olofsson et al., 1996], [Maglione et al., 1991]). VEGF-A, -B and PlGF with their binding to the VEGF receptors (VEGFR) 1 and 2 (flk and flt-1), expressed on endothelial cells, are critical to tumour

angiogenesis and vasculogenesis ([Millauer et al., 1993], [Fong et al., 1995]). These critical functions include increasing vascular permeability, promoting the migration and proliferation of endothelial cells, functioning as endothelial cell survival factors, mobilising endothelial progenitor cells (EPC) from bone marrow and upregulation of leukocyte adhesion molecules on endothelial cells. Other members of the VEGF family, including VEGF-C and VEGF-D, which bind to VEGFR-3 (flt-4), are involved in lymphangiogenesis (Karkkainen et al., 2002).

EPCs, identified by the expression of the cell surface marker CD133, are mobilised from the bone marrow and are then recruited to tumour sites by a number of chemokines including VEGF, stromal-derived factor-1 (SDF-1 or CXCL12) and angiopoietin ([Hattori et al., 2001], [Peichev et al., 2000]). This leads to a self-perpetuating effect as recruited EPCs then produce VEGF, HGF, G-CSF and GM-CSF, which recruit further EPCs (Li et al., 2007). SDF-1 acts by binding to CXCR4 on circulating vasculogenic stem cells and facilitates their adhesion, migration and homing to the tumour microenvironment ([Ceradini et al., 2004], Burger and Kipps, 2006]). This interaction between SDF-1 and CXCR4 is not limited to vasculogenic stem cells, with similar effects described in cancer stem cells and also normal stem cells, including the mobilisation of polymorphonuclear neutrophils and haemopoietic progenitor cells from the bone marrow ([Kucia et al., 2005], [Pelus et al., 2005]).

Active remodelling and integration of new cells into existing structures is required for tumour angiogenesis. Stromal fibroblasts, macrophages and endothelial cells release matrix metalloproteinases (MMP) to hydrolyse extracellular proteins of the surrounding tissue, degrade the basement membranes and facilitate cell movement ([Sternlicht and Werb, 2001], [Genis et al., 2006]). Macrophage-derived MMP-9 mobilises VEGF from matrix stores and is critical for recruitment and engraftment of EPCs into tumour vasculature (Jodele et al., 2005). The resultant blood vessel

formation occurs by a variety of processes including budding from existing vasculature, recruitment of vascular progenitor cells to form new vessels or tumour cell-lined channels mimicking vascular function (Ribatti et al., 2003).

1.2.3 Metabolic microenvironment

Both the abnormal structure and function of the vasculature of solid tumours contribute to the abnormal metabolic environment of hypoxia and acidosis that commonly exists (Harris, 2002). Hypovascular regions within tumours are often produced due to the imbalance between cell proliferation and neovascularisation. Given the tissue diffusion limit of oxygen, a distance of only 100-200μm, diffusion-limited or chronic hypoxia is seen in tumour regions where the distance from blood vessels exceeds this limit (Krogh, 1922). This was demonstrated in human lung cancer where necrotic cells were identified at 180μm from the nearest vessel (Thomlinson and Gray, 1955). In keeping with these findings, the mitotic index of tumour cells has also been demonstrated to decrease with increasing distance from endothelial cells (Tannock, 1968).

Intermittent or acute hypoxia (also known as cycling or perfusion limited hypoxia) arises due to the intermittency of tumour blood flow leading to periodic oxygen starvation in regions of tumour ([Brown and Giaccia, 1998], [Dewhirst, 1998]). In individual tumour vessels the blood flow rate has no clear relationship with oxygen tension (pO_2) (Helmlinger et al., 1997). The abnormalities of tumour microcirculation also commonly result in a low extracellular pH, a consequence of increased H^+ ion production combined with reduced removal, although the intracellular pH of cancer cells remains neutral or alkaline. The mean extracellular pH has been shown to decrease with increasing distance from blood vessels, reaching a plateau at between 100-170 μm. Despite the apparent similarities, no spatial correlation

between low extracellular pH and hypoxia has been demonstrated (Helmlinger et al., 1997).

The metabolic microenvironment of tumours plays a key role in tumour angiogenesis. Whilst incipient angiogenesis has been observed three days post inoculation of cells, preceding development of hypoxia, it has been demonstrated that further progression of angiogenesis two days later is related to areas of detectable hypoxia (Cao et al., 2005). The consequence of hypoxic stress is the upregulation of angiogenic factors, the effect of which is the creation of a new vascular supply ([Allalunis et al., 1999], [Fukumura, Xu et al., 2001]). In later stages hypoxia strongly induces neoangiogenesis, especially via hypoxia-inducible factor 1 alpha (HIF-1α) pathway. Activation of this pathway by hypoxia induces the production of proangiogenic factors, including VEGF ([Forsythe et al.,1996], [Ravi et al., 2000]). Peptide blockage of HIF-1α degradation has similar effects producing stimulation of angiogenesis (Willam et al., 2002). In addition to these effects, the recruitment of CXCR4-positive progenitor cells is also mediated by HIF-1 activation in endothelial cells, regulating SDF-1 gene expression (Ceradini et al., 2004). The proangiogenic factors that hypoxia upregulates include VEGF, Ang-2, PDGF, PlGF, TGF-α, IL-8 and HGF (Harris, 2002). Low extracellular pH also upregulates expression of proangiogenic factors, including VEGF and IL-8 (Xu et al. 2002).

The hostile hypoxic and acidotic tumour microenvironment plays a key role in the behaviour of tumours, but also in their responsiveness to treatment. It selects tumour cells resistant to apoptosis, more genetically unstable and of increased malignant, invasive and metastatic potential (Fukumura and Jain, 2007). It has been known since the early 1950s that tissue oxygen concentration is an important factor in tumour radiosensitivity (Gray et al., 1953). Not only does hypoxia in solid tumours significantly reduce radiosensitivity, it also reduces sensitivity to certain

chemotherapeutic agents including carboplatin and bleomycin (Koch et al., 2003). A reduction in effect of chemotherapy is also described with acidic extracellular pH, producing an accumulation of cells in G1 phase and also reducing cellular uptake of weak base agents including doxorubicin and mitoxantrone (Vukovic and Tannock, 1997).

1.3 Therapeutic targeting of tumour vasculature

1.3.1 Vascular disruption

Vascular disruptive agents (VDAs) exert their effect by the targeting of existing tumour vasculature, exploiting the differences between tumour and normal blood vessels. These treatments have been developed with the aim of producing rapid tumour cell ischaemia, resulting in tumour cell death. The exact mechanisms of how these agents exert their anti-tumour action are complex and remain under investigation. The vascular disruptive agents currently in development can be broadly divided into two classes: small molecule and ligand directed. The small molecule vascular disruptive agents can be further subdivided into two groups based on modes of action, which are the tubulin-binding agents and the flavonoids

1.3.2 Small molecule vascular disruptive agents

1.3.2.1 Tubulin-binding agents

Colchicine is the classic example of a tubulin-binding agent. Studies as far back as 1937 have explored its effects on tumour vasculature and demonstrated, in both animal and human tumours, the ability to induce haemorrhage and extensive necrosis ([Boyland and Boyland, 1937], [Seed et al., 1940]. Significant vascular effects have also been observed with the cytotoxic and potent tubulin-binding vinca alkaloids, vincristine and vinblastine (Hill et al., 1993). The vascular effects

observed with both colchicines and the vinca alkaloids occur only at doses close to the maximum tolerated (MTD), with a very narrow therapeutic window, preventing the therapeutic exploitation of this vascular disruptive effect.

1.3.2.2 Combretastatin A-4 phosphate (CA4P)

Newer tubulin-binding vascular disrupting agents offering a larger therapeutic window, including the combretastatins, have since been developed. These act at the colchicine-binding site of β-subunit of endothelial cell tubulin (Lin et al., 1988). Typically they produce a rapid reduction in tumour perfusion with maximal tumour vascular shutdown seen one to six hours post administration, with substantial recovery of tumour blood flow by 24 hours (Prise et al., 2002). Activation of the Rho/Rho-kinase pathway causes microtubule depolymerisation and remodelling of the actin cytoskeleton (Kanthou and Tozer, 2002). Activation of stress-activated protein 2 (SAPK2) also occurs. These effects produce three-dimensional changes in the shape of endothelial cells; more pronounced in newly formed ones as they lack a well-developed actin cytoskeleton and pericytic infiltration. Increased vascular resistance and also increased vascular permeability occurs, as there is disruption of the molecular engagement of the endothelial cell-specific junctional molecules, including vascular endothelial-cadherin (VE-cadherin) (Vincent et al., 2005). Combretastatin-induced vascular collapse, observed with CA4P and AC7700, may be related to arteriolar vasoconstriction reducing intravascular pressure, which results in an increase in the differential between interstitial fluid pressure and the intravascular capillary pressure ([Tozer et al., 2001], [Hori and Saito, 2003]). Contrary to previous conjecture on the mechanism leading to this vascular collapse, direct measurements of tumour interstitial fluid pressures following CA4P in an in vivo tumour model revealed no resultant increase (Ley et al., 2007).

Tumours with increased vascular permeability are more susceptible to vascular disruptive therapies (Beauregard et al., 2001). The vascular effect of CA4P, with the disruption of interphase microtubules in endothelial cells, results in a visible loss of a large proportion of the smallest tumour blood vessels (Tozer et al., 2001). Increases in the viscous resistance to blood flow and haematocrit, as a result of fluid loss from the vascular space and exposure of the basement membrane to flowing blood, can result in initiation of the coagulation cascade producing thrombus and reducing tumour blood flow (Tozer et al., 2005). Increased neutrophil recruitment is also described and this, in addition to upregulation of endothelial cell surface adhesion molecules, may contribute to both the vascular and cytotoxic effects of these small molecule VDAs (Brooks et al., 2003). Under aerobic conditions CA4P increases HIF-1 expression resulting in an increased production of VEGF-A, however under hypoxic conditions a reduction in the accumulation of HIF-1 has been observed (Dachs et al., 2003). The angiogenic response to CA4P has been studied using an in vivo non small cell lung carcinoma (NSCLC) xenograft model, with increased expression of both VEGF and bFGF demonstrated (Boehle et al., 2001). As a consequence of CA4P-induced vascular disruption, there is an acute mobilisation of circulating endothelial progenitor cells from the bone marrow, with these cells migrating to and localising in the residual viable rim of tumour (Shaked et al., 2006).

CA4P (fosbretabulin [Zybrestat]) is a synthetic, water soluble, phosphorylated prodrug of the natural product combretastatin A4 (CA4). Originally isolated from the bark of the Cape bushwillow, *Combretum caffrum,* CA4 is a tubulin-binding agent that has potent activity in preventing tubulin polymerization and microtubule assembly (Dark et al., 1997). It has been produced in two formulations; shown to be biologically equivalent in preclinical studies. Combretastatin A4 disodium phosphate was the initial formulation produced followed subsequently by combretastatin A4 tris monophosphate, which has been used in all clinical trials initiated since April 2006.

Acute vascular shutdown was observed at ten percent of MTD in preclinical studies. A single dose of i.p. CA4P 100mg/kg produced a greater than ninety percent loss of functional vascular volume at six hours, an effect that persisted for the following 12 hours (Dark et al., 1997). Extensive haemorrhagic necrosis and tumour cell loss were observed, but with no demonstrable effect on tumour growth. This effect is attributed to the actively proliferating rim of tumour cells remaining, thought to receive its blood supply from surrounding normal tissue (Chaplin et al 1999). The vascular architecture of the tumour periphery and the precipitous rise in interstitial fluid pressure from the tumour periphery to the centre are also thought to be contributing factors to the persistence of this viable rim (Tozer et al., 2005).

The clinical pharmacokinetic data from three Phase I clinical trials has now been reported. The plasma AUC and Cmax of CA4P and its active metabolite CA4 have been demonstrated to increase linearly with dose (Stevenson et al., 2003). CA4P is rapidly converted to CA4, which is then extensively converted to the glucuronide (CA4G). Estimates of mean plasma half-life for CA4P, CA4, and CA4G were approximately 0.41, 3.80, and 4.48 hours, respectively. Between 58% and 67% of the CA4P dose is excreted as CA4G in the urine within 24 hours of administration. At the 54mg/m^2 dose level, given as a single dose every 21 days, the mean ($\pm$standard deviation) maximum concentration (Cmax) values of CA4P and CA4 were 40 ($\pm$4) and 2.6 ($\pm$ 0.8) μM respectively, (n=6).

The dose limiting toxicities (DLTs) with single dose CA4P every 21 days were cardiac ischaemia and dyspnoea, seen at the 90mg/m^2 dose level (Dowlati et al., 2002). One patient, treated at the 60mg/m^2 dose level, had proven clinical evidence of myocardial ischaemia with ECG changes and raised troponin levels, with another patient at this dose level developing significant QTc prolongation (QTc ≥ 500 ms). The DLTs, for CA4P administered as five daily doses every 21 days, included

tumour pain, reversible sensorimotor neuropathy, syncope and dyspnoea at the 75mg/m^2 dose level (Stevenson et al., 2003). In the study looking at three weekly doses of CA4P every 28 days the DLTs were reversible ataxia at 114mg/m^2, vasovagal syncope and motor neuropathy at 88mg/m^2 and fatal ischaemia in previously irradiated bowel at 52mg/m^2 (Rustin et al., 2003). Other than the bowel ischaemia, these events all resolved in less than 12 hours. Other Grade 2 or higher toxicities observed were pain, fatigue, lymphopenia, diarrhoea, anaemia, hypertension, hypotension, vomiting, visual disturbance and dyspnoea.

Blood pressure changes are frequently seen following CA4P, with an average rise in both systolic and diastolic blood pressures of between 5 to 10 mmHg seen at 30 to 60 minutes post administration ([Anderson et al., 2003a], [Rustin et al., 2005]). Only a small percentage of patients experience Grade 3 or higher hypertension requiring treatment with anti-hypertensive agents. An acute 10% reduction in cardiac output that returns to baseline by 24 hours has also observed at 30 minutes post CA4P. These changes in blood pressure and cardiac output are thought to be due to CA4P-induced vascular smooth muscle contraction producing increased peripheral vascular resistance, an independent effect that is not required for the disruption of tumour vasculature (Anderson et al., 2003a). Preclinical studies have shown that, in the presence of preexisting hypertension, a greater blood pressure rise is seen following CA4P, associated with increased cardiac strain demonstrable by a rise in cardiac enzymes (Ke Q et al., 2007). These blood pressure and cardiac effects can be prevented by treatment with anti-hypertensive agents, using either calcium-channel antagonists or nitrates.

The other main cardiovascular effect observed following CA4P is prolongation of the QTc interval, with an increase of <20 msec commonly seen at doses ranging between 37 and 90mg/m^2. Increases greater than 60 msec have been observed in a

small number of patients, although no QTc interval of ≥500 msec was seen in the three main Phase I studies. The patients in these studies were however carefully screened prior to trial entry and those with pre-existing cardiac conduction defects excluded.

In those receiving CA4P once every three weeks, a complete response was seen in one patient with anaplastic thyroid carcinoma and greater than 12 month disease stabilisation seen in two other patients. With the five daily doses every three weeks, one patient with sarcoma had a partial response and fourteen others had stable disease. One partial response, in a patient with metastatic adrenocortical carcinoma, was also seen with the scheduling of three weekly doses every four weeks. With the characteristic viable tumour rim left after treatment with CA4P in addition to single agent studies showing little response, it is apparent that there is a need to combine CA4P with other treatment modalities to fully exploit its potential anti-tumour effect. Based on the clinical tolerability and assessment of effect by DCE-MRI and PET the recommended Phase 2 doses were 52 to 68mg/ m^2.

CA4P has been shown to enhance or act synergistically with several cytotoxic chemotherapy agents. In vivo studies have shown benefit with the addition of CA4P to cisplatin in mammary carcinoma, ovarian carcinoma and sarcoma models; 5-fluorouracil in a colonic carcinoma model; doxorubicin in a medullary thyroid carcinoma model; cyclophosphamide in breast carcinoma and sarcoma models; paclitaxel and carboplatin or manumycin A in an anaplastic thyroid cancer model; and CPT-11 in a rhabdomyosarcoma model ([Chaplin et al., 1999], [Horsman et al., 2000], [Siemann et al., 2002], [Grosios et al., 2000), [Nelkin and Ball, 2001], [Yeung et al., 2007], [Wildiers et al., 2004]). The scheduling of chemotherapy and a VDA is an important consideration. Preclinical studies have shown a benefit when CA4P was given one to two hours after chemotherapy, but no improvement in tumour cell

kill when CA4P was given one to two hours prior (Siemann et al., 2002). A phase I study looking at CA4P given one hour after carboplatin AUC 4-5, reported Grade 3/4 thrombocytopenia in seven of the sixteen patients studied (Bileuken et al.,2005). A further study looked at different scheduling, with CA4P administered 18 to 22 hours prior to carboplatin AUC 5 and/ or paclitaxel demonstrating a well tolerated combination with minimal myelosuppression. Current Phase II/III trials are ongoing, including a Phase II trial combining CA4P, carboplatin and paclitaxel in platinum resistant ovarian carcinoma and a randomised Phase II/III trial looking at this combination in anaplastic thyroid carcinoma.

To further enhance the anti-tumour effects of CA4P, attempts to exploit the resultant tumour ischaemia have been undertaken, combining it with treatments targeting hypoxia. In vivo studies, using a CaNT murine tumour model, have shown enhanced tumour growth delay with the addition of the bioreductive cytotoxic agents tirapazimine or banoxantrone (AQ4N) to CA4P (Tozer et al., 2008). Combining radioimmunotherapy with vascular disruption has also shown early promise. In preclinical studies, using a colorectal xenograft, Iodine-131 labelled anti-carcinoembryoinic antigen IgG (^{131}I-A5B7), in addition to CA4P produced sustained compete responses in five of the six mice studied (Pedley et al., 2001). Although, a phase I study of this combination revealed no significant responses and enhanced toxicity, with DLT of myelosuppression seen at 66% of the MTD for A5B7 alone (Meyer et al., 2009). The combination of CA4P and radiotherapy, anti-angiogenic agents or nitric oxide synthase inhibitors will be discussed later.

1.3.2.3 Other tubulin-binding vascular disruptive agents

There are a number of other tubulin-binding vascular disrupting agents currently in development. OXi4503 (CA1P) is a sodium phosphate prodrug of combretastatin A-1 shown to be ten times more potent than CA4P in terms of tumour vascular

shutdown, with preclinical studies demonstrating a similar MTD to CA4P (Hill et al., 2002). The vascular disruption is again most pronounced in central regions, although CA1P produces greater vascular disruption at the tumour periphery compared to CA4P. In addition to its effect on the tumour vasculature, it also displays a potent anti-tumour effect with tumour regression seen in preclinical studies at doses greater than 25mg/kg (Hua et al., 2003). The additional cytotoxicity of CA1P, despite comparatively lower tumour concentrations than are seen with CA4P, may be a result of the generation of the more reactive quinone species, ortho-quinone Q1 ([Kirwan et al., 2004], [Folkes et al., 2007]). A dose escalating Phase 1 study of single agent OXi4503 is currently in progress. Preclinical studies have again shown potentiation of the antitumour effect of cytotoxic chemotherapy when given in combination ([Shnyder et al., 2003], [Staflin et al., 2006]).

AC7700 (AVE8062A) is a water-soluble synthetic analogue of CA4. It is a prodrug cleaved by aminopeptidases to produce the active drug. In preclinical studies it has demonstrated the ability to produce the rapid and irreversible stasis of tumour blood flow (Hori et al., 1999). This is attributed to prolonged constriction of host arterioles and not through a direct effect on tumour blood vessels (Hori and Saito, 2003). Initial phase I studies examining daily and weekly schedules were halted following four vascular events of myocardial ischaemia, transient asymptomatic hypotension, transient cerebral ischaemia, and asymptomatic ventricular tachycardia. Three weekly scheduling of up to 22mg/m^2 is well tolerated, with no DLTs observed in 23 treated patients (Sessa et al., 2005). In preclinical studies, the combination of AC7700 with docetaxel, in an ovarian tumour model, produced enhanced inhibition of tumour growth (Kim et al., 2007). Three weekly AC7700 is currently under investigation combined with cisplatin in an ongoing phase 1 trial (Soria et al., 2008).

N-acetylcolchinol-*O*-phosphate (ZD6126) a colchicine analogue and phosphate prodrug of N-acetylcolchinol is currently undergoing both preclinical and clinical evaluation. Producing similar effects on tumour vasculature to CA4P, it has also been demonstrated that pre-treatment with antihypertensive agents can prevent the cardiovascular sequelae without compromising the ability to induce tumour necrosis (Gould et al., 2007). Preclinical studies have again shown an inconsistent effect on tumour growth when given as a single agent but an enhancement in tumour growth delay in combination with cytotoxic chemotherapies, including cisplatin in a lung cancer model and paclitaxel in a head and neck squamous cell carcinoma (HNSCC) model ([Blakey et al., 2002], [Davis, Dougherty et al., 2002]). Phase I studies have shown the MTD with weekly scheduling to be 20mg/m^2/wk and when administered as a single dose every 2 or 3 weeks the MTD is 80mg/m^2 ([Beerepoot et al., 2006], [LoRusso et al., 2008]). The main dose limiting toxicities with both schedules were cardiac ischaemia and asymptomatic left ventricular dysfunction.

Other novel tubulin-binding vascular disruptive agents in development include Auristatin PE (TZT1027), derived from dolastatin 10 (isolated from a marine mollusc); ABT-751, an oral sulphonamide that binds to the colchicines-binding site; Denibulin (MN-029), a benzimidazole that binds to the colchicines-binding site; and arsenic trioxide (Trisenox), currently used to treat acute promyelocytic leukaemia and able to induce vascular disruption in solid tumours.

1.3.2.4 Flavonoid vascular disruptive agents

The flavonoids work by causing partial dissolution of the actin cytoskeleton, resulting in DNA strand breaks and the induction of endothelial cell apoptosis. Inhibition of endothelial cell migration and tubulogenesis, leads to the formation of imperfect blood vessels and increases the probability of apoptosis. The anti-tumour effect is mediated through the activation of macrophages causing the release of cytokines, in

particular TNF. Antivascular effect is aided by the activation of platelets, which causes the release of serotonin. Both TNF and serotonin act as VDAs in their own right.

Flavone acetic acid ester, a flavonoid initially screened by the National Cancer Institute, showed sufficient in vivo anti-tumour activity for it to be selected for phase I testing by the Cancer Research Campaign in the United Kingdom (Bibby and Double, 1993). It did not proceed to phase II trials as significant hypotension was observed and it was also determined to be a prodrug of flavone acetic acid (FAA). FAA was found to have high anti-tumour action in murine tumour models and noted to induce haemorrhagic necrosis ([Plowman et al., 1986], [Smith et al., 1987]). Mechanistic studies revealed FAA to cause selective shutdown of tumour blood vessels ([Hill et al., 1989], [Zwi et al., 1989]). Both phase I and II clinical testing were subsequently undertaken, examining FAA as a single agent and also in combination with other anti-cancer treatments. These trials of FAA did not demonstrate any significant clinical activity, which has lead to further research focusing on new analogues, in an effort to clinically harness the anti-tumour effect of these compounds and overcome this apparent species-specific effect of FAA.

The tricyclic analogue of FAA, xanthenone-4-acetic acid (XAA), is highly amenable to synthesis of derivatives, including 5,6-dimethylxanthenone-4-acetic acid (DMXAA [ASA404]), which is 16-fold more potent than FAA (Baguely 2003). DMXAA induces apoptosis in a significant proportion of both murine and human tumour endothelial cells (Ching et al., 2002). Weekly and three weekly scheduling of DMXAA were tested in two parallel phase I studies, which determined the MTD of 3700mg/m^2. In these studies, levels of 5-hydroxyindoleacetic acid, a biomarker of vascular damage, increased in a dose dependant manner up to 1200mg/ m^2 and then plateaued. A dose of 1200mg/m^2 was subsequently selected for phase II testing of combinations

with cytotoxic chemotherapies, with doses of 1800mg/m^2 also looked at in NSCLC. These phase II studies have reported good tolerability and enhanced clinical activity with DMXAA in combination with docetaxel in HRPC, and with carboplatin and paclitaxel in advanced NSCLC. Phase III trials of these combinations are currently recruiting ([Pili et al., 2008], [McKeage et al., 2008]). A phase II trial of DMXAA combined with carboplatin and paclitaxel in ovarian carcinoma showed improved response rate but no improvement in time to progression or survival (Gabra et al., 2007).

1.3.2.5 Ligand directed vascular disruptive agents

Ligand directed VDAs are composed of separate targeting and effector moieties, which are chemically linked together (Thorpe, 2004). Antibodies, peptides or growth factors are used and selectively bind to molecules that are upregulated on tumour endothelial cells. These target molecules include those involved in angiogenesis and vascular remodelling, cell adhesion and prothrombotic changes. By coupling them to an effector moiety they are able to exert their vascular disruptive effect, through the induction of coagulation or endothelial cell death. Types of effector moiety that have been investigated include procoagulants (e.g. coagulation factor III), toxins (e.g. ricin), radioisotopes (e.g. Iodine-131), cytokines (IL-2), cytotoxic agents (e.g. doxorubicin) and inducers of apoptosis (e.g. *RAF-1* gene).

Several ligand directed vascular disruptive strategies are currently undergoing preclinical investigation. Strategies targeting tumour neovascularisation include combining VEGF121, which binds to both VEFR1 and VEGF2, (although is internalised only by binding to VEGFR2), with the plant toxin gelonin. VEGF121/rGel has demonstrated significant inhibition of tumour growth in preclinical prostate, bladder and breast cancer models ([Mohamedali et al., 2006], [Mohamedali et al 2005], [Ran et al., 2005]). Vascular targeted cancer gene therapy has also utilised

the upregulation of VEGF in tumour vasculature: Flk-1/Fas, a chimeric cell surface protein where the membrane-spanning and cytoplasmic 'death domain' of the pro-apoptotic protein Fas is fused to the extracellular ligand-binding domain of VEGFR2, has been demonstrated to produce apoptosis in tumour cells which are overexpressing VEGF (Dougherty and Dougherty, 2009). The delivery of suicide genes such as herpes simplex virus thymidine kinase (HSVtk) to tumour endothelial cells through a novel targeted adeno-associated virus/phage vector has also been demonstrated to suppress tumour growth (Trepel et al 2009). Other ligand directed strategies include L19(scFv), a monoclonal antibody that binds to the EDB domain fibronectin, a marker of angiogenesis, and localises to tumour blood vessels (Santimaria et al., 2003). The L19(scFv) antibody has been combined with different cytokines including IL-12 and TNF-α, demonstrating anti-tumour effect and also an adaptive anti-tumour immune response in murine teratocarcinoma, fibrosarcoma, colon carcinoma and neuroblastoma models ([Gafner et al., 2006], [Balza et al., 2006]) [Balza et al 2010].

1.3.3 Anti-angiogenesis

Inhibitors of angiogenesis can be subdivided by whether they have a direct or indirect mode of action. Indirect angiogenesis inhibitors act by interfering with the activity or preventing the expression of proangiogenic factors or their receptors (Kerbel and Folkman, 2002). By restoring the balance of pro-angiogenic and anti-angiogenic factors, this results in a reduction in the size and length of intratumoural vessels, greater pericyte coverage, decreased interstitial fluid pressure and reduced permeability of the basement membrane ([Yuan et al., 1996], [Tong et al., 2004]). This normalisation of the tumour vasculature is subsequently followed by further reduction in vessel density and the reappearance of hypoxia and reduced pericyte coverage (Winkler et al., 2004). Direct angiogenesis inhibitors act by blocking the

ability of tumour endothelial cells to proliferate, migrate and form new blood vessels (Gasparini et al., 2005). The targeting of genetically stable endothelial cells rather than unstable tumour cells means these compounds are theoretically less likely to induce acquired drug resistance (Boehm et al., 1997). A further subset of agents has both a direct and an indirect inhibitory action on angiogenesis, including multitargeted tyrosine kinase inhibitors (TKIs) and cytotoxic chemotherapeutic agents, which target both endothelial and malignant cells (Gasparini et al., 2005).

1.3.3.1 Indirect and mixed angiogenesis inhibition

Inhibitors of the VEGF pathway are the most clinically advanced anti-angiogenic agents. Multiple strategies targeting the main proangiogenic factor VEGF have entered clinical trials. These include monoclonal antibodies targeting VEGF-A or the VEGFRs, chimeric soluble receptors such as 'VEGF trap', extracellular inhibitors that bind the heparin-binding domain of VEGF165 and small molecule VEGFR TKIs (Ferrara and Kerbel, 2005). The concept that VEGF inhibition suppresses angiogenesis and thus tumour growth has been demonstrated in preclinical studies with the humanised murine monoclonal antibody inhibitor of VEGF-A, bevacizumab (Avastin) (Kim et al., 1993). Phase 3 trials of bevacizumab reported improved progression free survival (PFS) and overall response rate in combination with cytotoxic chemotherapy in metastatic colorectal and breast carcinomas and combined with interferon-α in metastatic renal cell carcinoma ([Hurwitz et al., 2004], [Salz et al., 2008]), [Miller et al., 2007], [Rini et al, 2008]). In Stage IIIB/IV NSCLC, significant improvement in both median survival and PFS was reported with bevacizumab in addition to paclitaxel and carboplatin (Sandler et al., 2006).

A number of the small molecule TKIs have also shown promising activity in clinical trials. SU11248 (sunitinib [Sutent]), an inhibitor of VEGFR, PDGFR, *c*-kit and Flt-3, has produced improved PFS in metastatic renal cell carcinoma in comparison to

interferon-α, as well as in imatinib-resistant gastrointestinal stromal tumours ([Motzer et al., 2007], [Heinreich et al., 2008]). Bay 43-9006 (sorafenib [Nexavar]), an inhibitor of C-RAF, B-RAF, a mutant B-RAF, VEGFR-2, VEGFR-3, PDGFRß, Flt-3, and *c*-kit, is thought to inhibit both tumour proliferation and angiogenesis. In placebo controlled randomised phase III studies it significantly improved median overall survival in advanced hepatocellular carcinoma and also improved progression-free survival in advanced clear cell renal carcinoma in patients where previous treatment has failed ([Llovet et al., 2008], [Escudier et al., 2007]). ZD6474 (vandetanib [Zactima]) is a potent inhibitor of VEGFR-2 that also inhibits EGFR. Phase II studies have shown promising effects with this agent in the second line treatment of advanced NSCLC, both as a single agent and in combination with docetaxel ([Kiura et al., 2008], [Heymach et al., 2007]). Other agents in clinical trials currently include: PTK787/ZK222584 (Vatalanib), an inhibitor of VEGFRs 1 and 2 in addition to PDGFR, c-Kit and c-Fms; AZD2171 (Cediranib), which inhibits the tyrosine kinase of VEGFRs 1, 2 and 3.

Novel agents targeting other cellular processes, including proliferation, are known to to indirectly inhibit angiogenesis. The monoclonal antibodies, cetuximab (C225), which targets EGFR, and trastuzumab (4D5), which targets the erbB2/ neu, have both been shown to reduce expression of VEGF (Petit et al., 1997). In further preclinical studies cetuximab has been shown to also reduce the expression of IL-8 and bFGF (Perrotte et al., 1999). Trastuzumab induces vascular normalisation and regression through reduced expression of pro-angiogenic factors, including VEGF, TGF-α, Ang-1 and PAI-1, as well as causing increased expression of the anti-angiogenic factor TSP-1 (Izumi et al., 2002). Selectively targeting EGFR with the small molecule TKI, gefitinib (Iressa), also inhibits angiogenesis, decreasing the production of VEGF, bFGF and TGF-α (Ciardiello et al., 2001). These anti-angiogenic effects may contribute to the overall anti-tumour action of these agents

and there is further scope to combine them with other vascular directed therapies, which is currently being explored in ongoing clinical studies.

Interferon-α is an established cytotoxic and anti-angiogenic treatment of cancers. In 1980 it was demonstrated to decrease endothelial cell motility and has since been shown to downregulate bFGF expression ([Brouty-Boyé and Zetter, 1980], [Singh et al., 1995]). It has been used as a treatment in a number of malignancies, in particular chronic myeloid and hairy cell leukaemias, and also including renal cell carcinoma, melanoma and Kaposi's sarcoma. The advent of new targeted strategies with superior efficacy however has lead to a marked decline recently in the use of interferon-α.

Thalidomide (α-(N-phthalimido)glutarimide), was initially used as a sedative antiemetic in the treatment of pregnancy-associated morning sickness until withdrawn in the 1960s when it was found to cause birth defects, particularly stunted limb development. There was a resurgence of interest in the 1990s when thalidomide was discovered to inhibit angiogenesis induced by bFGF (D'Amato et al., 1994). In addition to its anti-angiogenic properties, it has also been shown to have a direct anti-tumour action. TNF-α inhibition is thought to play an important role in these therapeutic effects. Following an initial report, showing a clinical response rate of 32% in patients with advanced and refractory multiple myeloma, it is now widely used to treat all stages of the disease in combination with dexamethasone and other agents including melphalan (Singhal et al., 1999). It has led to the development of new immunomodulatory drugs (IMiDs), thalidomide analogues including lenalidomide.

Temsirolimus, a soluble ester of rapamycin, has been found to have significant anti-tumour effects due to its inhibition of the serine/ threonine protein kinase,

mammalian target of rapamycin (mTOR). This inhibition has the downstream effect of reducing the translation of HIF1α resulting in a reduction of angiogenesis. In a phase III study examining the treatments of metastatic renal cell carcinoma, a significant improvement in overall survival of 3.6 months was seen compared to interferon-α (Hudes et al., 2007). It is now undergoing phase II testing, as a single agent and combined with other therapies, in a number of other tumour types including glioblastoma and melanoma, as are other mTOR inhibitors including everolimus. A number of other agents used in clinical practice for other indications have been subsequently discovered to have anti-angiogenic properties. These include doxycycline, zoledronate, roziglitazone and celecoxib ([Ginns et al., 2003], [Kalas et al.,2003], [Wood et al., 2002], [Panigrahy et al., 2002], [Masferrer et al., 2000]).

1.3.3.2 Direct angiogenesis inhibition

A vast number of studies have looked at identifying potential endogenous inhibitors of angiogenesis. The most widely studied is endostatin, a 20kDa fragment of collagen XVIII, which targets integrin $\alpha_5\beta_1$ inhibiting endothelial cell migration, proliferation and inducing apoptosis. However, the recombinant molecule used in the initial phase I and II studies, failed to demonstrate clinical anti-tumour activity. This may be a result of its relatively short half-life (approximately 2 hours) or the fact that 50% of molecules lacked 4 amino acids at the NH(2) termini, preventing binding to zinc and therefore producing a loss of anti-tumour effect ([Folkman, 2006], [Lee et al., 2008]). A phase II trial of recombinant human angiostatin, which binds to ATP synthase, angiomotin and annexin II on endothelial cells preventing endothelial cell migration and proliferation, combined with carboplatin and paclitaxel in advanced NSCLC has reported a disease control rate higher than historical controls although grade 3/4 vascular events were reported in 26.1% of patients (Kurup et al., 2006).

Other strategies for direct angiogenesis inhibition that are being explored include MEDI-522 (Vitaxin), a humanised monoclonal antibody that targets integrin $\alpha_v\beta_3$ that is highly expressed on tumour blood vessels compared to the low level seen on normal vessels. In a phase I study prolonged disease stabilisation was seen in three patients with metastatic renal carcinoma without any grade 3 or higher toxicities observed (McNeel et al., 2005). A current phase II study is looking at MEDI-522, 8mg/ kg, alone or in combination with dacarbazine in metastatic melanoma.

1.3.3.3 Combined anti-angiogenesis and vascular disruption

It has been hypothesized that combining anti-angiogenic agents with VDAs would produce enhanced anti-tumour effect, with the VDA significantly debulking the tumour and the anti-angiogenic agent preventing regrowth from the remaining viable tumour rim. In preclinical studies the combination of bevacizumab with either CA4P or CA1P showed enhanced tumour growth delay compared to the single agent treatments in a human renal cell carcinoma xenograft (Siemann and Shi, 2008). ZD6474 has also been looked at in combination with the VDA, ZD6126, in renal cell, Kaposi's sarcoma, colorectal and ovarian models. Both individual treatments showed activity in the renal cell and Kaposi's sarcoma models but the combination produced significantly superior tumour growth delays in all tumour models studied ([Siemann and Shi, 2004], [Shi and Siemann, 2005]). The EGFR inhibitor and indirect inhibitor of angiogenesis, gefitinib, has been studied in combination with ZD6126 in head and neck cancer xenografts. This combination showed both enhanced tumour growth delay and enhanced vascular effect, as evidenced by increased reduction in CD31 labelling (Bozec et al., 2006). Initial reports from a phase I study of bevacizumab and CA4P has shown this combination to be well tolerated with significant vascular effects (Nathan et al., 2008).

1.3.4 Nitric oxide and vascular function

The multi functional messenger molecule nitric oxide (NO) is an inorganic free radical gas. It is a product of the conversion of L-arginine, NADPH and oxygen to L-citrulline (de Wilt et al, 2000). NO is an important cell-signalling molecule at low concentrations, however, at high concentrations it can be cytotoxic (Ignarro, 2002). NO has a significant role in the mediation of tumour vascular function and angiogenesis (Fukumura, Gohongi et al., 2001). The production of NO is dependant on the NO synthase (NOS) enzymes (Marletta, 1993). Three isoforms of NOS have been identified, neuronal (nNOS or NOS1), inducible (iNOS or NOS2) and endothelial (eNOS or NOS3), each of which is expressed and regulated differently ([Nathan et al., 1994], [Hobbs et al., 1999]). Tumour cells often express one or multiple isoforms of NOS, dependant on the tumour type. The functions of NO depend on concentration and localisation of NO produced by these enzymes (Fukumura et al., 2006).

NO and VEGF have been shown to have distinct but complementary effects on tumour vasculature with one of the actions of VEGF being to increase NOS activity ([Camp et al., 2006], [Harris, 2002]). Vascular endothelial cell-derived NO mediates angiogenesis, perivascular recruitment and stabilisation of blood vessels in tumours and normal tissues ([Kashiwagi et al., 2005], [Yu et al., 2005], [Murohara et al., 1998]). Non-vascular cell derived NO interferes with vessel maturation in solid tumours (Kashiwagi et al., 2008).

1.3.4.1 Vascular effects of NOS inhibition

In terms of the therapeutic inhibition of NOS, the main compounds that have been explored are the analogues of L-arginine. These include N(G)-monomethyl-L-arginine (L-NMMA), N(omega)-nitro-L-arginine (L-NNA) and N(omega)-nitro-L-

arginine methyl ester (L-NAME). L-NMMA, at doses up to 20mg/kg/hr, and L-NAME, administered at 1mg/kg/hr, have both been explored clinically in the treatment of the hypotension and decreasing response to vasoconstrictive therapy commonly seen in septic shock (Avontuur et al., 1998). These treatments have not been widely adopted due to the toxicity observed in a phase III trial of infused L-NMMA, which was stopped early due to a higher Day 28 mortality in the treatment arm compared to those receiving placebo. In this trial a greater proportion of cardiovascular deaths was seen in the patients receiving L-NMMA, with observed cardiovascular effects including decreased cardiac output, heart failure and pulmonary or systemic arterial hypertension (Lopez et al., 2004).

Inhibition of all NOS isoforms with L-NAME or L-NMMA can reduce VEGF-induced angiogenesis, vascular permeability and can also reduce the accumulation of HIF-1α ([Ziche et al., 1997], [Quintero et al., 2006]). Similarly non-selective NOS inhibition with L-NNA can produce a selective increase in tumour vascular resistance and decrease tumour blood flow ([Tozer et al., 1995], [Tozer et al., 1997]). Inhibition of either eNOS, with the selective inhibitor cavtratin, or of all NOS isoforms, with L-NMMA, leads to decreased vessel density and increased vessel diameter (Kashiwagi et al., 2008). By comparison, nNOS silenced cells showed increased vessel density with more evenly distributed, less tortuous vessels and increased pericyte coverage. These effects, in addition to the observed decrease in permeability, are indicative of vascular normalization in the absence of nNOS (Kashiwagi et al., 2008). Overexpression of iNOS, not only increases tumour growth as well as the degree of functionally perfused vasculature and angiogenesis, but it has also been shown that iNOS gene therapy can, in fact, reduce tumour radioresistance under hypoxic conditions ([Cullis et al., 2006], [Worthington et al., 2004], [Coulter et al., 2008]). iNOS is transcriptionally upregulated by hypoxia and proinflammatory cytokines, such as interferon-gamma.

Non-selective NOS inhibition with N(omega)-nitro-L-arginine (L-NNA) causes a selective decrease in tumour vessel diameter, most pronounced in the tumour arteriolar circulation (Tozer et al., 2001). L-NNA produces a selective increase in tumour vascular resistance and decreased tumour blood flow ([Tozer et al., 1995], [Tozer et al., 1997]). In comparative studies examining inhibitors of the NOS enzymes, including both L- arginine analogues and different structural classes, L-NNA has been shown to be the most effective at inducing tumour vascular effects (Davis, Tozer et al., 2002). This has led to it being investigated in the clinical setting where a recent clinical Phase 1 study has reported significant vascular effects even at relatively low doses (Ng et al., 2007c). The optimal scheduling and method of administration for L-NNA, to maximise its anti-tumour effects, remains uncertain. Whilst pharmacokinetic data of single dose i.v. administered L-NNA in humans has been published, no comparative clinical or preclinical data exists comparing single or multiple dose injected L-NNA versus chronic oral administration.

1.3.4.2 Combined NOS inhibition and other vascular directed therapies

The interaction between the vascular effects of NO and tubulin binding vascular disruptive agents is well documented ([Davis, Tozer et al., 2002], [Parkins et al., 2000], [Cullis et al., 2006], [Wachsberger et al., 2005]). NO mediates protection against vascular disruption and has a protective effect against CA4P induced vascular injury, potentially through NO mediated limitation of neutrophil infiltration (Parkins et al., 2000). Over expression of iNOS confers resistance to the vascular disrupting agent ZD6126 (Cullis et al., 2006). In preclinical studies, the combination of NOS inhibition, with L-NNA 10mg/kg i.p. plus CA4P, compared to CA4P alone, produced enhanced reduction of perfused vascular volume and enhanced necrosis (Davis, Tozer et al., 2002). Other non-specific NOS inhibitors of different structural

classes have also shown similar activity, suggesting that the mechanism for this effect is related to inhibition of NOS (Davis, Tozer et al., 2002). Combined L-NNA and CA4P produces a tumour specific vascular effect (Tozer et al., 1999).

In P22 rodents, the addition of i.v. L-NNA (10mg/kg) to CA4P produced a marked increase in tumour necrosis; a 9 fold increase was seen with 3mg/kg CA4P and a 2.5 fold increase with 10mg/kg CA4P (Tozer et al., 2009). No cytotoxic dose response was seen when looking at L-NNA doses of 2.5mg/kg and increasing up to 20mg/kg. This is attributed to a balancing of the greater vascular resistance by the increase in MABP. In the CaNT model, the most effective combination of L-NNA with CA4P was seen with the highest dose of CA4P (100mg/kg), where a greater than additive cytotoxicity was produced. In terms of vascular volume reduction, simultaneous administration of these 2 agents appeared superior, but the cytotoxicity data suggested that giving the CA4P 3 hours prior to L-NNA conferred some benefit. L-NAME (1mg/ml) added to the drinking water for 24 hours prior to CA4P also showed enhanced blood flow reduction in P22 tumours. The optimal scheduling of CA4P and NOS inhibition to maximise this combined vascular effect remains uncertain.

Other preclinical studies have looked at the combination of ZD6126, a tubulin binding vascular disruptive agent, with L-NNA. ZD6126 alone produced 2-18% necrosis in U87 human glioblastoma xenografts compared with L-NNA (20mg/kg) alone, which produced 10-38%. The combination of these agents led to 89-95% necrosis in this tumour model (Wachsberger et al., 2005). L-NNA has also been studied in combination with the VEGFR-2 targeting monoclonal antibody, DC101, using an in vivo pancreatic cancer model. This combination enhanced tumour growth delay and produced an enhanced vascular effect, with a reduction in both microvessel density and vessel diameter (Camp et al., 2006).

1.3.5 Vascular effects of conventional anti-cancer therapies

1.3.5.1 Radiotherapy

The damage to the microvasculature of normal tissues following radiotherapy is well documented. This tumour bed effect has been demonstrated in preclinical models, where tumours implanted in a previously irradiated site grow back more slowly than control tumours at an unirradiated site (Leith et al, 1992). Radiotherapy appears to affect the tumour microvasculature through activation of the RhoA/Rho kinase pathway, resulting in rapid and persistent remodelling of the endothelial cytoskeleton and increase in the permeability of the microvasculature (Gabryś et al., 2007). It has been postulated that tumour radiosensitivity may be related to microvascular sensitivity, with more resistant cells lines displaying reduced endothelial cell apoptosis, although this theory has been contested (Garcia-Barros et al., 2003). This effect may also contribute to the normal tissue effects, including the gastrointestinal sequelae of radiotherapy. Endothelial cell apoptosis has been shown to occur in microvasculature of the gut following a single high dose of radiotherapy, an effect that was pharmacologically inhibited following the administration of an intravenous infusion of bFGF (Paris et al., 2001). Radiation-induced necrosis, a late normal tissue effect resulting from endothelial cell dysfunction, has been shown to be associated with increased vascular permeability and raised levels of VEGF. Exploratory clinical trials have been undertaken where the monoclonal antibody inhibitor of VEGF-A, bevacizumab, has been used in the treatment of radiation necrosis of the brain (Gonzalez et al., 2007).

Radiotherapy is also thought to have local and systemic effects on angiogenesis and has been shown to induce the expression of VEGF (Gorski et al., 1999). The formation of recurrent tumours after radiotherapy is preceded by angiogenesis, usually occurring within 20 days of completing radiotherapy (Hast et al., 2002).

Upregulation and stabilisation of HIF1α occurs as a result of increased VEGF expression from radiotherapy, which has the effect of increasing endothelial cell survival, angiogenesis and also tumour cell survival and proliferation (Dewhirst et al., 2008). Reduced levels of the endogenous angiogenesis inhibitor, angiostatin, have also been observed as a result of radiotherapy to the primary tumour, with a subsequent increase in growth of previously dormant metastases (Camphausen et al., 2001). However, enhanced inhibition of angiogenesis at uninvolved secondary (distal) sites, including the brain, following tumour irradiation has also been described (Hartford et al., 2000). This is thought to be a host- tumour interaction, as this effect was not observed following irradiation of normal tissues. The interaction of radiotherapy with tumour and normal tissue vasculature is complex, although it undoubtedly plays an important role in the response to treatment and has the potential to be exploited further.

1.3.5.2 Chemotherapy and hormonal therapy

Systemic anti-cancer treatments are also known to have effects on tumour vasculature. Androgen blockade, in the context of prostate adenocarcinoma, has been shown to down regulate VEGF production (Mazzucchelli et al., 2000). In addition to the vascular disruptive effects of the vinca alkaloids, described earlier, a number of cytotoxic chemotherapies have been demonstrated in preclinical studies to have anti-angiogenic properties. Paclitaxel, an inhibitor of microtubule polymerisation, inhibits the proliferation of endothelial cells and tumour angiogenesis (Belotti et al., 1996).

Metronomic or anti-angiogenic scheduling of chemotherapy, with the more frequent administration of lower doses, using cyclophosphamide has also been shown to be effective in controlling tumour growth in both drug sensitive and drug resistant

murine tumour models (Browder et al., 2000). The scheduling in this study produced sustained apoptosis of microvascular endothelial cells in the tumour vascular bed. It is hypothesized that the disease stabilising effects that have been observed in clinical studies, with schedules such as, continuous infusional 5-FU, weekly paclitaxel or daily oral etoposide, are a result of such anti-angiogenic effects (Kerbel and Folkman, 2002).

1.4 Combining radiotherapy and vascular directed therapy

Radiotherapy is a highly effective treatment in a large number of malignancies, yet a significant proportion of patients receiving radical treatment are not cured of their disease. Radiotherapy has been combined with other cancer treatments to improve its efficacy and the use of concurrent cytotoxic chemotherapy is the standard of care for specific tumours, in particular squamous cell carcinomas of the uterine cervix, anus, oesophagus and head and neck region. In assessing the potential benefits of adding a new treatment to radiotherapy, the key features to ascertain are whether it offers improved anti-tumour effect, spatial cooperation or non-overlapping toxicities (Steel, 1979).

There are potential exploitable non-interactive mechanisms supporting the concept for combining vascular directed therapies and radiotherapy, with each individual treatment exerting independent effects. Interactive mechanisms may also result from these combinations, where the vascular effects of radiotherapy and the vascular directed therapies enhance the effects of one or even both. An ideal combination therapy enhances tumour cell kill without enhancing damage to critical normal tissues. This is defined as the therapeutic index: the tumour response produced for a given level of normal tissue damage (Steel, 2002). The critical events

producing radiation-induced cell killing are thought to be DNA damage, in particular double strand breaks. The mechanisms of how vascular directed therapies actually exert their therapeutic effect on tumour vasculature are complex and dependent on the agent employed.

Timing, sequence and schedule are of particular importance when combining vascular directed therapies with radiotherapy. The vascular effects of each component of these combination treatments have to be considered, in addition to any potential interaction between the individual treatments. As vascular disruptive agents produce markedly different effects to the effects seen with anti-angiogenic agents, strategies to incorporate them must reflect these differences. These effects on tumour vasculature can produce significant acute and chronic changes in the tumour microenvironment, which in turn can affect the radioresponsiveness of the tumour or even how it responds to the vascular directed therapy. The main concerns expressed regarding the concept of combining vascular treatments and radiotherapy has been the potential for increased tumour hypoxia. Tumour oxygenation is an important radiobiological factor in determining the potential response to radiation, with hypoxia increasing radioresistance; this is therefore an important consideration in the sequencing of these treatments (Gray et al., 1953).

1.4.1 Vascular disruptive agents and radiotherapy

Since the introduction of VDAs, there has been extensive investigation into strategies to therapeutically exploit their potential. The effects of VDAs are most marked in the central portion of tumours, where significant necrosis is seen in tumours sensitive to this treatment. Despite this, VDAs, when given as single agents, have demonstrated only minimal impact on tumour growth, in both preclinical and clinical studies. The persistence of a viable residual rim of tumour

following treatment with VDAs is thought to be a significant contributing factor facilitating tumour regrowth, in addition to the resultant tumour revascularisation that occurs following this induced acute vascular disruption. Combining radiotherapy with VDAs offers a means for enhancing the effects of both treatments. The potential advantages and also disadvantages for this combination of treatments are summarised in Table 1.2.

Due to the inadequate nature of its vasculature, the central region of a tumour is usually chronically hypoxic, which has the effect of rendering the cells in this region relatively resistant to radiotherapy. By comparison, peripheral regions of a tumour, with a good vascular supply and greater levels of oxygenation, are sensitive to the effects of ionising radiation. Combining radiotherapy with VDAs is a means of spatial cooperation, with VDAs more effective in the centre and radiotherapy more effective at the rim. Following treatment with a VDA the remaining cells surviving in the peripheral tumour rim are likely to be well oxygenated; combined treatment with radiotherapy has been demonstrated to reduce the proportion of hypoxic cells compared to radiotherapy alone (Li et al., 1998).

Despite this spatial cooperation, the exact mechanism for interaction between these two therapeutic modalities remains unclear. Radiation-induced damage to the tumour vasculature is an important determinant of tumour cell survival, with the resultant endothelial cell apoptosis contributing to the overall anti-tumour effect (Garcia-Barros et al., 2003). The addition of a VDA will likely result in an increase in endothelial cell apoptosis and it is also possible that the damage to tumour blood vessels from radiotherapy enhances the sensitivity of endothelial cells to the effects of VDAs.

The non-overlapping toxicities of radiotherapy and VDAs add further weight to the argument for combining these treatments. Radiotherapy produces mainly localised toxicities, with common acute effects including inflammation, swelling, erythema, hair loss, mucositis, and pain. The majority of these acute effects can be effectively treated or managed to allow the continuation and completion of treatment. However, it is the late normal tissue effects, including fibrosis, organ or gland dysfunction, disrupted lymphatic drainage, altered vascularity or even tissue necrosis, that ultimately limit the dose that that can be delivered. These late effects are difficult to treat, usually irreversible and can have significant resultant morbidity for the patient. Treatment-related normal tissue sequelae are very much dependant on the tumour site and the dose, technique and fractionation of radiotherapy used. In the phase 1 studies of VDAs, the majority of grade 1 to 3 toxicities observed were acute blood pressure changes, cardiovascular toxicity and neurological effects, all of which were reversible. CA4P treatment-induced vascular and cardiovascular toxicities were seen to resolve by 4 to 6 hours post treatment and ataxia resolving within 24 to 48 hours.

1.4.1.1 Combretastatin A4 phosphate and radiotherapy

CA4P is the VDA that has been most extensively studied in combination with radiotherapy. Studies have been undertaken in a variety of preclinical rodent tumour models using both single fraction radiotherapy and fractionated radiotherapy. Given the concerns, regarding potential VDA-induced acute hypoxia compromising the effects of radiotherapy, exploration of the optimal timing for the administration of CA4P has been has been a key component to this work.

The majority of studies that have been undertaken have used a single fraction of radiotherapy. CA4P at doses of 10mg/kg to 100mg/kg i.p. administered 30 to 60 minutes after a single fraction of radiotherapy, at a dose per fraction of 5Gy up to

20Gy, was investigated using the KHT sarcoma tumour model (Li et al., 1998). In this study, the addition of CA4P, 100mg/kg, to radiotherapy reduced tumour cell survival by 10 to 500 fold compared to radiotherapy alone. Further work using the KHT sarcoma cell line demonstrated that the addition of synchronous CA4P 100mg/kg i.p. to a single 10Gy fraction of radiotherapy significantly reduced the surviving fraction irrespective of whether it was administered 1 hour prior to, synchronously or 30 minutes after radiotherapy (Murata et al. 2001a). This was in contrast to their findings with the C3H murine mammary tumour when, following administration of a single fraction of radiotherapy, at doses of 25Gy up to 70Gy, they determined the TCD50 value for radiation alone to be 53.2Gy. This was reduced significantly to 45.1Gy by the addition of CA4P 250mg/kg i.p., given synchronously or 30 minutes after radiotherapy. No improvement in the TCD50 was seen when the CA4P was administered 1 hour prior to radiotherapy.

The effect of tumour size on the outcome with combined vascular disruption and radiation has been explored. Studies using a syngenic rat rhabdomyosarcoma model have reported tumour size to be an important factor in determining which of these tumours will benefit from the addition of CA4P to radiotherapy. In this work, a significant tumour growth delay was demonstrated when CA4P 25mg/kg i.p. was given 24 hours after a single 8Gy fraction of radiotherapy (Landuyt et al., 2001). Interestingly, however, this effect was only significant in large tumours, deemed to be those measuring between 7 and 14 cm^3. Further work using this rhabdomyosarcoma model has examined whether tumour size continues to be a factor when CA4P was combined with fractionated radiotherapy (Ahmed et al., 2006). In this study, 5 daily fractions of 3Gy were delivered on successive days with CA4P 25mg/kg i.p. given 24 hours after the final irradiation. Tumour growth delay in small tumours (2 cm^3) was compared to that in large tumours (10 cm^3). Only the group with large tumours showed a small delay in tumour growth with the

combination treatment compared to radiotherapy alone, whereas no difference was seen between the treatment groups with small tumours.

Studies using single fractions of radiotherapy are logistically easier to undertake and provide an excellent means of screening for the effects of new targeted therapies when added to radiotherapy. However, fractionated radiotherapy remains the mainstay of modern radiotherapy, especially for radical and curative treatments where generally a greater number of fractions and smaller fraction sizes are used. Fractionated radiotherapy schedules have been looked at in combination with CA4P. Using the murine adenocarcinoma CaNT, eight daily fractions of radiotherapy were delivered over 2 weeks, 4 fractions per week, at a dose per fraction of 5Gy (Chaplin et al., 1999). CA4P 100mg/kg i.p. was administered 24 hours after the final fraction of radiotherapy each week (i.e. 4^{th} and 8^{th} fractions). In addition to minimising the effects of any resultant hypoxia, the radiotherapy was delivered whilst the mice were breathing Carbogen (95% O2, 5% CO2). A 63% increase in tumour regression compared to radiotherapy alone, in addition to, complete regression of 50% of tumours in the combination group, was seen, with neither radiotherapy nor CA4P alone producing any complete regressions. In another study using the C3H mammary carcinoma model, CA4P was administered at a dose of 250mg/kg i.p. 30 minutes after the fifth and tenth fractions of radiotherapy, with 10 fractions given over 2 weeks at a dose per fraction of 4 to 8Gy (Murata et al. 2000). The addition of CA4P to fractionated radiotherapy reduced the TCD50 value significantly to 65.6Gy compared to 70.6Gy for radiotherapy alone.

When combining any new agent with radiotherapy, it is critical to determine whether the normal tissue effects of radiotherapy are increased by the combination treatment. A study by Murata et al (2001a) looked at the acute skin toxicity of CA4P 250mg/kg i.p. given immediately following single fraction radiotherapy. There was

no significant difference in the percentage of animals with moist desquamation between the group receiving the combined treatment and those receiving radiotherapy alone. In addition to assessing the early responding skin effects of CA4P in combination with radiotherapy, the late effects of this combination have also been examined, looking at the late responding bladder and lung effects (Horsman et al., 2002). No significant difference in bladder reserve or ventilation rate was observed. This work demonstrated no enhancement of radiation response or damage in either the early or late responding normal tissues studied.

Another strategy to exploit the complimentary effects of VDAs and irradiation that is being investigated is the use of CA4P encapsulated in liposomes. These anti-E-selectin conjugated liposomes have specific peptide sequences on their surface for preferential targeting of irradiated tumour blood vessels via intergrin αVβ3. Enhanced tumour growth delay has been seen in both B16-F10 melanoma and Mca-4 mammary tumours with a single 5Gy fraction of radiotherapy in combination with immunoliposomes, at a CA4P concentration of 15mg/kg, given 5 minutes post irradiation via retro-orbital injection (Pattillo et al., 2005, Pattillo et al., 2009). In these experiments, free CA4P at a dose of 81mg/kg did not significantly improve tumour growth delay in combination with single fraction radiotherapy. However, when fractionated radiotherapy (20Gy in 10# over 10 days) was used in combination with CA4P or immunoliposomes given every other day (at the same dose as in the single fraction studies), both regimes enhanced tumour growth delay and there was no significant difference between the two treatments.

1.4.1.2 Other combretastatins and radiotherapy

OXI4503 has been looked at in combination with single fraction radiotherapy in the C3H mammary carcinoma model. When given i.p. 1 hour after radiotherapy, at a dose of 50mg/ kg, it significantly reduced the TCD50 value to 41Gy compared to a

value of 52Gy for radiotherapy alone (Hokland and Horsman, 2007). AC7700 combined with radiotherapy has been investigated in a variant of Yoshida sarcoma, LY80, examining the effects on tumour blood flow and tumour growth (Hori et al., 2008). A single i.v. dose of 10mg/kg was administered at 2 hours, 2 days, 3 days or 4 days following radiotherapy. There were significant increases in tumour blood flow at 48 hours with radiotherapy alone, reaching its maximum value at 3 to 4 days post treatment. A marked reduction in tumour blood flow was produced by the co-administration of AC7700, irrespective of when it was given. A greater than additive tumour growth delay was produced by AC7700 when given post irradiation and additionally it prevented locoregional lymph node metastasis in 50% of the mice receiving the combined treatment. In the groups receiving radiotherapy alone or in combination with AC7700 given 48 hours prior to radiotherapy, 100% of the mice developed lymph node metastases.

1.4.1.3 Other tubulin-binding VDAs and radiotherapy

ZD6126 has been studied in combination with radiotherapy in a number of preclinical tumour models. Using the U87 glioblastoma model, ZD6126 was given at a dose of 150mg/kg i.p. either 1 hour prior to or 1 hour after a single 10Gy fraction of radiotherapy (Wachsberger et al., 2005). When given 1 hour prior to radiotherapy, acute hypoxia was detected and this resulted in reduced tumour growth delay compared to radiotherapy alone. The tumour growth delay seen with ZD6126 given 1 hour after radiotherapy was comparable but not greater than radiotherapy alone.

Combined treatment with ZD6126 and radiotherapy on human umbilical vein endothelial cells (HUVECs) has shown augmented cell killing in clonogenic survival assays, with reduced irradiated endothelial cell survival and radiation induced apoptosis (Hoang et al., 2006). In this work, using a Matrigel plug assay with a lung carcinoma xenograft, the greatest reduction in vascularisation was observed with

combined ZD6126 and radiotherapy. Tumour growth delay, using head and neck squamous cell carcinoma xenografts, was also examined. Radiotherapy, at a dose of 2.5Gy was delivered twice weekly for 4 to 5 weeks with ZD6126, 200mg/kg i.p. given once per week, 1 hour after the second fraction of radiotherapy each week, producing only non significant enhancement of tumour growth delay.

The optimal timing for combining these treatments has been explored in work using the KHT sarcoma model (Siemann and Rojani 2002). With ZD6126, at a dose of 150mg/kg, tumour cell survival was reduced when given either prior to or after radiotherapy. The greatest cell kill was observed if ZD6126 was given 1 to 4 hours after or 24 hours prior to radiotherapy. In combination with fractionated radiotherapy, 25Gy in 10 fractions over 2 weeks, ZD6126, 150mg/kg i.p. administered 1 hour after the final fraction of radiotherapy each week, produced a significant delay in tumour regrowth, compared to radiotherapy alone. Further work has looked at whether tumour size has an impact on the effect of ZD6126 and radiation (Siemann and Rojiani 2005). A decrease in size of tumour surviving fraction post treatment was seen with increasing tumour size.

1.4.1.4 Flavonoid VDAs and radiotherapy

FAA was one of the first VDAs to be examined in combination with radiotherapy. When given at a dose of 170mg/kg i.v., it was shown to enhance the tumour response to a single 10Gy fraction of radiotherapy in Glasgow's murine ^{239}Pu-induced osteogenic sarcoma model (De Neve et al 1990). This enhancement was only seen when FAA was given immediately prior to radiotherapy and was not seen when administered either 1 hour prior or 48 hours after. FAA has also been shown to be more effective than TNF in inhibiting the growth of irradiated HUVECs (Lin et al. 1996). The TCD50 in C3H mammary carcinoma, treated with a single fraction, was reduced from 52Gy with radiotherapy alone to 42Gy with the addition of FAA

administered i.p. 1 hour after radiotherapy, at a dose of 150mg/kg (Horsman et al., 2001).

Simultaneous administration of DMXAA, 20mg/kg i.p., and a single 15Gy fraction of radiotherapy increased the mean tumour growth time (time to grow to three times treatment volume) to 18.5 days from 15.5 days with radiation alone, in the C3H mammary carcinoma model (Murata et al., 2001b). Altering the timing of administration of DMXAA to 1 to 3 hours post radiotherapy produced a further significant improvement in the mean tumour growth time to 21 to 22 days. DMXAA given 24 hours post radiation was no better than simultaneous administration, but if given prior to radiotherapy any beneficial effect was lost with the mean tumour growth time similar to radiotherapy alone. The survival of KHT sarcoma cells were also studied following a 10Gy single fraction in combination with DMXAA 17.5mg/kg. The greatest cell killing was seen when DMXAA was given 1 to 3 hours after radiotherapy, compared to just prior and 6 hours after. The final component of this examined the acute cutaneous toxicity of the combination treatment, with the feet of CDF1 mice irradiated with or without DMXAA, given 1 hour after irradiation. The dose that 50% of the animals developed moist desquamation was not significantly different between the two groups; 33Gy for the combined treatments and 32Gy for radiotherapy alone.

Potentiation of the radiation response has been seen in both RIF-1 fibrosarcoma and the MDAH-Mca-4 mammary carcinoma models (Wilson et al., 1998). DMXAA (80μmol/kg i.p.) was given 5 minutes after a single 20Gy fraction of radiotherapy, producing a calculated dose modification factor of 2.3 and 3.9 respectively in the two tumour models. The effect of timing was examined in the MDAH-Mca-4 tumour model. The combination schedule produced a greater tumour growth delay than radiotherapy, although the effect was less when DMXAA was given 1 to 4 hours prior to radiotherapy. In this work, DMXAA was also examined in combination with a

fractionated radiotherapy schedule of 20Gy in 8 fractions over 4 days, a dose per fraction of 2.5Gy. Following the final fraction of radiotherapy, DMXAA, 80μmol/kg i.p., was given immediately and produced a tumour growth delay of 9 days compared to 3.1 days for radiotherapy alone. This fractionation was then used in both the RIF-1 and MDAH-Mca-4 models to examine the effect of concurrent daily i.p. DMXAA, given 5 minutes after the second fraction of radiotherapy each day at a reduced dose of 56μmol/kg due to the associated increased toxicity of the daily treatment. The combined treatment produced the greatest tumour growth delay in both models and was significantly better than radiotherapy alone.

1.4.2 Hyperthermia in combination with VDAs and radiotherapy

Hyperthermia has been extensively investigated as an anticancer treatment, as a single agent and in combination with other therapeutic modalities, including radiotherapy. It is a potent radiosensitiser of both tumour cells and normal tissue (Horsman and Overgaard, 2007). Sequential treatment, with radiotherapy followed by hyperthermia, seems to provide the best combination, with anti-tumour effects still seen when heating is delivered 4 to 6 hours after irradiation. At an interval of 4 hours, there is negligible enhancement of normal tissue effects, whilst some enhancement of radiation damage in tumours still occurs. The efficacy of hyperthermia can be improved through a reduction in blood flow; resulting in better tumour heating and increased tumour damage (Horsman et al. 1989, Honess et al. 1991).

In studies using the C3H mammary carcinoma model, there was a marked improvement in the TCD50 for radiotherapy alone (53Gy), with the addition of FAA (150mg/kg), DMXAA (20mg/kg) or CA4P (25mg/kg), when given i.p. 30 to 60

minutes after the single fraction of radiotherapy (Horsman and Murata, 2002). These combination therapies produced TCD50 values of between 41Gy to 48Gy, and when hyperthermia (41.5°C for 1 hour) was added, the TCD50 values were decreased further to between 28 to 33Gy. The addition of a VDA to radiotherapy and hyperthermia improved tumour control by a greater extent than radiotherapy and hyperthermia alone, at both 41.5°C and 43°C. In further work the triple combination of radiotherapy, DMXAA and hyperthermia (41.5°C) has been shown to lower the TCD50 value from 52Gy, for radiotherapy alone, to 30Gy; an enhancement ratio of 1.75. This beneficial effect was still evident at 40.5°C, where an enhancement ratio of 1.29 was produced; an equivalent effect to that seen with radiotherapy and hyperthermia at 43°C without DMXAA (Murata and Horsman, 2004).

1.4.3 Bioreductive cytotoxics in combination with VDAs and radiotherapy

With tumour hypoxia providing a major stumbling block to the success of conventional anticancer strategies, this has led to the development of bioreductive agents, such as tirapazamine, a hypoxia-activated topoisomerase II poison. Given the increased hypoxia following the administration of VDAs, preclinical studies have explored their combined effects. DMXAA has been shown to enhance the anti-tumour effects, in MDAH-Mca-4 tumours, of the bioreductive drugs tirapazamine, CI-1010 and SN23816 (Lash et al., 1998). Enhanced tumour growth delay has also been reported with the addition of CA4P to both tirapazamine and AQ4N, in experiments using the mouse mammary tumour CaNT (Tozer et al., 2008). With both VDAs and bioreductive agents demonstrating potential enhancement of the anti-tumour effects of radiotherapy, this provides a rationale for looking at all three treatments together.

Further preclinical work using the MDAH-Mca-4 tumour model has examined DMXAA in combination with fractionated radiotherapy, 20Gy in 8 fractions over 4 days, and tirapazamine (Wilson et al., 1998). The addition of i.p. tirapazamine, given 5 minutes after each fraction of radiotherapy at a dose of 75μmol/kg, extended the tumour growth delay to 8 days compared to 3.1 days for radiotherapy alone. DMXAA, 80μmol/kg i.p. given immediately after the final fraction of radiotherapy, produced a tumour growth delay of 9 days, but the combination of radiotherapy, tirapazamine and DMXAA gave the greatest tumour growth delay of 12 days.

1.4.4 Dual targeting of tumour vasculature in combination with radiotherapy

1.4.4.1 Anti-angiogenesis

Numerous preclinical studies have been undertaken to ascertain the potential beneficial therapeutic effects of combining novel anti-angiogenic agents and radiotherapy. Most of these studies have, as with VDAs, used single fraction radiotherapy. Despite the heterogeneity in these studies of antiangiogenic agents, tumour type, fractionations, timings and scheduling, their findings suggest that this combination of angiogenesis inhibition and radiotherapy produces an increase in anti-tumour effect that is, at least, additive (Horsman and Siemann, 2006). Beneficial effects have been observed when they are given concurrently, adjuvantly, neoadjuvantly or in any combination of these schedules. Comparative studies have not elicited a definitive scheduling for the administration of anti-angiogenics with radiotherapy.

It has been demonstrated that tumour blood vessels, arising from tissue that has been irradiated to a high dose, are sensitised to the effects of angiogenesis inhibition. The growth rate of tumours implanted at a previously irradiated site is

comparatively slower than in non-irradiated sites. A study examining the effects on FaDu xenografts demonstrated further growth inhibition by the addition of the anti-angiogenic agent PTK787/ ZK222584, whereas this combination did not significantly delay tumour growth in the same tumours implanted at a non-irradiated site (Zips et al., 2005). VEGF is an important endothelial cell survival factor, its withdrawal induces cell death and it has a protective role in tumour blood vessels, helping to counteract the sequelae of radiotherapy. Interruption of this protective mechanism, by the combined radiotherapy and angiogenesis inhibition, results in increased endothelial cell apoptosis; the inhibition of the signalling cascade induced by angiogenic factors, including VEGF, directly radiosensitising tumour endothelial cells (Gorski et al., 1999). Apoptosis is the main death pathway for endothelial cells following radiotherapy and this provides further rationale for combining anti-VEGF and other anti-angiogenic strategies with radiation.

The normalisation of tumour vasculature following anti-angiogenic therapy provides another potential vascular strategy to enhance the effects of radiotherapy. This vascular normalisation has been shown to increase tumour oxygenation and, as a consequence of this, increase tumour radiosensitivity (Winkler et al., 2004). Continued use of these agents can produce a further reduction in vessel density, which, as a result, may increase tumour hypoxia. With these findings, there appears to be a therapeutic window for combining anti-angiogenic agents and radiotherapy, in order to achieve the maximal therapeutic benefit through exploiting this vascular normalisation.

Combined angiogenesis inhibition and radiotherapy can also produce enhanced effects on distant metastases in addition to the effects seen at the primary site. The effect of adding thrombospondin-1 (TSP-1) to single fraction radiotherapy has been looked at using the human melanoma xenograft D12 (Rofstad et al., 2003).

Following the discovery that a dose of 30Gy produced a significant reduction in endogenous TSP-1, the effects of TSP-1, administered at a dose of 25 or 50μg i.p. 24 hours prior to and then again 1 hour prior to radiotherapy, were examined. TSP-1 significantly reduced the frequency of lung metastases and improved control of the primary tumour. Adjuvant TSP-1, 50μg i.p. given three times per week, further delayed the regrowth of the primary tumours.

1.4.4.2 EGFR inhibition

ZD6474, which inhibits both EGFR and VEGFR-2, has been evaluated in combination with radiotherapy. In a study with fractionated radiotherapy (20Gy/ 10#/ 2weeks) using the HT29 colon carcinoma xenograft model, ZD6474, 25mg/kg, was orally (p.o) administered daily, five days per week for two weeks either neoadjuvantly, concurrently or adjuvantly (Brazelle et al., 2006). An additive beneficial effect was seen with the combination therapy, but this was independent of the timing of ZD6474. Similarly, in a study with daily ZD6474, 30mg/kg p.o. in combination with radiotherapy (12Gy/4#/2weeks), a beneficial effect, independent of sequence, was observed in the EGFR-positive head and neck squamous cell carcinoma xenograft, UMSCC2; although concurrent administration had superior anti-tumour activity compared to adjuvant treatment in the EGFR-negative xenograft, UMSCC10 (Gustafson et al., 2008). These findings are in contrast to those of a further study, where the CaLu 6 NSCLC xenograft was used in combination with fractionated radiotherapy (6Gy/3#/3days) and compared to daily ZD6474, 50mg/kg p.o., given, either, two hours prior to each fraction, or 30 minutes after the final fraction, then continued for the duration of the experiment (Williams et al., 2004). In this study, the sequential administration, with radiotherapy followed by ZD6474, produced the greatest tumour growth delay.

Beneficial anti-tumour activity has also been reported in preclinical studies, combining ZD6474 with concurrent chemoradiation using temozolamide in malignant glioma xenografts and with gemcitabine in pancreatic carcinoma xenografts, ([Sandström et al., 2008], [Bianco et al., 2006]). Other combinations that have shown promise in preclinical studies include erlotinib, bevacizumab and radiotherapy and also sunitinib, cetuximab and radiotherapy; both studies used the same fractionated radiotherapy schedule (24Gy/4#/1.5weeks) and same head and neck cancer xenograft, CAL33 ([Bozec et al., 2008], [Bozec et al., 2009]). Clinical trials are awaited to establish whether this dual targeting of EGFR and VEGF in combination with radiotherapy can produce this enhanced anti-tumour activity in humans, in addition to determining the impact of scheduling on this combination in different tumour types, given the variable effects seen in the preclinical trials with different tumours.

EGFR inhibitors have been looked at in combination with VDAs and radiotherapy. Gefitinib has been combined with ZD6126 and fractionated radiotherapy, 16Gy in 4 fractions over 2 weeks, in the NSCLC xenograft model, A549 (Raben et al., 2004). ZD6126 was given weekly at a dose of 150mg/kg i.p. after the completion of radiotherapy each week and gefitinib was given at a dose of 100mg/kg daily for 2 weeks. This triple combination of radiotherapy, gefitininib and ZD6126 significantly increased tumour growth delay compared to radiotherapy and either gefitinib or ZD6126 alone.

1.4.4.3 NOS inhibition

Following evidence showing enhancement of the vascular effects of VDAs by the addition of NOS inhibition, the combination of these two vascular directed therapies has been looked at in combination with single fraction radiotherapy. In a study looking at the combination of ZD6126 and radiotherapy, nitric oxide synthase

inhibition was incorporated into the schedule, as the U87 glioblastoma model is known to be relatively resistant to the induction of tumour necrosis by ZD6126 (Wachsberger et al., 2005). The addition of L-NNA (20mg/kg) to ZD6126 (200mg/kg), both given i.p., increased the percentage of necrosis produced at 24 hours post treatment to 89 to 95%, compared with 10 to 38% with ZD6126 alone. However this combination of L-NNA and ZD6126, when given after a single 10Gy of radiotherapy, did not show any additional benefit compared with radiotherapy and ZD6126 alone.

1.5 Functional imaging

1.5.1 The role of functional imaging in assessing response to vascular directed therapies

As the transition from conventional cancer treatments to more targeted therapies evolves, questions have arisen regarding the best way to assess tumour response. The World Health Organisation published the WHO handbook for reporting results of cancer treatment in 1979, with the aim of providing a standard and reproducible means for the assessment of tumour response. Despite the widespread adoption of these criteria, using the measurement of tumours with multiplication of two measured diameters, they were, ultimately, felt to be cumbersome and unnecessarily complex. This led to the subsequent development of the 'Response Evaluation Criteria in Solid Tumours (RECIST)' (Therasse et al., 2000). The assessment process was significantly simplified, with only the longest diameter of the tumour required, whilst maintaining a level of accuracy and reproducibility. RECIST has since been further updated and simplified (Eisenhauer et al., 2009). Whilst FDG-PET identification of new lesions is now accepted as evidence of progressive disease, tumour size remains the major component to RECIST, potentially limiting its use in assessing newer targeted agents. Tumour shrinkage

may reflect a substantial effect, but it cannot accurately reflect acute functional changes within the tumour. Conversely, significant anti-tumour effect can occur without significant tumour shrinkage occurring. There is inherent observational error in the measurement of tumours and it can be extremely difficult to measure the full extent of some tumours, in particular diffuse intraperitoneal malignancies or pulmonary lymphangitis.

In the search for non-invasive means to assess tumour vascular function and detect response at an early stage, functional imaging techniques using CT, MRI, PET and ultrasound have come to the forefront. The ability of these novel techniques to assess subtle acute microcirculatory changes has been of particular importance in both the diagnostic setting and therapeutic monitoring of tumours. These techniques can be used to provide reliable biomarkers for the monitoring of anticancer therapies, especially anti-angiogenic and vascular disruptive strategies, both in the clinical trials setting and also in everyday clinical practice. The characteristic features of tumour vasculature are distinguishable from the vascular patterns observed in non-malignant tissue. Many of the features are amenable to study by functional techniques, such as the high permeability to macromolecules, a feature that can be exploited with the use of specific contrast agents. The pros and cons of these different functional imaging techniques for assessing tumour vasculature are shown in table 1.3.

1.5.2 Dynamic contrast enhanced CT

The use of rapid sequence perfusion or dynamic contrast-enhanced (DCE) computed tomography (CT) in the assessment of tissue vasculature was first reported in 1980, in a study of intracranial blood volume (Axel, 1980). Following on from this, preclinical studies have looked at DCE-CT in the assessment of

myocardial and renal blood flow ([Wolfkiel et al., 1987], [Jaschke et al., 1990]). As technology and software have developed, this has led to the production of scanners capable of helical CT, with the benefits of higher resolution, faster scan speeds and smaller slice thickness. Advancement in computing methods enabled the production of parametric vascular maps, using a colour scale to provide a visual representation of the rate of enhancement in each pixel (Miles et al., 1991). Clinical studies have since been undertaken using DCE-CT for quantification of tissue blood volume and as a measure of perfusion in the kidney, liver and pancreas. Further refinement of DCE-CT and increased potential applications for these techniques have resulted from the development of multi-detector (MD) CTs. MDCT allows the simultaneous acquisition of multiple slices, thus improving spatial resolution, reducing scanning time and enabling scanning of a greater volume.

The principle of DCE-CT involves acquisition of a baseline non-contrast enhanced CT. This is then followed by the administation of an i.v. contrast agent and the acquisition of a series of further CTs. The resultant enhancement of tissue is dependent on the following factors: the volume and concentration of the contrast agent and the rate at which it is delivered; the surface area and permeability of the vasculature; the rate of back flux into the intravascular space from the extravascular-extracellular space; the rate at which the contrast agent is excreted. There is a direct linear relationship between enhancement (Hounsfield Units [HU]) and iodine concentration. The sequential CT scans acquired allow assessment of the acute temporal changes in contrast enhancement following administration of i.v. contrast. This provides information on the functioning vasculature of the tissue, which can be semi-quantitative, such as peak enhancement and time to peak enhancement, and quantitative, such as tissue blood flow and blood volume.

The two main types of contrast agent used in DCE-CT are defined as low molecular weight (<1kDa) or macromolecular (>30kDa). Low molecular weight agents are used in everyday clinical practice with diagnostic CT and are iodine based, usually derivatives of iodobenzoic acid, with a molecular weight of around 700Da. This type of contrast remains in the intravascular compartment for the first few cardiac cycles post injection then diffuses into the extravascular-extracellular space, with minimal intracellular uptake (<1%). It is excreted mainly via the kidneys, although there can be a component of hepato-biliary excretion too. Macromolecular agents have a much greater retention within the intravascular space, with <1% first pass extraction, allowing a more accurate assessment of vascular volume. As tumour vasculature, but not normal tissue vasculature, is permeable to these macromolecules, there is the potential for this to be exploited using this type of contrast in perfusion CT. Currently these agents, despite showing promise in preclinical trials, are not licensed for clinical use and results from clinical trials are awaited (Simon et al., 2005).

A number of mathematical modelling techniques have been used in DCE-CT to study different vascular parameters. Analysis methods based on the Fick principle have been commonly used to assess blood flow per tissue volume (also termed perfusion), including the ‘peak’ method or the ‘slope’ method ([Mullani and Gould, 1983], [Miles 1991]). Dual compartment modelling has been used, based upon an analysis method for the modelling of radionuclide tracer kinetics, having been adapted and simplified for use with CT ([Patlak et al., 1983], [Patlak and Blasberg, 1985]). This, Patlak analysis, can be used to provide estimates of tissue blood volume (BV) and also vascular leakage (extraction fraction, K_1). The tissue contrast concentration is deemed to be equivalent to the sum of the intravascular and extravascular-extracellular concentration of contrast. When divided by the whole blood contrast concentration, this can be plotted graphically to produce the Patlak

plot, with K1 derived from the slope of this line, and BV from the y-intercept. Flow and vascular permeability have to be considered when interpreting extraction fraction values. This is because when flow is greater than permeability, then K_1 will equal permeability, taking into account the given surface area (permeability surface area product). In flow limited situations, K_1 will reflect flow rather than permeability surface area product.

The acquistion of perfusion CT data can either be undertaken as a first pass study, a delayed phase study, or, as is becoming more common, both first pass and delayed. The first pass of contrast is usually within 40 seconds of administration and imaging this requires a high temporal sampling rate, up to one acquisition every 0.5 second. First pass imaging is used in determining blood flow, blood volume and mean transit time. In delayed phase studies, data is acquired over a longer period, typically around two minutes, with less frequent sampling, of up to one acquisition every five seconds. Delayed phase studies are used in determining vascular leakage.

Due to the constraints of technology, the initial development of DCE-CT was undertaken using single level studies. The data for these studies is acquired from an anatomical volume, with the maximal z-axis coverage defined by the number and arrangement of detectors on the scanner. The z-axis coverage for a CT scanner with four detectors is around 2cm and increases with 64 detectors to around 4cm. Modern CT scanners with 256 detectors will allow increased coverage of almost 13cm. With advancement in scanner technology, volumetric helical techniques have now been developed that use multiple helical acquisitions, rather than single level. With serial acquisitions every five to seven seconds, this allows breath-holding techniques to be incorporated into the technique for scanning the thorax and upper abdomen. With volumetric DCE-CT, Patlak analysis is used to produce estimates of

extraction fraction (approximating to permeability surface area product in tumours) and blood volume. These volumetric techniques enable greater volume coverage, such that whole tumour or organ measurements can be acquired, providing an improved measure of the spatial heterogeneity that may exist. It has also been shown to potentially have better measurement reproducibility (Ng et al., 2006).

In providing information on both morphological features and vascular function, DCE-CT is a useful tool in the assessment of tumour angiogenesis. In confirmation of this, DCE-CT parameters have been shown to correlate with immunohistochemical-derived measures of tumour vascularity in renal cell carcinoma, NSCLC and colorectal carcinoma ([Jinzaki et al., 2000], [Tateishi et al., 2002], [Yi et al., 2004], [Wang et al., 2006], [Goh et al., 2008]). Its use as an imaging biomarker of tumour vascularity and in the assessment of treatment related changes in tumour vascularity has increased, especially with the availability of commercial versions of the required software. DCE-CT has been used in this context in clinical trials of vascular directed therapies, including the evaluation of bevacizumab in rectal cancer and pharmacodynamic phase 1 studies of endostatin, SU6668, L-NNA and the combination of AZD2171 and gefitinib ([Willett et al., 2004], [Thomas et al., 2004], [Xiong et al., 2004], [Ng et al., 2007c], [Meijerink et al., 2007]). It has also been used in early phase clinical trials, examining the vascular effects in NSCLC of radiotherapy alone and in combination with a single dose of CA4P ([Ng et al., 2007b], [Ng et al., 2007a]).

1.5.3 Other functional imaging techniques

1.5.3.1 Dynamic contrast enhanced MRI

This is an established imaging biomarker for tumour angiogenesis and has been widely used in clinical trials of vascular directed therapies. DCE-magnetic resonance

imaging (MRI) derived parameters have been shown to correlate with immunohistochemical measures of tumour vascularity in carcinomas of the lung, rectum, oral cavity and breast ([Schaefer et al., 2006], [Zhang et al., 2008], [Unetsubo et al., 2009], [Teifke et al., 20067]). Pharmacodynamic studies of anti-angiogenic agents utilising DCE-MRI include phase I trials of endostatin, vatalanib, axitinib, cediranib and a phase II study of bevacizumab in locally advanced breast cancer ([Eder et al., 2002], [Morgan et al., 2003], [Liu et al., 2005], [Drevs et al., 2007], [Wedam et al., 2006]). It has been used to document the vascular response in phase I trials of the VDAs, including CA4P, DMXAA and ZD6126 ([Galbraith et al., 2003], [Galbraith, Rustin et al., 2002], [Evelhoch et al., 2004]). The vascular effects of cytotoxic chemotherapy have also been examined using DCE-MRI and it has been evaluated as a predictor of response to neoadjuvant chemotherapy for carcinoma of the breast ([Lankester et al., 2005], [Ah See et al., 2008]). Similarly, it has been studied as a predictor of treatment outcome in patients undergoing radiotherapy for carcinomas of the uterine cervix or rectum ([Mayr et al., 2000], [Devries et al., 2001]).

DCE-MRI techniques commonly incorporate low molecular weight, gadolinium-based, paramagnetic contrast agents, such as gadolinium diethylenetriamine pentaacetic acid (Gd-DTPA), which have similar kinetics to the low molecular contrast agents used in DCE-CT, although macromolecular contrast agents are also under clinical investigation. The effect of the i.v. contrast is to produce inhomogeneities in the magnetic field, which result in a decrease in tissue relaxation time. The change in MR signal intensity is dependent on a number of factors, including dose of contrast, type of MR sequence, native tissue relaxation and intrinsic tumour heterogeneity.

T_2*- and T_1- weighted sequences are the two main sequences that are utilised in the techniques of DCE-MRI (Padhani and Leach, 2005). T_2*-weighted (dynamic susceptibility contrast) sequences use i.v. bolus tracking techniques to examine transit time, relative blood flow and blood volume. Contrast produces a reduction in signal intensity. Within the extracranial circulation, T_2* measurements are relative rather than absolute, due to difficulties in accurately determining arterial input and also vascular leakage of contrast as this produces T_1 signal enhancing effects that counteract the T_2* signal reducing effects. With T_1-weighted (relaxivity based) sequences, contrast produces shortening of T_1 relaxation, thus increases signal enhancement. Quantitative kinetic parameters can be derived from concentration-time curves using pharmacokinetic modelling (Tofts et al., 1999).

The standard parameters from these T_1-weighted sequences are the volume transfer constant of contrast agent (K^{trans} or permeability-surface area product per unit volume of tissue), leakage space as a percentage of unit volume of tissue (v_e) and the rate constant (k_{ep}); $k_{ep} = K^{trans}/ v_e$ is the equation showing mathematical relationship between these factors (Tofts, 1997). These models require measurement of arterial input function and, due to difficulties in measuring the actual tumour arterial supply, this is often done by indirect measurement from a large artery in close proximity or by using an idealised mathematical function. It has been suggested that these model-based assumptions, used in the calculation of these parameters, may lead to systematic overestimation of K^{trans} (Buckley, 2002). With flow or permeability limited situations, K^{trans} will predominantly reflect flow or permeability respectively; similar to the kinetics for extraction fraction described with DCE-CT. In addition to these quantitative parameters, the signal intensity curves generated from T_1-weighted DCE-MRI can be used to derive semi-quanitative parameters, which include onset of enhancement, initial and mean upsweep of enhancement curves, maximal signal intensity, washout gradient and integral areas

under enhanced curves over fixed periods of time. The reproducibility of these parameters has been investigated, showing v_e and area under the curve (AUC) to be highly reproducible with K^{trans} and k_{ep} sufficiently reproducible to detect changes greater than 14 to 17% (Galbraith, Lodge et al., 2002).

1.5.3.2 PET

Positron emission tomography (PET) relies upon the production of positrons by the decay of radioisotopes. These positrons are highly unstable and therefore, almost instantaneously, combine with electrons, each collision producing two photons with energy of 511KeV that travel in opposite directions at 180° to each other. These annihilation photons are then detected by a ring of PET detectors and allow the construction of an image based upon the concentration and distribution of the tracer. PET on its own lacks the fine anatomical detail of CT. This has led to development of combined CT and PET, which produces images with a higher degree of accuracy.

The most common radiotracer used in diagnostic PET imaging of malignancy is ^{18}F-fluorodeoxyglucose (FDG), which is used mainly to provide more accurate staging or to determine response to treatment. This exploits the higher level of glycolysis in tumour cells, with increased uptake of glucose as a result of upregulation of cell surface glucose transporters, including GLUT-1, GLUT-5 and SGLT1 (Brown et al., 1999). Intracellular FDG is phosphorylated to FDG-6-phosphate and is retained intracellularly, as it is resistant to the further metabolic processes normally occurring to glucose-6-phosphate and dephosphorylates slowly (Young et al., 1999). As glucose uptake reflects cellular metabolism, FDG avidity is also observed in non-malignant processes, with uptake by macrophages, neutrophils and muscle cells under tension. Fluorine-18 (^{18}F) has a half-life of 110 minutes, making it ideal for use in radiotracer production, as it allows the tracers to be produced by a cyclotron at one site and to have sufficient activity to then be delivered for use at other hospital

sites. ^{18}F is utilised in a number of different radiotracers, including fluoromisonidazole (FMISO), a hypoxia tracer and 3-deoxy-3-fluorothymidine (FLT), which examines cellular proliferation.

PET imaging has also been used in the assessment of tumour vascularity, although its use is not as widespread as either DCE-CT or DCE-MRI. These PET tracers use the radioisotope Oxygen-15 (^{15}O), which, with a half-life of 2 minutes, limits their use to hospitals with a cyclotron on site. This can be used to label water ($H_2\ ^{15}O$), a freely diffusible PET tracer, where regional uptake directly and specifically represents tissue perfusion and which has been demonstrated to be a reproducible measure in tumours (de Langen et al., 2008). $H_2\ ^{15}O$ PET has been used in early phase clinical trials to determine the *in vivo* effects on tumour perfusion, including phase I studies of CA4P and endostatin and a phase II study of razoxane in renal cell carcinoma ([Herbst et al., 2002], [Anderson et al., 2003a], [Anderson et al., 2003b]). Using the radioisotope ^{15}O it is also possible to measure blood volume, using labelled inhaled carbon monoxide (C ^{15}O)-PET. Once a steady state has been reached with inhalation of C ^{15}O, the volume of distribution of carboxyhaemoglobin within a tumour can be calculated, equating to the relative tumour blood volume (Aboagye and Price, 2003). This technique has also been used in phase I trials of VDAs, as part of the pharmacodynamic assessments undertaken (Anderson et al., 2003a).

1.5.3.3 Ultrasound

Doppler ultrasound (US), using frequencies of 2 to 10MHz, can be used to map blood flow in vessels with a diameter 200μm or greater. It does not, however, have the sensitivity to determine blood flow within capillaries and cannot differentiate between tumour arteries and veins. New techniques, including digital devices, that

can increase signal to noise ratio, and high frequency probes, increasing axial and lateral resolutions, have improved accuracy further. These improvements, with the addition of ultrasound contrast agents and vascular recognition software, enable the detection of vessels with diameters as small as 40μm (Lassau et al., 2007). The raw data from these microbubble-enhanced US techniques can be used to derive similar semi-quantitative parameters to DCE, including peak intensity, time to peak intensity, mean transit time, coefficient of wash-in slope and AUCs (for the total curve, for the wash-in or for the wash out).

Contrast-enhanced US quantification of blood flow and fractional blood volume can be undertaken by assessing the rate of microbubble replenishment after destruction of the microbubbles using pulses of high power US (mechanical index >1). Using emission processors at a low mechanical index avoids destruction of the microbubbles and allows detection of both perfusion and the direction of microvessel flow (Lassau et al., 2007). In animal studies, gray-scale contrast enhanced US and low mechanical index have been used to quantitatively assess tumour blood flow (McCarville et al., 2006).

Contrast-enhanced US measures of blood flow and vascular volume have been shown to compare favourably to similar DCE-CT derived parameters in preclinical studies (Broumas et al., 2005). Further preclinical work has shown a strong and significant relationship between DCE-MRI and microbubble contrast-enhanced US measures of tumour perfusion (Yankeelov et al., 2006). DCE-Doppler US has been used to assess angiogenesis inhibitor-induced changes within tumour vasculature in animal tumour models and has also been used in clinical studies, including a pilot study examining the vascular effects of sorafenib in metastatic renal cell carcinoma ([McCarville et al., 2006], [Lamuraglia et al., 2006]).

1.6 Laboratory techniques for the assessment of tumour vasculature and response

1.6.1 Immunohistochemical quantification of tumour vascularity

The techniques for the immunohistochemical identification of microscopic tumour vessels use several different vessel wall antigens as markers. The most commonly used antibodies are anti-CD34, anti-CD31 and anti-Factor VIII related antigen (Von Willebrand's factor). Each of the antibodies has different sensitivities and immunostaining characteristics: anti-CD34 also stains immature haemapoetic cells and anti-CD31 stains plasma cells, macrophages and even carcinoma cells in certain circumstances. As anti-CD34 and anti-CD31 antibodies are endothelial specific, rather than tumour specific, they have been used widely in identifying microvessels in both preclinical studies, including those using the poorly differentiated head and neck squamous cell carcinoma (SCC) xenograft FaDu, and also in clinical studies of tumours from many different sites, including NSCLC ([Bhattacharya et al., 2004], [Irion et al., 2008], [Giatromanolaki et al., 1998]).

As anti-CD34 and anti-CD31 are pan-endothelial markers, that identify both established and newly formed vessels, techniques have been developed to examine vascular proliferation and maturity. CD105 (Endoglin) is a proliferation-associated and hypoxia-inducible protein, expressed in proliferating endothelial cells, which has been examined as a marker of angiogenesis in a number of human tumours, including NSCLC and breast cancer ([Tanaka et al., 2001], [Beresford et al., 2006]). Another feature of tumour vasculature that has been studied is the lack of pericyte coverage in immature microvessels, which are both irregular and have increased permeability. The absence of staining for smooth muscle actin-positive pericytes,

has been shown to correlate with increased haematogenous metastases and also poorer prognosis in patients with colorectal carcinoma (Yonenaga et al., 2005). Simultaneously staining with anti-CD34 and anti-alpha smooth muscle actin allows the calculation of the pericyte coverage index: the proportion of vessels with pericyte coverage. Immunohistochemical assessment of tumour angiogenesis can also be undertaken through staining for the presence of pro-angiogenic factors or their receptors, in particular staining for VEGF is now relatively commonplace (Giatromanolaki et al., 1998).

Microvessel density (MVD) is the most commonly used measure of tumour vascularity and has been shown to be a prognostic indicator in breast, prostate and other cancers ([de Jong et al., 2000], [Borre et al., 1998]). It has been used in preclinical studies as an assessment of effect for VDAs and anti-angiogenic agents, although changes in MVD are not proven to necessarily reflect treatment efficacy ([Seshadri et al., 2006], [Hlatky et al., 2002]). Traditionally, it has relied upon the counting of stained microvessels within an area of tumour; which can either be selected at random or can be specifically defined areas within the tumour, such as the tumour edge or the areas of highest vascularity at low magnification (also known as ‘hot spots’).

The techniques for counting vessels also vary greatly, for example, the numbers of fields the counts are derived from, the magnification used, the methods of choosing the fields to be counted and also the exact nature of what is counted within each field. There can be marked observer variability in MVD counts from the same tumour, with uncertainty regarding whether multiple positive staining spots represent one or more vessels. One method that can be employed in an effort to reduce this variability is Chalkley point counting. This involves a 25 piece graticule applied over a vascular ‘hotspot’ at x250 magnification, with the grid orientated so that the

maximum number of points are superimposed over stained microvessels (Chalkley, 1943). The Chalkley point count is equivalent to the number of grid points that hit these stained microvessels and is, therefore, a relative area estimate, rather than a true vessel count. Despite consensus statements suggesting standardisation of techniques with the counting of vessels in the highest angiogenic area, this is not suitable for all tumour types and neither this proposed standardised method nor Chalkley point counting have been universally adopted (Vermeulen et al., 2002).

The advent of computerised analysis methods has provided means to quantify the extent and intensity of staining. By ostensibly removing observer variability, it is possible to produce a more reproducible quantification. Following acquisition of high resolution digital images of the stained histological slide, computer software then differentiates the component colours; brown for the component being identified when using DAB staining, which can, in turn, be differentiated from the background staining, usually blue with haematoxylin. Although this method has been used with systems to produce MVD counts, results are commonly displayed as the ratio or percentage of DAB-thresholded pixels (or area) compared to the number of pixels (or area) for a defined region of interest or for the whole image. This is defined as the mean total vascular area when used with vascular stains, such as CD34 or CD31, to examine tumour microvessels. These new techniques have been used increasingly in both preclinical and clinical studies as a measure of tumour vascularity and also as a predictor of outcome in patients receiving chemoradiation ([Chantrain et al.,2003], [Wester et al.,1999], [Irion et al., 2008], Zhang et al., 2006]).

1.6.2 Quantification of tumour angiogenesis by circulatory biomarkers

With the explosion in vascular directed therapies, especially novel anti-angiogenic agents, there is a need for robust and clinically relevant circulatory biomarkers, to complement the imaging biomarkers currently available. In the assessment of the effects of neoadjuvant therapies, (treatments given prior to surgical resection), as is routinely done in rectal and breast cancers, MVD counts or mean total vascular areas can be easily determined. Outside this setting, they require extra biopsies to be taken, which are prone to sampling errors and may not be representative of the tumour as a whole.

To circumvent these problems, there is an ongoing quest, utilising the increasing knowledge regarding the key components of tumour angiogenesis, to identify circulatory biomarkers that may be easily extracted by relatively non-invasive diagnostic techniques, such as venesection. Circulating levels of pro-angiogenic cytokines and receptors are one avenue that has been explored. These are now being incorporated into clinical studies, using enzyme-linked immunosorbent assays (ELISA) or similar techniques to detect these cytokines. Various cytokines have been looked at in clinical trials, including SDF-1, PDGF, bFGF, Ang-2, IL-6 and IL-8, as well as, the most commonly used, concentrations of circulating VEGF and the VEGFRs (Vermeulen et al., 2002). Similarly, levels of circulating endothelial cells and circulating EPCs have been demonstrated as feasible circulatory biomarkers and are now also being incorporated into early phase clinical trials of vascular directed therapies ([Lowndes et al., 2008], [Zhu et al., 2009]).

1.6.3 Immunohistochemical quantification of tumour hypoxia

Histological assessment of hypoxia provides insight on the interaction between hypoxia and other tumour microenviromental features, including vascularity, necrosis, proliferation and apoptosis. The detection and quantification of intra-tumoural hypoxia by immunohistochemistry can be performed using either extrinsic or intrinsic markers; one of the most widely used and extensively investigated extrinsic markers of hypoxia is the nitroimidazole group. Initial *in vitro* studies investigated misonidazole as a hypoxic cell radiosensitiser, with further *in vivo* work demonstrating a higher concentration of misonidazole in tumour tissue compared to normal tissue and, additionally, the production and retention of reduced metabolites under hypoxic conditions (Varghese et al., 1976). Despite the variable binding observed in different tumours, within a tumour it is the local cellular oxygen concentration that determines the rate of binding for nitroimidazoles ([Urtasun et al., 1986], [Chapman, 1991]). With misonidazole in totally anoxic conditions, binding is proportional to the square root of its extracellular concentration (Chapman et al., 1983). The metabolism of 2-nitroimidazoles occurs in a series of single electron reductions. Of this group of compounds, pimonidazole and EF5 are the two most commonly used in the immunohistochemical identification and quantification of hypoxia.

Pimonidazole is a 2-nitroimidazole with a piperidine side chain, which is water soluble, stable, and is widely distributed in tissues. It has a half-life of 5.1 hours, with dose limiting toxicities observed at doses >1g/$m^{2,}$ including, severe acute central neurotoxicity, malaise, fever, disorientation and sweating ([Saunders et al., 1984], [Roberts et al., 1984]). When used as an extrinsic marker of hypoxia, it is given i.v. at a dose of 0.5g/m^2, at which level such toxicities were not observed. The reduction and resultant activation of pimonidazole under hypoxic conditions results in the

formation of protein adducts, which have been shown to persist intracellularly for a prolonged time (Azuma et al., 1997). These pimonidazole adducts are effective immunogens for the production of both monoclonal and polyclonal antibodies, a feature that has been key to its success as a marker in immunohistochemical and immunofluorescent techniques.

The hypoxic fraction measured by pimonidazole, gives a reliable estimate of radiobiologically relevant hypoxia with high spatial resolution and has been shown to correlate with the hypoxic fraction measured by comet assay in both animal and human tumours (Olive et al., 2000). Pimonidazole is not metabolised in necrotic cells, which is one explanation for the poor correlation between its measurements of hypoxia and microelectrode readings. The pimonidazole-derived hypoxic fraction has, however, been shown to correlate inversely with the density of perfused blood vessels, measured with Hoechst 33342, in preclinical studies using a glioma xenograft model (Rijken et al., 2000). In this work, pimonidazole identified hypoxia occurred at critical distances from perfused vessels, especially when beyond 100mm, suggesting that it is detecting predominantly diffusion-limited hypoxia.

Hypoxia can also be identified with intrinsic markers, which do not require the prior administration of an agent and hence provide a useful means for examining hypoxia in archived histological material. These techniques rely on the identification of hypoxia-related genes and proteins. Given the critical function of HIF-1 as a transcription factor, upregulated in hypoxic conditions, it has been evaluated as an intrinsic marker. The over expression of HIF-1α, the nuclear protein product and oxygen regulated subunit of the HIF-1 gene, is a common finding in solid tumours and their metastases (Zhong et al., 1999). The immunohistochemical staining pattern of HIF-1α correlates with hypoxia, as detected by the 2-nitroimidazole EF5 in tumours, but more diffuse staining patterns correlating with CD31 detected

vasculature have also been reported ([Vukovic et al., 2001], [Zhong et al., 1999]). Increased expression has shown correlation with higher rates of locoregional failure in head and neck cancers, although it has not shown a similar correlation in cervical cancers and in this study showed only a weak correlation with pimonidazole staining ([Aebersold et al., 2001], [Hutchison et al., 2004]). This lack of reliable correlates has restricted the use of HIF-1 α as an intrinsic marker of hypoxia.

Some of the most promising intrinsic markers of hypoxia are the glucose transporters (Glut-1 and Glut-3), which mediate cellular uptake of glucose. These are controlled by the HIF-1 pathway and are upregulated in hypoxic conditions to enable anaerobic glycolysis. Upregulation of Glut-1 has been shown to confer a poor prognosis in a number of tumour types, including NSCLC, SCC of the uterine cervix, colorectal adenocarcinoma and transitional cell carcinoma of the bladder ([Younes et al., 1997], [Airley et al., 2001], [Haber et al., 1998], [Younes et al., 2001]). In SCC of the uterine cervix, a weak, yet significant, correlation has been demonstrated between Glut-1 and microelectrode detected hypoxia, in addition to, a correlation of Glut-1 expression with both pimonidazole binding and CA IX expression ([Airley et al., 2001], [Airley et al., 2003]). Glut-1 staining seems to identify mainly diffusion-limited hypoxia.

Another promising intrinsic marker of hypoxia is carbonic anhydrase-IX (CA IX). The carbonic anhydrases are critical components in cellular respiration and the regulation of the acid-base balance. They are a group of cell membrane zinc metalloenzymes that catalyse the hydration of carbon dioxide, producing carbonic acid. The expression of CA IX is regulated through the hypoxia response pathways of both HIF-1 and the unfolded protein response (van den Beucken et al., 2009). A predominantly perinecrotic staining pattern indicative of diffusion-limited hypoxia is seen with CA IX and this has been shown to be similar, but not identical, to that

seen with pimonidazole (Lal et al., 2001). In a study of the effects of hypoxia on different tumour cells lines, of all the hypoxia markers studied, CA IX was the most consistently expressed in these different tumours (Lal et al., 2001). High to moderate expression of CA IX has been observed in multiple common epithelial tumour types (Ivanov et al., 2001). In locally advanced carcinomas of the uterine cervix, the extent of CA IX expression positively correlated with microelectrode measured tumour hypoxia; increased expression of CA IX was also associated with a poor prognosis (Loncaster et al., 2001).

1.7 Aims

This work attempts to address the questions as to whether the anti-tumour and vascular effects of combined CA4P and radiotherapy can be enhanced with the addition of the nitric oxide synthase inhibitor, L-NNA, or the anti-EGFR monoclonal antibody, cetuximab. These preclinical studies have also investigated the pharmacokinetic impact of the combinations. The aims of the clinical component of this work have been twofold. Firstly, the validation of the novel functional imaging technique, volumetric DCE-CT, as a biomarker of tumour hypoxia and vascularity in NSCLC, has been undertaken; using digitised immunohistochemically-stained resected lung tissue as the baseline for comparison, and further comparison with FDG PET-CT parameters. Secondly, DCE-CT and circulatory biomarkers have been used to examine the tumour vascular changes in patients receiving concurrent CA4P and radiotherapy as part of a phase IB trial, with the cohort of head and neck carcinoma patients also receiving cetuximab.

Pro-Angiogenic Factors	Anti-angiogenic Factors
Vascular endothelial growth factor (VEGF)	Thrombospondin-1 (TSP-1)
Placental growth factor (PlGF)	Interferon α/β
Basic fibroblast growth factor (bFGF)	Platelet factor-4
Acidic fibroblast growth factor (aFGF)	16kD Prolactin
Fibroblast growth factors 3 and 4 (FGF-3,-4)	Angiostatin
Transforming growth factor-α (TGF-α)	Canstatin
Transforming growth factor-β (TGF-β)	Tumstatin
Hepatocyte growth factor (HGF)	
Interleukins (IL)-1, -2, -6, -8	
Angiogenin	
Angiotropin	
Epidermal growth factor (EGF)	
Fibrin	
Nicotinamide	
Platelet-derived endothelial growth factor (PD-ECGF)	
Platelet derived growth factor (PDGF)	
Tumour necrosis factor-α (TNF-α)	
Thrombin	
Matrix metalloproteinases (MMP)-2, -9	
Angiopoietin-2 (Ang-2)	

Table 1.1

Pro- and Anti-angiogenic Factors.

Advantages	Disadvantages
Enhanced tumour control	VDA-induced tumour hypoxia
Spatial cooperation	Cardiovascular effects
Increased endothelial cell apoptosis	Acute blood pressure changes
Non-overlapping toxicities	Reversible neurological sequelae
No enhancements of normal tissue effects of radiotherapy	Loss of beneficial effects with incorrect timing and sequence

Table 1.2

Advantages and disadvantages of combining VDAs and radiotherapy.

	DCE-CT	DCE-MRI	PET	Ultrasound
Tracer	Iodinated contrast	Gadolinium based contrast	15-O labelled H_20 or CO	Microbubbles
Measured Parameters	BF, BV, MTT, PS	K^{trans}, k_{ep}, v_e Relative BF, BV	BF, BV	BF, BV, MTT
Advantages	Straightforward quantification Good spatial resolution Relatively cheap Widely available	Good contrast resolution No radiation burden	Direct quantification	No radiation burden Relatively cheap Widely available
Disadvantages	Radiation burden	Quantification challenging Limited availability	Radiation burden Limited availability Expensive	Limited to superficial sites Unable to assess microvasculature Regional perfusion only

BF= blood flow, BV= blood volume, MTT= mean transit time, PS= permeability surface area product, K^{trans}= transfer constant, k_{ep}= rate constant, v_e= extravascular-extracellular volume for a given tissue volume

Table 1.3

Different functional imaging techniques for the assessment of tumour vasculature

CHAPTER 2

Materials and Methods

2.1 Preclinical Studies

All animal procedures were carried out in compliance with UK Animals (Scientific Procedures) Act 1986, and with the approval of the Ethical Review Committee of the Gray Cancer Institute.

2.1.1 Tumours

2.1.1.1 CaNT

Murine poorly differentiated mammary adenocarcinoma NT (CaNT) were implanted into the rear dorsum of 10 to 16 week old female CBA/ Gy f TO mice, by injecting 0.05 ml of a crude cell suspension prepared by mechanical dissociation of an excised tumour from a donor animal. Tumours were selected for treatment when the geometric mean diameter (GMD) reached 4.5mm to 6.5 mm, approximately 3 to 4 weeks after implantation.

2.1.1.2 FaDu

Tumour cells from the human poorly differentiated hypopharyngeal squamous cell carcinoma, FaDu, were incubated under 19.6% O_2, 5% CO_2 and 75.4% N_2 at 37^{o}C. The cells were maintained in Dulbecco's Modified Eagle Media (DMEM) supplemented with 10% foetal calf serum (FCS), 2mM L-glutamate, 100 units penicillin and 100ug/ml streptomycin. Tumour implantation was by subcutaneous injection of 2 x 10^6 cells in 0.05ml into the rear dorsum of 5 to 14 week old female

nude mice. Using a previously described schedule, whole body irradiation, with 5Gy delivered to the mice 24 hours prior to implantation, was given to increase immunosuppression (Perez et al., 1995). Tumours were selected at 4.5 to 6.5 mm GMD, approximately 2 to 3 weeks after implantation.

2.1.2 Drug Treatments

2.1.2.1 Combretastatin A4 Phosphate (CA4P)

The disodium salt of CA4P (Oxigene Inc., Watertown, MA) was dissolved in 0.9% saline at appropriate concentrations to allow each dose to be injected at 0.1ml/ 10g body weight.

2.1.2.2 N(omega)-nitro-L-arginine (L-NNA)

L-NNA (Sigma-Aldrich Co. Ltd., Gillingham, UK) was dissolved initially in a few drops of 1M HCl then water for injection at appropriate concentrations to allow each dose to be injected at 0.1ml/ 10g body weight or in sufficient water to produce a concentration of 1mg/ml when administered in drinking water. Drinking water was prepared freshly each day.

2.1.2.3 Cetuximab (C225)

The monoclonal antibody C225, cetuximab, (Merk KG aA, Germany) was administered at a dose of 1mg/ 0.5ml intraperitoneally (i.p).

2.1.3 Tumour Irradiation

Tumour irradiation was delivered to unanaesthetised animals using an X-ray source (Pantak, Windsor, UK), 240 kV/ 15 mA Xrays (0.25 mm Cu, 1.0 mm Al, half value layer of 1.3 mm Cu). Dosimetries of the in vivo irradiation systems were checked with an ion chamber prior to the initial treatment.

2.1.3.1 Local tumour irradiation

Animals were placed in a purpose-built lead irradiation jig with the tumours exposed. Each fraction was delivered to the midplane dose. After 50% of intended dose was delivered, to minimise dose non-uniformity, the mice were rotated horizontally 180º and positions changed on the jig. The required monitor units for each treatment were calculated, taking into account the atmospheric pressure (*P*) and the temperature (*T*) in the treatment room, as follows: 119.4 x *P/ T* x Dose (Gray).

2.1.3.2 Whole body irradiation

Nude mice, 24 hours prior to implantation of tumour xenograft cells, were placed in a housing container lined only with single sheet of paper and were able to freely move around. The container was placed on a frame for whole body irradiation at a designated distance from the source (point A) and fixed into position, with the head of the Pantak unit lowered and pointing vertically. A dose of 5 Gy was then delivered to point A, with the required monitor units for each treatment calculated as follows: 3907 x *P/ T* x Dose (Gray)

2.1.4 Tumour Growth Delay

Callipers were used to measure tumours in 3 orthogonal diameters (width, length and depth), at regular intervals, with tumours allowed to grow to but not exceed a geometric mean diameter of 12.5mm. The initial measurements were undertaken prior to the administration of the first dose of radiation, L-NNA, CA4P or C225. Tumour volumes were then calculated from the geometric mean diameter. The time to tumour regrowth was calculated as the time taken for tumours to grow to either 1 or 2 times (FaDu) or 3 times (CaNT) their original volume, with the specific time to achieve this calculated for each tumour. The tumour growth delay was calculated as the difference in time to tumour regrowth between different treatment or control

cohorts. Statistical comparison between the treatment groups, including calculation of the mean tumour growth delay for each group, was undertaken using the specific time to tumour regrowth data from each tumour in a treatment group. Additionally the tumour volumes were normalised to allow calculation and comparison of mean growth curves for each group of animals, 3 to 6 animals per group.

2.1.5 Pharmacokinetic studies

Mice were sacrificed at the time points specified and blood was collected. In addition tumours, livers and leg muscles were excised, weighed and homogenised. Plasma was obtained from the blood samples by centrifugation (14 000g, 2 min). The plasma samples and tissue homogenates were then transferred to tubes for storage; heparinised tubes were used for L-NNA and EDTA tubes for CA4P.

2.1.5.1 L-NNA

LNNA was determined in plasma and tissue samples by high-performance liquid chromatography (HPLC) with ultraviolet (UV) detection after extraction with methanol, using a method based on that of Tabrizi-Fard and Fung (Tabrizi-Fard & Fung, 1996) and similar to that described by Ng et al (Ng et al., 2007b). Tissues were homogenised in four volumes (tumour and liver) or nine volumes (muscle) of phosphate buffered saline containing 1 mM EDTA. To 50 µL plasma, 250 µL tumour/liver or 500 µL muscle homogenate was added 20 µl internal standard (theophylline, 200 µM), followed by 1 mL methanol, with mixing after each addition. Samples were centrifuged (20,000g, 10 min) and the supernatant taken to dryness in a centrifugal evaporator. The samples were reconstituted in 100 µL eluent A (see below) containing an additional 0.1 M H_3PO_4 and put in HPLC vials for analysis.

HPLC was carried out on a Waters 2695 system with diode array detection (Waters 2996). The column was a Hichrom RPB (5 µm, 250 x 3.2 mm) maintained at 30 ºC. Separation was achieved with eluent A: 25 mM KH_2PO_4, 25 mM H_3PO_4, 20 mM octane sulphonic acid, filtered through a 0.45 µm polypropylene membrane (Pall, VWR); Eluent B: 75 % acetonitrile, using a gradient from 5 % B to 25 % B in 13 min, then to 35 % B over 2 min, held at this for 1 min then back to 5 % over 0.1 min. The flow rate was 0.7 mL/min and the detection wavelength was 268 nm. Data was acquired and quantitated using Waters Empower software. For the two groups receiving i.p. L-NNA, half lives were calculated by weighted non-linear-least squares regression; area under the curve (AUC) was calculated by use of the linear trapezoidal rule, extrapolated to infinity by the use of the terminal half-life.

2.1.5.2 CA4P

CA4P was determined in plasma and tissues by HPLC using fluorescence detection, as initially described by Stratford and Dennis and then, with refinement of the technique, by Stratford in 2008 ([Stratford and Dennis, 1999], [Stratford, 2008]). Tissues were homogenised in either 4 (tumour and liver) or 9 (muscle) volumes of 2mg/ml EDTA. To 50 µL plasma, 250 µL tumour/liver or 500 µL muscle homogenate was added 25 µl internal standard (*trans*-3,4,5-trimethoxy-4'-methylstilbene, 5µM), followed by 1 mL methanol, with mixing after each addition. Samples were centrifuged (20,000g, 10 min) and the supernatant taken to dryness in a centrifugal evaporator. The samples were reconstituted in 100 µL 25% acetonitrile and put in HPLC vials for analysis.

HPLC was carried out on a Waters 2695 system with a 474 fluorescence detector (5 µl flow cell). The column was a Hichrom RPB (5 µm, 250 x 3.2 mm) maintained at 30ºC. Separation was achieved with eluent A: 50% methanol, 1.5mM potassium dihydrogen orthophosphate, 7.5mM TBA, filtered through a 0.45 µm polypropylene

membrane (Pall, VWR); eluent B: methanol; eluent C: acetonitrile. A linear gradient was used from 100% A to 50% B, 50 % C in 14 min, returning to initial conditions over 1 min, with a flow rate of 0.6ml/ min. A photolysis coil was placed between the column and fluorescence detector (excitation 330 nm, emission 390 nm, bandwidth 18 nm). Waters Empower software was used for data acquisition.

2.2 Clinical treatments

2.2.1 Radiotherapy

All radiotherapy treatments were delivered in concordance with standard practice at Mount Vernon Cancer Centre and as stated in the UKR-104 protocol.

2.2.1.1 High dose palliative lung radiotherapy

Patients with inoperable non small cell lung carcinoma (NSCLC), unsuitable for radical radiotherapy were planned using virtual simulation or conventional simulator at the discretion of the designated practitioner planning the treatment. All known disease was encompassed within the radiotherapy field with a margin used to take into account set-up error and internal margin. Treatment was delivered using megavoltage anterior - posterior parallel opposed photon fields, with MLC shielding of uninvolved tissue where possible. A dose of 27Gy in 6 fractions (4.5Gy per fraction) over 3 weeks was delivered to the midplane dose, with 2 fractions per week given either on Monday and Thursday or Tuesday and Friday (Corner et al., 2007).

2.2.1.2 Radical head and neck radiotherapy

Patients with locally advanced squamous cell carcinoma of the head and neck (HNSCC) were planned by CT simulation. Treatment was delivered using a 3D conformal megavoltage technique, with matched electron fields for treatment of the posterior neck when this region required treatment to a dose greater than spinal

cord tolerance (defined as 46Gy in 2Gy per fraction). A dose of 64 to 70Gy in 32 to 35 fractions (2Gy per fraction) over 6.5 to 7 weeks was delivered to the 100% isodose.

2.2.2 Concurrent CA4P

CA4P for Injection is a white to off-white powder. It was supplied as a sterile freeze-dried, disodium salt, with sufficient excess in the vial to provide 90mg of the free acid. The dosing and scheduling of i.v. CA4P and radiotherapy are shown in Table 2.1. CA4P was administered as a 10 minute i.v. infusion, 2 hours after the final fraction of radiotherapy each week, except in the NSCLC cohort 7 where CA4P was administered 2 hours after every fraction of the twice-weekly radiotherapy. An infusion pump with an inline filter (<5 microns) was used for the administration of CA4P and the i.v. infusion was protected from light by photoprotective tubing and plastic covers. A nurse was present and a physician was in close proximity to the patient area during the administration of CA4P and for the post-treatment observation period.

The total dose of CA4P as free acid that was administered was rounded to the nearest mg. In calculating the body surface (BSA), actual heights and weights were used, with no adjustment to an ideal body weight. The BSA and dose of CA4P were recalculated prior to each treatment. For patients with a BSA >2.0m^2, the CA4P dose was calculated using a capped BSA of 2.0m^2. A CA4P dose of 50mg/ m^2 was given in all cohorts except prostate cohort 5, where a dose of 63mg/ m^2 was used. In addition to this dose escalation, an increase in dose intensity was also explored with CA4P given as a single dose in the first 2 cohorts, weekly in the next 3 cohorts (including the Head and Neck cohort 6, where it was given concurrently with cetuximab and radiotherapy), and then twice weekly in the final lung cohort.

If during CA4P infusion or during the post infusion observation period, an acute hypertensive event (defined by a systolic pressure >180mmHg or diastolic blood pressure >110mmHg) occurred, immediate intervention with anti-hypertensive medication was instigated. Frequent blood pressure monitoring was then continued throughout the rest of the post-treatment period to ensure the adequate control of hypertension. During the week of CA4P treatment, any medications known to prolong QTc were to be omitted at least 72 hours prior to the administration of CA4P and resumed no earlier than 6 hours after dosing with CA4P, provided that any QTc prolongation had resolved to baseline.

2.2.3 Concurrent Cetuximab

Cetuximab was delivered according to standard Mount Vernon Hospital protocol, which was derived from the phase III study of cetuximab and radiotherapy in squamous cell carcinoma of the head and neck (Bonner et al., 2006). In the week prior to commencing radiotherapy, a test dose of i.v. cetuximab (20mg given over 10 minutes) was administered together with premedication of i.v. chlorpheniramine 10 mg. This was followed by an observation period of 30 minutes. Provided no hypersensitivity was observed, patients then received 400mg/ m^2 i.v. cetuximab as a loading dose. Following the commencement of radiotherapy, cetuximab 250mg/ m^2 i.v. maintenance was given weekly throughout the planned radiotherapy. The patients then received external beam radiotherapy 64 to 70Gy, in 2Gy per fraction over 6.5 to 7 weeks, plus weekly CA4P as stated in section 2.2.1.2.

2.2.4 Pimonidazole

Pimonidazole was reconstituted with water for injection and a dose of 0.5mg/m^2 was measured. This was then added to 100 mls 0.9% saline, which was then administered intravenously over 20 minutes. An infusion pump with an inline filter (<

5 microns) was used for the administration of pimonidazole and the i.v. infusion was protected from light by photoprotective tubing and plastic covers. A nurse was present and a physician was in close proximity to the patient area during the administration.

2.3 Imaging Techniques

2.3.1 DCE-CT

Patients were scanned using a MDCT scanner (Sensation 16, Siemens Medical Solutions or Somaton Definition). No additional patient preparation was required over and above that for a routine thoracic or head and neck CT examinations. An 18-gauge cannula was placed in an antecubital fossa vein while the patient lay supine on the scanner table.

2.3.1.1 Volumetric Technique

An initial unenhanced breath-hold helical scan was obtained using the following parameters: 80kV; 120mAs; table feed, 30mm; rotation time, 0.5 seconds; collimation, 2mm; detector width, 1.5mm; scanning field of view (SFOV), 500mm; matrix, 512 x 512mm. This scan provided baseline unenhanced images and was used to plan the subsequent perfusion study. Using a dual-headed pump injector (Injektron CT2, Medtron), 100mL of iobitridol 300mg I/ mL (Xenetix 300, Guerbet) was administered with a decreasing bolus infusion rate (32mL at 4mL/s, 16mL at 2mL/s, and 60mL at 1mL/s) and followed by a saline flush (20mL at 1mL/s). The rationale for the contrast-infusion protocol was to optimise conditions for the mathematic analysis model, Patlak analysis, by maintaining a more constant intravascular concentration of contrast material, minimizing the concentration gradient between the intravascular and extravascular spaces, and improving the signal-to-noise ratio during the acquisition.

A single-level bolus tracking scan (CARE bolus, Siemens) at the level of the aortic arch was commenced at the same time as contrast administration using the following parameters: 80 kV; 20mAs; scanning time, 0.5 seconds; collimation, 4.5mm; detector width, 0.75mm. The dynamic study was triggered when peak aortic enhancement was identified from the aortic time–density curve during the bolus tracking scans. The dynamic study consisted of a total of eight breath-hold helical acquisitions, encompassing the entire tumour using the following parameters: 80kV; 120mAs; table feed, 30mm; rotation time, 0.5 seconds; collimation, 2mm; detector width, 1.5mm; SFOV, 500mm; matrix, 512 x 512mm. Total dynamic acquisition time varied from patient to patient but was approximately 90 seconds. The entire CT perfusion study was repeated within 24 hours without intervening treatment, using identical technical parameters to allow assessment of measurement reproducibility.

Data were transferred to a dedicated workstation (Leonardo, Siemens Medical Solutions). Each perfusion study consisted of nine helical scans (one baseline scan and eight contrast enhanced dynamic scans) that required post-processing before quantitative perfusion analysis. For each scan, the 2mm collimated axial images were reformatted, into 5mm thick axial images for smaller tumours undergoing surgical resection and 10mm thick axial images for larger tumours receiving palliative radiotherapy and CA4P, using 3D software (3D Analysis, Siemens) to permit analysis within a clinically acceptable time. Reformatted scans were checked to ensure that the whole tumour was included and that each of the reformatted axial images corresponded to a similar position along the z-axis of the patient on all nine scans by comparing the position of the tumour to adjacent anatomical structures. Then each reformatted axial image from the same position along the z-axis of the patient from each of the nine helical scans was saved as a separate series on the workstation for further analysis. Thus, for every patient, multiple series were obtained for each of the two dynamic studies, encompassing the entire tumour; each

series consisted of a single baseline unenhanced image and eight dynamic contrast-enhanced axial images at the same tumour level. The number of series per patient varied, depending on tumour size.

For each patient, all series of reformatted dynamic images, encompassing the whole tumour, were loaded into the prototype perfusion software (Siemens) based on Patlak analysis. The arterial input was determined from the bolus tracking scan images for each patient; using an electronic cursor and mouse, a circular region of interest (ROI) was placed within the aorta. An arterial time–attenuation curve was generated automatically, and this information was saved using the software for subsequent analysis. A single, central tumour level was chosen, and an ROI was drawn freehand around the tumour by a single experienced observer using an electronic cursor and mouse, taking care to exclude surrounding air and atelectatic lung where possible. A tissue attenuation–time curve was generated automatically by the software along with parametric maps of permeability and blood volume. Each pixel location within the functional map corresponded to a single quantitative perfusion value resulting from the mathematic calculation of the data at that location. Data were analysed on a pixel-by-pixel basis for all levels encompassing the tumour. By amalgamating data from all individual pixels from these levels, median values for permeability surface area product and blood volume were calculated, producing values for whole tumour coverage; these values were recorded for each patient. Thus, for all patients, median values of tumour permeability surface area product and blood volume for whole tumour coverage were documented for subsequent statistical evaluation. To determine the true value for the different parameters, the scaling factors used to produce an appropriate colour display (as shown in Figure 2.1) were taken in to account: Blood Volume (ml/100ml), a scaling factor of 10 was used (i.e. a value of 30 means a blood volume of 3 ml/100ml or 3%); Permeability surface area product (ml/100ml/min), a scaling factor of 2 was

used (i.e. a value of 100 means a permeability of 50 ml/100ml/min); Blood Flow (ml/100ml/min) did not require a scaling factor.

2.3.1.2 Single level technique

A low dose unenhanced study was performed initially to identify the tumour; scan co-ordinates were noted for the tumour mid point, and these co-ordinates used to plan the subsequent dynamic study. Four contiguous slices each reconstructed to 7mm (as shown in Figure 2.2) were obtained through the mid-point of the tumour using the following acquisition parameters: 80kV; 120mAs; detector width, 1.5mm; SFOV, 500mm; matrix, 512 x 512mm; 1 second interval for the first 30 seconds, and 2 second interval for the next 30 seconds. Acquisition commenced 5 seconds following the start of intravenous injection to allow acquisition of baseline unenhanced images. The entire CT perfusion study was repeated within 24 hours without intervening treatment, using identical technical parameters to allow assessment of measurement reproducibility.

Data were transferred to a dedicated workstation (Leonardo, Siemens Medical Solutions). Analysis was performed using commercial perfusion software (Body perfusion, Siemens) in order to obtain quantitative measurements (blood volume, blood flow, mean transit time and permeability surface area product). A representative 7mm axial image in which the tumour was best visualised was loaded into the software. A processing threshold between -150 to +150 Hounsfield units (HU) was chosen to optimise soft tissue visualisation. An arterial input was defined by placing a circular region of interest (ROI), 10mm^2 in size, within the best-visualised artery on the selected image; the common, internal or external carotid arteries on either side. The arterial enhancement-time curve was derived automatically by the software and resulting parametric maps of blood volume, blood

flow, mean transit time and permeability surface area product were produced, with each individual pixel representing a parameter value.

Mean blood volume, blood flow, transit time and permeability surface area product measurements were obtained by using a mouse and electronic cursor to trace a freehand ROI around the tumour margins. Care was taken to exclude surrounding air or uninvolved neighbouring blood vessels. Mean values for blood volume, blood flow, transit time and permeability surface area product, for this representative 5mm axial section, were recorded for each individual. Peak enhancement and time to peak enhancement derived from the resulting enhancement curves were recorded also for the arterial input vessel and for the tumour. Analysis was repeated for the remaining two 5mm axial images in exactly the same manner so that an overall mean value could be obtained for blood volume, blood flow, mean transit time and permeability surface area product for the tumour volume scanned.

2.3.1.3 DCE-CT Reproducibility

The standard consensus approach was used in the assessment of reproducibility for the volumetric and single level DCE-CT techniques (Bland and Altman, 1996a,b,c). Difference (*d*) between the measurements of a parameter in the two reproducibility scans was calculated. The distribution of all the differences (*d*) was tested for normality with Shapiro-Wilk test. Kendall's tau rank correlation coefficient was used to determine the association between the size of *d* and the mean parameter value. If it was demonstrated that error was proportional to the mean, at the 95% confidence interval, then the data was transformed using natural logarithms (*ln*), with the Shapiro-Wilk and Kendall's tau rank correlation coefficient repeated subsequently.
Using a one way ANOVA on either the original or the transformed data, the following statistical measures of reproducibility were calculated:

1) Mean square difference (*dsd*) = $\sqrt{(\sum d^2/n)}$
2) Within patient standard deviation (*wSD*) = dsd/$\sqrt{2}$
3) Within patient coefficient of variance (*wCV*)
    a) Original data *wCV = wSD/mean*
    b) *ln* transformed data *wCV = Exp(wSD)-1*
4) Repeatability parameter (*r*)
    a) Original data *r% = (r/mean) x 100*
    b) *ln* transformed data *r% = [100x Exp(ln mean ± r)]/mean*
5) Variance ratio (*F*): the ratio of the between patient variance and within patient variance = $[X_n^2/n]/[X_d^2/d]$; where *n* is the numerator and *d* is the denominator.

Intraclass correlation coefficient (*ICC*) = $mSS_B - SS_T/(m-1)SS_T$; where *m* is the number of observations per subject, SS_B is the sum of squares between subjects and SS_T is the total sum of squares (as per one way ANOVA above).

2.3.2 FDG-PET/ CT

All patients in the DCE-CT Lung tumour control group underwent routine PET-CT staging, to determine their suitability for radical surgical resection.^{18}FDG-PET/ CT was performed as follows, according to the standard protocol of the Paul Strickland Scanner Centre, Mount Vernon Hospital, Northwood, Middlesex, UK. Fasted patients received an intravenous injection of 4.5MBq/kg ^{18}FDG. Following a 60 to 90 minute uptake period, imaging was performed on an integrated PET/ CT instrument incorporating a 4 or 64-slice MDCT (Discovery LS or Discovery VCT, GE Healthcare, Chalfont St Giles, UK). CT for attenuation correction was performed from the skull base to upper thigh: 140kV, 80mA, pitch 1.5, 3.75mm detectors. The PET scan was obtained over the same anatomical area as CT. All acquisitions were carried out in 2D mode, consisting of an emission scan of 4 minutes per bed position. PET images were reconstructed using CT for attenuation correction by

employing CT maps. Transaxial emission images of 3.9 x 3.9 x 4.25mm (in plane matrix size 128 x 128) were reconstructed using ordered subsets expectation maximisation (OSEM) with two iterations and 28 subsets. The axial field of view was 148.75mm. Images were viewed on a standard reporting workstation (Advantage 4.4, GE Healthcare, Chalfont St Giles, UK). A rectangular volume of interest (VOI) was placed over the entire tumour. The standard uptake value (SUVmax, SUVmean) based on a standard pre-defined PET-threshold of 42% was derived automatically for the tumour VOI.

2.4 ELISA

Blood samples were taken at 4 time points for these tests through the course of this study: Prior to first CA4P administration (Day 5); 4 hours post CA4P administration (Day 5); 6 to 8 hours post CA4P administration (Day 5); 7 days post CA4P administration (Day 12). At each selected time point venepuncture was performed and one 5ml EDTA blood tube filled. Immediately after collection, the tube was inverted to mix the anticoagulant and blood adequately, then the sample was placed on ice in a closed container. Within 15 minutes of collection the EDTA tube containing the blood sample was centrifuged for 15 minutes at 1000x g, at 2°C to 7°C, to separate out the plasma. Following this the plasma was immediately aliquoted equally into 3 polypropylene screw capped cryogenic vials; the vials having been labelled with the protocol number, subject ID, time point, date and time of sampling. The vials were then placed in a container to prevent light reaching the sample and were transferred on ice to the Gray Cancer Institute. They were immediately placed in a –80°C freezer, monitored to ensure –80°C temperature or colder maintained, and the freezer log was completed to show number and position of samples.

Following collection of all required samples, arrangements were made with the analytical laboratory for shipping. All samples were couriered on dry ice to National Blood Service (NHSBT) in Oxford, where they were tested using R+D Systems Quantikine® Colorimetric Sandwich ELISA Kits. Each kit contained: pre-coated 96-well microplate, conjugated detection antibody, calibrated immunoassay standard, assay diluent, calibrator diluent(s), wash buffer, colour reagent A and B, stop solution and plate sealers.

The cytokines tested for were SDF-1, VEGF, VEGFR-1 and G-CSF. The assays employed used a quantitative sandwich enzyme immunoassay technique. A monoclonal antibody specific for the cytokine to be identified was pre-coated onto a microplate. Standards and samples were then pipetted into the wells, with the immobilized antibody binding any of the target cytokine present. After washing away any unbound substances, an enzyme-linked polyclonal antibody specific for the cytokine was added to the wells. Following a wash to remove any unbound antibody-enzyme reagent, a substrate solution was added to the wells to allow colour to develop in proportion to the amount of cytokine bound in the initial step. The colour development was stopped and the intensity of the colour measured using a microplate reader to determine the optical density of each well. The wavelength for this reader was set to 540nm or 570nm, unless wavelength correction was unavailable when a subtraction was performed to correct for the optical imperfections in the plate.

To calculate the results, optical density for the standards was plotted versus the concentration of the standards, with the best curve drawn. The data underwent logarithmic transformation to facilitate production of a linear plot and also regression analysis. In order to determine the concentration of the specific cytokine for each sample, the absorbance value on the y-axis was found and a horizontal line

extended to the standard curve. At the point of intersection, a vertical line was extended to the x-axis where the corresponding concentration for the cytokine could be read.

2.5 Immunohistochemistry

2.5.1 Human lung specimens

At surgery the lung or lung lobe(s) containing the tumour were excised and immediately placed in formalin. Following transfer to the pathology laboratory the specimens were then reinflated in formalin for 24 to 48 hours, allowing the specimen to be cut and assessed in three dimensions. The reinflated specimen was orientated, into the same plane that it would have existed in situ, and then the whole specimen was cut into 5 to 10mm sections, with the incisions made in the same plane as that of the axial DCE-CT sections. The tumour was then identified and samples taken for routine pathological staging. Additional samples were acquired for the study. Up to 3 sections were obtained, depending on the size of the tumour, corresponding to the superior, middle and inferior DCE-CT sections, as shown in Appendix A. The uninvolved lung was cut from around the tumour to allow them to be placed in a cassette (maximum dimensions available 5 x 5cm); the specimen ID plus orientation of specimen, including which surface lay uppermost, were marked on to the cassette. A diagram was drawn of each section taken for the study, where possible, showing the orientation of the tumour within the lung and the tissue removed prior to the specimen being placed in the cassette. If the tumour section diameter was greater than 5cm, the specimen was then cut and stored in either 2 or 3 separate cassettes: each labelled for orientation and a diagram drawn to depict how the tumour had been divided.

2.5.2 Materials

Immunohistochemical staining was undertaken using a very sensitive labelled polymer method for human tissue. The materials and methods described below were adapted from Gray Cancer Institute guidelines, with the key materials used shown in Table 2.2

Other equipment used:

- Panasonic NN-6453BBPQ 800W 2450MHz Microwave
- Grant Sub6 water bath IH9520002
- Pipettes: Gilson models P20, P100, P200, P1000, P5000 and disposable pipette tips, Anachem, UK
- Avery Berkel analytical balance FA64 reading to 0.0001g
- Universal staining system vial and cap, Dako S3425
- Dako Seymour glass labelling system, Eltron TLP2642
- Dako slide label kit S3417

2.5.3 Preparation of solutions and reagents

2.5.3.1 0.5M Tris buffer saline (TBS)

- Tris base 61g
- Na Cl 81g
- Distilled water 1000ml

Mixed to dissolve and concentrated HCl used to adjust pH to 7.6. Stored at room temperature and prior to use diluted to 1: 10 with distilled water, with pH adjustment if required.

2.5.3.2 Zinc Fixative

0.1M Tris buffer pH 7.4 1000mls (recipe below)

- Tris base 12.1g
- Deionised water 900ml
- 1.0M HCl 81.5mls

Mixed to dissolve and pH adjusted to 7.4

- Calcium Acetate 0.5g
- Zinc Acetate 5.0g
- Zinc Chloride 5.0g

Mixed to dissolve, with final pH 6.5 to 7.0. Stored at room temperature.

2.5.4 Preparation of histological slides for staining

Paraffin-embedded sections of 4µm thickness were cut from specimen blocks and were then labelled with their unique identifier using either pencil or a permanent marker. These were then mounted onto microscope slides and dried for 1 hour at 57°C. Dewaxing was undertaken by placing slides in xylene for 5 minutes. The slides were rehydrated through graded alcohols (100%, 90% and 70%) to water they were then placed in a slide tray and circled with a resin pen before washing with TBS.

2.5.5 Antigen retrieval

2.5.5.1 Pretreatment with 0.1% Chymotrypsin

Two dishes, each containing 200ml distilled water, were preheated to 37ºC in a waterbath. The slides were then placed into one of the dishes. 200mg calcium chloride was added to the second dish and stirred to dissolve. Subsequently 200mg alpha chymotrypsin was added to the same dish and again stirred to dissolve. Using 0.2M sodium hydroxide the pH was adjusted to 7.8. The slides were then transferred to the enzyme bath for 5 minutes then were removed and placed in running tap

water for a further 5 minutes to halt the enzymatic reaction. Following this the staining process was undertaken.

2.5.5.2 Heat induced epitope retrieval (HIER)

A plastic rack containing slides was placed into a plastic trough with 250ml of 10mM citric acid at pH 6 (pH adjusted using 2M sodium hydroxide). The lid was placed on the trough, which was then placed on an outer area of microwave turntable and heated at full power for 4 minutes. The lost fluid was then replaced with distilled water. This process of heating at full power for 4 minutes with replacement of the lost fluid was repeated twice more. Following the final heating and topping up with water, the trough with slides, was left to stand for 20 minutes. The slide rack was then removed and placed in the sink under running water for 5 minutes prior to continuing the staining process.

2.5.6 Immunohistochemical staining

2.5.6.1 CD34

No pre-treatment was undertaken, unless specimens stained poorly, when 0.1% Chymotrypsin pre-treatment (as per section 2.5.5.1) was used prior to staining further sections from the same specimen. At this point the slides were washed well in water and peroxidase block (DakoCytomation S2023) was applied for 5 minutes. The slides were then washed well in water, rinsed with TBS and protein block (DakoCytomation X0909) was applied for 5 minutes, with the excess then tipped off. Mouse anti-human CD34 (Qbend10) antibody (Novocastra NCL-End), diluted to 1/100 in antibody diluent (DakoCytomation S2022), was applied for 1 hour at room temperature. The slides were then rinsed in TBS 3 times over 3 to 5 minutes. Dako Envision Horseradish peroxidase (HRP) mouse polymer (DakoCytomation K5007) was applied for 30 minutes with the slides then washed again in TBS.

2.5.6.2 Pimonidazole

HIER (as per section 2.5.5.2) at pH 6, was used to pretreat the slides. They were then washed well in water and peroxidase block (DakoCytomation S2023) was applied for 5 minutes. Following this, the slides were washed well in water, rinsed with TBS and protein block (DakoCytomation X0909) was applied for 5 minutes, then the excess was tipped off. Hypoxyprobe 1Mab1 (4.3.11.3) (Natural Pharmacia), diluted to 1/100 in antibody diluent (DakoCytomation S2022) was applied for 1 hour at room temperature. The slides were then rinsed in TBS 3 times over 3 to 5 minutes. Dako Envision Horseradish peroxidase (HRP) mouse polymer (DakoCytomation K5007) was applied for 30 minutes with the slides washed again in TBS.

2.5.6.3 Glut-1

Slides were pre-treated by HIER (as per section 2.5.5.2) at pH 6. They were then washed well in water and peroxidase block (DakoCytomation S2023) was applied for 5 minutes. Following this the slides were washed well in water, rinsed with TBS and protein block (DakoCytomation X0909) was applied for 5 minutes, then the excess was tipped off. Glut-1 (SPH-498) antibody (Abcam ab40084), diluted to 1/300 in antibody diluent (DakoCytomation S2022), was applied for 1 hour at room temperature. The slides were then rinsed in TBS 3 times over 3 to 5 minutes. Dako Envision Horseradish peroxidase (HRP) mouse polymer (DakoCytomation K5007) was applied for 30 minutes with the slides then washed again in TBS.

2.5.6.4 Completion of staining and slide preparation

After the drainage of excess fluid, Diaminobenzadine (DAB) substrate (Vector SK-4100) was applied at a concentration of 20µl DAB/ 1ml for 5minutes followed by further rinsing in TBS and then washing well in running tap water. Slides were then

counterstained in Gills I haematoxylin (to stain the nuclei blue) for 10 to 30 seconds and washed well in running tap water for 5 minutes. Finally the slides were dehydrated through graded alcohols, cleared in xylene and mounted in DPX.

2.5.7 Digitisation of histology slides

The selected histology slide was cleaned of dust and any residual unwanted external marks, then fixed in position on the microscope stage. A Nikon eclipse TE200 microscope (4x objective) and a JVC KY-F75U camera (1360 x 1024 pixel) were used in conjunction with in-house microscope control software ('Lister'- Gray Cancer Institute, Northwood, Middlesex, UK) to acquire digital images. In preparation for image acquisition, background corrections were performed to compensate for discolouration and illumination non-uniformities: A white average image (W) was acquired from a clean area on the slide adjacent to the region of interest (ROI); A black average image (B) was acquired whilst the light source was occluded. The corrected image was then created from the original image (I) by calculating (I-B)/(W-B). The limits of the ROI were then defined using x and y stage coordinates and then the focal plane was defined by the user focussing on 3 points within the ROI that were selected by the computer. The software was then able to take into account the specimen's mounting angle and ensure all acquired images were in focus. The region scan was then started: multiple images were acquired sequentially for the whole ROI, with a predefined overlap of 10% between each image, the motorised stage moving the specimen between each image acquisition. All the resultant images were saved under the relevant filename as .ics files (Dean et al., 1990). An in-house software program ('Image Stitching' – Gray Cancer Institute, Northwood, Middlesex) was then used to produce a single image from the multiple acquired images, with the 10% overlap removed. To produce this image within the memory requirements of the program the individual image files were

subsampled by a factor of 4, although subsampling by a factor of 8 was required on 4 occasions due to the large size of the resultant stitched image. The settings used for the image stitching were defined as: Confident of overlap but no edge correction and no blend. The new stitched image was then saved as a .tif image file. Every pixel of the image containing information, in an 8-bit format: values between 0 (total absence of colour) and 255 (complete saturation of colour) for each of the colours red, green and blue.

2.5.8 Quantification of immunohistochemical staining

The acquisition of digital histological section images, with the quantification of colour on a pixel-by-pixel basis, enabled analysis of immunohistochemical stain colour intensity to be undertaken. This analysis was performed using in-house software ('TRI2' – Gray Cancer Institute, Northwood, Middlesex, UK). Reference intensity red-green-blue spectral patterns for the brown of the DAB staining and the blue of the haematoxylin staining were determined from the stored .tif images by analysing strongly stained areas of each colour, in each experiment for every one of the individual immunohistochemical stains, prior to the analysis and then saved in .spec file format.

After opening each .tif image file for analysis, resampling by 25% then again by 50% was undertaken using a standard binning method, due to the large size of these image files. A mask was drawn, delineating the ROI on each slide, with these ROIs saved as a binary .bmp (bitmap) files, where 1 indicates a selected pixel and 0 an unwanted pixel. 'Linear unmixing' was then opened in the software and the brown and blue references for the specific stain loaded. Linear unmixing was initiated by clicking on 'Go' and then a separated reference 1 (the brown staining pixels within the mask area) image was produced and saved as an .ics file. This image was

copied onto a new workspace, with the mask then copied and pasted on. The process was repeated for all the images of the same stain, allowing the analysis of them to be done with a multiple image statistics macro.

The multiple image statistics macro analyses all images in the designated new workspace determining total intensity, average intensity, standard deviation, standard error, modal value, modal frequency and mask area. The data produced was automatically saved in an Excel spreadsheet (.xls) format. This analysis was used to examine the whole mask area (ROI) by selecting 'Apply mask' and 'Normalise' on the multiple image statistics macro. It was also used to examine all of the brown staining pixels within the mask area. To examine the stained pixels, one of the images stored in the new workspace was highlighted and then the 'Histogram' icon on the tool bar was selected. The intensity levels for the detection of the brown stain were set, with Minimum at 0.2 and Maximum at 1000; this scale was then copied and applied to all images in the workspace. The multiple image statistics macro was then run as before with the 'Apply mask' selected but without normalisation. Again the resultant data was saved as a .xls file.

In addition to calculating the intensity and summary statistics of the immunohistochemical staining, the percentage of the slide staining with each was also examined. Initially the fraction of the mask area (number of pixels) stained by each immunohistochemical stain was derived using the following equation: Mask area (stained pixels)/ Mask area (whole ROI). This enabled the calculation of the percentage staining by multiplying the Stained fraction by 100.

2.6 Statistical Analysis

Statistical analysis was performed using Microsoft® Excel 2000 (Microsoft Corporation, Washington State, USA) and either StatsDirect version 2.6.5 (StatsDirect, Cheshire, UK) or SPSS software v13 (SPSS Inc., Illinois, USA).

2.6.1 Tumour Growth Delay

One way analysis of variance (ANOVA) followed by Tukey-Kramer multiple comparisons testing was used to compare the difference in time to tumour regrowth between the treatment groups. Differences were considered significant when p was ≤0.05.

2.6.2 Lymph node metastases

One way ANOVA, followed by Tukey-Kramer multiple comparisons testing, and Mann-Whitney U test were used to compare group means for the times to the development of lymph node metastases or end of study. Differences were considered significant when p was ≤0.05.

2.6.3 Immunohistochemical, DCE-CT and FDG-PET derived parameters

Correlation between DCE-CT measurements (PS, BV and BF) and immunohistochemical parameters (pimonidazole and Glut-1 expression) was assessed by Spearman rank correlation. Mann-Whitney U-test was used to assess associations between DCE-CT measurements or immunohistochemical parameters and clinico-pathological parameters (histological subtype, grade, stage and nodal status). In order to evaluate the effects of tumour heterogeneity on both DCE-CT and immunohistochemical parameters, coefficients of variance were calculated

where there were more than one tumour slice evaluated. Statistical significance was at 5%.

2.6.4 Blood count and cytokine parameters

The changes in blood count and cytokine parameters, between the measured time points, were compared using a paired samples t-test. Differences were considered significant when p was ≤0.05.

Cohorts				Week 1							Week 2							Week 3							Week 4							Week 5							Week 6							Week 7				
No.	**Disease/Trt.**	**Fraction/Dose**	**Gy/day/wk**	M	T	W	Th	F	S	S	M	T	W	Th	F	S	S	M	T	W	Th	F	S	S	M	T	W	Th	F	S	S	M	T	W	Th	F	S	S	M	T	W	Th	F	S	S	M	T	W	Th	F
	NSCLC																																																
1	Radiation	27/6 Gy	4.5/9	R			R				R			R				R			R																										
	CA4P	50 mg/m2					C																																									
2	Radiation	27/6 Gy	4.5/9	R			R				R			R				R			R																										
	CA4P	50 mg/m2					C							C							C																										
7	Radiation	27/6 Gy	4.5/9	R			R				R			R				R			R																										
	CA4P	50 mg/m2		C			C				C			C				C			C																										
	Prostate																																																
3	Radiation	55-57/19-20 Gy	2.75/13.75	R	R	R	R	R			R	R	R	R	R			R	R	R	R	R			R	R	R	R	R																		
	CA4P	50 mg/m2						C																																								
4	Radiation	55-57/19-20 Gy	2.75/13.75	R	R	R	R	R			R	R	R	R	R			R	R	R	R	R			R	R	R	R	R																		
	CA4P	50 mg/m2						C							C							C								C																	
5	Radiation	55-57/19-20 Gy	2.75/13.75	R	R	R	R	R			R	R	R	R	R			R	R	R	R	R			R	R	R	R	R			R	R	R	R	R			R	R	R	R	R			R	R	R	R	R
	CA4P	63 mg/m2						C							C							C								C								C								C
	H&N																																																
6	Radiation	64-70/32-35 Gy	2/10	R	R	R	R	R			R	R	R	R	R			R	R	R	R	R			R	R	R	R	R			R	R	R	R	R			R	R	R	R	R			R	R	R	R	R
	CA4P	50 mg/m2						C							C							C								C								C								C
	Cetuximab*	250 mg/m2					C							C							C							C							C							C					
				*Cetuximab should be given on the same day every week although the actual day may vary between patients																																												

Table 2.1

Phase Ib Trial of CA4P (Combretastatin A-4 Phosphate) in Combination with Radiotherapy in Patients with Advanced Cancer of the Lung, Head & Neck or Prostate, CA4P Protocol: UKR-104.

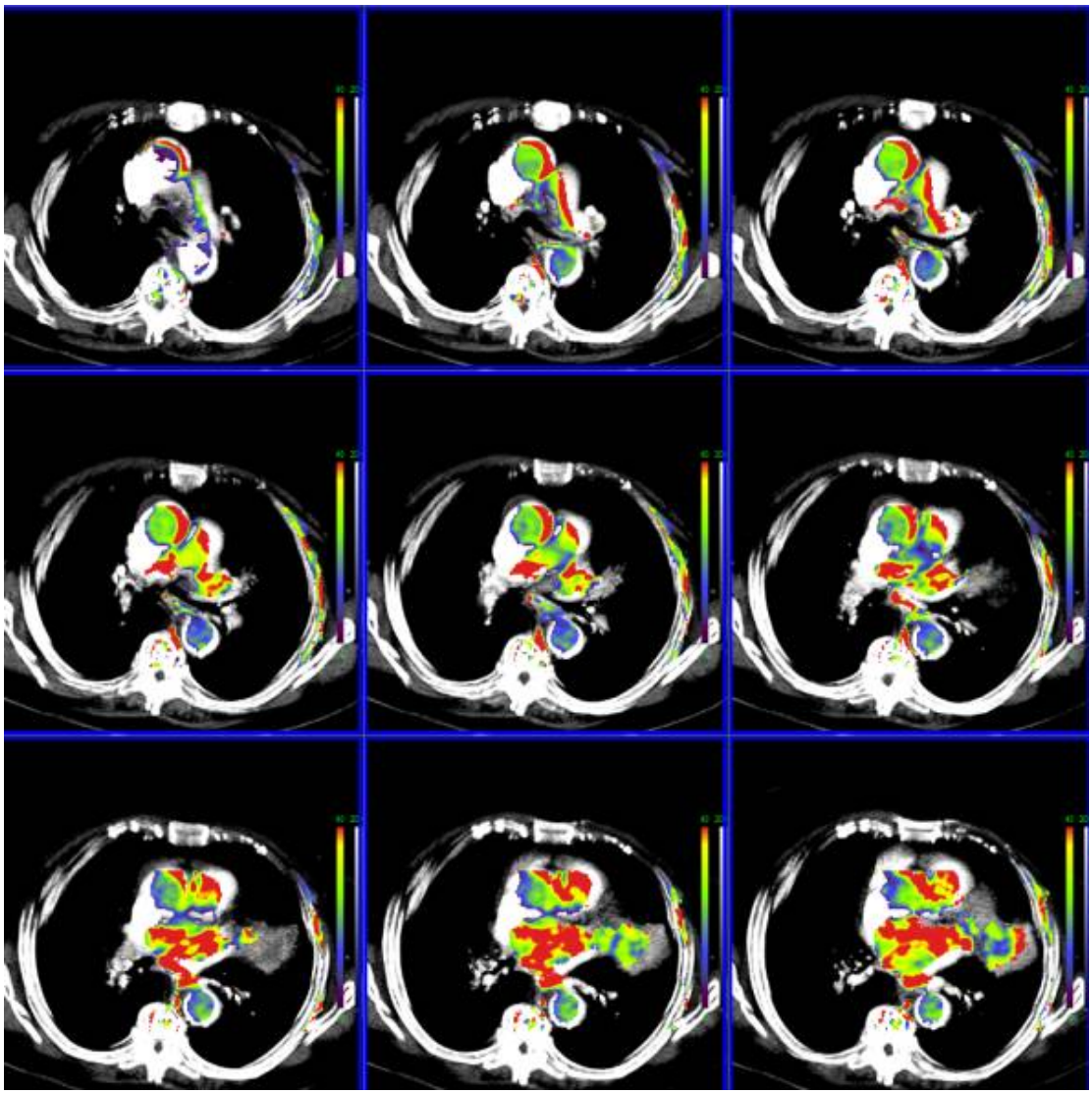

Figure 2.1

Colour parametric maps of permeability surface area product (PS), from a patient with NSCLC. The volumetric DCE-CT acquisition encompasses the whole tumour.

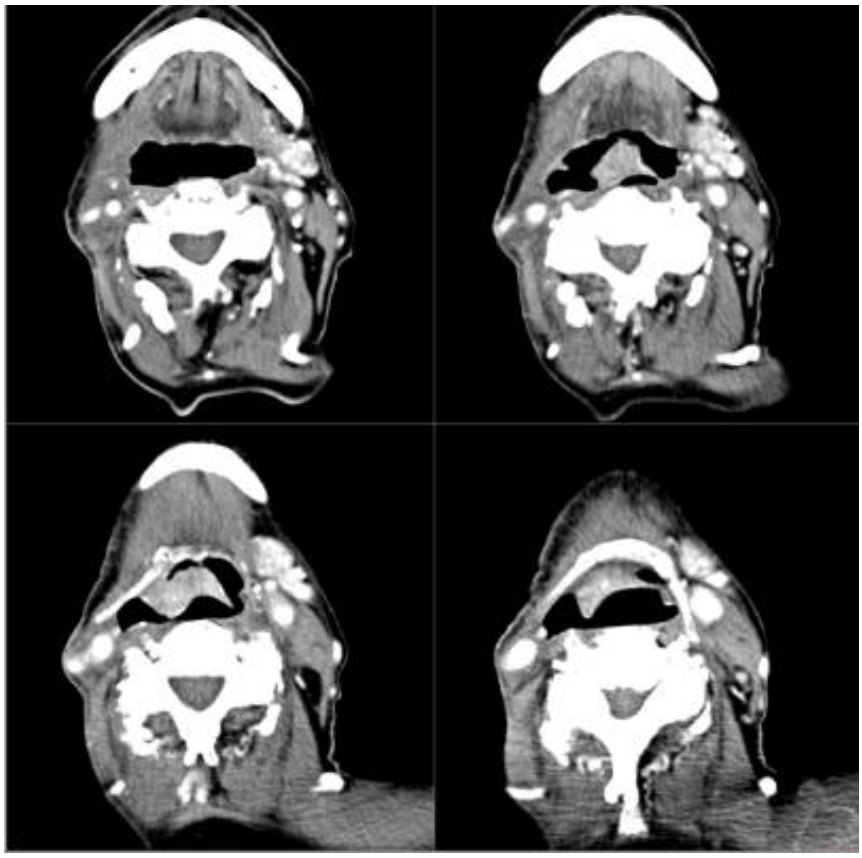

Figure 2.2

Parametric images of blood volume (BV) in a patient with HNSCC, showing the extent of z-axis coverage for this single level DCE-CT.

Product	Supplier	Cat. No.
Citric acid	VWR International	277814N
Alpha Chymotrypsin	Sigma	C4129
Protease	Sigma	P6911
Hydrochloric acid (HCl)	VWR International	28507
Sodium Chloride (NaCl)	VWR International	30123
Protein Block	DakoCytomation	X0909
CD34 (Qbend10) antibody	Novocastra	NCL-End
CD31 (pecam-1) antibody	Novocastra	CD31-1A10
Hypoxyprobe 1Mab1 (4.3.11.3)	Natural Pharmacia	Hypoxyprobe^{TM}1kit
Glut-1 (SPH-498) antibody	Abcam	ab40084
Antibody diluent	DakoCytomation	S2022
Peroxidase blocking solution	DakoCytomation	S2023
ChemMate Envision antibody detection kits	DakoCytomation	K5007
Calcium Chloride	VWR International	27587
Aqua hold PAP Resin Pen	M-Tech Diagnostics	9084
DPX	Surgipath Ltd	08600E

Table 2.2

Key materials used for immunohistochemical staining.

CHAPTER 3

Preclinical evaluation of nitric oxide synthase inhibition alone or in combination with radiation and vascular disruption.

3.1 Aims

- To determine plasma, tumour and normal tissue uptake and clearance of L-NNA when administered as a single dose i.p., 5 daily doses i.p. or by chronic oral schedule.
- To determine whether the addition of chronic oral or i.p. L-NNA enhances tumour growth delay in combination with fractionated radiotherapy.
- To determine whether the addition of chronic oral or i.p. L-NNA enhances tumour growth delay in combination with weekly combretastatin A4 phosphate.
- To determine whether the addition of chronic oral L-NNA enhances tumour growth delay in combination with daily low dose combretastatin A4 phosphate.
- To determine whether the addition of chronic oral L-NNA enhances tumour growth delay in combination with external beam fractionated radiotherapy and either weekly or daily low dose combretastatin A4 phosphate.

3.2 Introduction

This chapter contains details of preclinical experiments, examining the pharmacokinetics and effects on tumour growth of different schedules of the non-isoform specific NOS inhibitor, L-NNA. The murine mammary adenocarcinoma tumour model CaNT was selected as it had been used successfully, in studies demonstrating the effects of L-NNA, CA4P and also radiotherapy in previous preclinical work at Gray Cancer Institute, ([Parkins et al., 2000], [Davis, Tozer et al., 2002], [Rojas et al., 2004]).

Despite the encouraging tumour vascular effects observed with DCE-CT in a recent clinical phase 1 study of single dose L-NNA, it is likely that multiple doses of L-NNA or combination with other therapeutic modalities will be required to fully harness its potential (Ng et al., 2007c). These animal experiments enabled comparison of the plasma, tumour and normal tissue uptake and clearance of L-NNA, which would not be feasible in the clinical setting. Additionally they allowed comparison of the pharmacokinetics of different schedules of L-NNA: single i.p. dose, five daily i.p. doses and chronic oral administration in the drinking water. Using a tumour growth delay assay, experiments were undertaken to assess the impact of different schedules of L-NNA and establish whether their combination with fractionated radiotherapy and CA4P (both weekly and daily low dose schedules) could enhance the anti-tumour effects of these treatments.

3.3 Methods

3.3.1 Tumours and Treatments

This work was undertaken using the CaNT tumour model (as per section 2.1.1.1). The treatments under investigation were L-NNA and CA4P (as per section 2.1.2), and local tumour irradiation (as per section 2.1.3)

3.3.2 Pharmacokinetics

The pharmacokinetics of three different L-NNA schedules were analysed, as per sections 2.1.5. For Group 1, a single ip dose of L-NNA, 10mg/ kg, was given with sampling on day 1 at 10, 20, 30, 40, 60, 90, 120mins. Group 2 received five daily doses of ip L-NNA, 10mg/ kg, with sampling on day 5 at 10, 20, 30, 40, 60, 90, 120mins. L-NNA, 1mg/ml, was administered continuously in the drinking water for group 3, with sampling at 10am on days 2, 5, 8, 9 and 4pm on days 2, 5, 8. In groups 1 and 2 there were 2 mice used for every time point, with 3 mice per time point used for group 3. L-NNA concentrations in plasma and tissues were then determined using the technique described in section 2.1.5.1.

3.3.3 Tumour Growth Delay Treatment Groups

The treatment groups, with the various combinations of treatments studied, are shown in Table 3.1. In the initial experiment three different schedules of L-NNA were studied: *L-NNA 2qw:* 10mg/ kg i.p. twice per week (on days 3, 4, 10 and 11), *L-NNA 5qw:* 10mg/ kg i.p. five times per week (on days 0 to 4 and 7 to 11) and *L-NNA O:* orally in the drinking water at a concentration of 1 mg/ ml continuously. The drinking water consumption for each cage (3 to 6 mice) receiving the *L-NNA O* schedule was measured every 24 hours, producing a mean daily consumption of 4.08mls/ mouse/ day (Range 1.83 to 9.67mls/ mouse/ day). These L-NNA schedules were studied

alone, in combination with *CA4P (100)*: 100mg/ kg i.p. once per week (on day 4 and repeated on day 11) or in combination with radiotherapy (*RT*): 40Gy in 8 fractions over 2 weeks, as per section 2.1.3. On the days when radiotherapy was also given i.p. L-NNA was given within one hour after radiotherapy. In the schedules where i.p. L-NNA and i.p. CA4P were both administered, they were given concurrently using separate i.p. injections.

Further experiments were then undertaken to investigate the combination of *L-NNA O*, radiotherapy and either *CA4P (100)* or *CA4P (50)*: 50mg/ kg i.p. five times per week (on days 0-4 and 7-11). In these experiments *L-NNA O* alone, CA4P alone (both schedules) and *L-NNA O* with CA4P (both schedules), all without radiotherapy, were also examined. On the days when radiotherapy was also given, *CA4P (50)* was given one hour after radiotherapy. In the experiment where *CA4P (100)* was used, it was given 24 hours after the final fraction of radiotherapy each week. All treatment schedules were administered with an overall treatment time of two weeks, to ensure uniformity and allow direct comparison between treatment groups. Controls were used for all experiments, with i.p. saline administered 5 days per week except in the experiment where *L-NNA O* was combined with weekly *CA4P (100)*, where weekly i.p. saline was used (the volume of each control injection was determined in the same manner as i.p. CA4P or L-NNA, with a volume of 0.01ml/g administered). Drinking water was changed daily for all groups, to provide comparable conditions to the *L-NNA O* treatment groups.

The time to tumour regrowth was calculated for each tumour, as per section 2.1.4, with the difference observed between the mean times to tumour regrowth for the study cohorts, defined as tumour growth delay. To facilitate concurrent running of these experiments, back extrapolations from day 2 measurements were used to give day 0 tumour volumes for the groups receiving single agent L-NNA 2qw alone and

L-NNA 2qw combined with CA4P (100); no therapeutic intervention being scheduled for these two groups until day 3.

3.3.4 Statistical analysis

This was performed as stated in section 2.6. The comparison of the tumour growth delays produced by the various treatment groups is described in section 2.6.1.

3.4 Results

3.4.1 Pharmacokinetic studies

The plasma half-life after i.p. L-NNA was 122 minutes for the single dose group and 130 minutes for the five daily doses, as shown in Figure 3.1A. The tumour and other tissue concentrations of L-NNA (Figure 3.1B) were not significantly different between the single dose and five daily i.p. administrations. For the single i.p. dose of L-NNA, tumour Cmax was 72.2 mM and Tmax was 20 minutes, compared to a Cmax of 49.7 mM and Tmax 30 minutes for five daily i.p. doses of L-NNA. A relatively rapid increase in concentration was seen in both the tumour and liver with the i.p. schedules of L-NNA, which is in contrast to muscle where the drug appears to be taken up relatively slowly; the Tmax for muscle with the single dose and five daily doses respectively were 120 minutes and 60 minutes. L-NNA was taken up by a greater extent in the tumours compared to liver or skeletal muscle. As would be expected with a half-life of little more than 2 hours, there was no evidence for accumulation of drug after repeated daily administration, or induction of metabolism during the time-scale of the experiment. The tumour concentration remained significantly higher than that of the other tissues evaluated throughout the study period for both the single and five daily doses of L-NNA.

No significant accumulation occurred after Day 2 in the drinking water cohort, consistent with the relatively short half-life (Figure 3.2). Variability was observed in the drinking water cohort where plasma and tissue concentrations were lower at 4 pm compared with those at 10 am. This reflects diurnal variation in uptake of drinking water despite continuous exposure. Cmax was seen for all tissues in the samples collected on day 5 at 10 am, with a mean tumour Cmax of 76.4 mM. The tumour concentration at 10 am was maintained throughout the study period, which is consistent with the delay in tumour growth observed with this schedule. After L-NNA in the drinking water was replaced by plain water, at 4 pm on Day 8, low concentrations of drug were still detectable in the samples from the last time point at 10 am on Day 9 (18 h later).

3.4.2 Tumour Growth Delay Studies

3.4.2.1 Single agent L-NNA schedules

The mean tumour growth curves for the three schedules of L-NNA are shown in Figures 3.3. Both *L-NNA 5qw* and *L-NNA O* significantly enhanced tumour growth delay compared to controls. The mean time to tumour regrowth to 3 times original volume for *L-NNA 5qw* was 9.4 days and for *L-NNA O* was 10.3 days; tumour growth delays of 2.2 days (p=0.0224) and 3.1 days (p=0.0012) respectively. No statistically significant tumour growth delay between *L-NNA 5qw* and *L-NNA O* was produced. *L-NNA 2qw* did not significantly enhance tumour growth delay compared to controls and was significantly inferior to *L-NNA O* (p=0.0175). *L-NNA O* was tested on two further occasions with enhanced tumour growth delay compared to controls of 2.4 days (p=0.0222) and 1.6 days (p=0.0578) respectively (data not shown).

3.4.2.2 Combined L-NNA and CA4P

Similar significant results were seen in the cohort receiving *CA4P (100)* and the cohort receiving *L-NNA O*, with significant tumour growth delays of 2.6 days (p=0.0098) and 2.3 days (p=0.0222) respectively, compared to controls. The mean tumour growth curves for the combination of the three schedules of L-NNA studied with weekly *CA4P (100)* are shown in Figures 3.4. Enhanced tumour growth delays were produced by both *L-NNA O,* 3.6 days (p=0.0085), and *L-NNA 5qw,* 3.3 days (p=0.0095), in combination with *CA4P (100),* compared to *CA4P (100)* alone (Figure 3.4). No additional tumour growth delay was produced by *L-NNA 2qw* in combination with *CA4P (100).* Repeated daily dosing with *CA4P (50)* resulted in a substantial tumour growth delay relative to a large single dose. Figure 3.5 shows the mean tumour growth curves for *CA4P (50)* in combination with *L-NNA O*. The curve for *CA4P (50)* alone demonstrates the enhanced tumour growth delays found with this schedule in comparison to both *L-NNA O,* 1.9 days (p=0.0283), and controls, 3.6 days (p<0.0001). There was an additive enhancement in tumour growth delay with the combination of *L-NNA O* and *CA4P (50)*, with this combination producing the longest tumour growth delay of 5.5 days (p<0.0001), compared to controls, and of 3.5 days (p=0.001) compared to CA4P *(50)* alone.

3.4.2.3 Combined L-NNA, CA4P and Radiotherapy

Radiotherapy alone produced an enhancement in tumour growth delay of 42.9 days compared to that for controls (p<0.0001), with the curves for all of the groups receiving radiotherapy lying in close proximity (Figure 3.6). Prolongation of tumour growth delays were observed in the cohorts where radiotherapy was combined with *L-NNA 2qw*, *L-NNA 5qw* or *L-NNA O*, producing tumour growth delays of 4.7 days, 3.9 days and 3.5 days respectively; although none of these tumour growth delays were statistically different to radiotherapy alone. In contrast to the results shown in

Figure 3.6, on repeat testing a significant benefit was observed for the combination of radiotherapy and *L-NNA O* compared to radiotherapy alone (Figure 3.7), with an additional tumour growth delay of 5.6 days (p= 0.0285). The time for tumour regrowth for radiotherapy alone in Figure 3.7 was 35.2 days, shorter than in the previous experiment, and this may explain why a significant effect was observed on only one occasion with this combination.

The combination of *L-NNA O* with CA4P was investigated in combination with radiotherapy. The combination of *CA4P (100)* with radiotherapy showed an enhanced tumour growth delay compared with radiotherapy alone 6.5 days (p=0.0093). However, the combination of *L-NNA O*, *CA4P (100)* and radiotherapy was no more effective than either *L-NNA O* or *CA4P (100)* alone combined with radiotherapy (Figure 3.7). *L-NNA O* in combination with *CA4P (50)* and radiotherapy (Figure 3.8) resulted in little separation between the mean tumour growth curves for all the groups receiving radiotherapy. Single agent *CA4P (50)* also did not enhance the response to radiotherapy. Regardless of the CA4P dosing schedule, it has been demonstrated that there is no further tumour growth delay from the addition of continuous oral L-NNA to the combination of CA4P and radiotherapy.

3.5 Discussion

NO and the NOS enzymes play key roles in the regulation of tumour vasculature and angiogenesis and have the potential to be targeted as part of new therapeutic strategies ([Kashiwagi et al., 2005], [Murohara et al., 1998], [Yu et al., 2005]). L-NNA acting through NOS inhibition may exploit this target. The tumour vascular effects that can result from non-isoform specific inhibition of NOS are complex; the inhibition of vascular endothelial cell derived NOS being a major component of these effects; tumour specific arteriolar constriction and the inhibition of angiogenesis by

stabilisation of HIF-1α and downstream of VEGF ([Tozer et al., 2001], [Ziche et al., 1997], [Quintero et al., 2006]). Fractionated irradiation has been shown to promote NO-dependent angiogenesis, an effect that can be suppressed with non-isoform specific NOS inhibition (Sonveaux et al., 2003). Using DCE-CT assessment, a recent clinical phase 1 trial has shown significant reduction in tumour blood volume at 1 hour after a single dose of i.v. L-NNA, and this effect was sustained at 24 hours (Ng et al., 2007c). These effects were seen at doses of up to 0.9mg/ kg and are in keeping with previous preclinical studies examining i.v. and i.p. L-NNA schedules, which have shown differential reduction in the blood flow of tumours compared to normal tissues ([Tozer et al., 1995], [Tozer et al., 1997]).

This study has demonstrated that effective plasma and tumour concentrations of L-NNA can be achieved with either i.p. or oral delivery, in this animal model. Tumour concentrations produced were high relative to other tissues with all three of the L-NNA schedules studied, which may reflect trapping of the drug within the tumour following vascular shutdown. With oral administration in the drinking water there was a reduction in plasma and tissue concentrations between the morning and afternoon samples in keeping with the known drinking behaviour of the mice studied with maximum intake overnight. Chronic oral dosing achieved similar plasma and tumour levels of L-NNA to i.p. schedules of L-NNA. In keeping with this, significant enhancement in tumour growth delay compared to saline controls was observed for both the chronic oral L-NNA (*L-NNA O*) and daily i.p. LNNA (*L-NNA 5qw*) schedules, with the chronic oral dosing of L-NNA demonstrated to be as effective as daily L-NNA administered i.p. five times per week.

The dose intense schedule of daily low dose CA4P, 50mg/ kg i.p. five times per week, produced the greatest tumour growth delay observed in any single agent treatment group. A significant improvement in tumour growth delay was seen with

chronic oral L-NNA in combination with weekly CA4P (100mg/ kg) or daily CA4P (50mg/kg), compared to either schedule of CA4P alone. This enhanced effect between L-NNA and the tubulin-binding vascular disruptive agents, CA4P or ZD6126 has been previously described ([Tozer et al., 2009], [Wachsberger et al., 2005]).

CA4P is known to enhance radiotherapy in a schedule dependent manner; the optimal effect seen when given either simultaneously or after radiotherapy (Murata et al., 2001a). In this study, weekly CA4P (100 mg/ kg) when given i.p. 24 hours after the final fraction of radiotherapy each week produced the expected enhanced tumour growth delay. However, daily CA4P (50 mg/ kg) i.p., with four of the five daily doses each week given within an hour of the prior radiotherapy, demonstrated no improvement in tumour growth delay. It has been proposed that when VDAs are administered prior to radiotherapy, the resultant acute tumour hypoxia may negate the beneficial effects of this combination. Tumour oxygenation is an important radiobiological factor in determining the potential response to radiation, with hypoxia increasing radioresistance; this is therefore an important consideration in the sequencing of these treatments (Gray et al., 1953). It is feasible that CA4P-induced radioresistance due to tumour hypoxia is the reason no benefit was observed with the regime of daily CA4P (50mg/kg). Alternatively the angiogenic response to the intensive scheduling of this vascular disruptive therapy, including the mobilisation of endothelial progenitor cells from the bone marrow, may negatively impact radiation-induced damage to the tumour vasculature; this vascular damage is thought to be an important determinant of tumour cell survival ([Boehle et al., 2001], [Shaked et al., 2006], [Garcia-Barros et al., 2003]).

Despite the anti-tumour effects observed with single agent schedules, the addition of concurrent chronic oral or i.p. L-NNA alone to radiotherapy failed to increase the

efficacy of radiotherapy. The combination of oral L-NNA with either the weekly or daily CA4P schedules and radiotherapy also did not confer any additional benefit. Other work examining combined nitric oxide synthase inhibition with L-NNA, radiotherapy and ZD6126 did not show any enhancement of anti-tumour effects, compared to the combined treatment without L-NNA (Wachsberger et al., 2005). It may be that these findings are related to the scheduling of each treatment modality. Increased tumour hypoxia may have resulted in increased radioresistance. In addition NO can be a potent radiosensitiser in hypoxic conditions and this effect will be diminished in the presence of L-NNA ([De Ridder et al., 2008], [Gray et al., 1958], [Mitchell et al., 1998]).

In setting out to ascertain the impact of the combined vascular effects of L-NNA and CA4P with radiotherapy, a fractionated schedule was selected rather than a single fraction schedule, with the aim of optimising the clinical relevance of this work. Due to logistical constraints, this combination was studied in only one murine mammary tumour; CaNT was selected as it had previously demonstrated responsiveness to the effects of L-NNA and CA4P (Tozer et al., 2009). It is feasible that, in fact, the effects of L-NNA are greater in other human tumours, such as NSCLC, where 89% expression of eNOS and 40% expression iNOS has been reported in a case series (Puhakka et al., 2003). This would be in keeping with the observed vascular effects of L-NNA in NSCLC in the published phase 1 study (Ng et al., 2007c).

3.6 Conclusion

After chronic oral or i.p. administration LNNA is concentrated and retained in the CaNT mouse tumour model. L-NNA enhances tumour growth delay in this model, with greatest efficacy observed when delivered by chronic oral dosing. The enhanced tumour growth delay seen with L-NNA in combination with the tubulin

binding VDA, CA4P is consistent with an increased vascular damaging effect. Paradoxically, in combination with radiotherapy no consistent improvement in growth delay was seen with LNNA alone or in combination with CA4P. Clearly the interaction of RT with these vascular directed therapies, and their different modes of action, is complex, reflecting the interaction between vascular disruption, consequent changes in tumour microenvironment and radiation cell kill mechanisms which requires further study.

	L-NNA 2qw	L-NNA 5qw	L-NNA O
CA4P (100)	x	x	x
CA4P (50)	-	-	x
RT	x	x	x
RT + CA4P (100)	-	-	x
RT + CA4P (50)	-	-	x

Table 3.1

Combinations of treatments studied: L-NNA 2qw - 10mg/ kg ip on days 3, 4, 10, and 11; L-NNA 5qw - 10mg/ kg ip on days 0- 4 and 7- 11; L-NNA O- 1mg/ ml continuously in drinking water; CA4P (100)- 100mg/ kg ip on days 4 and 11; CA4P(50)- 50mg/ kg ip on days 0-4 and 7- 11; RT- radiotherapy, 40 Gray in 8 daily fractions on days 0-3 and 7-10.

A

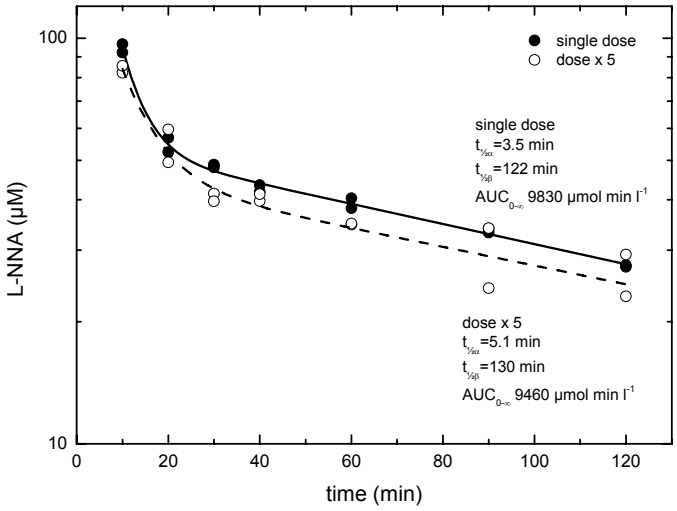

B

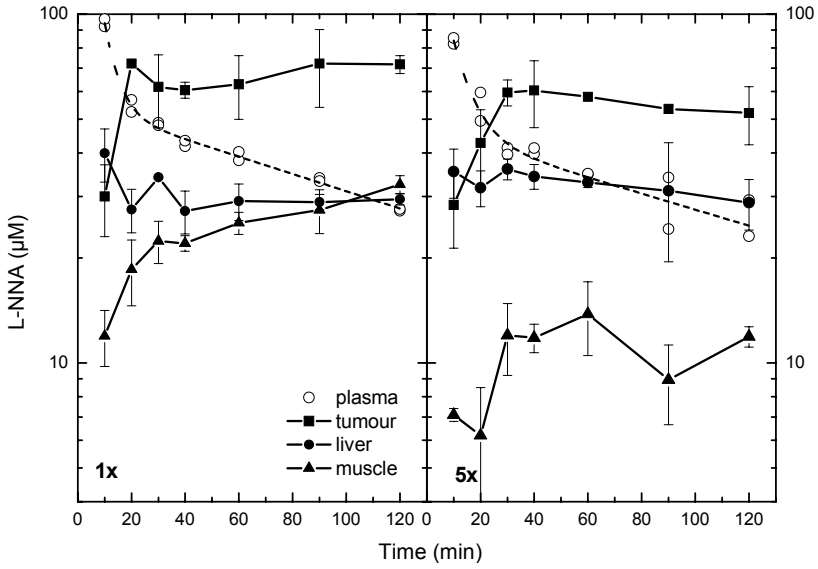

Figure 3.1

A- Plasma concentrations of L-NNA in CBA female mice after single or five daily doses of 10 mg/kg i.p.; B- Plasma and tissue concentrations of L-NNA in female CBA mice after a single i.p. dose (1x) or 5 x 10 mg/kg i.p. (5x).

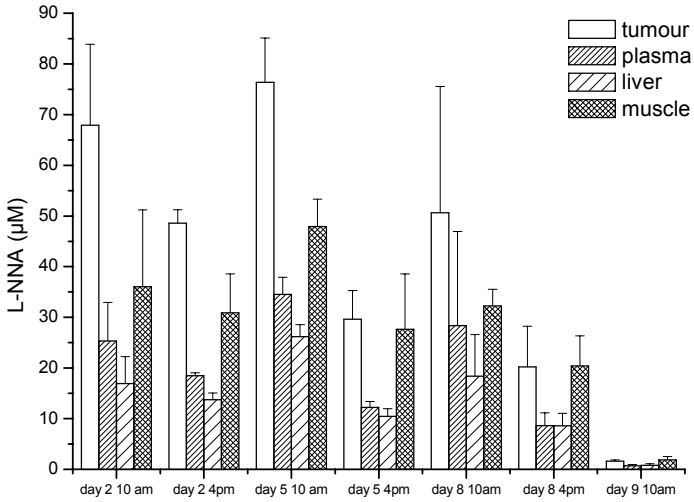

Figure 3.2

Plasma and tissue concentrations of continuous oral L-NNA (1 mg/ml drinking water) in female CBA mice. Columns represent means + 1 SD for 3 animals.

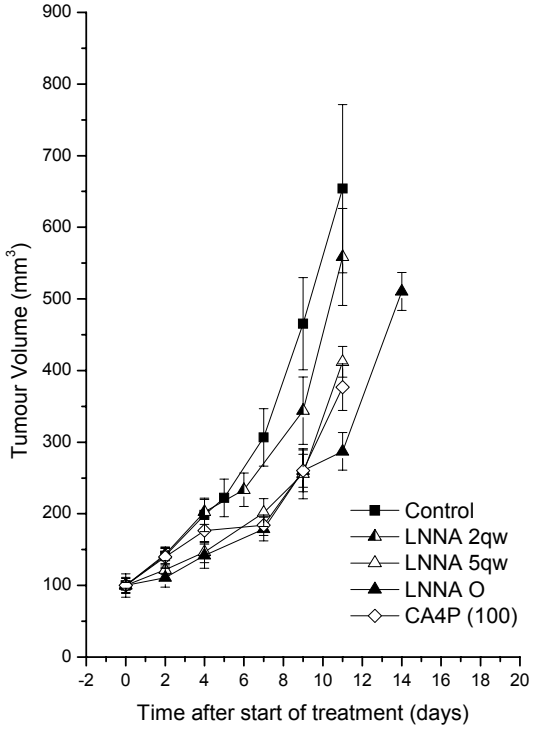

Figure 3.3

Effect of different L-NNA schedules when administered as a single agent or weekly CA4P on the growth of CaNT murine tumours. Points represent means ± 1 SEM for 5-6 animals. Comparison of single agent L-NNA schedules: *L-NNA 2qw:* 10mg/ kg i.p. twice per week (on days 3, 4, 10 and 11), *L-NNA 5qw:* 10mg/ kg i.p. five times per week (on days 0 to 4 and 7 to 11) and *L-NNA O:* orally in the drinking water at a concentration of 1 mg/ ml continuously; *L-NNA O* and *L-NNA 5qw* significantly enhancing tumour growth delay compared to controls. Weekly *CA4P (100)* alone, 100mg/ kg i.p. once per week (on day 4 and repeated on day 11) providing comparison.

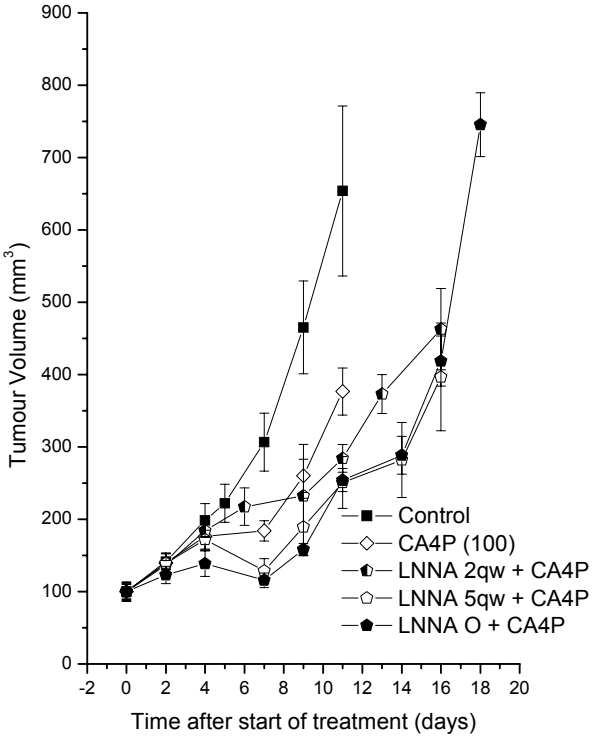

Figure 3.4

Effect of weekly CA4P combined with different L-NNA schedules on the growth of CaNT murine tumours. Points represent means ± 1 SEM for 5-6 animals. Weekly *CA4P (100)* alone, 100mg/ kg i.p. once per week (on day 4 and repeated on day 11), and in combination with either *L-NNA 2qw:* 10mg/ kg i.p. twice per week (on days 3, 4, 10 and 11), *L-NNA 5qw:* 10mg/ kg i.p. five times per week (on days 0 to 4 and 7 to 11) and *L-NNA O:* orally in the drinking water at a concentration of 1 mg/ ml continuously*;* the combinations of *CA4P (100)* with *L-NNA O* and *L-NNA 5qw* significantly enhancing tumour growth delay compared to *CA4P (100)* alone.

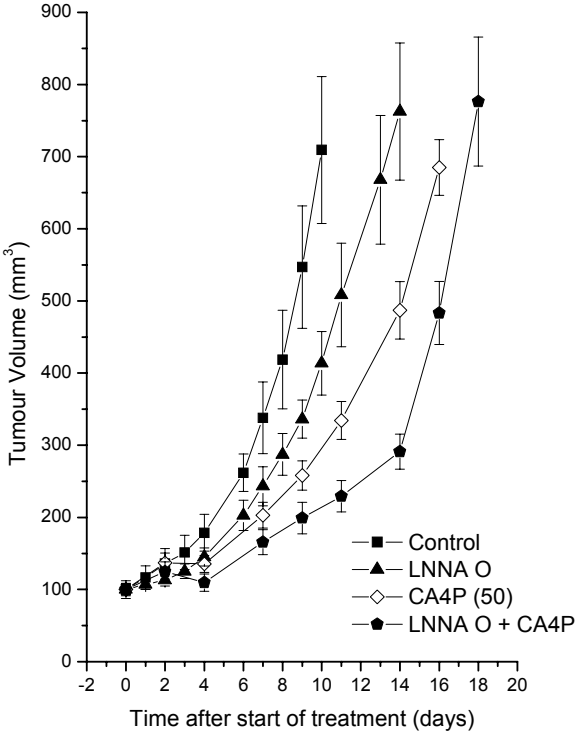

Figure 3.5

Effect of daily CA4P in combination with oral L-NNA schedule on the growth of CaNT murine tumours. Points represent means ± 1 SEM for 5-6 animals. Daily *CA4P (50),* 50mg/ kg i.p. five times per week (on days 0-4 and 7-11), alone and in combination with *L-NNA O,* orally in the drinking water at a concentration of 1 mg/ ml continuously; the combination of *CA4P (50)* and *L-NNA O* significantly enhancing tumour growth delay compared to *CA4P (50)* alone.

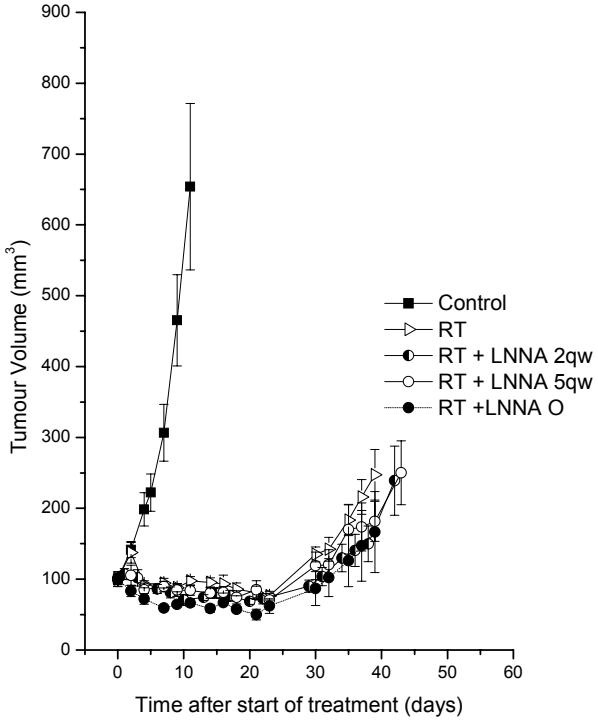

Figure 3.6

Effect of different L-NNA schedules on the growth of CaNT murine tumours in combination with fractionated radiotherapy. Points represent means ± 1 SEM for 5-6 animals. **A** RT, 40Gy in 8 fractions over 2 weeks, in combination with either *L-NNA 2qw:* 10mg/ kg i.p. twice per week (on days 3, 4, 10 and 11), *L-NNA 5qw:* 10mg/ kg i.p. five times per week (on days 0 to 4 and 7 to 11) and *L-NNA O:* orally in the drinking water at a concentration of 1 mg/ ml continuously; no enhancement of tumour growth delay seen with combination treatments.

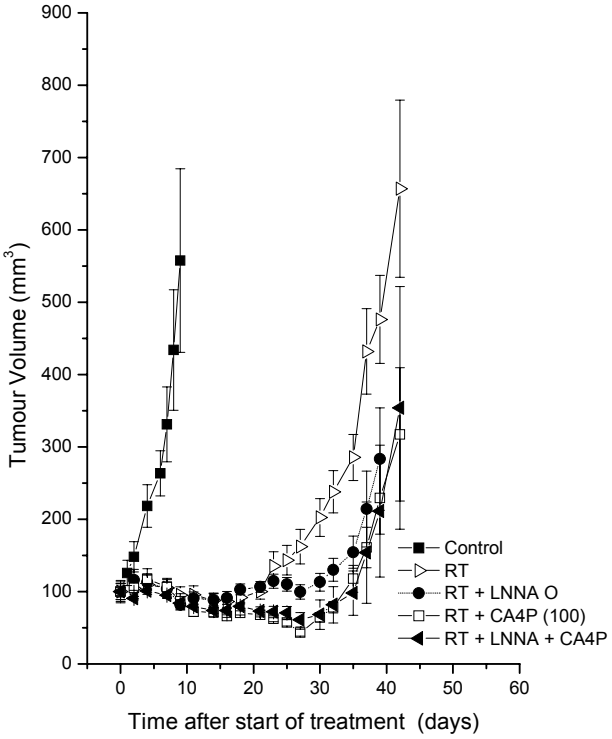

Figure 3.7

Effect of oral L-NNA schedule on the growth of CaNT murine tumours in combination with fractionated radiotherapy and weekly CA4P. Points represent means ± 1 SEM for 5-6 animals. *RT*, 40Gy in 8 fractions over 2 weeks, in combination with *L-NNA O,* orally in the drinking water at a concentration of 1 mg/ ml continuously; or *CA4P (100)*, 100mg/ kg i.p. once per week (on day 4 and repeated on day 11)*; RT* and *CA4P (100)* significantly enhanced tumour growth delay compared to *RT* alone.

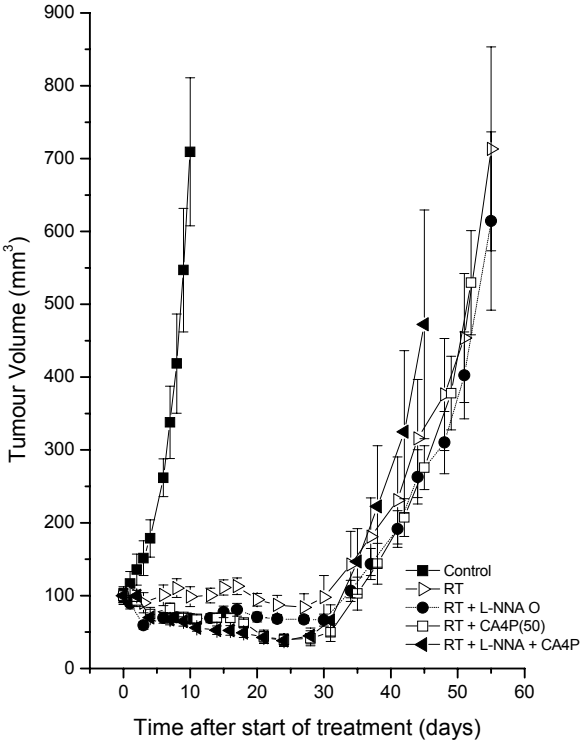

Figure 3.8

Effect of oral L-NNA schedule on the growth of CaNT murine tumours in combination with fractionated radiotherapy and daily CA4P. Points represent means ± 1 SEM for 5-6 animals. *RT,* 40Gy in 8 fractions over 2 weeks, in combination with *L-NNA O,* orally in the drinking water at a concentration of 1 mg/ ml continuously, or *CA4P (50),* 50mg/ kg i.p. five times per week (on days 0-4 and 7-11); no enhancement of tumour growth delay seen with combination treatments.

CHAPTER 4

Preclinical evaluation of EGFR inhibition in combination with radiation and vascular disruption.

4.1 Aims

- To determine whether the addition of combretastatin-A4 phosphate to cetuximab leads to enhanced growth delay when used to treat implanted human squamous cell xenograft, FaDu, tumours on female nude mice.
- To determine whether the addition of combretastatin-A4 phosphate to cetuximab in combination with radiotherapy leads to enhanced growth delay when used to treat implanted human squamous cell xenograft, FaDu, tumours on female nude mice.
- To determine whether radiotherapy fraction size has an effect on the response of FaDu tumours to combined cetuximab, combretastatin A4 phosphate and radiotherapy.
- To ascertain whether the plasma and tumour uptake and clearance of CA4P when given i.p. is altered when given in combination with cetuximab.

4.2 Introduction

This chapter contains details of preclinical experiments, examining the effects on tumour growth of monoclonal antibody inhibitor of EGFR, cetuximab, in combination

with CA4P and fractionated radiotherapy. The poorly differentiated hypopharyngeal SCC tumour model FaDu was selected as it has been used successfully in previous preclinical studies, where the addition of cetuximab to fractionated radiotherapy decreased repopulation and increased reoxygenation resulting in improved local tumour control (Krause et al., 2005).

As cancer treatments evolve towards a multi-targeted approach, different combinations of therapies are being examined. EGFR overexpression in HNSCC is associated with high levels of VEGF-A and VEGF-C, and also with poor prognosis (O-charoenrat P et al., 2000). EGFR signalling induces HIF1α synthesis, and the inhibition of EGFR by cetuximab has been shown to have anti-angiogenic effects, with reductions in the expression of VEGF, IL-8 and bFGF ([Laughner et al., 2001], [Petit et al., 1997], [Perrotte et al., 1999]). Combining EGFR inhibition with vascular disruption has shown some promise. Gefitinib given in combination with ZD6126, in head and neck cancer xenografts, resulted in both enhanced tumour growth delay and enhanced vascular effect (Bozec et al., 2006). Gefitinib has also been combined with ZD6126 and fractionated radiotherapy in a non small cell lung cancer (NSCLC) xenograft model, with this triple combination significantly increasing tumour growth delay compared to radiotherapy and either gefitinib or ZD6126 alone. (Raben et al., 2004). Using a tumour growth delay assay, experiments were undertaken to assess the impact of cetuximab and establish whether its combination with fractionated radiotherapy and CA4P could enhance the anti-tumour effects of these treatments. These animal experiments also enabled the impact of co-administration of cetuximab on the plasma, tumour and normal tissue uptake and clearance of CA4P to be determined, which would not be feasible in the clinical setting.

4.3 Methods

4.3.1 Tumours and Treatments

This work was undertaken using the FaDu tumour model (as per section 2.1.1.2). The treatments under investigation were C225 and CA4P (as per section 2.1.2), and whole body and local tumour irradiation (as per section 2.1.3).

4.3.2 Treatment Groups

All treatment schedules were administered over a comparable two week period to ensure uniformity. CA4P (100mg/ kg) i.p. once per week (on the 5th day of each week) was studied alone, in combination with C225 (1mg/ mouse) i.p. every 3 days for 4 doses in total, in combination with radiotherapy (schedule as described previously) plus all possible combinations of these three treatments. When cetuximab was given in combination with radiotherapy, the first dose was given at least 6 hours prior to the commencement of radiotherapy. CA4P, when combined with radiotherapy, was given on the following day after the final fraction of radiotherapy each week. Control groups received 0.5mls normal saline i.p. every 3 days for 4 doses. Radiotherapy doses of 2, 2.5 or 3 Gray per fraction were delivered to the midplane dose. Eight fractions were delivered over two weeks, four fractions per week delivered on consecutive days with a three day treatment gap.

4.3.3 Pharmacokinetics

Mice were sacrificed at the time points specified below and blood was collected in EDTA tubes. Tumours were excised, weighed and homogenised. 2 mice per time point were used for both groups. Group 1 received a single i.p. dose of CA4P, 100mg/ kg. Group 2 received i.p. cetuximab, 1mg in 0.5ml on day 1 then again on

day 4, followed by a single i.p. dose of CA4P, 100mg/ kg on day 5. Sampling for both groups was performed at 10, 20, 30, 60, 90, 120, 240mins.

4.3.4 Statistical analysis

This was performed as stated in section 2.6. The comparison of the tumour growth delays and the time to development of lymph node metastases, produced by the various treatment groups, are described in section 2.6.1 and section 2.6.2 respectively.

4.4 Results

4.4.1 Tumour Growth Delay Studies

4.4.1.1 CA4P and cetuximab

The mean tumour growth curves for the single agent schedules of cetuximab and CA4P, and the combination of both, are shown in Figure 4.1. Cetuximab alone, 1mg i.p every 3 days for 4 doses, produced a time to tumour regrowth (to twice original volume) of 9.2 days, with the greatest tumour growth delay of 3.4 days compared to controls. By comparison, CA4P alone, 100mg/ kg i.p weekly for 2 doses, produced a tumour growth delay of 1.8 days and CA4P combined with cetuximab, a tumour growth delay of 2.7 days, both compared to controls. None of the delays observed, between treatment groups or controls, reached statistical significance.

4.4.1.2 CA4P, cetuximab and radiotherapy

At 2Gy per fraction, radiotherapy alone produced a mean time to tumour regrowth of 26.3 days, a tumour growth delay of 10.5 days compared to that for controls ($p<0.0001$). The curves for all of the groups receiving radiotherapy at 2Gy per fraction, to a total dose of 16Gy, delivered over 2 weeks, are shown in Figure 4.2.

The greatest tumour growth delay, at this dose per fraction, was produced by the combination of radiotherapy, cetuximab and CA4P. This triple combination resulted a time to tumour regrowth (to twice original volume) of 32.2 days, with tumour growth delays of 5.9 days compared to radiotherapy alone, 4.8 days compared to radiotherapy combined with cetuximab and 3.7 days compared to radiotherapy combined with CA4P. Despite these improvements in tumour growth delay, none achieved statistical significance.

The curves for all the groups receiving radiotherapy at 2.5Gy per fraction to a total dose of 20Gy, delivered over 2 weeks, are shown in Figure 4.3. Radiotherapy alone, at 2.5Gy per fraction, produced a mean time to tumour regrowth of 38.6 days. Again the group receiving cetuximab and CA4P, in combination with radiotherapy at a dose per fraction of 2.5Gy, demonstrated the greatest time to tumour regrowth (to twice original volume) of 53.3 days. This combination produced significant tumour growth delays at this dose per fraction; 14.7 days ($p=0.0193$) compared to radiotherapy alone, and 14.9 days ($p=0.0293$) compared to radiotherapy combined with CA4P. These calculations were undertaken excluding data from 1 mouse in the radiotherapy alone group and from 2 mice in the radiotherapy and CA4P group. These were excluded, as the tumours did not reach 200% of the original volume, due to the development of large lymph node metastases requiring the mice to be sacrificed. The group sizes as a result were 4 mice and 3 mice respectively.

With extrapolations for the tumour growth curves (with between 0.3 and 0.5 days beyond the final data point) for 2 mice in the radiotherapy combined with CA4P group, this enabled data from all 5 mice in this cohort to be used in the comparison. Using this extrapolated data the tumour growth delays produced by the combination of cetuximab, CA4P and radiotherapy remained significant; 14.9 days ($p=0.0058$), compared with radiotherapy combined with CA4P, and 14.7 days ($p=0.0101$),

compared with radiotherapy alone. The major difference resulting from these extrapolations were that radiotherapy combined with cetuximab also had significant tumour growth delays compared to radiotherapy combined with CA4P and radiotherapy alone, 11.6 days (p=0.0319) and 11.4 days (p=0.0494) respectively.

The time to tumour regrowth to original volume was also examined for those cohorts receiving 2.5Gy per fraction, to provide comparison for the groups receiving 3Gy per fraction. This was not possible for the groups receiving radiotherapy at 2Gy per fraction and those groups not receiving radiotherapy, due to insufficient magnitude of effect on tumour growth. Using this alternative endpoint of time to tumour regrowth to original volume, cetuximab combined with CA4P and radiotherapy was the only treatment cohort to demonstrate significant tumour growth delays, compared to radiotherapy combined with CA4P, and radiotherapy alone, 12.7 days (p=0.0161) and 13.9 days (p=0.0083) respectively. No significant difference was observed between radiotherapy combined with cetuximab and radiotherapy combined with cetuximab and CA4P, for either the time for tumour regrowth to original or twice original volume, even when extrapolated data was included.

The curves for all the groups receiving radiotherapy at 3Gy per fraction to a total dose of 24Gy, delivered over 2 weeks, are shown in Figure 4.4. For this dose level of radiotherapy alone, only one tumour regrew to twice its original volume, in a time of 53.9 days. The other mice in the radiotherapy alone group had to be sacrificed prior to their primary tumour regrowing, due to the development of lymph node metastases, which prevented valid statistical comparison between the radiotherapy alone group and the other treatment groups, at this time point. The remainder of the groups had 3 evaluable mice, with the combination of cetuximab, CA4P and radiotherapy producing the greatest time to tumour regrowth (to twice original volume) of 95.6 days. The triple combination produced tumour growth delays of 37.8

days compared to radiotherapy combined with CA4P alone and 19.6 days compared to radiotherapy combined with cetuximab alone. None of these tumour growth delays were, however, statistically significant.

The 3Gy per fraction treatment groups were also examined in respect to the time to tumour regrowth to original volume. Without any extrapolation, this increased the numbers of mice per group where the data could be included; 4 mice in the radiotherapy combined with cetuximab group, 3 mice in both the radiotherapy combined with CA4P and radiotherapy combined with cetuximab and CA4P groups, with 2 mice in the radiotherapy alone group. As before, the greatest time to tumour regrowth (to original volume) of 86.6 days, was produced by radiotherapy combined with cetuximab and CA4P. This produced tumour growth delays of 45.3 days ($p=0.0677$) and 49.9 days ($p=0.094$), compared with radiotherapy combined with CA4P and radiotherapy alone respectively.

One tumour, from the group receiving radiotherapy (3Gy per fraction) combined with cetuximab and CA4P, never regrew throughout the study period, up to 137 days. The remaining small skin nodule was resected at the conclusion of the study, although light microscopy with H+E immunohistochemical staining revealed no evidence of residual malignancy.

4.4.1.3 Lymph node metastases

During the post treatment phase for the first treatment cohort in the tumour growth delay experiments, it was noted that lymph node metastases commonly developed in the groups that received radiotherapy. These were not seen in the cohorts that did not receive radiotherapy, which had a much faster rate of tumour growth and therefore a much shorter follow up period. The times when lymph node metastases

first appeared were noted for the mice in the groups receiving radiotherapy, at all 3 radiotherapy dose levels, and are shown in Table 4.1.

In the group receiving radiotherapy combined with cetuximab, at 2Gy per fraction to a total dose of 16Gy over 2 weeks, the mean time to development of lymph node metastases, or end of experiment if no metastases were seen, was significantly longer by 18 days, than seen with the radiotherapy combined with CA4P cohort, and 15 days longer than radiotherapy alone. The cohort receiving radiotherapy combined with both cetuximab and CA4P also had a significantly longer mean time to the development of lymph node metastases, compared to the same two cohorts by 23 days and 20 days respectively. All these differences were significant with a p-value of <0.0001. There was no significant difference between the groups receiving radiotherapy combined with cetuximab and CA4P or radiotherapy combined with cetuximab alone, and also between the groups receiving radiotherapy combined with CA4P or radiotherapy alone.

A similar picture was observed in the groups receiving radiotherapy at a dose of 2.5Gy per fraction to a total dose of 20Gy over 2 weeks, with mean differences of 39.2 days (p=0.0004) and 34.2 days (p=0.0016) respectively, between radiotherapy combined with cetuximab and CA4P and the groups receiving radiotherapy alone or radiotherapy combined with CA4P. At 3Gy per fraction, to a total dose of 24Gy over 2 weeks, the only difference that was significant was between the radiotherapy combined with cetuximab and CA4P and the group receiving radiotherapy alone, producing an increase in the mean time to development of lymph node metastases of 53.8 days (p=0.0447). The next greatest mean increase of 37 days (radiotherapy combined with cetuximab and CA4P compared with radiotherapy combined with CA4P) was not significant (p=0.2261).

For the cohort receiving 2Gy per fraction, only one mouse in the radiotherapy combined with cetuximab cohort developed lymph node metastases, although in the group receiving the same combination treatment, at 2.5Gy per fraction, none of the mice developed lymph node metastases. This is in contrast to the radiotherapy combined with CA4P groups where 5 out of 5 and 4 out of 5 developed lymph node metastases, at 2Gy per fraction and 2.5Gy per fraction respectively. When the groups were combined for each dose per fraction, into those that received cetuximab and those that did not, significant differences were detected. Using the Mann-Whitney U test, the median increase in the time to development of lymph node metastases or end of experiment was 19 days ($p<0.0001$) at 2Gy per fraction, 37.5 days ($p<0.0001$) at 2.5Gy per fraction and 30 days ($p=0.0112$) at 3Gy per fraction. A significant median increase of 23 days ($p<0.0001$) was noted between 2Gy per fraction and 2.5Gy per fraction, in the groups receiving radiotherapy combined with cetuximab. No other significant differences were noted between the different dose per fractions in the groups either receiving concomitant cetuximab or not.

4.4.2 Pharmacokinetic studies

Comparison of the plasma and tissue pharmacokinetics of CA4P and its metabolite CA4 were undertaken; examining a single dose of CA4P 100mg/kg i.p. and the same dose of CA4P administered after 2 preceding doses of cetuximab, 1mg i.p., given initially 4 days and then 1 day prior to CA4P. As a result of tissue degradation during the storage process, which was evident when the whole tissues were defrosted, prior to being homogenised, the data from the liver and muscle samples was thought to be unreliable and unsuitable for comparative analysis. The tumour samples, however, were deemed suitable for analysis and this data is presented here, in addition to the plasma pharmacokinetic data.

There was no significant difference in the tumour concentrations of CA4P and its metabolite, CA4, between the i.p. administration of CA4P alone and its administration following prior cetuximab (Figure 4.6). Analysis of the tumour from the group receiving CA4P alone, revealed the CA4P tumour Cmax to be 9.45μM, with a Tmax of 10 minutes. This compared to the combination group of CA4P and cetuximab, with a CA4P Cmax of 5.45μM and a Tmax of 20 minutes. For the metabolite, CA4, Cmax was 26.85μM with a Tmax of 10 minutes for the CA4P alone group. In comparison the Cmax for the group receiving CA4P in combination with cetuximab was 27.25 μM with a Tmax of 30 minutes.

4.5 Discussion

The targeting of EGFR using monoclonal antibodies or small molecule TKIs provides a new therapeutic strategy; the upregulation of EGFR a common feature in many malignancies, such as squamous cell carcinoma of the head and neck (HNSCC), NSCLC and colorectal carcinoma. EGFR has a key role in tumour proliferation but its inhibition affects other downstream pathways, including the indirect inhibition of angiogenesis (Petit et al., 1997). Cetuximab, the monoclonal antibody therapy targeting EGFR, is now widely used, administered concomitantly with radiotherapy in the treatment of SCCs of the head & neck. This follows the phase III study demonstrating that cetuximab combined with radiotherapy improved both progression-free and overall survival in locally advanced SCC of the head & neck, compared to radiotherapy alone (Bonner et al., 2006).

There are potentially exploitable interactive mechanisms and non-interactive mechanisms supporting the concept for combining vascular directed therapies and radiotherapy. Radiation-induced damage to the tumour vasculature is an important determinant of tumour cell survival, with the resultant endothelial cell apoptosis

contributing to the overall anti-tumour effect (Garcia-Barros et al., 2003). The addition of a VDA has been shown to augment radiation-induced damage to HUVECs and it is possible that the damage to tumour blood vessels from radiotherapy also enhances the sensitivity of endothelial cells to the effects of VDAs (Hoang et al., 2006). The combination of radiotherapy and angiogenesis inhibition results in increased endothelial cell apoptosis, with the inhibition of the signalling cascade induced by angiogenic factors directly radiosensitising tumour endothelial cells (Gorski et al., 1999). There is the potential for antiangiogenic agents, in addition to VDAs, to further enhance the vascular damage and thus antitumour effects of radiotherapy. EGFR inhibitors have shown enhanced antitumour effects in combination with VDAs and radiotherapy; Radiotherapy with concomitant gefitininib and ZD6126 significantly increased tumour growth delay in a NSCLC xenograft model, compared to radiotherapy and either gefitinib or ZD6126 alone (Raben et al., 2004).

In this study we have used tumour growth delay as a surrogate for anti-tumour effect and have demonstrated that cetuximab plus CA4P in combination with radiotherapy, consistently produced the greatest tumour growth delay; 3.7 days at 16Gy (2Gy per fraction), 14.9 days at 20Gy (2.5Gy per fraction) and 37.8 days at 24Gy (3Gy per fraction), all compared to radiotherapy combined with CA4P. The magnitude of this delay increased with both increasing radiation dose and increasing dose per fraction. One tumour cure was observed in this study at the highest dose level of radiotherapy; this mouse was from the cohort receiving 24Gy in combination with both cetuximab and CA4P. It is likely that, particularly in the group receiving 24Gy, the small numbers achieving the target size for tumour regrowth was an important factor in the statistical comparison. With the greater control of the primary tumour produced at this higher dose, an increased incidence of lymph node metastases was observed late into the follow up period.

One of the factors that reduced the number of animals available for comparison of tumour growth delay, was the development of lymph node metastasis contributing to tumour burden; this effect was particularly seen in the groups receiving the highest radiation dose. These metastases curtailed the length of follow up possible, due to the need to carefully restrict the overall tumour burden on the mice. Even in the lowest radiation dose group, receiving 2Gy per fraction, a marked difference in the time to development of lymph node metastasis or end of experiment existed between the groups receiving cetuximab in addition to radiotherapy (range 47 to 59 days) compared with those receiving radiotherapy but not cetuximab (range 33 to 46 days). This difference was borne out at the other 2 dose levels where significant differences were also observed between the radiotherapy groups receiving cetuximab or not, with the greatest median difference 37.5 days. These findings are consistent with cetuximab reducing the ability of FaDu tumours to metastasise, in addition to enhancing the control of the primary tumour.

Despite the enhanced anti-tumour effects produced by weekly CA4P in combination with fractionated radiotherapy in other tumour models, this combination did not produce a significant improvement compared with radiotherapy alone, at any of the radiotherapy 3 dose levels in this study, using this head & neck SCC tumour model ([Chaplin et al., 1999], [Murata et al. 2000]). Whilst radiotherapy plus cetuximab did produce a significant tumour growth delay compared with radiotherapy alone or in combination with CA4P, this was only significant in the 20Gy group, when extrapolated tumour growth delay data was included. The EGFR inhibitor, gefitinib, has been studied in combination with ZD6126, in head and neck cancer xenografts. This combination showed both enhanced tumour growth delay and enhanced vascular effect, as evidenced by increased reduction in CD31 labelling (Bozec et al., 2006). In this work, enhanced tumour growth delays were produced with the addition of CA4P to radiotherapy plus cetuximab compared with radiotherapy plus cetuximab

alone, with a delay of 19.6 days seen between the cohorts at the 24Gy dose level. The triple combination of EGFR inhibition, VDA and radiotherapy consistently produced the longest time to tumour regrowth in these experiments, however, no significant difference was demonstrated between the cohorts receiving radiotherapy plus cetuximab with or without CA4P. This may be, as already discussed, due to the sensitivity of the tumour model used and the confounding factor produced by the development of lymph node metastases.

Having demonstrated enhanced tumour growth delay with cetuximab, CA4P and radiotherapy, we set out to investigate whether the addition of cetuximab could have an impact on the pharmacokinetics of CA4P. Our findings show no significant difference in plasma or tumour levels of CA4P or its metabolite following the addition of cetuximab. This lack of interference supporting the potential combination of these 2 targeted therapies.

4.6 Conclusion

In this work enhanced anti-tumour effect was observed between cetuximab, CA4P and radiotherapy, with this combination consistently producing the longest time to tumour regrowth. It was also the only treatment to produce a signicant tumour growth delay compared to radiation alone. The anti-tumour effects of radiotherapy plus cetuximab in this tumour model were confirmed, demonstrated by the reduced ability of the primary tumours to metastasise to local lymph nodes. Despite the beneficial effects seen in combination with cetuximab and radiotherapy, single agent CA4P in combination with radiotherapy demonstrated no beneficial anti-tumour effect in this FaDU tumour model. The combination of cetuximab, CA4P and fractionated radiotherapy has shown promising anti-tumour effects and warrants further investigation.

2Gy/f	2Gy/f + Cet	2Gy/f + CA4P	2Gy/f + Cet + CA4P
35	47	33	59
33	52*	33	59
33	52*	33	59
46*	52*	33	47
33	52*	33	56*

2.5Gy/f	2.5Gy/f + Cet	2.5Gy/f + CA4P	2.5Gy/f + Cet + CA4P
30	74*	28	74*
56*	84*	51	74*
56*	84*	58	86*
28	70*	58*	86
28	70*	28	74*

3Gy/f	3Gy/f + Cet	3Gy/f + CA4P	3Gy/f + Cet + CA4P
56*	28	42	44
28	72	28	137*
42	94	84*	114*
28	100*	84*	98
28	49*	28	58

**No lymph node metastases by final day of experiment*

Table 4.1

Time (days) to development of lymph node metastases, or end of experiment for those not developing lymph node metastases. Data shown for each of the mice in the experiment. Three dose levels of radiotherapy studied: 16Gy in 2Gy per fraction (2Gy/f), 20Gy in 2.5Gy per fraction (2.5Gy/f), 24Gy in 3Gy per fraction (3Gy/f). Radiotherapy was administered alone and in combination with cetuximab (Cet), 1mg i.p. every 3 days foe 4 doses, and/ or combrestastatin A4 phosphate (CA4P), 100mg/kg i.p. weekly for 2 doses.

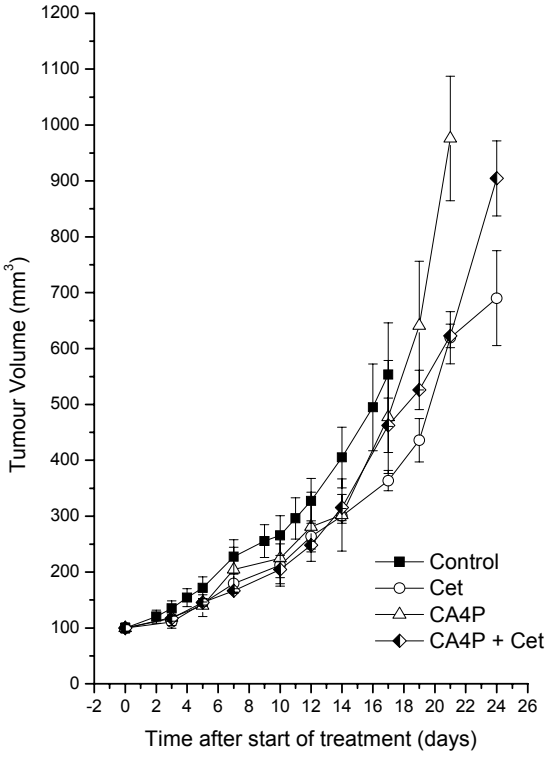

Figure 4.1

Effect of CA4P 100mg/kg i.p. weekly or cetuximab (Cet) 1mg i.p. every 3 days for 4 doses on growth of FaDu tumours when administered as single agents or in combination. Points represent means ± 1 SEM for 3-4 animals.

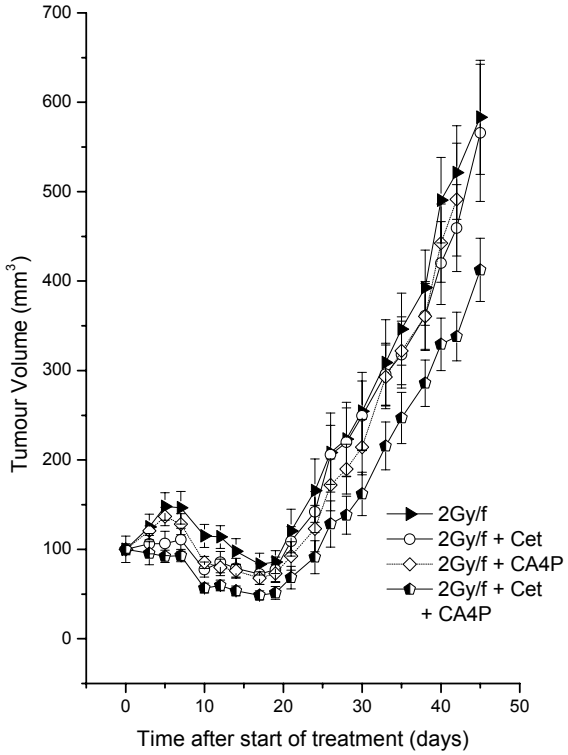

Figure 4.2

Effect of fractionated radiotherapy 16 Gray in 8 fractions (2 Gray per fraction), 4 fractions per week with a 3 day treatment gap on growth of FaDu tumours when administered either alone, plus CA4P 100mg/kg i.p. weekly or cetuximab (Cet) 1mg i.p. every 3 days for 4 doses or in combination with both CA4P and cetuximab. Points represent means ± 1 SEM for 4-5 animals.

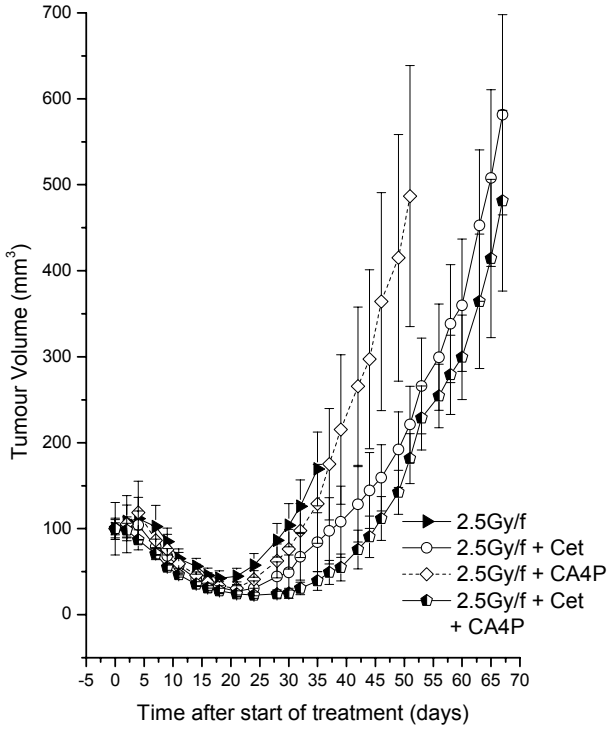

Figure 4.3

Effect of fractionated radiotherapy 20 Gray in 8 fractions (2.5 Gray per fraction), 4 fractions per week with a 3 day treatment gap on growth of FaDu tumours when administered either alone, plus CA4P 100mg/kg i.p. weekly or cetuximab (Cet) 1mg i.p. every 3 days for 4 doses or in combination with both CA4P and cetuximab. Points represent means ± 1 SEM for 3-5 animals.

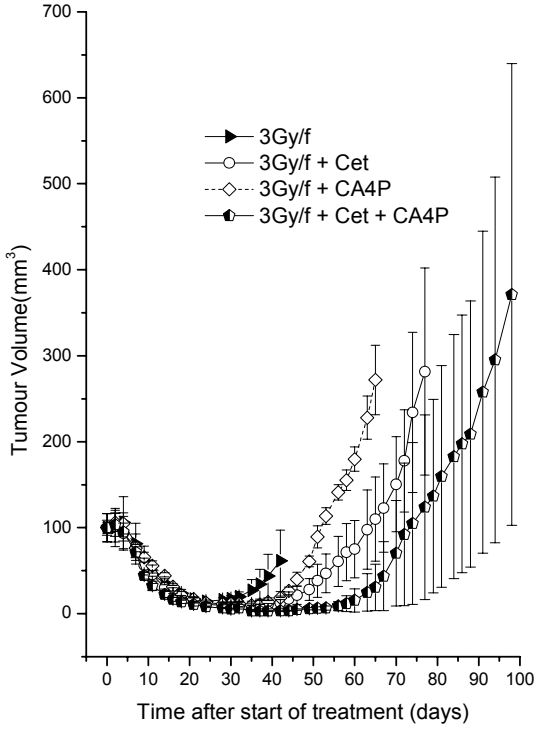

Figure 4.4

Effect of fractionated radiotherapy 24 Gray in 8 fractions (3 Gray per fraction), 4 fractions per week with a 3 day treatment gap on growth of FaDu tumours when administered either alone, plus CA4P 100mg/kg i.p. weekly or cetuximab (Cet) 1mg i.p. every 3 days for 4 doses or in combination with both CA4P and cetuximab. Points represent means ± 1 SEM for 3-5 animals.

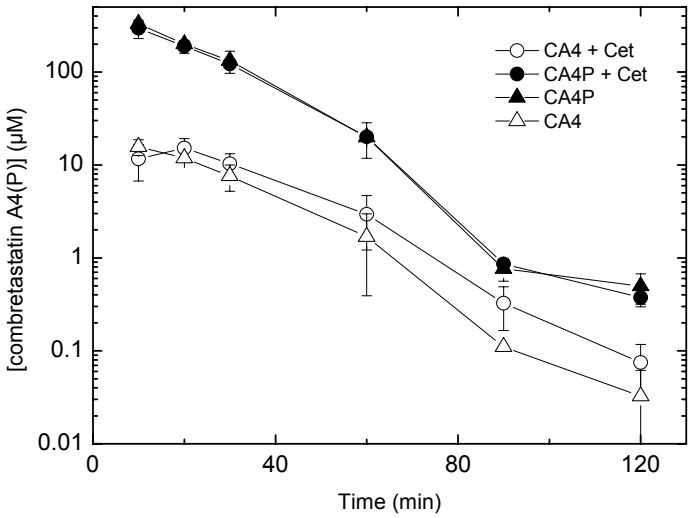

Figure 4.5

Plasma combretastatin A4 and combretastatin A4 phosphate concentrations, following CA4P 100mg/kg ip +/- cetuximab (Cet) 1mg ip every 3 days for 2 doses.

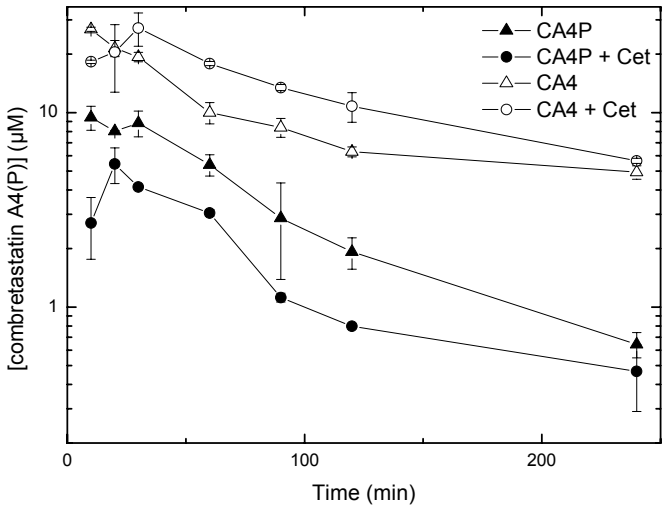

Figure 4.6

Tumour combretastatin A4 and combretastatin A4 phosphate concentrations, following CA4P 100mg/kg i.p. +/- cetuximab (Cet) 1mg ip every 3 days for 2 doses.

CHAPTER 5

Pathophysiological correlates of volumetric DCE-CT in resected lung cancers.

5.1 Aims

- To establish whether there is a relationship between volumetric dynamic contrast enhanced computed tomography (DCE-CT) measures of tumour vascularity and immunohistochemical assessment of tumour vascularity and hypoxia in resected NSCLC.
- To establish how volumetric DCE-CT measures of tumour vascularity correlate with clinico-pathological parameters: FDG-PET SUV and pathological stage

5.2 Introduction

In this chapter, the potential of volumetric DCE-CT as a biomarker of tumour angiogenesis and hypoxia is explored.

The structure and function of the vasculature contribute to the abnormal metabolic environment of hypoxia and acidosis that commonly exists in solid tumours, with hypoxic stress producing the upregulation of angiogenic factors ([Harris, 2002] [Allalunis et al., 1999], [Fukumura, Xu et al., 2001]). Hypoxia can also influence the response of solid tumours to treatment, as it significantly reduces radiosensitivity and also diminishes sensitivity to certain chemotherapeutic agents ([Gray et al.,

1953], [Koch et al., 2003]). Following the demonstration of improved survival with the addition of the anti-angiogenic agent, bevacizumab, to conventional chemotherapy in advanced NSCLC, the search for reliable markers to predict prognosis and monitor treatment has escalated (Sandler et al., 2006).

Immunohistochemistry can be used in the assessment of angiogenesis. However, although high microvessel density (MVD) count in surgically resected NSCLC has been shown to correlate with poor prognosis, a more recent meta-analysis did not confirm this finding ([Meert et al., 2002], [Tirella et al., 2007]). The traditional manual techniques for MVD counting are affected by subjectivity, with the use of different methodologies and the operator dependence of these techniques. Another potential confounding factor when using selected tumour sections or regions of interest for analysis, or through the use of biopsy material, is sampling error, as these may not be representative of the complex heterogeneity of the whole tumour.

DCE-CT provides information on both the vascular supply and vascular function of tumours. To date only a few studies in head and neck cancers, but not in lung cancers, have explored the relationship between DCE-CT parameters and immunohistochemical biomarkers of angiogenesis and hypoxia (Newbold et al., 2009). DCE-CT of the entire lung tumour volume, potentially, allows whole tumour vascularity and hypoxia to be assessed, and also to be compared with other clinicopathological prognostic biomarkers, such as FDG-PET SUV and pathological stage.

5.3 Methods

5.3.1 Patients and Treatments

All patients were recruited as part of the study, entitled “Phase 1b trial of CA4P (combretastatin A-4 phosphate), in combination with radiotherapy in patients with advanced cancer of the lung, head & neck or prostate: CA4P protocol number UKR104”. This trial commenced recruitment in January 2003 after receiving both local ethics and MHRA approval. Explicit approval for the exposure of patients to radiation for research purposes was granted, as required by IR(ME)R (Ionising Radiation (Medical Exposure) Regulations) legislation. Each patient gave written informed consent, prior to undergoing screening to determine suitability for participation in this study. A control cohort validating the use of volumetric DCE-CT in NSCLC, from this phase 1b clinical trial is examined in this chapter.

For the DCE-CT lung tumour control group the inclusion and exclusion criteria were defined as follows:

Inclusion Criteria

1) Cytologically or histologically confirmed lung cancer, or presumed lung cancer on the basis of imaging, suitable for surgical resection
2) Males or females, 18 years of age or older.
3) Able and willing to consent.

Exclusion Criteria

1) Routine exclusion criteria for CT including pregnancy and known reaction to intravenous contrast agent.

5.3.2 Treatment Group

Twenty consecutive consenting patients, within the inclusion criteria, presenting to Harefield Hospital, for surgical resection of lung cancer, either histologically confirmed or presumed on the basis of imaging, were prospectively recruited. All patients had undergone preoperative staging of their lung lesion with ^{18}FDG-PET/CT at Mount Vernon Hospital, performed as per section 2.3.2. PET/CT was performed within 4 weeks of the planned date for surgery.

5.3.3 Volumetric DCE-CT

Pre-operative DCE-CT was performed 24 hours prior to the planned date for surgery. These volumetric helical CT acquisitions (comprising an unenhanced and 8 post contrast breath-held acquisitions) encompassing the entire tumour were obtained as per section 2.3.1.1. Contiguous 5mm thick axial reformatted overlapping images were analysed on a pixel-by-pixel basis and tumour permeability surface area product (PS; ml/100ml/min), blood volume (BV; ml/100ml) and blood flow (BF; ml/100ml/min) were derived, using commercial software (Siemens Healthcare, Forchheim, Germany). Comparison between whole tumour values for DCE-CT and FDG-PET parameters was undertaken. To enable comparison with immunohistochemistry, 5mm thick axial reformatted images were selected, corresponding with each histological section obtained; this comparison was undertaken on a layer-by-layer basis. Immediately following completion of DCE-CT scanning, i.v. pimonidazole (0.5mg/m^2) was administered, as per section 2.2.4.

5.3.4 Histology

The post surgical re-inflated lung specimen was orientated into the same plane that would have existed in situ in vivo, and sectioned sequentially every 5 to 10mm, in the same plane as the axial DCE-CT images, as per section 2.5.1.

Immunohistochemical staining was undertaken, as per section 2.5.6, using a labelled polymer method for CD34, Glut-1 and pimonidazole, with up to 3 representative sections per tumour, matched to the DCE-CT images, as shown in Appendix A. The acquisition of digital histological section images (section 2.5.7), with the quantification of colour on a pixel-by-pixel basis (section 2.5.8), enabled analysis of immunohistochemical stain colour intensity to be undertaken, deriving the intensity of the stain and the stained tumour fraction, which is described as the relative vascular area (CD34) or hypoxic fraction (Glut-1, and pimonidazole).

5.3.5 Statistical analysis

This was undertaken as described in section 2.6.3. Correlation between DCE-CT parameters (PS, BV, and BF), FDG PET parameters (SUVmax) and immunohistochemical parameters (pimonidazole, Glut-1 and CD34 expression) were assessed by Spearman rank correlation. To determine the associations between DCE-CT parameters (PS, BV, and BF), FDG PET parameters (SUVmax) and clinico-pathological parameters (histological subtype, grade, stage and nodal status), the Mann-Whitney U-test was used. Statistical significance was defined by $p<0.05$.

5.4 Results

5.4.1 Patient and tumour characteristics

Six female and 14 male (mean age 64.4 years) patients underwent DCE-CT, demographics as shown in Table 5.1. Nineteen patients received pimonidazole; one patient did not receive this due to the temporary unavailability of drug. Two patients did not proceed to surgical resection due to the discovery of more advanced and unresectable disease prior to operation.

The time between CT and surgery was 18 to 24 hours for 14 of the 18 operated patients and was 3, 4, 6 and 9 days for the other 4 patients, giving a median difference of 1 day. Of those undergoing surgical resection one had benign bronchiectasis with squamous metaplasia, one had synovial sarcoma and 2 were found to have metastatic lung disease (colon and prostate). The remaining 14 patients, had early stage resectable NSCLC (8 squamous cell carcinomas and 6 adenocarcinomas), as shown in Table 5.1.

5.4.2 Tumour blood volume, vascularity and hypoxia

The Spearman rank correlations between BV and fraction stained for CD34, pimonidazole and Glut-1 are shown in Figure 5.1 and the data shown in Table 5.2. A significant negative correlation was seen between BV and pimonidazole fraction (ρ=-0.485, p=0.004). This demonstrated that low tumour BV, derived by volumetric DCE-CT, is closely linked to increased levels of tumour hypoxia, as defined by pimonidazole staining, in NSCLC. Neither CD34 fraction nor Glut-1 fraction correlated significantly with BV.

5.4.3 Tumour permeability surface area product, vascularity and hypoxia

The Spearman rank correlations between PS and fraction stained for CD34, pimonidazole and Glut-1 are shown in Figure 5.2 and the data shown in Table 5.2. A significant negative non-linear correlation was seen between PS and Glut-1 fraction (ρ=-0.496, p=0.002) suggesting that NSCLC tumours with low PS and reduced vascular permeability, are associated with upregulation of the intrinsic HIF-1 hypoxia pathway, and greater expression of the glucose transporter, Glut-1. Neither CD34 fraction nor pimonidazole fraction correlated significantly with PS.

5.4.4 Tumour blood flow, vascularity and hypoxia

There were no statistically significant non-linear correlations between BF and fraction stained for CD34, pimonidazole and Glut-1, as shown in Figure 5.3, with the data shown in Table 5.2.

5.4.5 Tumour maximum standard uptake value, vascularity and hypoxia

The Spearman rank correlations between maximum standard uptake value (SUVmax) and fraction stained, for CD34, pimonidazole and Glut-1, are shown in Figure 5.4 and the data shown in Table 5.2. A positive non-linear correlation between Glut-1 and SUVmax was observed (ρ=0.348, p=0.041), demonstrating an association between the amount of FDG uptake and the expression of Glut-1. A negative non-linear correlation between CD34 and SUVmax was observed (ρ=-0.331, p=0.049), consistent with greater uptake of FDG in poorly vascularised NSCLC tumours. However, no statistically significant correlations were seen between pimonidazole and SUVmax.

5.4.6 Tumour DCE-CT and PET parameters

The Spearman rank correlations between BV, PS, BF and SUVmax are shown in Figures 5.5 and 5.6, with the data shown in Table 5.3. A negative non-linear correlation between whole tumour PS and SUVmax was observed (ρ=-0.538, p=0.05). This, again, is in keeping with the greater uptake of FDG in vascularly compromised NSCLC tumours. No other significant correlations were seen.

The relationships between DCE-CT and pathological features of these NSCLC tumours were explored, and are shown in Table 5.4. PS was significantly lower in

squamous cell compared to adenocarcinoma (11.2 vs 17.0, p=0.043) and for SUVmax the opposite was true, with higher values in squamous cell carcinoma (18.0 vs 12.3, p=0.043). BF was significantly lower in stage I than stage II/III tumours (34.4 vs 51.0, p=0.008), and node negative (N0) versus node positive (N1/2) tumours (35.4 vs 52.7, p=0.016).

5.4.7 Qualitative and quantitative analysis of immunohistochemistry

The quality of staining was good in all cases and pimonidazole and Glut-1 staining were well demarcated from non-stained areas and varied in intensity (Median intensity value 0.12 [0.06 to 0.49] vs 0.15 [0.02 to 0.33]). A difference was observed in the pattern of staining between adenocarcinomas and squamous cell carcinomas (SCCs), as depicted in Figure 5.7. Relatively high staining of Glut-1 was observed in SCCs (7 out of 8 patients), in comparison to poorer Glut-1 staining in adenocarcinomas. This differed from pimonidazole staining where higher intensity was observed in adenocarcinomas (3 out of 5 patients), and poorer staining in squamous cell carcinomas. These findings were also reflected in the results for the fraction stained, where the median fraction stained for Glut-1 was 33% (7% to 77%) for SCCs and 14% (1% to 22%) for adenocarcinomas, and for pimonidazole was 13% (0% to 45%) for SCCs, compared to 38% (0% to 70%) for adenocarcinomas.

5.4.8 Immunohistochemical assessment of tumour vascularity and hypoxia

The Spearman rank correlations between the stained fractions of CD34, Glut-1 and pimonidazole are shown in Figure 5.8, with the data shown in Table 5.5. A significant negative non-linear correlation between pimonidazole fraction and CD34 fraction was observed (ρ=-0.370, p=0.031), suggesting that a reduction in the

relative vascular area of these NSCLC tumours is associated with increased tumour hypoxia. No other significant correlations were seen.

5.4.9 Fraction and intensity of immunohistochemical stain

The Spearman rank correlations between the stained fractions, average intensity and total intensity of CD34, Glut-1 and pimonidazole are shown in Figure 5.9, with the data shown in Table 5.6. For all three stains, significant positive non-linear correlations were observed between the total intensity of staining, the average intensity of staining and the fraction stained.

5.5 Discussion

The primary objective of this study was to explore the potential of volumetric DCE-CT parameters as biomarkers of tumour angiogenesis and hypoxia in NSCLC. Correlations with immunohistochemistry-derived measures of tumour vascularity and DCE-CT parameters have been demonstrated in various tumour types, including NSCLC, renal cell, oesophageal, gastric and colorectal carcinoma ([Ma et al., 2008], [Chen et al., 2009], [Jinzaki et al., 2000], [Wang et al., 2006], [Chen et al.,2010], [Yao et al., 2010], [Goh et al., 2008]). In NSCLC, the semi quantitative single level DCE-CT derived parameter (maximum attenuation value of time attenuation curves) was shown to be greater in NSCLC staining positive for VEGF (Tateishi et al., 2002). It was also shown to correlate with the average microvessel density (MVD), from 20 fields at 200x magnification, in these tumours.

In the assessment of solitary pulmonary nodules, semi-quantitative single level DCE-CT derived peak attenuation correlated with MVD, which was defined as the sum of vessel counts from 3 ‘hotspots’ within the nodule at 100x magnification (Yi et al., 2004). Further work examining the role for DCE-CT in the assessment of solitary

peripheral lung nodules has shown greater BF, BV and PS in malignant nodules, compared to either inflammatory or benign ones, as well as demonstrating a significant correlation between these three parameters and MVD (assessed by 'hotspot' counting) in VEGF positive NSCLC (Ma et al., 2008).

With regards to hypoxia, single level DCE-CT parameters have been examined in a small series of 7 patients with SCC of the head and neck, but no correlations were observed with either pimonidazole or CAIX staining, assessed using a visual scoring system based on estimates of percentage staining (Newbold et al., 2009). Similarly, in another head and neck cancer study with 67 patients, no correlation was observed between the DCE-CT derived tumour perfusion rate and the fraction stained for either Glut-1 or CAIX (De Schutter et al., 2005). However, these studies were technically limited to 2cm coverage at a selected level and, therefore, may not have encompassed the entire tumour. Some of these studies had only very small numbers (less than 10 patients) and all used a visual scoring system to quantify the extent of immunohistochemical staining, where observer variability can be a source of error. The study described in this chapter, is the first to demonstrate significant correlations between DCE-CT parameters and immunohistochemical staining of intra-tumoural hypoxia.

Hypoxia is an important factor in determining tumour response to treatment in NSCLC and in other cancers, by reducing radiosensitivity and sensitivity to some chemotherapeutic agents ([Gray et al., 1953], [Koch et al. 2003]). It is well established that increasing radiation doses are needed to gain equivalent cell kill at low tumour oxygen partial pressures ([Gray et al., 1953], [Rojas et al., 1990], [Grau et al., 1992]). Hypoxic tumour regions result from an imbalance between oxygen supply and consumption, which is caused by abnormal structure and function of the microvessels supplying the tumour (causing intermittent or cycling hypoxia),

increased diffusion distances between the feeding blood vessels and the tumour cells (causing chronic or diffusion-limited hypoxia), reduced O2 transport capacity of the blood due to the presence of anaemia and cellular proliferation ([Höckel and Vaupel, 2001], [Vaupel and Harrison 2004]). Hypoxia selects tumour cells resistant to apoptosis, more genetically unstable and of increased malignant, invasive and metastatic potential (Fukumura and Jain, 2007). It leads to the overexpression of hypoxia-inducible factor 1 (HIF-1), which activates the transcription of genes that are involved in angiogenesis, cell survival, glucose metabolism and invasion (Semenza, 2003). Angiogenesis, induced by hypoxia, contributes to malignant progression and enhances metastatic dissemination (Rofstad et al., 2010).

Pimonidazole, in addition to the other most commonly used 2-nitroimidazole (EF5), is regarded as a gold standard exogenous hypoxia marker. It is water soluble, stable, widely distributed in tissues, reflecting hypoxia at the time of its administration (both intermittent and chronic), and is capable of detecting levels of pO2 less than 10 mm Hg (Raleigh et al., 1999). The reduction and resultant activation of pimonidazole under hypoxic conditions results in the formation of stable protein adducts, which persist intracellularly (Azuma et al, 1997). Pimonidazole binding has been shown to correlate with oxygen electrode measurements of pO2 in C3H mammary tumours. However, in clinical studies of cervix carcinoma, a poor correlation has been observed between its measurements of hypoxia and microelectrode readings, which may be a reflection of the lack of metabolism of pimonidazole in necrotic cells ([Raleigh et al., 1999], [Nordsmark et al., 2003]). In our study we found a significant inverse correlation, between the pimonidazole fraction (often termed the hypoxic fraction or pHF) and DCE-CT derived BV. This finding is in keeping with a reduction in the functional vessel volume in tumour regions with increased chronic hypoxia, given that pimonidazole binding has been shown to mainly reflect chronic hypoxia (Rijken et al., 2000).

The results seen with pimonidazole in this study were not replicated with Glut-1, and no correlation between pimonidazole and Glut-1 was observed (p=0.898). Despite it's proven role as an endogenous hypoxia marker, controlled by the HIF-1 pathway and upregulated in hypoxic conditions promoting anaerobic glycolysis, Glut-1 is not hypoxia specific. In a study of HNSCC tumours, different geographic distributions of HIF-1α and pimonidazole were produced, indicating that HIF-1α might not be suitable as a marker for chronic hypoxia (Janssen et al 2002). Other studies in different tumour types have demonstrated areas of mismatch between pimonidazole and Glut-1 staining, with no significant correlation between them (van Laarhoven et al., 2006).

The expression of HIF-1α, and thus Glut-1, can be increased by factors other than hypoxia. Aerobic glycolysis, or the Warburg effect, is a well described phenomenon in malignant tumours (Warburg et al., 1927). Cancer cells exhibit increased glycolysis compared to normal cells even in aerobic conditions; with this evident by increased production of lactic acid, and resulting in an estimated 10% increase in ATP production (Koppenol et al., 2011). This has been attributed to oncogenic mutations in mitochondrial metabolic enzymes, such as fumarate hydratase and succinate dehydrogenase, producing increased levels of fumarate and succinate (King et al., 2006). Both of these are known to inhibit prolyl hydroxylases that are responsible for the oxygen-dependent modification of HIF1α and its degradation (Koppenol et al., 2011). HER2 and EGFR signalling have also been demonstrated to increase the rate of HIF1α protein synthesis under non-hypoxic conditions (Laughner et al., 2001). This increase in HIF1α is produced by HER2 or EGFR activation of the phosphatidylinositol-3 kinase/ Akt pathway, and the downstream FKBP-rapamycin-associated protein.

In this study, differences were observed between the subtypes of NSCLC, with a greater fraction stained with Glut-1 compared to pimonidazole in SCCs and a greater fraction stained with pimonidazole compared to Glut-1 in adenocarcinomas. This variation between tumour cell types may be a significant factor in the differences observed when comparing correlations between BV and PS and the hypoxic fractions, measured by pimonidazole and Glut-1. Other factors, which could contribute to a mismatch, include the requirement for intravenous administration and the potential for variations in uptake with pimonidazole, in comparison to the intrinsic expression of Glut-1.

Overexpression of Glut-1 has previously been shown to correlate with poor prognosis in NSCLC (Younes et al., 1997). Whilst no negative correlation was seen between Glut-1 and BV, a negative correlation was seen between Glut-1 and PS. Glut-1 is a well-described endogenous marker of hypoxia and Glut-1 score has been shown to correlate weakly ($r=0.28$; $p=0.04$) with pO_2 measured by Eppendorf electrodes in cervix carcinoma (Airely et al., 2001). In regions of intermittent or acute hypoxia (also described as cycling or perfusion limited hypoxia), HIF-1 activation produces increased expression of downstream molecules, including Glut-1. This is in contrast to pimonidazole binding, which is limited to the areas actually hypoxic at the time of administration. It is possible that the mismatch of staining and lack of correlation between Glut-1 and pimonidazole in this study of NSCLC tumours is due to Glut-1 staining reflecting a greater proportion of intermittent hypoxia. This points to the possibility that reduced functional tumour vascular leakage is associated with increased intermittent hypoxia, although the functional tumour vascular volume does not appear to significantly contribute to the process. This is in keeping with the effects on DCE-MRI parameters, observed with the inhibition of HIF-1alpha in preclinical tumour models, where dramatic decreases in the tumour permeability

surface area product were observed, with no significant change in tumour vascular volume (Jordan et al. 2005).

Glut-1 also had a significant positive correlation with SUVmax, confirming the relationship between FDG uptake in NSCLC and the expression of this glucose transporter. The demonstration of a significant negative correlation between SUVmax and PS further supports the interplay between these parameters. A strong correlation between Glut-1 expression and SUVmax has previously been reported in NSCLC ([Higashi et al., 2000], [Duan et al., 2008], [2007]). In a previous surgical series of stage I and II NSCLC, tumours with a high SUVmax showed greater expression of Glut-1, and a high SUVmax was shown to predict for reduced 2 year survival (van Baardwijk et al., 2007).

The digitisation of microscopic images, using computerised methods, has provided a means for the reproducible assessment of immunohistochemical staining of tissue, removing the observer variability that exists with non-digitised techniques. Despite some studies showing MVD counts to be a correlate for prognosis in NSCLC, this is an inconsistent finding ([Meert et al., 2002], [Tirella et al., 2007]). A variety of different techniques are used in studies using MVD and even when efforts to standardise this have been put in place, observer variability remains a factor. In this study the relative vascular area and hypoxic fraction for each entire tumour slice were computer derived, with only the delineation of the tumour region of interest (ROI) undertaken manually, by the same operator for all the tumours in the study. This utilised in-house digital microscopy software, and enabled the elimination of observer error, as well as a reduction in sampling error. Similar digitised techniques defining the relative or mean total vascular area, with vascular stains, such as CD34 or CD31, have been used increasingly as a measure of tumour vascularity in both preclinical studies, including mammary carcinoma and neuroblastoma models, and in clinical studies, including NSCLC, bladder and breast cancers ([Chantrain et

al.,2003], [Irion et al., 2003], [Irion et al., 2008], [Wester et al.,1999], [Sullivan et al., 2009]).

An unexpected finding from this study was the lack of significant correlation between the relative vascular area (CD34 fraction) and any of the DCE-CT parameters. In keeping with this finding, a recent preclinical study, where digital microscopic images were captured and analysed using ImageJ software from the National Institutes of Health in Bethesda, also failed to demonstrate a correlation between luminal vessel area and CT perfusion parameters, including BV, PS and BF (Park et al., 2009). In this chapter, significant negative correlations were demonstrated between relative vascular area (derived from CD34) and hypoxic fraction (derived from pimonidazole), confirming the known inverse relationship between microvessel density and hypoxia in tumours.

The comparison between immunohistochemistry and DCE-CT, especially when undertaken on a whole tumour basis, provides challenges. The reinflation of the resected specimen with formalin cannot accurately recreate the original size and shape in vivo and the process of paraffin embedding results in tissue shrinkage and distortion. In this study, paraffin-embedded sections of 4μm thickness were being compared to 5mm CT sections, the smallest section size thought to be feasible, without sacrificing the accuracy of this DCE-CT technique. To minimize the potential inaccuracies, we reorientated all of the resected lung specimens into the same positions as they had been in situ and then sections were cut in the same plane as the transaxial CT slices. Using the orientation of the slices obtained, (which was recorded at the time of cut up), and the stained slides, the CT slices to be used for comparison on the layer level were selected. Despite these efforts, inherent inaccuracies still exist, which have to be taken into account when interpreting the results from this study. For tumour BF, measurement was from a central 5mm

tumour slice only, due to technical limitations imposed by the CT scanner configuration (16 MDCT), and this prohibited both the multiple layer and whole tumour analysis used for the other DCE-CT and FDG-PET parameters.

In the assessment of lung tumour vascularity and hypoxia, CT holds advantages over MRI. With faster scan speeds, distortion from respiratory movement is less of a problem and, as with this study, it lends itself to the use of breath holding or respiratory-gated techniques, that enable sequential scans to be done in the same phase of respiration. This is in addition to the good spatial resolution it affords and the relatively straightforward quantification with DCE-CT. For extrathoracic disease sites, functional MRI techniques have been used successfully in the identification of intratumoural hypoxia, as detected by pimonidazole. Blood oxygen level dependent (BOLD)-MRI has been used in prostate cancer, where R(2)* displayed a high sensitivity, and a number of DCE-MRI parameters have shown statistically significant correlations in head and neck cancer ([Hoskin et al., 2007], [Newbold et al., 2009]). We have demonstrated in this study, that volumetric DCE-CT shows potential as a biomarker of intratumoural hypoxia in NSCLC.

The results from this study point towards the potential use of BV as a non-invasive biomarker of hypoxia in NSCLC, with uses such as monitoring the effects of novel targeted therapies, given alone or in combination with radiotherapy, and with conventional cytotoxic chemotherapies. There is also the possibility that this technique can be harnessed into the radiotherapy planning process, to identify hypoxic subvolumes within NSCLC tumours, which can then be targeted by dose painting techniques, delivering higher radiation doses to combat the relative radioresistance in these regions.

Both DCE-CT and FDG-PET parameters may be used to aid in the identification of poor prognosis tumours and provide further information for the stratification of patients prior to surgical resection or radiotherapy. The significant inverse correlation between PS and both Glut-1 and SUVmax, points to low values for whole tumour PS as an indicator of poor prognosis in NSCLC. Significant differences in PS and SUVmax, demonstrated between adenocarcinomas and squamous cell carcinomas, and the significantly greater BF, seen in higher stage and node positive NSCLC, compared to stage I and node negative cases respectively, also point to the use of these parameters as prognostic biomarkers in these tumours.

5.6 Conclusion

The data presented in this chapter has demonstrated the potential ability to quantify whole tumour hypoxia in NSCLC using volumetric DCE-CT; the parameter of BV correlates negatively with the hypoxic fraction, as defined by pimonidazole, and PS correlates negatively with the hypoxic fraction, as defined by Glut-1. The dependence of the FDG-PET parameter, SUVmax, on both Glut-1 and reduced tumour vascular leakage (PS) was highlighted. Differences were revealed between the subtypes of NSCLC, with greater staining of Glut-1 compared to pimonidazole in SCCs and the reverse picture seen with adenocarcinomas.

Using novel digitisation of microscope images, with in house software, the inverse relationship between the relative vascular area and hypoxic fractions in NSCLC were confirmed. However, no direct correlation between relative vascular area and any of the DCE-CT parameters was observed. This may be a consequence of the small numbers of patients in this study or due to the inherent inaccuracies of the technique: comparison between 4μm thick histological sections and 5mm CT sections; shrinkage and distortion of resected tissue; difficulties in selection of

corresponding CT slice; potential normal lung vasculature inclusion in DCE CT analysis.

To fully realise the potential of volumetric CT as a biomarker of intratumoural hypoxia in NSCLC, further work is required to see whether the same correlations are observed when examining small subvolumes of 5mm^3 or less. This would allow it to be utilised for dose painting techniques, in the planning of complex radiotherapy treatments. In providing accurate functional data on NSCLC, volumetric DCE-CT, in addition to FDG-PET, has the potential to be harnessed as a tool to aid the prognostic stratification of patients and selection for treatment.

Parameter	Number (%)
Histological subtype	
Adenocarcinoma	6 (43)
Squamous cell carcinoma	8 (57)
Grade	
2	8 (57)
3	6 (43)
Pathological stage	
IB	5 (36)
IIA	1 (7)
IIB	5 (36)
IIIA	3 (21)
Pathological nodes	
N0	6 (43)
N1	6 (43)
N2	2 (14)

Table 5.1

Staging and histopathological features of 14 resected NSCLC tumours.

A

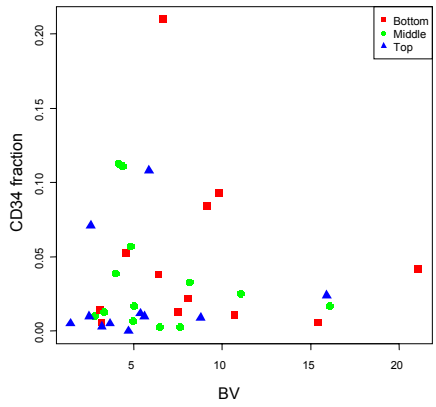

B

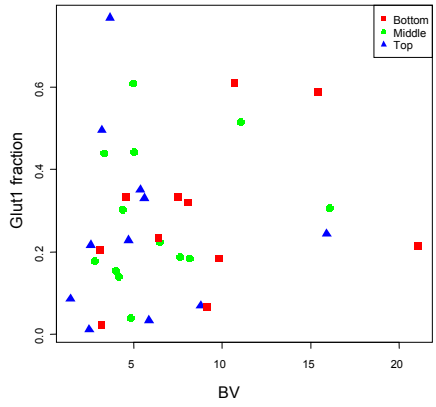

C

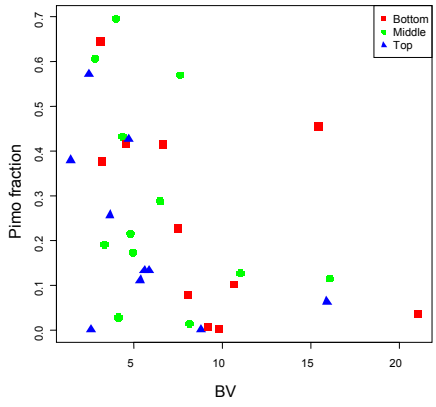

Figure 5.1

Correlation of mean DCE-CT derived blood volume (BV) with the fraction stained for 3 different immunohistochemical stains: **A** endothelial marker (CD34), **B** glucose transporter-1 (Glut-1) and **C** pimonidazole (Pimo).

A

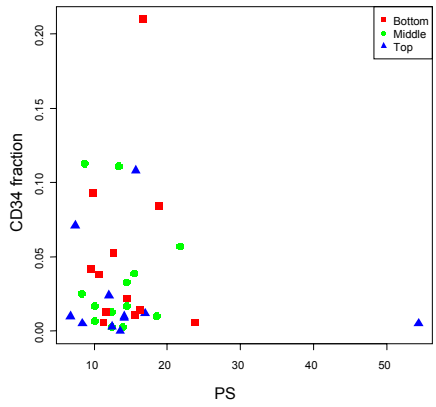

B

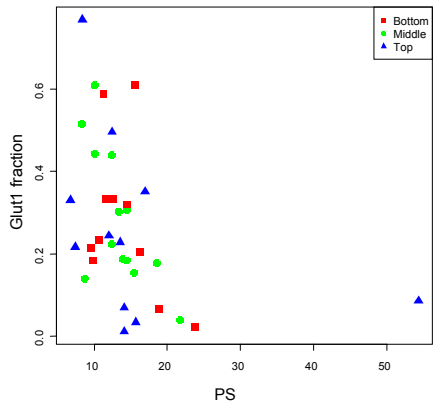

C

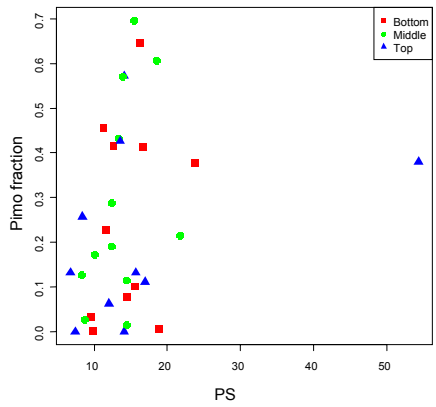

Figure 5.2

Correlation of mean DCE-CT derived permeability surface area product (PS) with the fraction stained for 3 different immunohistochemical stains: **A** endothelial marker (CD34), **B** glucose transporter-1 (Glut-1) and **C** pimonidazole (Pimo).

A

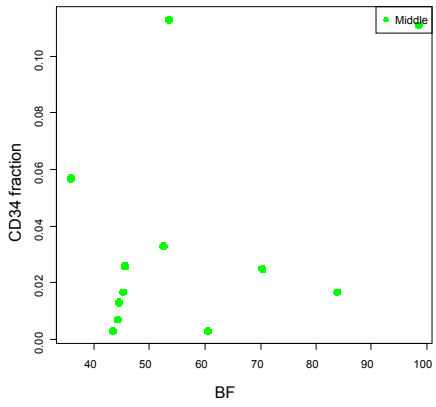

B

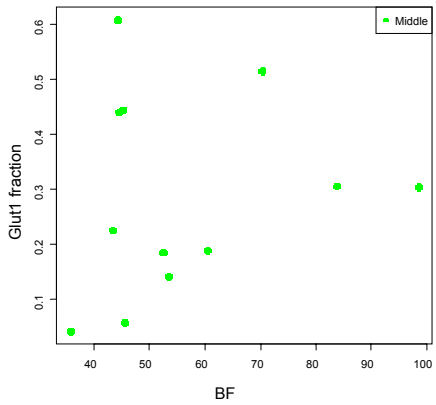

C

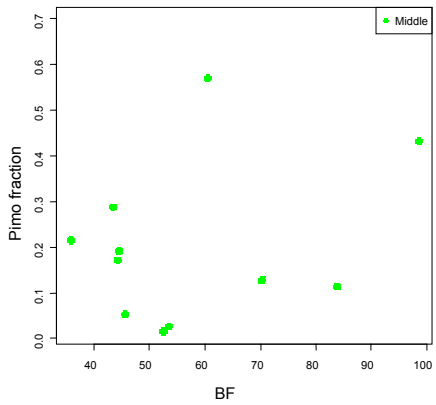

Figure 5.3

Correlation of mean DCE-CT derived blood flow (BF) with the fraction stained for 3 different immunohistochemical stains: **A** endothelial marker (CD34), **B** glucose transporter-1 (Glut-1) and **C** pimonidazole (Pimo).

A

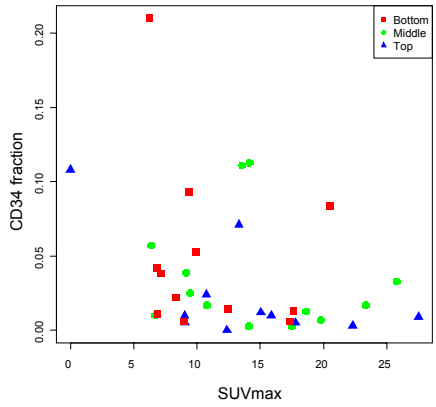

B

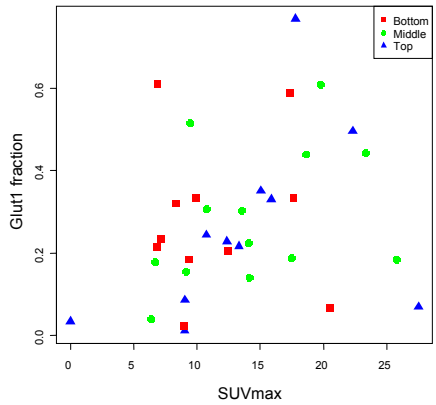

C

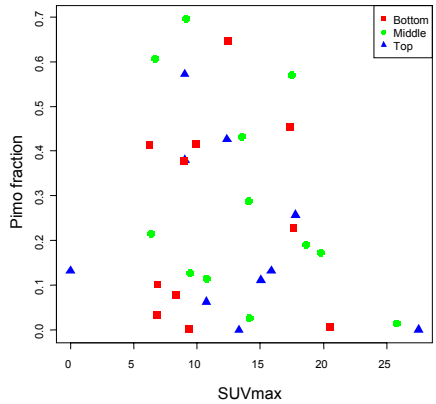

Figure 5.4

Correlation of maximum standard uptake value (SUVmax) with the fraction stained for 3 different immunohistochemical stains: **A** endothelial marker (CD34), **B** glucose transporter-1 (Glut-1) and **C** pimonidazole (Pimo).

	Pimo		Glut-1		CD34	
BV	ρ=-0.485	**p=0.004***	ρ=0.225	**p=0.194**	ρ=0.187	**p=0.274**
PS	ρ=0.278	**p=0.117**	ρ=-0.496	**p=0.002***	ρ=-0.031	**p=0.856**
BF	ρ=-0.055	**p=0.881**	ρ=0.133	**p=0.683**	ρ=0.291	**p=0.358**
SUVmax	ρ=-0.212	**p=0.235**	ρ=0.348	**p=0.041***	ρ=-0.331	**p=0.049***

*significant at 5% level

Table 5.2

Spearman rank correlations of mean DCE-CT derived blood volume (BV), permeability surface area product (PS), blood flow (BF) and maximum standard uptake value (SUVmax) with the fraction stained for 3 different immunohistochemical stains: endothelial marker (CD34), glucose transporter-1 (Glut-1) and pimonidazole (Pimo).

A

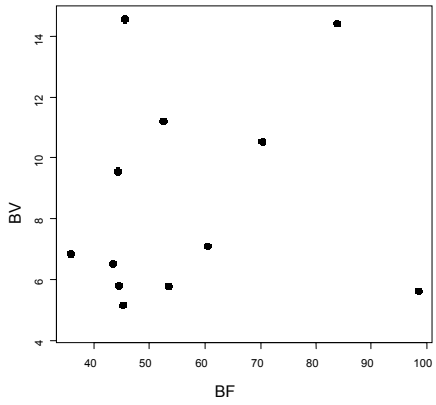

B

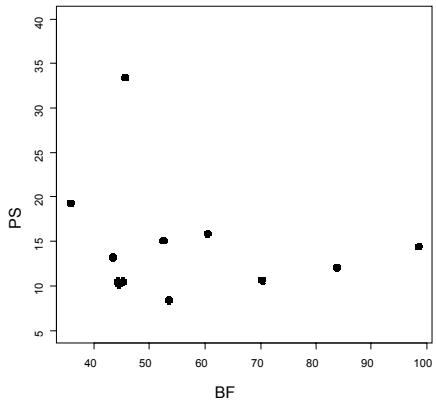

C

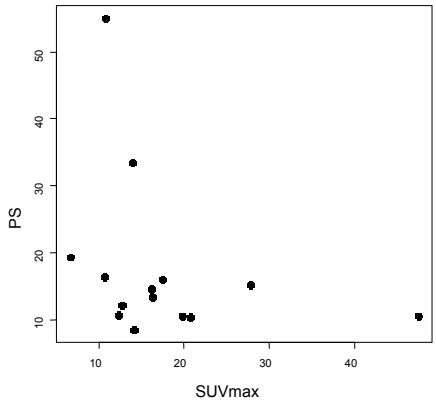

Figure 5.5

Correlation between the mean DCE-CT derived parameters: **A** blood flow (BF) and blood volume (BV), **B** blood flow (BF) and permeability surface area product (PS), and **C** blood volume (BV) and permeability surface area product (PS).

A

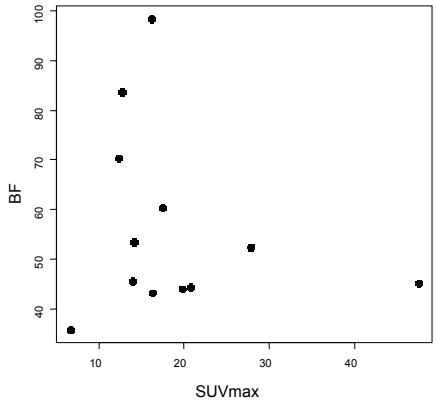

B

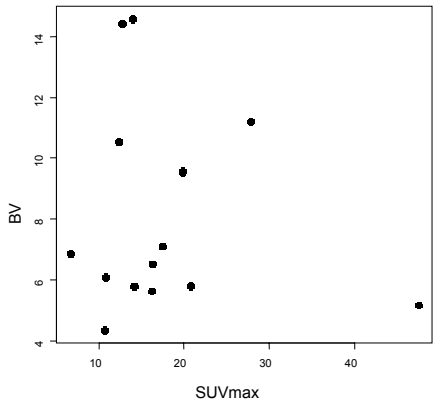

C

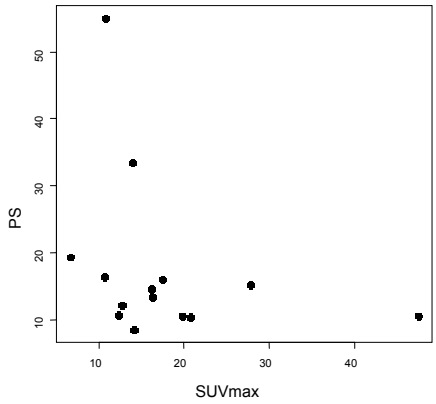

Figure 5.6

Correlation between maximum standard uptake value (SUVmax) and the mean DCE-CT derived parameters: **A** blood flow (BF), **B** blood volume (BV) and **C** permeability surface area product (PS).

	BV		PS		BF	
BV	-	-	ρ=0.218	**p=0.454**	ρ=0.126	**p=0.700**
PS	ρ=0.218	**p=0.454**	-	-	ρ=-0.014	**p=0.974**
BF	ρ=0.126	**p=0.700**	ρ=-0.014	**p=0.974**	-	-
SUVmax	ρ=-0.033	**p=0.916**	ρ=-0.538	**p=0.050***	ρ=-0.189	**p=0.558**

*significant at 5% level

Table 5.3

Spearman rank correlations between the mean DCE-CT derived parameters of blood flow (BF), blood volume (BV) and permeability surface area product (PS), and for each of these with maximum standard uptake value (SUVmax).

	BF	BV	PS	SUVmax
Histological subtype				
Adenocarcinoma	47.7 (15.9)	5.6 (2.4)	**17.0 (5.3)**	**12.2 (3.7)**
Squamous cell	41.0 (8.2)	7.9 (3.6)	**11.2 (1.9)**	**21.7 (11.6)**
Differentiation				
Moderate	49.4 (15.9)	6.6 (3.9)	14.0 (3.9)	19.1 (13.3)
Poor	41.6 (11.3)	7.4 (2.4)	13.3 (6.0)	15.6 (2.7)
Pathological stage				
I	**34.4 (3.9)**	6.0 (2.4)	16.3 (5.5)	13.6 (5.4)
II/III	**51.0 (13.7)**	7.4 (3.7)	12.2 (3.7)	19.8 (11.6)
Pathological nodes				
N0	**35.4 (4.0)**	6.7 (2.8)	15.8 (5.1)	16.0 (7.6)
N1/2	**52.7 (13.9)**	7.1 (3.7)	12.1 (4.0)	18.8 (12.0)

Table 5.4

Mean (standard deviation) DCE-CT and FDG-PET parameters according to the pathological features of resected NSCLC tumours. Significant Mann Whitney U Tests ($p<0.05$) are highlighted in bold.

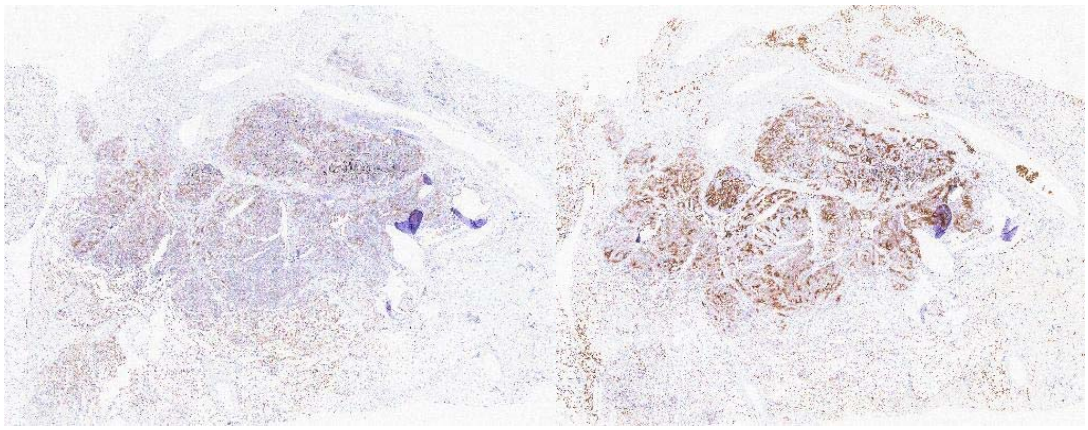

(i) Pimonidazole **(ii)** Glut-1

A Squamous Cell Carcinoma

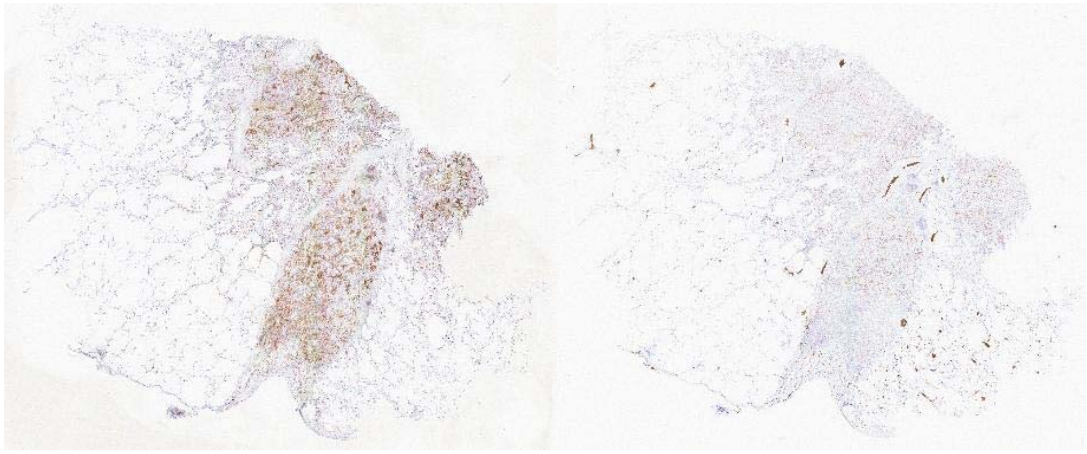

(i) Pimonidazole **(ii)** Glut-1

B Adenocarcinoma

Figure 5.7

Digital microscope images of immunohistochemical stained whole tumour sections from resected NSCLCs, showing the staining intensity for **(i)** Pimonidazole and **(ii)** Glut-1, in different tumour subtypes: **A** Squamous cell carcinoma; **B** Adenocarcinoma

A

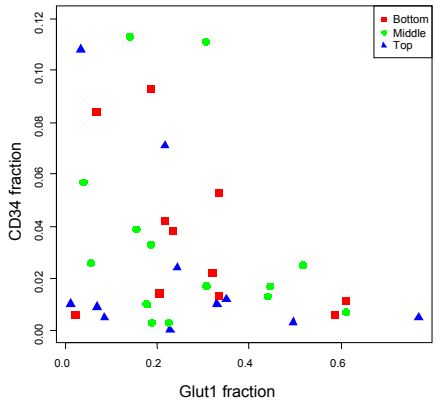

B

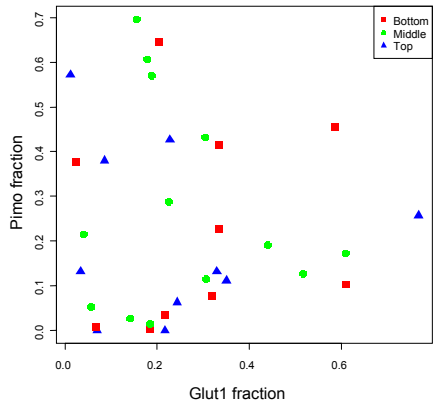

C

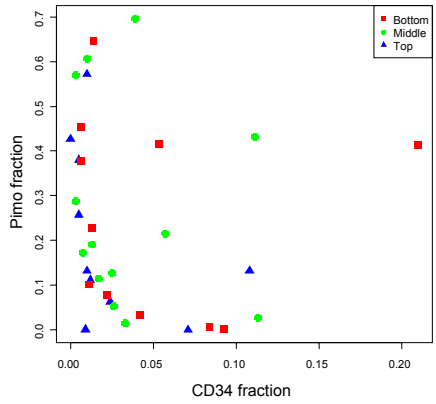

Figure 5.8

Correlation between 3 different immunohistochemical stains: **A** endothelial marker (CD34) and glucose transporter-1 (Glut-1), **B** pimonidazole (Pimo) and glucose transporter-1 (Glut-1) and **C** pimonidazole (Pimo) and endothelial marker (CD34).

	CD34 fraction		Glut1 fraction	
CD34 fraction	-	-	ρ=-0.276	**p=0.103**
Glut1 fraction	ρ=-0.276	**p=0.103**	-	-
Pimo fraction	ρ=-0.37	**p=0.031***	ρ=0.03	**p=0.868**

*significant at 5% level

Table 5.5

Spearman rank correlations between 3 different immunohistochemical stains: Endothelial marker (CD34), Glucose transporter-1 (Glut-1) and Pimonidazole (Pimo).

A

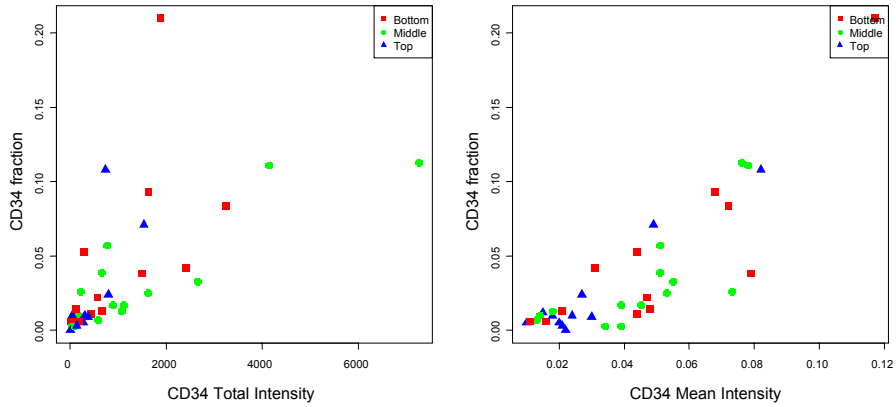

B

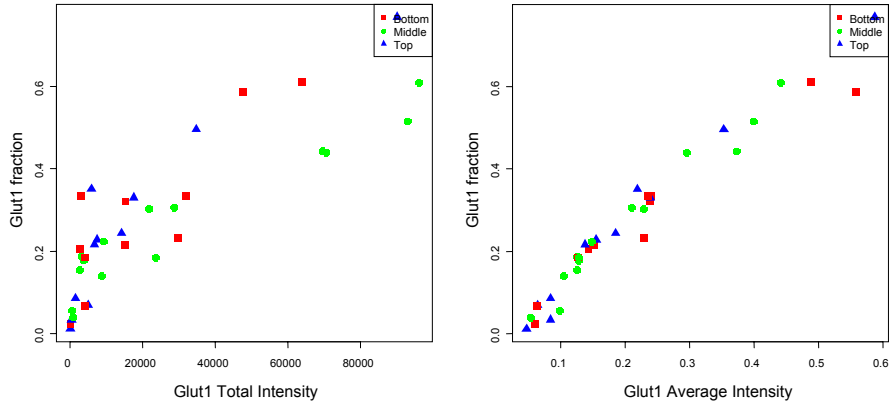

C

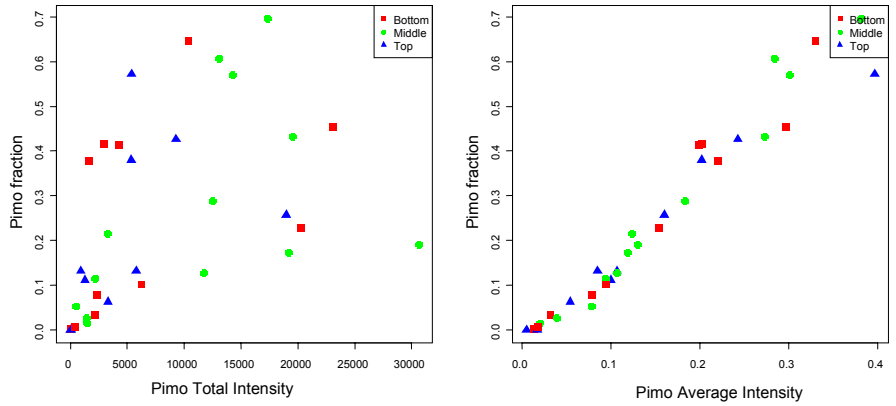

Figure 5.9

Correlation between the fraction stained, average intensity and total intensity for the 3 different immunohistochemical stains: **A** Endothelial marker (CD34), **B** Glucose transporter-1 (Glut-1) and **C** Pimonidazole (Pimo).

Fraction Stained	Total Intensity		Mean Intensity	
CD34	ρ=0.813	**p=0.000***	ρ=0.802	**p=0.000***
Glut1	ρ=0.863	**p=0.000***	ρ=0.982	**p=0.000***
Pimo	ρ=0.469	**p=0.000***	ρ=0.989	**p=0.000***

*significant at 5% level

Table 5.6

Spearman rank correlations between the fraction stained, average intensity and total intensity for the 3 different immunohistochemical stains: Endothelial marker (CD34), Glucose transporter-1 (Glut-1) and Pimonidazole (Pimo).

CHAPTER 6

Tumour vascular effects of combined vascular disruption and radiation in advanced NSCLC

6.1 Aims

- To determine the reproducibility and repeatability of the volumetric DCE-CT technique in assessing whole tumour vascular changes in advanced NSCLC.
- To determine tumour vascular effects of high dose palliative radiotherapy in combination with twice weekly combretastatin A-4 phosphate in advanced NSCLC, using volumetric DCE- CT.

6.2 Introduction

In this chapter, clinical experiments using DCE-CT assessment of the tumour vascular changes in patients receiving the VDA CA4P, in addition to radiotherapy, for advanced NSCLC are described.

Around 65% of cases of NSCLC present with advanced disease, either Stage IIIB or IV. Only 15 to 25% of cases are deemed to be potentially curable by surgical resection or radical radiotherapy (Lester et al., 2006). For the remainder of cases non-curative treatments and supportive care are the available treatment options, with radiotherapy commonly used as a palliative treatment. It was estimated in 1993 that in the UK 20-30% of cases of NSCLC received palliative radiotherapy (Maher et

al., 1993). Many different palliative radiotherapy doses and fractionations are currently in clinical use. A high dose palliative lung radiotherapy fractionation, delivering 27Gy in 6# over 3 weeks, has been developed at Mount Vernon Hospital, Middlesex, UK. In a retrospective study it was shown to have achieved symptomatic improvement in 48% of those treated; median survival was 8 months, 1 year overall survival was 27% and no grade 3 or 4 toxicities were observed (Corner et al., 2007). This radiotherapy fractionation was selected for use in this study as it lends itself to the planned escalation of CA4P dose intensity, from single dose up to twice weekly administration for the duration of the radiotherapy treatment.

It is well documented that timing, sequence and schedule are of particular importance when combining vascular directed therapies with radiotherapy. In preclinical studies, the administration of CA4P after or simultaneously with radiotherapy has been shown to improve tumour control, but when given prior to radiotherapy this beneficial effect was lost (Murata et al. 2001a). A twice weekly fractionation offers a minimum 72 hour recovery period after each dose of CA4P, therefore avoiding this potential negative effect, by allowing tumour cell reoxygenation following the acute CA4P-induced vascular shutdown. Volumetric DCE-CT has been used for all 3 NSCLC treatment cohorts in this phase IB study, to facilitate comparison of the whole tumour vascular effects, resulting from twice weekly CA4P scheduling with the weekly and single dose scheduling from the previous 2 cohorts.

6.3 Methods

6.3.1 Patient selection and recruitment

All patients were recruited as part of a “Phase 1b trial of CA4P (combretastatin A-4 phosphate) in combination with radiotherapy in patients with advanced cancer of the

lung, head & neck or prostate: CA4P protocol number UKR104"; the full inclusion and exclusion criteria of which are shown in Appendix B. Trial recruitment commenced in January 2003 following ethical and MHRA approval. Explicit approval for the exposure of patients to radiation for research purposes was granted, as required by the IR(ME)R (The Ionising Radiation (Medical Exposure) Regulations 2000) legislation. Each patient gave written informed consent, prior to undergoing screening to determine suitability for participation in this study.

The analysis of one cohort of the UKR-104 trial (cohorts 7) is reported in this chapter, the treatment scheduling of which is shown in Table 2.1. Patients with histologically proven advanced NSCLC (Cohort 7) deemed unsuitable for radical treatment, were prospectively recruited. Having fulfilled the criteria for inclusion in the study, patients proceeded to receive high dose hypofractionated palliative lung radiotherapy, 27Gy in six fractions over 3 weeks (as per section 2.2.1.1). This was delivered in combination with CA4P (as per section 2.2.2), 50mg/m^2 i.v., administered after every fraction of radiotherapy. Each patient was scheduled to receive a total of 6 doses of CA4P, the final dose level of a dose escalation study. Comparative analysis between the results from cohort 7 and the previously reported NSCLC cohorts 1 and 2 was undertaken. The first cohort (cohort 1) had received a single dose of CA4P, at a dose of 50mg/m^2 i.v. administered following the second fraction of radiotherapy only and cohort 2 had received weekly CA4P, 50mg/m^2 i.v. given after the second, fourth and sixth fractions of radiotherapy. Data from a further NSCLC radiotherapy alone cohort were also included when examining the impact of changes in technique reproducibility.

6.3.2 Imaging

DCE-CT was performed as described in section 2.3.1. Volumetric DCE-CT of the thorax (as per section 2.3.1.1) was selected to assess changes in lung tumour vascularity, on a whole tumour basis, resulting from the combination treatment described above. Eight DCE-CT scans were performed for cohort 7 as follows: 2 baseline pretreatment scans; further scans at 1 hour after radiotherapy (1 hour prior to administration of CA4P) and another at 4 hours after administration of CA4P were scheduled with the second, fourth and sixth fractions of radiotherapy and doses of CA4P.

6.3.3 Statistical analysis

Statistical comparison of changes in the DCE-CT derived parameters (blood volume and permeability surface area product) between time points were assessed using reproducibility analysis, as per section 2.3.1.3. To allow assessment of measurement reproducibility, the two initial pretreatment perfusion studies from each patient were analysed by the same observer for both studies, cross-referencing between studies from the same patient to ensure similar tumour levels. This reproducibility statistic enabled the calculation of whether a change in blood volume or permeability surface area product post treatment for an individual patient or a group of patients was statistically significant.

6.4 Results

6.4.1 Lung Volumetric DCE- CT

Six patients were treated in cohort 7: 3 males and 3 females, mean age 71 years (Range 61 to 83 years). The combination treatment was well tolerated, with no dose limiting toxicities (DLTs) produced. All of the six patients received the intended 6

fractions of radiotherapy, 6 doses of CA4P and underwent volumetric DCE-CT scanning as planned; there were 48 CT studies for analysis from the 6 patients treated. An example of the colour DCE-CT parametric maps for 1 patient is shown in Figure 6.1.

6.4.2 Reproducibility

The reproducibility statistics for both blood volume and permeability surface area product are shown in Table 6.1. These were derived from the baseline volumetric DCE-CT scans from 24 patients with NSCLC in the UKR-104 study; 6 patients in cohort 1, 4 patients in cohort 2, 6 patients in cohort 7 and 8 patients in a radiotherapy alone control group. The Kendall's tau test confirmed the proportionality of error on the mean value for both parameters, indicating dependence of error on the mean. As a result of this, both parameters were logarithmically transformed.

The percentage group change, in each parameter resulting from therapy, required to achieve significance at the 95% level, was calculated for the different cohort sizes. For blood volume a change greater than –21.5% to 27.4% was required for cohort 7 (n=6), a change greater than –18.9% to 23.4% for the combined cohorts 1 and 2 (n=8), and a change greater than –25.7% to 34.6% was required for cohort 2 alone (n=4). For permeability surface area product a change greater than –11.4% to 12.9% was required for cohort 7 (n=6), a change greater than –10.0% to 11.1% for the combined cohorts 1 and 2 (n=8), and a change greater than –13.8% to 16.0% required for cohort 2 alone (n=4).

6.4.3 Blood Volume

The blood volume (BV) results for the 6 patients in cohort 7 and the mean values and standard deviations for the cohort, at each of the time points where DCE-CT was performed, are shown in Tables 6.2 and 6.3. These results were then plotted to produce the graph seen in Figure 6.2.

In this cohort, following the second fraction of radiotherapy (2# RT), having received both the first fraction of radiotherapy and first dose of CA4P 3 days earlier, the mean blood volume increased significantly by 42.2%. Four of the 6 patients in the cohort had a rise in BV between these time points, yet only patient, BS37, had a significant individual increase (193.6%). A reduction in BV was seen for 4 patients after the second dose of CA4P (CA4P2), compared to 1 hour after the second fraction of radiotherapy. However, differing effects in BV were observed between these time points, with patient BS37 having a significant individual reduction of -57.5%, whereas patient JW35 had a significant individual rise of 110.9%. There were no significant individual changes after the second dose of CA4P compared to the mean baseline (MB). The only other group change observed that was significant on reproducibility testing was the change in blood volume after the sixth fraction of radiotherapy compared with 4 hours after the fourth dose of CA4P (CA4P4), with a mean increase of 36.8%.

Further significant individual changes in blood volume compared to previous time points were observed for patient JW35: a reduction of -48% at 4 hours after the fourth dose of CA4P, an increase of 259% after the sixth fraction of radiotherapy (6# RT) and a reduction of -50.7% at four hours after the sixth dose of CA4P (CA4P6). Again compared to previous time points, patient RD32 had a significant individual decrease of -74.3% after the sixth fraction of radiotherapy, and a significant

individual increase of 107.4%, 4 hours after the sixth dose of CA4P. Further to this, patient RD32 had a significant increase of 118.8% 4 hours after the fourth dose of CA4P, compared to mean baseline. The only other significant change seen was patient AA34 after the fourth fraction of radiotherapy, with a reduction of -47.1%, compared to mean baseline.

The blood volume (BV) results for 8 patients from cohorts 1 and 2, in addition to the group mean values for the combined cohorts, are shown in Tables 6.4 and 6.5. These results were then plotted to produce the graph seen in Figure 6.3. There were no significant group changes compared with either mean baseline or the previous time point, for any of the eight patients. The only significant individual change produced was a reduction of 46.9% compared to mean baseline, with patient HC07 at 1 hour after the sixth fraction of radiotherapy (6# RT).

6.4.4 Permeability surface area product

The permeability surface area product (PS) results for the 6 patients and the mean values and standard deviations for the cohort, at each of the time points where DCE-CT was performed, are shown in Tables 6.6 and 6.7. These results were then plotted to produce the graph seen in Figure 6.4.

A significant group increase of 20.3% in the whole tumour permeability surface area product was seen 1 hour after the second fraction of radiotherapy (2# RT), the patients having received both the first fraction of radiotherapy and first dose of CA4P 3 days earlier. Of the 6 patients in cohort 7, 4 had a rise in PS, with patient BS37 having a significant individual increase (77.8%), compared to mean baseline (MB), and one patient showing no change. At 4 hours after the second dose of CA4P (CA4P2) compared to after the second fraction of radiotherapy, PS was reduced for 5 out of the 6 patients, patient BS37 having a significant individual reduction of -

30%. However, patient RD32 was noted to have a significant rise (50%) at this time point, compared to after the second fraction of radiotherapy and mean baseline; these 2 values being identical.

After the fourth fraction of radiotherapy (4# RT), the patients having received 3 doses of CA4P previously, 4 of the 6 patients showed an increase in PS. The increase for patient JS33, was significant compared to 4 hours after the second dose of CA4P (35.5%) and also mean baseline (40%). However, a significant individual decrease in whole tumour PS (–33.3%), compared to 4 hours after the second dose of CA4P, was also observed at this time point for patient RD32. The only other significant group changes observed after this point were a rise of 14.8% at 4 hours after the fourth dose of CA4P (CA4P4) and a rise of 14.6% after the sixth dose of CA4P (CA4P6), both significant in comparison with mean baseline. Patient JW35 had a significant individual decrease in PS after the sixth fraction of radiotherapy (6# RT), compared with the previous time point (–27.3%) and with mean baseline (54.4%). At the same time point, a significant increase in PS was noted for patient AA34 (37.9%), in comparison to mean baseline, with this significant increase maintained at 4 hours after the subsequent sixth dose of CA4P. Patient AL31 had significant decreases in PS, compared to mean baseline, at 4 hours after the fourth dose of CA4P (-26.0%) and after the sixth fraction of radiotherapy (-39.7%).

The permeability surface area (PS) results for 8 patients from cohorts 1 and 2, in addition to the mean values for the combined cohorts, are shown in Tables 6.8 and 6.9. These results were then plotted to produce the graph seen in Figure 6.5. Significant group changes were seen 1 hour after the second fraction of radiotherapy (2# RT) compared to mean baseline (MB), with a 14.6% increase in whole tumour PS. A significant group increase of 18.9% was also produced 1 hour after the fourth fraction of radiotherapy (4#RT), compared to 4 hours after the first

dose of CA4P (CA4P1). Significant individual changes in PS were also observed in cohorts 1 and 2. Significant rises were seen in PS after the second fraction of radiotherapy, compared with mean baseline, for patients FR03 (45.3%) and SF06 (39.38%), although 4 hours after the first dose of CA4P they had changes in different directions, with a significant decrease (–31.4%) compared with the previous time point and a significant rise (74.1%) compared to mean baseline, respectively. Patient SD12 had a significant decrease in PS after the first dose of CA4P, compared to 1 hour after the second fraction of radiotherapy (-42.2%) and mean baseline (-34.9%). Following this decrease, patient SD12 then had a significant increase in PS of 49.8% 1 hour after the fourth fraction of radiotherapy (4# RT), compared with the previous time point. The only other significant individual change was patient HC07, where a reduction of –29.9% was seen after the sixth fraction of radiotherapy (6# RT) compared to 4 hours after the second dose of CA4P (CA4P2).

6.5 Discussion

Volumetric DCE-CT, an imaging biomarker of tumour vascularity, is being used increasingly to assess treatment related changes in tumour vasculature. DCE-CT has been used in this context in clinical trials of anti-angiogenic and other vascular directed therapies, including bevacizumab, endostatin, SU6668, L-NNA and the combination of AZD2171 and gefitinib ([Willett et al., 2004], [Thomas et al., 2004], [Xiong et al., 2004], [Ng et al., 2007c], [Meijerink et al., 2007]). Whole tumour measurements, have been made possible by novel volumetric techniques, which enable superior assessment of the spatial heterogeneity that exists within tumours.

Previously some early phase clinical trials utilising volumetric techniques have examined the vascular effects in NSCLC of radiotherapy alone and in combination with a single dose of CA4P ([Ng et al., 2007b], [Ng et al., 2007a]). In this work, we

have built upon these previous studies, assessing the changes resulting from treatment with radiotherapy and the increased dose intensity of CA4P: from single dose to weekly then twice weekly. Whilst this chapter focuses on the final cohort of 6 patients, within the whole UKR-104 study there were 24 NSCLC patients with the required two baseline scans, derived from 3 treatment and 1 control cohorts, from which reproducibility could be assessed, to determine the extent of treatment-related change required to indicate significance on an individual and group basis. This was done for whole tumour blood volume and permeability surface area product in the patients from the 3 treatment cohorts; with the increased number of patient data providing more accurate assessment of the intra-tumoural variability in derived parameters with the volumetric DCE-CT technique in NSCLC (Bland and Altman, 1996a,b,c). Given the marked heterogeneity that exists in tumour vascularity and blood flow between different tumours and in the same tumour at different time points, this is an important step. It also enables potential confounding patient factors, including variability in cardiac output or haemoglobin, to be taken into account. In addition to their role in the UKR-104 study, these measures of reproducibility will allow the significance of changes in volumetric DCE-CT parameters in NSCLC to be assessed in future studies utilising this technique at our centre.

For all the NSCLC treatment cohorts in this study, the first DCE-CT scan during treatment was performed after the second fraction of radiotherapy. This provides an interesting point for comparison as cohort 7 had already received a dose of CA4P following the first fraction of radiotherapy, whereas cohorts 1 and 2 had not received any prior CA4P. A significant group increase in blood volume was seen for cohort 7, yet not the first 2 cohorts. The only patient to have a significant individual rise in blood volume was also in cohort 7. Receiving a dose of CA4P 72 hours previously did not impede this increase in blood volume, which could be due to greater blood

flow in the remaining larger vessels, resulting from the smaller and more immature blood vessels of the tumour being damaged by CA4P (Tozer et al., 2001). This effect on tumour blood volume was not seen in cohort 2 after the fourth fraction of radiotherapy, when they had received a dose of CA4P 1 week previously. It would suggest that this improvement in tumour blood flow in larger vessels post CA4P is due to a transient functional change, with a return to the more chaotic vascular state after 1 week. However, it could be that, as only 4 patients had volumetric DCE-CT scans in cohort 2, a similar effect is produced but has not been detected due to the small sample size.

A different pattern was observed with permeability surface area product after the second fraction of radiotherapy. Significant group increases were seen in cohort 7 and also in cohorts 1 and 2, seemingly independent of whether they had received a previous dose of CA4P or not. A further significant group increase in permeability surface area product after the fourth fraction of radiotherapy was observed with cohorts 1 and 2, but was not seen in cohort 7 or in any of the cohorts after the sixth fraction of radiotherapy. This suggests that it is the first dose of concurrent CA4P that has the greatest effect, further enhancing the increase in permeability of the tumour vasculature resulting from radiotherapy. The diminishing of this effect with further doses of CA4P may arise from the loss of small blood vessels within the tumour, due to the CA4P-induced disruption of interphase microtubules in endothelial cells; these small vessels being more sensitive to its vascular disruptive effects (Tozer et al., 2001).

Indicative of the expected vascular shutdown produced by VDAs, individual decreases in whole tumour blood volume were produced at 4 hours following the administration of CA4P for 4 of the 6 patients in cohort 7 (after the second dose of CA4P) and 5 of the 8 patients in the combined cohorts 1 and 2 (after the first dose of

CA4P). Despite this, the only significant decreases were observed in cohort 7 and occurred in patients where significant individual increases in blood volume had been previously observed, following the commencement of radiotherapy. These findings are in keeping with sensitisation of the tumour vasculature to the effects of CA4P by radiotherapy, an effect that may be more pronounced in tumours sensitive to the effects of CA4P. Tumours with increased vascular permeability have been shown to be more susceptible to vascular disruptive therapies and in these experiments we have seen that radiotherapy increases both tumour blood volume and permeability (Beauregard et al., 2001). It is possible that these vascular changes reflect treatment-induced enhanced endothelial cell damage, adding support for combining CA4P and radiotherapy, especially as radiation-induced damage to the tumour vasculature is known to be an important determinant of tumour cell survival (Garcia-Barros et al., 2003).

In preclinical studies, CA4P has been shown to increase tumour vascular permeability through disruption of the molecular engagement of endothelial cell-specific junctional molecules, including VE-cadherin (Vincent et al., 2005). Significant rises in permeability surface area product after CA4P were seen with patients RD32 and JW35, followed by a significant decrease after the subsequent fraction of radiotherapy, yet patient BS37 displayed the exact opposite effect with a decrease after CA4P and a rise after radiotherapy. The twice weekly scheduling of concurrent CA4P (cohort 7) produced a significant rise in permeability surface area product for 5 of the 6 patients, compared with only 2 of the eight patients receiving a once weekly schedule of CA4P (cohorts 1 and 2). This difference is, however, not statistically significant and whether a true additive benefit is being observed with the more dose dense regimen remains uncertain.

6.5 Conclusion

In this experiment we were able to detect significant treatment-induced changes in both whole tumour blood volume and permeability surface area product in these cases of NSCLC. Through inclusion of DCE-CT data from 24 patients, we were able to accurately determine the reproducibility of the volumetric technique at our centre. We have observed a greater proportion of significant group increases in blood volume and permeability surface area product plus a greater number of significant changes in these parameters in cohort 7, with the twice weekly scheduling of CA4P combined with twice weekly fractions of radiotherapy, compared to the single dose and weekly scheduling used in cohorts 1 and 2 respectively. The increase seen in functional tumour vascular leakage after radiotherapy was, however, lost in the twice weekly scheduling of CA4P after the second fraction, and was only present with the weekly scheduling of CA4P after the fourth fraction.

Given the small number of patients in each treatment cohort, it is impossible to fully establish the significance of these observed differences. It is very likely that differences in tumour cell type, grade, stage and tumour volume may contribute to these findings. Our data would support the hypothesis that enhanced endothelial cell damage results from the combination of radiotherapy and concurrent administration of CA4P in advanced NSCLC, without any significant overlapping or enhanced acute toxicity. Further phase 2 studies are required to fully establish the role for this combination therapy in NSCLC, using either weekly CA4P at a dose of 50mg/m^2 for standard daily radiotherapy fractionations (5 days per week) or, potentially, twice weekly CA4P, at a dose of 50mg/m^2, if using a twice weekly radiotherapy fractionation, as in this study.

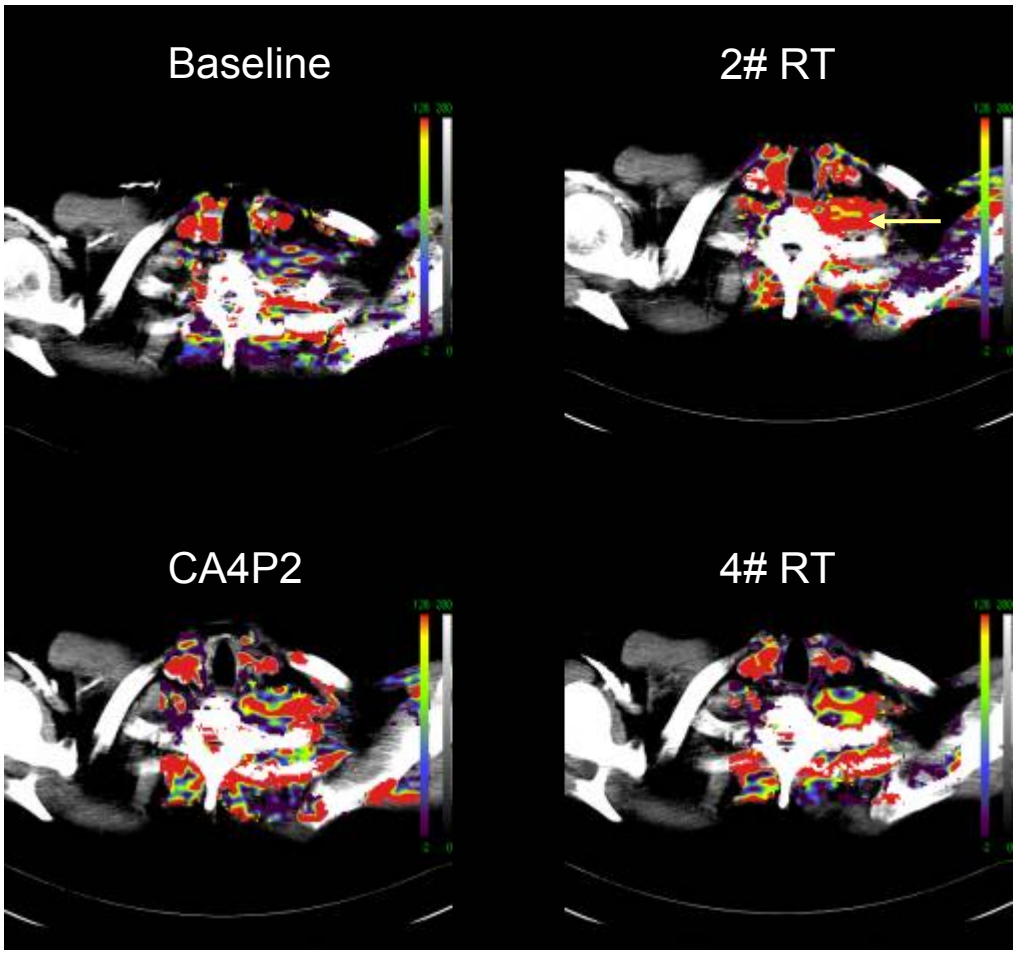

Figure 6.1

Colour parametric maps of DCE-CT derived whole tumour blood volume (BV) for patient BS37, who received twice weekly CA4P and RT, as part of Cohort 7. The yellow arrow points to the left apical lung primary tumour. An increase in blood volume (compared to baseline) is seen in the lung tumour 1 hour after the second fraction of radiotherapy (2# RT), then a decrease at 4 hours after the subsequent (second) dose of CA4P (CA4P2), on the same day. In comparison to CA4P2, only slight changes were observed in BV with the next DCE-CT scan, 1 hour after the fourth fraction of radiotherapy (4# RT).

	PS (ml/100ml/min)	BV (ml/100ml)
Mean (SD)	11.49 (4.05)	5.82 (2.14)
Mean difference	0.16	-1.19
95% limits of agreement	-25.7% to 34.5%	-44.8% to 81.1%
WSD	0.11[a]	0.21[a]
WCV (%)	11.3[a]	23.9[a]
Repeatability	0.30	0.59

[a]Ln transformed data

SD – standard deviation; WCV – within subject coefficient of variation; WSD – within subject standard deviation

Table 6.1

Reproducibility and repeatability statistics from paired studies performed on 24 patients, with NSCLC due to receive high dose palliative radiotherapy, measuring whole tumour permeability surface area product (PS) and blood volume (BV).

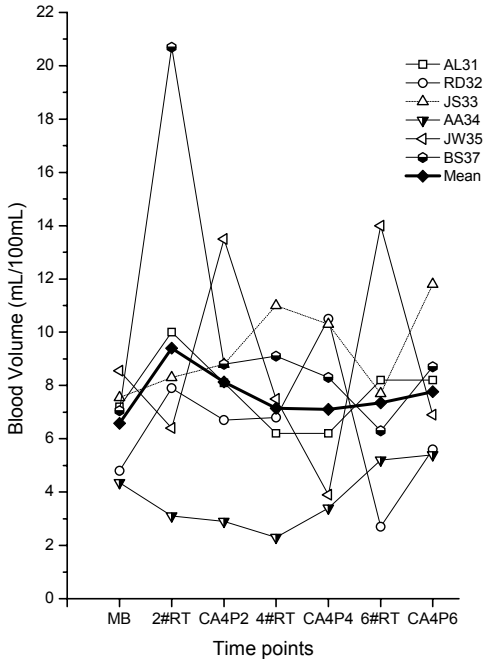

Figure 6.2

Graph of median whole tumour blood volume for NSCLC patients receiving twice weekly CA4P and RT (Cohort 7), plotted at the following time points: MB- mean baseline; 2# RT- 1 hour after second fraction of radiotherapy; CA4P2 – 4 hours after the second dose of CA4P; 4# RT- 1 hour after fourth fraction of radiotherapy; CA4P4 – 4 hours after the fourth dose of CA4P; 6# RT- 1 hour after sixth fraction of radiotherapy; CA4P6 – 4 hours after the sixth dose of CA4P.

	MB	2# RT	*change (%)*	CA4P2	*change (%)*	4# RT	*change (%)*
AL31	7.20	10.00	*38.89*	8.10	*12.50*	6.20	*-13.89*
RD32	4.8	7.90	*64.58*	6.70	*39.58*	6.80	*41.67*
JS33	7.55	8.30	*9.93*	8.80	*16.56*	11.00	*45.70*
AA34	4.35	3.10	*-28.74*	2.90	*-33.33*	2.30	***-47.13***[a]
JW35	8.55	6.40	*-25.15*	13.50	*57.89*	7.50	*-12.28*
BS37	7.05	20.70	***193.62***[a]	8.80	*24.82*	9.10	*29.08*
Mean	6.58	9.40	***42.19***[b]	8.13	*19.67*	7.15	*7.19*

	CA4P4	*change (%)*	6# RT	*change (%)*	CA4P6	*change (%)*
AL31	6.20	*-13.89*	8.20	*13.89*	8.20	*13.89*
RD32	10.50	***118.75***[a]	2.70	*-43.75*	5.60	*16.67*
JS33	10.30	*36.42*	7.70	*1.99*	11.80	*56.29*
AA34	3.40	*-21.84*	5.20	*19.54*	5.40	*24.14*
JW35	3.9	***-54.39***[a]	14	*63.74*	6.9	*-19.30*
BS37	8.30	*17.73*	6.30	*-10.64*	8.70	*23.40*
Mean	7.10	*13.80*	7.35	*7.46*	7.77	*19.18*

[a]*Significant individual change in BV* [b]*Significant group change in BV*

MB- mean baseline; 2# RT- 1 hour after second fraction of radiotherapy; CA4P2 – 4 hours after the second dose of CA4P; 4# RT- 1 hour after fourth fraction of radiotherapy; CA4P4 – 4 hours after the fourth dose of CA4P; 6# RT- 1 hour after sixth fraction of radiotherapy; CA4P6 – 4 hours after the sixth dose of CA4P.

Table 6.2

DCE-CT derived median blood volume (BV) values (ml/100ml) and percentage change from mean baseline for NSCLC patients receiving twice weekly CA4P and RT (UKR104 cohort 7).

	MB	2# RT	*change (%)*	CA4P2	*change (%)*	4# RT	*change (%)*
AL31	7.20	10.00	*38.89*	8.10	*-19.00*	6.20	*-23.46*
RD32	4.8	7.90	*64.58*	6.70	*-15.19*	6.80	*1.49*
JS33	7.55	8.30	*9.93*	8.80	*6.02*	11.00	*25.00*
AA34	4.35	3.10	*-28.74*	2.90	*-6.45*	2.30	*-20.69*
JW35	8.55	6.40	*-25.15*	13.50	***110.94***[a]	7.50	*-44.44*
BS37	7.05	20.70	***193.62***[a]	8.80	***-57.49***[a]	9.10	*3.41*
Mean	6.58	9.40	***42.19***[b]	8.13	*3.14*	7.15	*-9.78*

	CA4P4	*change (%)*	6# RT	*change (%)*	CA4P6	*change (%)*
AL31	6.20	*0.00*	8.20	*32.26*	8.20	*0.00*
RD32	10.50	*54.41*	2.70	***-74.29***[a]	5.60	***107.41***[a]
JS33	10.30	*-6.36*	7.70	*-25.24*	11.80	*53.25*
AA34	3.40	*47.83*	5.20	*52.94*	5.40	*3.85*
JW35	3.9	***-48.00***[a]	14	***258.97***[a]	6.9	***-50.71***[a]
BS37	8.30	*-8.79*	6.30	*-24.10*	8.70	*38.10*
Mean	7.10	*6.51*	7.35	***36.76***[b]	7.77	*25.31*

[a]*Significant individual change in BV* [b]*Significant group change in BV*

MB- mean baseline; 2# RT- 1 hour after second fraction of radiotherapy; CA4P2 – 4 hours after the second dose of CA4P; 4# RT- 1 hour after fourth fraction of radiotherapy; CA4P4 – 4 hours after the fourth dose of CA4P; 6# RT- 1 hour after sixth fraction of radiotherapy; CA4P6 – 4 hours after the sixth dose of CA4P.

Table 6.3

DCE-CT derived median blood volume (BV) values (ml/100ml) and percentage change from previous time point for NSCLC patients receiving twice weekly CA4P and RT (UKR104 cohort 7).

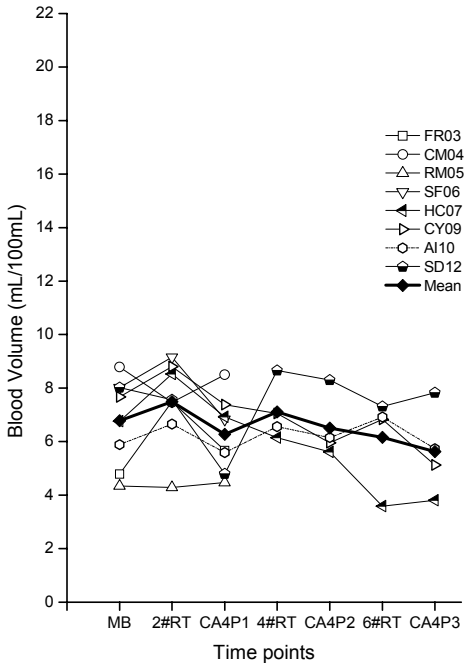

Figure 6.3

Graph of median whole tumour blood volume for NSCLC patients receiving single dose or weekly CA4P and RT (Cohorts 1 + 2), plotted at the following time points: MB- mean baseline; 2# RT- 1 hour after second fraction of radiotherapy; CA4P1 – 4 hours after the first dose of CA4P; 4# RT- 1 hour after fourth fraction of radiotherapy; CA4P2 – 4 hours after the second dose of CA4P; 6# RT- 1 hour after sixth fraction of radiotherapy; CA4P3 – 4 hours after the third dose of CA4P.

	MB	2# RT	*change (%)*	CA4P1	*change (%)*
FR03	4.79	7.50	*56.58*	5.67	*18.37*
CM04	8.79	7.47	*-15.02*	8.50	*-3.30*
RM05	4.34	4.29	*-1.15*	4.47	*3.00*
SF06	8.02	9.16	*14.29*	6.83	*-14.78*
HC07	6.76	8.53	*26.18*	6.93	*2.51*
CY09	7.67	8.81	*14.86*	7.38	*-3.78*
AI10	5.89	6.66	*13.17*	5.59	*-5.01*
SD12	8.02	7.57	*-5.55*	4.80	*-40.11*
Mean	6.78	7.50	*12.92*	6.27	*-5.39*

	4# RT	*change (%)*	CA4P2	*change (%)*	6# RT	*change (%)*	CA4P3	*change (%)*
HC07	6.15	*-9.02*	5.62	*-16.86*	3.59	***-46.89***[a]	3.81	*-43.64*
CY09	7.05	*-8.08*	5.96	*-22.29*	6.83	*-10.95*	5.13	*-33.12*
AI10	6.56	*11.47*	6.15	*4.50*	6.92	*17.59*	5.74	*-2.46*
SD12	8.66	*8.05*	8.30	*3.56*	7.31	*-8.80*	7.83	*-2.31*
Mean	7.11	*0.60*	6.51	*-7.77*	6.16	*-12.26*	5.63	*-20.38*

[a]*Significant individual change in BV* [b]*Significant group change in BV*

MB- mean baseline; 2# RT- 1 hour after second fraction of radiotherapy; CA4P1 – 4 hours after the first dose of CA4P; 4# RT- 1 hour after fourth fraction of radiotherapy; CA4P2 – 4 hours after the second dose of CA4P; 6# RT- 1 hour after sixth fraction of radiotherapy; CA4P3 – 4 hours after the third dose of CA4P.

Table 6.4

DCE-CT derived median blood volume (BV) values (ml/100ml) and percentage change from mean baseline for NSCLC patients receiving single dose and weekly CA4P and RT (UKR104 cohorts1+2).

	MB	2# RT	*change (%)*	CA4P1	*change (%)*
FR03	4.79	7.50	*56.58*	5.67	*-24.40*
CM04	8.79	7.47	*-15.02*	8.50	*13.79*
RM05	4.34	4.29	*-1.15*	4.47	*4.20*
SF06	8.02	9.16	*14.29*	6.83	*-25.44*
HC07	6.76	8.53	*26.18*	6.93	*-18.76*
CY09	7.67	8.81	*14.86*	7.38	*-16.23*
AI10	5.89	6.66	*13.17*	5.59	*-16.07*
SD12	8.02	7.57	*-5.55*	4.80	*-36.59*
Mean	6.78	7.50	*12.92*	6.27	*-14.94*

	4# RT	*change (%)*	CA4P2	*change (%)*	6# RT	*change (%)*	CA4P3	*change (%)*
HC07	6.15	*-11.26*	5.62	*-8.62*	3.59	*-36.12*	3.81	*6.13*
CY09	7.05	*-4.47*	5.96	*-15.46*	6.83	*14.60*	5.13	*-24.89*
AI10	6.56	*17.35*	6.15	*-6.25*	6.92	*12.52*	5.74	*-17.05*
SD12	8.66	*80.42*	8.30	*-4.16*	7.31	*-11.93*	7.83	*7.11*
Mean	7.11	*20.51*	6.51	*-8.62*	6.16	*-5.23*	5.63	*-7.18*

[a]*Significant individual change in BV* [b]*Significant group change in BV*

MB- mean baseline; 2# RT- 1 hour after second fraction of radiotherapy; CA4P1 – 4 hours after the first dose of CA4P; 4# RT- 1 hour after fourth fraction of radiotherapy; CA4P2 – 4 hours after the second dose of CA4P; 6# RT- 1 hour after sixth fraction of radiotherapy; CA4P3 – 4 hours after the third dose of CA4P.

Table 6.5

DCE-CT derived median blood volume (BV) values (ml/100ml) and percentage change from previous time point for NSCLC patients receiving single dose and weekly CA4P and RT (UKR104 cohorts1+2).

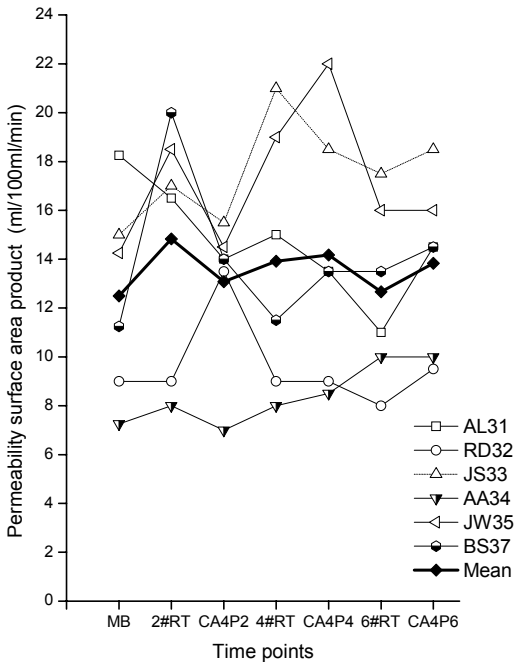

Figure 6.4

Graph of median whole tumour permeability surface area product for NSCLC patients receiving twice weekly CA4P and RT (Cohort 7), plotted at the following time points: MB- mean baseline; 2# RT- 1 hour after second fraction of radiotherapy; CA4P2 – 4 hours after the second dose of CA4P; 4# RT- 1 hour after fourth fraction of radiotherapy; CA4P4 – 4 hours after the fourth dose of CA4P; 6# RT- 1 hour after sixth fraction of radiotherapy; CA4P6 – 4 hours after the sixth dose of CA4P.

	MB	2# RT	*change (%)*	CA4P2	*change (%)*	4# RT	*change (%)*
AL31	18.25	16.50	*-9.59*	14.00	*-23.29*	15.00	*-17.81*
RD32	9.00	9.00	*0.00*	13.50	***50.00***[a]	9.00	*0.00*
JS33	15.00	17.00	*13.33*	15.50	*3.33*	21.00	***40.00***[a]
AA34	7.25	8.00	*10.34*	7.00	*-3.45*	8.00	*10.34*
JW35	14.25	18.50	*29.82*	14.50	*1.75*	19.00	*33.33*
BS37	11.25	20.00	***77.78***[a]	14.00	*24.44*	11.50	*2.22*
Mean	12.50	14.83	***20.28***[b]	13.08	*8.80*	13.92	*11.35*

	CA4P4	*change (%)*	6# RT	*change (%)*	CA4P6	*change (%)*
AL31	13.50	***-26.03***[a]	11.00	***-39.73***[a]	14.50	*-20.55*
RD32	9.00	*0.00*	8.00	*-11.11*	9.50	*5.56*
JS33	18.50	*23.33*	17.50	*16.67*	18.50	*23.33*
AA34	8.50	*17.24*	10.00	***37.93***[a]	10.00	***37.93***[a]
JW35	22.00	***54.39***[a]	16.00	*12.28*	16.00	*12.28*
BS37	13.50	*20.00*	13.50	*20.00*	14.50	*28.89*
Mean	14.17	***14.82***[b]	12.67	*6.01*	13.83	***14.57***[b]

[a]*Significant individual change in PS* [b]*Significant group change in PS*

MB- mean baseline; 2# RT- 1 hour after second fraction of radiotherapy; CA4P2 – 4 hours after the second dose of CA4P; 4# RT- 1 hour after fourth fraction of radiotherapy; CA4P4 – 4 hours after the fourth dose of CA4P; 6# RT- 1 hour after sixth fraction of radiotherapy; CA4P6 – 4 hours after the sixth dose of CA4P.

Table 6.6

DCE-CT derived permeability surface area product (PS) values (ml/100ml/min) and percentage change from mean baseline for NSCLC patients receiving twice weekly CA4P and RT (UKR104 cohort 7).

	MB	2# RT	*change (%)*	CA4P2	*change (%)*	4# RT	*change (%)*
AL31	18.25	16.50	*-9.59*	14.00	*-15.15*	15.00	*7.14*
RD32	9.00	9.00	*0.00*	13.50	***50.00***[a]	9.00	***-33.33***[a]
JS33	15.00	17.00	*13.33*	15.50	*-8.82*	21.00	***35.48***[a]
AA34	7.25	8.00	*10.34*	7.00	*-12.50*	8.00	*14.29*
JW35	14.25	18.50	*29.82*	14.50	*-21.62*	19.00	*31.03*
BS37	11.25	20.00	***77.78***[a]	14.00	***-30.00***[a]	11.50	*-17.86*
Mean	12.50	14.83	***20.28***[b]	13.08	*-6.35*	13.92	*6.13*

	CA4P4	*change (%)*	6# RT	*change (%)*	CA4P6	*change (%)*
AL31	13.50	*-10.00*	11.00	*-18.52*	14.50	*31.82*
RD32	9.00	*0.00*	8.00	*-11.11*	9.50	*18.75*
JS33	18.50	*-11.90*	17.50	*-5.41*	18.50	*5.71*
AA34	8.50	*6.25*	10.00	*17.65*	10.00	*0.00*
JW35	22.00	*15.79*	16.00	***-27.27***[a]	16.00	*0.00*
BS37	13.50	*17.39*	13.50	*0.00*	14.50	*7.41*
Mean	14.17	*2.92*	12.67	*-7.44*	13.83	*10.61*

[a]*Significant individual change in PS* [b]*Significant group change in PS*

MB- mean baseline; 2# RT- 1 hour after second fraction of radiotherapy; CA4P2 – 4 hours after the second dose of CA4P; 4# RT- 1 hour after fourth fraction of radiotherapy; CA4P4 – 4 hours after the fourth dose of CA4P; 6# RT- 1 hour after sixth fraction of radiotherapy; CA4P6 – 4 hours after the sixth dose of CA4P.

Table 6.7

DCE-CT derived permeability surface area product (PS) values (ml/100ml/min) and percentage change from previous time point for NSCLC patients receiving twice weekly CA4P and RT (UKR104 cohort 7).

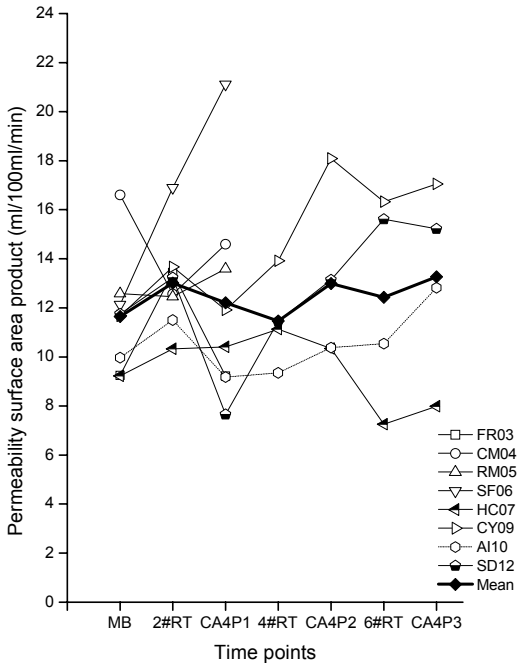

Figure 6.5

Graph of median whole tumour permeability surface area product for NSCLC patients receiving single or weekly CA4P and RT (Cohorts 1 + 2), plotted at the following time points: MB- mean baseline; 2# RT- 1 hour after second fraction of radiotherapy; CA4P1 – 4 hours after the first dose of CA4P; 4# RT- 1 hour after fourth fraction of radiotherapy; CA4P2 – 4 hours after the second dose of CA4P; 6# RT- 1 hour after sixth fraction of radiotherapy; CA4P3 – 4 hours after the third dose of CA4P.

	MB	2# RT	*change (%)*	CA4P1	*change (%)*
FR03	9.25	13.44	***45.30***[a]	9.22	*-0.32*
CM04	16.60	12.56	*-24.34*	14.59	*-12.11*
RM05	12.58	12.46	*-0.91*	13.59	*8.07*
SF06	12.13	16.90	***39.38***[a]	21.11	***74.10***[a]
HC07	9.23	10.33	*11.98*	10.41	*12.85*
CY09	11.68	13.67	*17.09*	11.91	*2.01*
AI10	9.97	11.50	*15.35*	9.18	*-7.92*
SD12	11.75	13.23	*12.60*	7.65	***-34.89***[a]
Mean	11.65	13.01	***14.55***[b]	12.21	*5.22*

	4# RT	*change (%)*	CA4P2	*change (%)*	6# RT	*change (%)*	CA4P3	*change (%)*
HC07	11.13	*20.65*	10.34	*12.09*	7.25	*-21.41*	7.99	*-13.39*
CY09	13.92	*19.23*	18.09	*54.95*	16.33	*39.87*	17.05	*46.04*
AI10	9.35	*-6.22*	10.38	*4.11*	10.54	*5.72*	12.82	*28.59*
SD12	11.46	*-2.47*	13.14	*11.83*	15.61	*32.85*	15.22	*29.53*
Mean	11.47	*7.80*	12.99	*20.74*	12.43	*14.26*	13.27	*22.69*

[a]*Significant individual change in PS* [b]*Significant group change in PS*

MB- mean baseline; 2# RT- 1 hour after second fraction of radiotherapy; CA4P1 – 4 hours after the first dose of CA4P; 4# RT- 1 hour after fourth fraction of radiotherapy; CA4P2 – 4 hours after the second dose of CA4P; 6# RT- 1 hour after sixth fraction of radiotherapy; CA4P3 – 4 hours after the third dose of CA4P.

Table 6.8

DCE-CT derived permeability surface area product (PS) values (ml/100ml/min) and percentage change from mean baseline for NSCLC patients receiving single dose and weekly CA4P and RT (UKR104 cohorts1+2).

	MB	2# RT	*change (%)*	CA4P1	*change (%)*
FR03	9.25	13.44	***45.30***[a]	9.22	***-31.40***[a]
CM04	16.60	12.56	*-24.34*	14.59	*16.16*
RM05	12.58	12.46	*-0.91*	13.59	*9.07*
SF06	12.13	16.90	***39.38***[a]	21.11	*24.91*
HC07	9.23	10.33	*11.98*	10.41	*0.77*
CY09	11.68	13.67	*17.09*	11.91	*-12.87*
AI10	9.97	11.50	*15.35*	9.18	*-20.17*
SD12	11.75	13.23	*12.60*	7.65	***-42.18***[a]
Mean	11.65	13.01	***14.55***[b]	12.21	*-6.96*

	4# RT	*change (%)*	CA4P2	*change (%)*	6# RT	*change (%)*	CA4P3	*change (%)*
HC07	11.13	*6.92*	10.34	*-7.10*	7.25	***-29.88***[a]	7.99	*10.21*
CY09	13.92	*16.88*	18.09	*29.96*	16.33	*-9.73*	17.05	*4.41*
AI10	9.35	*1.85*	10.38	*11.02*	10.54	*1.54*	12.82	*21.63*
SD12	11.46	***49.80***[a]	13.14	*14.66*	15.61	*18.80*	15.22	*-2.50*
Mean	11.47	***18.86***[b]	12.99	*12.13*	12.43	*-4.82*	13.27	*8.44*

[a]*Significant individual change in PS* [b]*Significant group change in PS*

MB- mean baseline; 2# RT- 1 hour after second fraction of radiotherapy; CA4P1 – 4 hours after the first dose of CA4P; 4# RT- 1 hour after fourth fraction of radiotherapy; CA4P2 – 4 hours after the second dose of CA4P; 6# RT- 1 hour after sixth fraction of radiotherapy; CA4P3 – 4 hours after the third dose of CA4P.

Table 6.9

DCE-CT derived permeability surface area product (PS) values (ml/100ml/min) and percentage change from previous time point for NSCLC patients receiving single dose and weekly CA4P and RT (UKR104 cohorts1+2).

CHAPTER 7

Tumour vascular effects of combined vascular disruption, EGFR inhibition and radiation in Head and Neck cancer.

7.1 Aims

- To determine tumour vascular effects, using single level perfusion CT in Head and Neck squamous cell carcinoma, of radical radiotherapy in combination with weekly combretastatin A-4 phosphate and cetuximab.
- To detect changes in cytokine production and blood composition in patients with Head and Neck squamous cell carcinoma receiving radical radiotherapy in combination with weekly combretastatin A-4 phosphate and cetuximab.

7.2 Introduction

This chapter contains details of clinical experiments using DCE-CT to assess the tumour vascular changes resulting from the administration of the VDA CA4P, in addition to radiotherapy and the EGFR inhibitor, cetuximab, in patients with SCCs of the head and neck region.

In the treatment of locally advanced SCC of the head & neck, radiotherapy is commonly employed, either preoperatively or postoperatively. Whilst hyperfractionated and accelerated regimens have been extensively studied, the

standard fractionation used in the UK is 2Gy per fraction for 6.5 to 7 weeks. However, radiotherapy alone is no longer the standard of care for the treatment of this patient group. A large meta-analysis, using individual patient data, most recently updated in 2009, examining the use of cisplatin-based chemotherapy in head and neck cancer has shown a more pronounced benefit with concomitant chemotherapy compared to induction chemotherapy, producing a hazard ratio of death of 0.81 ($p<0.0001$) and an absolute benefit 6.5% at 5 years (Pignon et al., 2009). Concomitant cetuximab has also been shown to improve outcome in locally advanced head and neck cancer, producing a median overall survival of 49 months compared to 29.3 months for radiotherapy alone; hazard ratio of 0.74 ($p=0.03$) (Bonner et al., 2006).

As previously discussed in Chapter 4, there have been preclinical studies that have demonstrated enhanced anti-tumour effects with the addition of a VDA to combined radiotherapy and EGFR inhibition ([Bozec et al., 2006], [Raben et al., 2004]). In the experiments described in Chapter 4, using the head and neck squamous cell carcinoma (HNSCC) tumour model FaDu, enhanced anti-tumour effect was observed with cetuximab, CA4P and radiotherapy; this combination being the only treatment to produce significant tumour growth delay compared to radiation alone. As part of a phase Ib study, we undertook to determine whether this triple combination was tolerable in the clinical setting and to explore the resultant effects on the tumour vasculature, using DCE-CT imaging and circulatory biomarkers.

7.3 Methods

7.3.1 Patient selection and recruitment

All patients were recruited as part of the study entitled “Phase Ib trial of CA4P (combretastatin A-4 phosphate) in combination with radiotherapy in patients with advanced cancer of the lung, head & neck or prostate: CA4P protocol number UKR104”. The full inclusion and exclusion criteria in the UKR-104 protocol for all cohorts receiving treatment with radiotherapy and CA4P are listed in Appendix B. The analysis of one cohort of this phase 1b clinical trial is examined in this chapter, the treatment scheduling of which is shown in Table 2.1. It was intended that 6 patients would be treated in each of the treatment cohorts, provided the combination treatment was well tolerated and no dose limiting toxicities (DLTs) were observed. The stopping criteria were defined as 2 patients in a single cohort experiencing DLTs.

Patients with histologically confirmed squamous cell carcinoma of the head and neck, suitable for radical treatment, were prospectively recruited; fulfilling the criteria for inclusion in the study, they proceeded to receive radical radiotherapy to the head and neck, 64 to 70Gy in 32 to 35 fractions over 6.5 to 7 weeks (as per section 2.2.1.2). This was delivered in combination with CA4P (as per section 2.2.2), 50mg/m2 i.v. after the final fraction of radiotherapy each week; it was intended that each patient was to receive a total of 7 doses of CA4P. Concurrent cetuximab was also delivered, as per section 2.2.3, with a loading dose given one week prior to radiotherapy and further doses given weekly for the duration of radiotherapy.

7.3.2 Imaging

Single level DCE-CT was used to assess changes in tumour vascularity, resulting from these combination therapies, using the technique described in section 2.3.1.

Up to 9 DCE-CT scans were performed at the following time points: 2 baseline pretreatment scans; 4 to 6 days after loading dose of cetuximab on the day of but prior to first fraction of radiotherapy; 1 hour after the final fraction of radiotherapy in the first week (1 hour prior to administration of CA4P), 4 hours after the first dose of CA4P and 72 hours after the first dose of CA4P; 1 hour after the final fraction of radiotherapy in week 5 (1 hour prior to administration of CA4P), with further CTs at 4 hours and 72 hours after the subsequent dose of CA4P.

7.3.3 Blood sampling

Following the insertion of a cannula, into a suitable forearm vein, 10 mls of blood was collected in EDTA tubes for full blood count and to provide plasma samples for ELISA (as per section 2.4). Blood samples were taken at four designated time points with the first dose of CA4P administered: preCA4P, 4 hours post CA4P, 6 to 8 hours post CA4P and 1 week post CA4P.

7.3.4 Statistical analysis

Statistical comparison of changes in blood count and cytokine parameters, between time points, were assessed using a paired samples t-test, as per section 2.6.4.

7.4 Results

7.4.1 Head and Neck Single Level DCE- CT

Four patients were treated in this cohort, 3 males and 1 female, mean age 73 years (range 65 to 86 years). DLTs of myocardial ischaemia were observed in the third and fourth patients treated, after the third and fourth doses of CA4P respectively, which fulfilled the stopping criteria for the cohort, therefore no further patients were treated. Only the first patient in the cohort received the intended 7 doses of CA4P,

the third and fourth patients only receiving 3 and 4 doses respectively. These three patients completed the planned radiotherapy and cetuximab treatment. The second treated patient developed aspiration pneumonia, attributed to his radical radiotherapy, and whilst an inpatient with this problem, he experienced a fall, resulting in a fractured neck of femur. As a result of these complications the second patient received only 4 doses of CA4P (on weeks 1,2,3 and 5) and did not complete the intended radiotherapy or cetuximab treatments.

There were 21 studies for analysis from 3 patients (6 studies each for the first and third patients and 9 studies for the second patient). The final three DCE-CT scans for the first patient were performed in the final week of the radiotherapy treatment, when it was noted that due to the complete response of his primary tumour no further measurements could be taken. Subsequently, there was rescheduling of the final 3 scans for the following patients in the cohort, initiating them at the end of the fifth week of radiotherapy. For the second patient the DCE-CT scans were undertaken as per the new schedule but the final scans were performed at the end of the fifth week with the fourth dose of CA4P, as the patient had missed one dose of CA4P in the previous week. The third patient did not have scans in the fifth week as the CA4P had been discontinued; due to the previously stated observed toxicity. The final patient in the cohort received her treatment as an adjuvant, with no residual macroscopic disease and was therefore not suitable for DCE-CT assessment of response. An example of the colour DCE-CT parametric maps for 1 patient is shown in Figure 7.1.

Due to only 3 patients having DCE-CT scanning, it was not possible to use reproducibility statistics to reliably ascertain the significances of any changes seen in the DCE-CT parameters. Descriptive analysis of the observed changes was

therefore undertaken. The changes in all parameters measured for the group mean and individual patients are summarised on Table 7.1.

7.4.2 Blood Volume

The median blood volume (BV) results for the 3 patients and the mean values for the cohort, at each of the time points where DCE-CT was performed, are shown in Tables 7.2 and 7.3. These results were then plotted to produce the graph seen in Figure 7.2.

No real change of any magnitude was seen in median tumour BV at 4 to 5 days after the loading dose of cetuximab (Cet) or 1 hour after the fifth fraction of radiotherapy (5#RT). A variable response was observed at 4 hours after the first dose of CA4P; patient JC36 had an individual increase of 84%, compared to mean baseline, and of 123.7%, compared to after the fifth fraction of radiotherapy, whereas the other 2 patients had decreases of –40.8% and –28.0% compared to mean baseline. Patient HC38 had an increase in BV of 127.9% at 72 hours after the first dose of CA4P (CA4P1), compared to 4 hours after the same dose of CA4P, although again JC36 showed changes in the other direction with a decrease of –47.5%. HC38 had a further large increase of 95.2% at 1 hour after the twenty-fifth fraction of radiotherapy (25#RT), compared to mean baseline.

7.4.3 Permeability surface area product

The median permeability surface area product (PS) results for the 3 patients and the mean values for the cohort, at each of the time points where DCE-CT was performed, are shown in Tables 7.4 and 7.5. These results were then plotted to produce the graph seen in Figure 7.3.

At 4 to 5 days after the loading dose of cetuximab (Cet) and prior to the first fraction of radiotherapy, a reduction in group mean PS was produced of -10.2%, compared to mean baseline (MB). At this time point, patient GK39 had an individual decrease in PS of -40.0%, patient HC38 had a decrease of lesser magnitude and patient JC36 actually had an increase of 19.7%, all compared to mean baseline. After the fifth fraction of radiotherapy (5#RT) there was a 20.3% increase in the group mean PS, compared to the previous time point (after the loading dose of cetuximab), with an increase of 42.3% seen with patient JC36 and of 25.0% with patient HC38. As seen before, a variation in response was observed; GK39 having a decrease of –43.9%, compared to patient JC36 who had an increase of 70.3%, both compared to mean baseline.

Four hours after the first dose of CA4P (CA4P1), patient JC36 had an individual increase in PS of 110% compared to mean baseline and 20% compared to 1 hour after the fifth fraction of radiotherapy. Although this remained raised at 72 hours after the first dose of CA4P and prior to the sixth fraction of radiotherapy (72h 1), compared to mean baseline (104.4%), there was, in fact, a small decrease compared to the previous time point. There were small increases in the group mean PS at 4 hours (16.0%) and 72 hours (18.7%) after the first dose of CA4P. At these two time points patient GK39 had individual decreases in permeability surface area product; at 4 hours after CA4P a decrease of -57.6% compared to mean baseline and a decrease of –24.5% compared to 1 hour after the fifth fraction of radiotherapy, and then at 72 hours a decrease of –51.9% compared to mean baseline.

At 1 hour after the twenty-fifth fraction of radiotherapy (25#RT) for patient HC38, there was an increase in PS compared to both mean baseline (25.3%) and 72 hours after the first dose of CA4P (21%). There were further individual increases for this patient at 4 hours after the fourth dose of CA4P of 55.3 % compared with mean

baseline and 24.0% compared with 1 hour after the twenty-fifth fraction of radiotherapy. Finally, at 72 hours after the fourth dose of CA4P, PS increased further to 82.15ml/100ml; a relatively large increase compared to mean baseline (75.6%), but no real change compared with the previous time point, 4 hours after the fourth dose of CA4P.

7.4.4 Blood Flow

The median blood flow (BF) results for the 3 patients and the mean values for the cohort, at each of the time points where DCE-CT was performed, are shown in Tables 7.6 and 7.7. These results were then plotted to produce the graph seen in Figure 7.4.

At 4 to 6 days after administration of the loading dose of cetuximab (Cet), patient GK39 demonstrated an individual increase in BF of 169.3% compared with mean baseline (MB). Despite no sizable changes observed with the 2 other patients, a group mean increase of 48.5% was still produced. After the fifth fraction of radiotherapy (5#RT), despite a slight reduction in blood flow for patient GK39 compared with the previous time point, there was an individual increase for this patient (131.3%) and a group mean increase (55.1%) in blood flow compared to mean baseline. At four hours after the first dose of CA4P, there were comparatively large individual reductions in BF compared with 1 hour after the fifth fraction of radiotherapy seen for 2 patients: patient HC38 (-57.1%) and patient GK39 (-63.5%). This reduction in BF was not seen for all patients at this time point, with patient JC36 having a significant individual increase compared with 1 hour after the fifth fraction of radiotherapy (95.5%) and mean baseline (91.7%). Following this, the individual increase in BF of greatest magnitude observed in this study was patient HC38 at 4 hours after the fourth dose of CA4P, compared with 1 hour after the twenty-fifth

fraction of radiotherapy, with an increase of 87.2%. No other large individual or group changes in BF were observed.

7.4.5 Blood Testing

All four patients in cohort 6 underwent blood testing. Blood samples for first patient, JC36, were delayed and collected with the sixth dose of CA4P. The final three patients treated in the cohort all had sampling as planned, with the first dose of CA4P.

7.4.6 Full Blood Count

The results from the full blood count testing, undertaken for all four head and neck patients are shown in Table 7.8. The results for white cell count, neutrophil count, lymphocyte count and monocyte count, including the mean values, were then plotted to produce the graphs seen in Figures 7.5, 7.6, 7.7 and 7.8 respectively.

All four patients demonstrated significant increases at 6 hours, compared to pre CA4P, in total white blood cells with a mean increase of 3.45 ($p=0.0151$), and neutrophils with a mean increase of 3.8 ($p=0.0152$). This compared to 4 hours after CA4P, when although there was an increase in the mean white cell and neutrophil counts, 2 patients (HC38 and GK39) in fact had a decrease in both of these parameters and these mean increases were not significant on paired t-testing (Figures 7.5 and 7.6). At 1 week post CA4P, both the white cell and neutrophil counts had decreased significantly compared with 6 to 8 hours after CA4P, with mean decreases of 4.5 ($p=0.0031$) and 4.6 ($p=0.0033$) respectively. There were no other significant decreases in these parameters between the various time points when samples were collected.

A significant reduction in lymphocyte count was seen at 4 hours after CA4P compared to preCA4P (Figure 7.7); a mean reduction of 0.275 (p=0.0222). At 4 hours after CA4P all four patients had a decrease in lymphocyte count. There was a further reduction in the lymphocyte count for patient GK39 but an increase for JC36, between 4 hours and 6 to 8 hours, returning to the same level as preCA4P. The lymphocyte counts for the other 2 patients between these time points were unchanged and paired t-testing at 6 to 8 hours compared to preCA4P revealed only a non-significant trend towards a sustained decrease at 6 to 8 hours (p=0.0632). The monocyte count also significantly changed following administration of CA4P with a mean increase of 0.25 (p=0.0154) between 4 hours and 6 to 8 hours after CA4P; this rise being produced in all four patients (Figure 7.8). At 4 hours after CA4P compared to preCA4P, a mean decrease of -0.3 was produced, with 3 patients having a decrease in monocyte count, although patient JC36 had a small increase, which was not statistically significant (p=0.1343). The same three patients had an increase between 4 hours and 1 week after CA4P, but, once again, their response differed from patient JC36, who had no change in the monocyte count between these time points, producing a mean increase of 0.25; a non-significant trend towards a sustained increase in monocyte count at 1 week (p=0.0632). No other significant changes in blood parameters, including basophils and eosinophils (data not shown in tables), were seen over the study time period.

7.4.7 ELISA

The results from the ELISA testing for the cytokines VEGF, VEGFR-1, G-CSF and SDF-1 are shown in Table 7.9. These results, including the mean values, were then plotted for each of the cytokines, to produce the graphs seen in Figures 7.9, 7.10, 7.11 and 7.12 respectively.

A mean increase in VEGF between preCA4P and 4 hours after CA4P of 44 pg/ml (p=0.1203) was produced; 3 patients showing an increase and patient HC38 showing no change (Figure 7.9). Between 4 hours and 6 to 8 hours after CA4P, a decrease in the mean by 24.75 pg/ml (p=0.0679) was produced; the only patient to show no decrease was HC38. By 1 week, the mean VEGF had increased by 16 pg/ml compared to 6 to 8 hours after CA4P, with patient GK39 having a decrease, although this was not significant. The variability of response between the time points seen with VEGF was not observed with VEGFR1, where all 4 patients had a similar direction of change throughout the study period, except between 4 and 6 to 8 hours after CA4P, where patient JC36 had a decrease in VEGFR1, whereas the other 3 showed rises (Figure 7.10). A highly significant mean increase was observed in VEGFR1 at 4 hours, compared to preCA4P, of 67.5 pg/ml (p=0.0108). At 6 to 8 hours, a mean increase of 96.75 pg/ml (p=0.065), compared to preCA4P, was produced but this was not significant. There was a mean increase in VEGFR1 of 29.25 pg/ml between 4 and 6 to 8 hours after CA4P, but this was also not significant. Significant decreases were seen at 1 week, compared to both 4 hours and 6 to 8 hours after CA4P, with mean decreases of 88.5 pg/ml (p=0.0252) and 117.75 pg/ml (p=0.0061) respectively.

The G-CSF results show a similar pattern of change, in mean concentration, to VEGFR1 (Figure 7.11). There was an increase in mean at 4 hours, further increase at 6 hours and a decrease at 1 week. These changes in direction of results were consistent for the same three patients at each time point but patient JC36 had changes in the opposite direction for each one. As a result, none of these changes were significant on paired t-testing. There were also no significant changes in SDF-1 between the tested time points (Figure 7.12). The validity of the SDF-1 results are uncertain, as, after analysis had been undertaken, it came to light that a further centrifugation step of 10000g for 10 minutes should have been performed. This was

required to remove platelets as they express a receptor for SDF-1 and this may affect the results of the assay.

7.5 Discussion

The scheduling of CA4P in this chapter was the final escalation of weekly CA4P dose intensity in the UKR104 study. Of the seven treatment cohorts in the study, 4 were delivered using radical radiotherapy with a once daily fractionation, 5 fractions per week. Previous prostate cohorts had received CA4P 50mg/m^2, either as a single dose or weekly for 4 weeks, with the final cohort receiving 63mg/m^2, also weekly for 4 weeks. CA4P was delivered after the final fraction of each week, to allow a recovery time of at least 72 hours, prior to recommencement of radiotherapy the next week. The radical fractionation used in cohort 6 for the treatment of SCC of the head & neck was delivered over 6.5 to 7 weeks, which allowed escalation of concurrent CA4P, with patients scheduled to receive 7 weekly doses at 50mg/m^2.

Concomitant cetuximab was incorporated into the treatment schedule for cohort 6, as a result of treatment with radiotherapy alone being superseded by combination therapies. This monoclonal antibody targets EGFR, inhibiting cellular processes, including proliferation, but also indirectly inhibits angiogenesis. It has been demonstrated to reduce expression of the pro-angiogenic factors VEGF, IL-8 and bFGF ([Petit et al., 1997], [Perrotte et al., 1999]). By combining one of the current standards of care, (cetuximab and radiotherapy), with CA4P, a vascular disruptive agent directed at a different target and with a different set of documented side effects, this treatment was designed to incorporate both vascular disruptive and antiangiogenic strategies. To determine the vascular effects resulting from this treatment single level DCE-CT, blood count and cytokine parameters were examined. Single level DCE-CT was selected to monitor the vascular changes in

this cohort, taking into account the relative size of the primary tumours to be assessed and also to allow assessment of blood flow. This gave z-axis coverage, for the CT scanner with four detectors, of approximately 2cm. From the 3 patients assessed, no consistent trends in any of the DCE-CT parameters measured were seen, but large changes were detected both between time points and in comparison with baseline values.

From Figure 7.2 the rapid increase in blood volume at 72h after the first dose of CA4P with patient HC38 is evident, in comparison to the low level at 4 hours post dose, with the blood volume increasing to a peak after the 25th fraction of radiotherapy. Decreases in blood volume, after the first and fourth doses of CA4P, were also seen with this patient. The use of DCE-CT allowed the identification of a reduction in the group mean PS, compared to mean baseline 4 to 5 days after the loading dose of cetuximab, followed by an increase after the fifth fraction of radiotherapy. The mean PS remained raised at 4 hours and 72 hours after the first dose of CA4P, with only changes of small magnitude between time points. However, at every time point, up to 72 hours after the first dose of CA4P, there were individual changes in the other direction to that seen with the group mean. Patient HC38 had no sizable individual change in PS until after the twenty-fifth fraction of radiotherapy, when there was a greater increase that persisted at 4 hours and 72 hours after the fourth dose of CA4P (Figure 7.3). For this patient, the cumulative effect of this combination treatment increased the tumour PS and resulted in no acute reduction in PS at four hours after the fourth dose of CA4P, compared to that seen after the first dose of CA4P.

Discernible changes in BF also resulted from the combination of therapies, with a large rise in BF seen after the loading dose of cetuximab for patient GK39, which resulted in a large increase in the group mean, despite the other 2 patients showing

only small decreases in BF. The group mean increase at 1 hour after the fifth fraction of radiotherapy was mainly due to the magnitude of increase of BF observed with patient GK, compared to mean baseline, when there had, in fact, been a small reduction in blood flow for this patient between 4 to 5 days after the loading dose of cetuximab and the fifth fraction of radiotherapy. The BF for the other 2 patients at this time point both increased, showing a further variable response. The expected reduction in blood flow 4 hours after CA4P was observed, with large reductions for patient HC38 and patient GK39, but in keeping with the variability previously observed, patient JC36 had a large increase at this time point.

There is an ongoing quest to identify circulatory biomarkers that may be easily extracted by relatively non-invasive diagnostic techniques, including circulating levels of endothelial progenitor cells (EPC), pro-angiogenic cytokines and receptors, and these are now being incorporated into early phase clinical trials of vascular directed therapies ([Shaked et al., 2006], [Bertolini et al., 2006], [Shaked et al., 2009], [Vermeulen et al., 2002.], [Lowndes et al., 2008], [Zhu et al., 2009]). EPCs from the bone marrow are recruited to tumour sites by a number of chemokines, including VEGF, SDF-1 and angiopoietin ([Hattori et al., 2001], [Peichev et al., 2000]). SDF-1 acts by binding to CXCR4 on circulating vasculogenic stem cells and facilitates their adhesion, migration and homing to the tumour microenvironment ([Ceradini et al., 2004], [Burger and Kipps, 2006], [Folkins et al., 2009]). This interaction between SDF-1 and CXCR4 is not limited to vasculogenic stem cells, with similar effects described in both cancer stem cells and normal stem cells, including the mobilisation of polymorphonuclear neutrophils and haemopoietic progenitor cells from the bone marrow ([Kucia et al., 2005], [Pelus et al., 2005]).

In this chapter, patients being treated with radical radiotherapy and cetuximab for SCCs of the head & neck, had significant increases in both neutrophil count (at 6 to

8 hours) and VEGFR1 (at 4 hours) after receiving CA4P, demonstrating the acute vasculogenic response resulting from the CA4P-induced damage to the tumour vasculature. In keeping with this, the graphs for neutrophils, VEGFR1 and G-CSF (Figures 7.6, 7.10 and 7.11) all show a similar shape in their mean curves and the mean curve for VEGF demonstrates an increase at 4 hours prior to a reduction at 6 to 8 hours. All three parameters demonstrate a statistically significant decrease, returning to baseline, when assessed at 1 week after receiving CA4P.

The changes seen for VEGF and G-CSF were often consistent for 3 patients, but due to the small numbers in the cohort, 100% of changes had to be in the same direction to achieve significance. The standard full blood count testing was sensitive enough to demonstrate these significant changes in neutrophil count, also reflected in the white cell count results. It was not possible to test for EPCs at the local hospital laboratory. Whether the significant reduction in lymphocyte count at 4 hours is related to this vasculogenic response is uncertain, but lymphopenia is a documented side effect of CA4P. It could also be due to a direct toxic effect or a sensitivity of the lymphocytes to the effects of CA4P.

By using both imaging and circulatory biomarkers, this enabled confirmation of the varied responses seen between the different patients. At 4 hours post CA4P, patient JC36 had documented rises in tumour BV, PS and BF, and rises in neutrophil count, VEGF and VEGFR, which peaked at 4 hours. In addition, the concentration of GCSF had decreased; with a further reduction at 6 to 8 hours post CA4P. These findings contrast with patient HC38, who had decreases in tumour BV, PS and BF, plus decreased neutrophil count, increasing VEGFR and increasing GCSF; these three circulatory parameters then continued to increase, peaking at 6 to 8 hours. These differences in patient HC38, may have resulted from a less well vascularised and more necrotic tumour, which would, therefore, be more reliant on the vessels

damaged by CA4P. A prolongation of the vasculogenic response, as seen with the further increases in neutrophil count and VEFR at 6 to 8 hours, may result from this increased vascular and tumour damage.

7.6 Conclusion

The experiments in this chapter have demonstrated that single level DCE-CT parameters can be used to detect acute changes in the vasculature of SCCs of the head & neck, undergoing treatment with radiotherapy, cetuximab and CA4P. However, a marked heterogeneity in the DCE-CT parameters was demonstrated, which may represent the inherent heterogeneity of the tumours. In this experiment, we have also harnessed the use of specific circulatory biomarkers and have demonstrated significant vasculogenic responses to CA4P- induced vascular damage; with significant acute rises in neutrophil count and VEGFR1. This indicates that the indirect antiangiogenic action of cetuximab does not prevent this vasculogenic response, in patients with SCC of the head & neck who are receiving radical radiotherapy, cetuximab and CA4P.

The findings from this study were limited by the observed toxicity of increased myocardial ischaemia with these combined therapies. Prior to the combination being looked at again in the clinical setting, further preclinical studies are required to determine whether the detrimental normal tissue cardiovascular effects, produced by the combination of CA4P and cetuximab, can be modulated by anti-hypertensive therapies or other agents, without the loss of the combined antitumour effects.

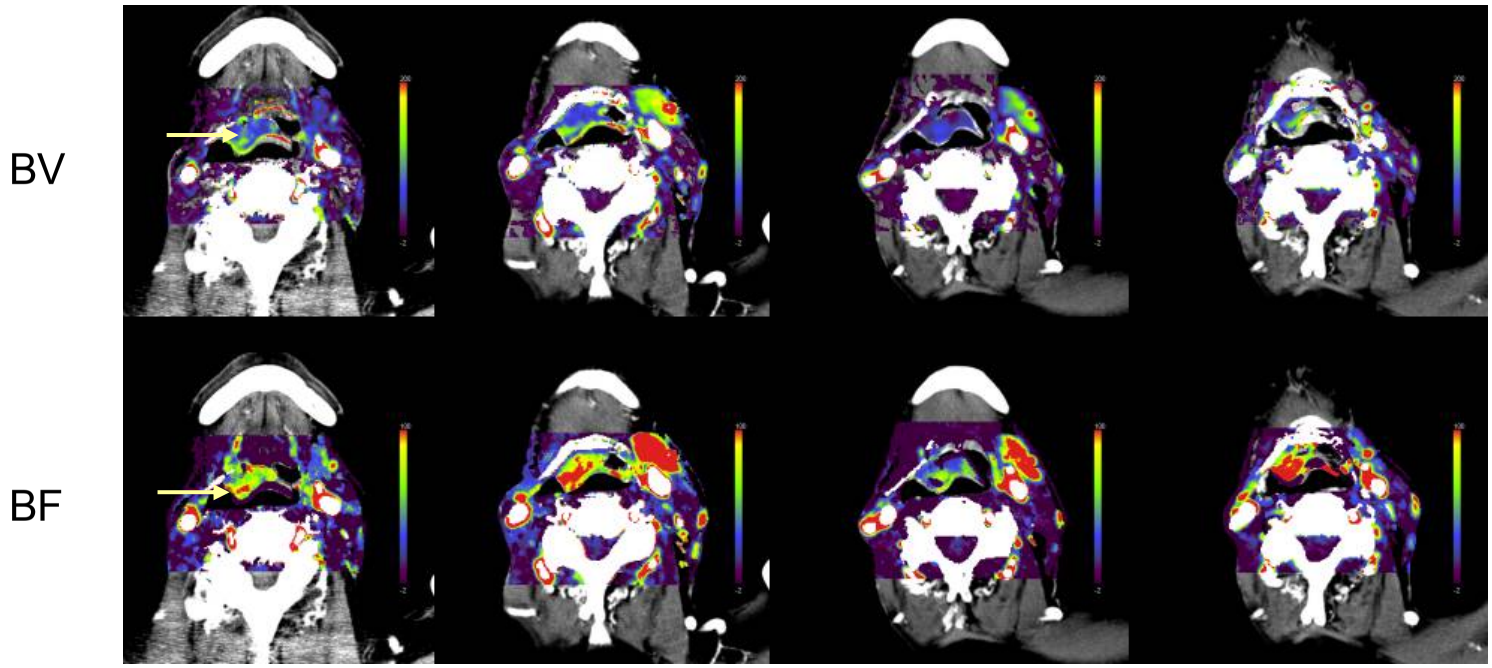

Figure 7.1

Colour parametric maps of single level DCE-CT derived tumour blood volume (BV) and blood flow (BF) for patient HC38, who received weekly CA4P, cetuximab and RT, as part of Cohort 6. The yellow arrows point to the supraglottic HNSCC primary tumour. A slight increase in BV and BF (compared to baseline) is seen in the lung tumour 1 hour after the fifth fraction of radiotherapy (5# RT), then a decrease in both parameters at 4 hours after the subsequent (first) dose of CA4P (CA4P1), on the same day. 72 hours later (72h 1) a recovery in BV and BF was seen.

	MB	Cet	*change (%)*	5#RT	*change (%)*	CA4P1	*change (%)*	72h 1	*change (%)*
Mean BV	62.69	57.38	*-7.17*	59.16	*0.17*	71.04	*20.54*	66.57	*24.84*
Mean PS	36.14	31.35	*-10.19*	**38.65**[b]	*20.30*	37.68	*-5.41*	39.19	*6.57*
Mean BF	47.60	52.99	*48.45*	63.34	*16.68*	54.20	*-8.40*	55.97	*29.80*

	MB	Cet	*change (%)*	5#RT	*change (%)*	CA4P1	*change (%)*	72h 1	*change (%)*
JC36 BV	77.90	66.45	*-14.70*	64.05	*-3.61*	**143.30**[a]	*123.73*	**75.20**[a]	*-47.52*
JC36 PS	25.28	30.25	*19.68*	**43.05**[a]	*42.31*	**53.25**[a]	*23.69*	51.65	*-3.00*
JC36 BF	55.98	**45.80**[a]	*-18.18*	54.90	*19.87*	**107.30**[a]	*95.45*	**72.95**[a]	*-32.01*

	MB	Cet	*change (%)*	5#RT	*change (%)*	CA4P1	*change (%)*	72h 1	*change (%)*
HC38 BV	74.22	70.30	*-5.28*	82.93	*17.97*	43.93	*-47.03*	**100.10**[a]	*127.85*
HC38 PS	46.78	42.00	*-10.22*	**52.50**[a]	*25.00*	**44.40**[a]	*-15.43*	48.43	*9.08*
HC38 BF	68.93	64.97	*-5.75*	93.73	*44.28*	**40.20**[a]	*-57.11*	**74.37**[a]	*84.99*

	MB	Cet	*change (%)*	5#RT	*change (%)*	CA4P1	*change (%)*	72h 1	*change (%)*
GK39 BV	35.95	35.40	*-1.53*	30.50	*-13.84*	25.90	*-15.08*	24.40	*-5.79*
GK39 PS	36.35	**21.80**[a]	*-40.03*	20.40	*-6.42*	15.40	*-24.51*	17.50	*13.64*
GK39 BF	17.90	**48.2**[a]	*169.27*	41.4	*-14.11*	**15.10**[a]	*-63.53*	20.60	*36.42*

[a]Individual change in BV/ PS/ BF >2x mean difference between 2 baseline scans

[b]Group change in BV/ PS/ BF >2x mean difference between 2 baseline scans

MB- mean baseline; Cet- 4 to 6 days after first dose of cetuximab and prior to the first fraction of radiotherapy; 5# RT- 1 hour after fifth fraction of radiotherapy; CA4P1 – 4 hours after the first dose of CA4P; 72h 1- 72 hours after the first dose of CA4P

Table 7.1

DCE-CT derived median blood volume (BV) values (ml/100ml), median permeability surface area product (PS) values (ml/100ml/min) and median Blood Flow (BF) values (ml/100ml/min), together with percentage change from previous time point, for each patient and group mean (UKR104 cohort 6).

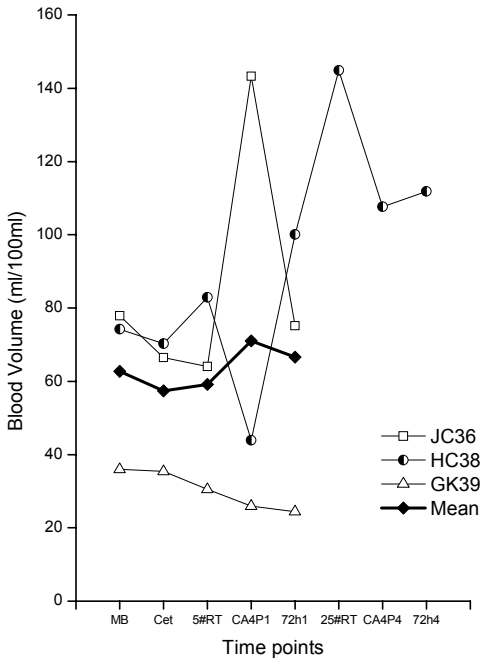

Figure 7.2

Graph of median single level tumour blood volume for HNSCC patients receiving weekly CA4P, weekly cetuximab and RT (Cohort 6), plotted at the following time points: MB- mean baseline; 2# RT- 1 hour after second fraction of radiotherapy; CA4P1 – 4 hours after the first dose of CA4P; 72h 4 – 72 hours after the first dose of CA4P; 25# RT- 1 hour after twenty fifth fraction of radiotherapy; CA4P4 – 4 hours after the fourth dose of CA4P; 72h 4 – 72 hours after the fourth dose of CA4P.

	MB	Cet	*change (%)*	5#RT	*change (%)*	CA4P1	*change (%)*	72h 1	*change (%)*
JC36	77.90	66.45	*-14.70*	64.05	*-17.78*	**143.30**[a]	*83.95*	75.20	*-3.47*
HC38	74.22	70.30	*-5.28*	82.93	*11.74*	43.93	*-40.80*	100.10	*34.88*
GK39	35.95	35.40	*-1.53*	30.50	*-15.16*	25.90	*-27.96*	24.40	*-32.13*
Mean	62.69	57.38	*-7.17*	59.16	*-7.06*	71.04	*5.06*	66.57	*-0.24*

	25#RT	*change (%)*	CA4P4	*change (%)*	72h 4	*change (%)*
HC38	**144.90**[a]	*95.24*	107.65	*45.05*	111.85	*50.71*

[a]***Individual change in BV >2x mean difference between 2 baseline scans***

[b]***Group change in BV >2x mean difference between 2 baseline scans***

MB- mean baseline; Cet- 4 to 6 days after first dose of cetuximab and prior to the first fraction of radiotherapy; 5# RT- 1 hour after fifth fraction of radiotherapy; CA4P1 – 4 hours after the first dose of CA4P; 72h 1- 72 hours after the first dose of CA4P; 25# RT- 1 hour after twenty fifth fraction of radiotherapy; CA4P4 – 4 hours after the fourth dose of CA4P; 72h 4- 72 hours after the fourth dose of CA4P; 6# RT- 1 hour after sixth fraction of radiotherapy; CA4P4 – 4 hours after the third dose of CA4P.

Table 7.2

DCE-CT derived median blood volume (BV) values (ml/100ml) and percentage change from mean baseline for patients with SCC Head & Neck receiving weekly CA4P, cetuximab and RT (UKR104 cohort 6).

	MB	Cet	*change (%)*	5#RT	*change (%)*	CA4P1	*change (%)*	72h 1	*change (%)*
JC36	77.90	66.45	*-14.70*	64.05	*-3.61*	**143.30**[a]	*123.73*	**75.20**[a]	*-47.52*
HC38	74.22	70.30	*-5.28*	82.93	*17.97*	43.93	*-47.03*	**100.10**[a]	*127.85*
GK39	35.95	35.40	*-1.53*	30.50	*-13.84*	25.90	*-15.08*	24.40	*-5.79*
Mean	62.69	57.38	*-7.17*	59.16	*0.17*	71.04	*20.54*	66.57	*24.84*

	25#RT	*change (%)*	CA4P4	*change (%)*	72h 4	*change (%)*
HC38	**144.90**[a]	*44.76*	107.65	*-25.71*	111.85	*3.90*

[a]***Individual change in BV >2x mean difference between 2 baseline scans***

[b]***Group change in BV >2x mean difference between 2 baseline scans***

MB- mean baseline; Cet- 4 to 6 days after first dose of cetuximab and prior to the first fraction of radiotherapy; 5# RT- 1 hour after fifth fraction of radiotherapy; CA4P1 – 4 hours after the first dose of CA4P; 72h 1- 72 hours after the first dose of CA4P; 25# RT- 1 hour after twenty fifth fraction of radiotherapy; CA4P4 – 4 hours after the fourth dose of CA4P; 72h 4- 72 hours after the fourth dose of CA4P; 6# RT- 1 hour after sixth fraction of radiotherapy; CA4P3 – 4 hours after the third dose of CA4P.

Table 7.3

DCE-CT derived median blood volume (BV) values (ml/100ml) and percentage change from previous time point for patients with SCC Head & Neck receiving weekly CA4P, cetuximab and RT (UKR104 cohort 6).

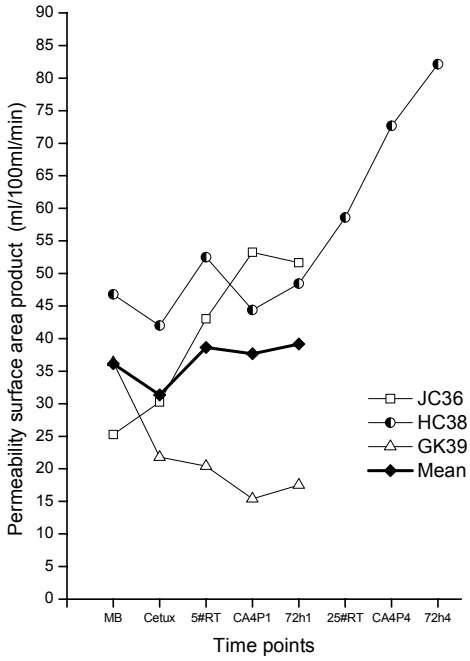

Figure 7.3

Graph of median single level tumour permeability surface area product for HNSCC patients receiving weekly CA4P, weekly cetuximab and RT (Cohort 6), plotted at the following time points: MB- mean baseline; 2# RT- 1 hour after second fraction of radiotherapy; CA4P1 – 4 hours after the first dose of CA4P; 72h 4 – 72 hours after the first dose of CA4P; 25# RT- 1 hour after twenty fifth fraction of radiotherapy; CA4P4 – 4 hours after the fourth dose of CA4P; 72h 4 – 72 hours after the fourth dose of CA4P.

	MB	Cet	*change (%)*	5#RT	*change (%)*	CA4P1	*change (%)*	72h 1	*change (%)*
JC36	25.28	30.25	*19.68*	**43.05**[a]	*70.33*	**53.25**[a]	*110.68*[a]	**51.65**[a]	*104.35*
HC38	46.78	42.00	*-10.22*	**52.50**[a]	*12.22*	44.40	*-5.09*	48.43	*3.53*
GK39	36.35	**21.80**[a]	*-40.03*	**20.40**[a]	*-43.88*	**15.40**[a]	*-57.63*[a]	**17.50**[a]	*-51.86*
Mean	36.14	31.35	*-10.19*	38.65	*12.89*	37.68	*15.98*	39.19	*18.67*

	25#RT	*change (%)*	CA4P4	*change (%)*	72h 4	*change (%)*
HC38	**58.60**[a]	*25.26*	**72.65**[a]	*55.29*	**82.15**[a]	*75.60*

[a]Individual change in PS >2x mean difference between 2 baseline scans

[b]Group change in PS >2x mean difference between 2 baseline scans

MB- mean baseline; Cet- 4 to 6 days after first dose of cetuximab and prior to the first fraction of radiotherapy; CA4P1 – 4 hours after the first dose of CA4P; 72h 1- 72 hours after the first dose of CA4P; 25# RT- 1 hour after twenty fifth fraction of radiotherapy; CA4P4 – 4 hours after the fourth dose of CA4P; 72h 4- 72 hours after the fourth dose of CA4P; 6# RT- 1 hour after sixth fraction of radiotherapy; CA4P3 – 4 hours after the third dose of CA4P.

Table 7.4

DCE-CT derived median permeability surface area product (PS) values (ml/100ml/min) and percentage change from mean baseline for patients with SCC Head & Neck receiving weekly CA4P, cetuximab and RT (UKR104 cohort 6).

	MB	Cet	*change (%)*	5#RT	*change (%)*	CA4P1	*change (%)*	72h 1	*change (%)*
JC36	25.28	30.25	*19.68*	**43.05**[a]	*42.31*	**53.25**[a]	*23.69*	51.65	*-3.00*
HC38	46.78	42.00	*-10.22*	**52.50**[a]	*25.00*	**44.40**[a]	*-15.43*	48.43	*9.08*
GK39	36.35	**21.80**[a]	*-40.03*	20.40	*-6.42*	15.40	*-24.51*	17.50	*13.64*
Mean	36.14	31.35	*-10.19*	**38.65**[b]	*20.30*	37.68	*-5.41*	39.19	*6.57*

	25#RT	*change (%)*	CA4P4	*change (%)*	72h 4	*change (%)*
HC38	**58.60**[a]	*20.99*	**72.65**[a]	*23.98*	**82.15**[a]	*13.08*

[a]***Individual change in PS >2x mean difference between 2 baseline scans***

[b]***Group change in PS >2x mean difference between 2 baseline scans***

MB- mean baseline; Cet- 4 to 6 days after first dose of cetuximab and prior to the first fraction of radiotherapy; CA4P1 – 4 hours after the first dose of CA4P; 72h 1- 72 hours after the first dose of CA4P; 25# RT- 1 hour after twenty fifth fraction of radiotherapy; CA4P4 – 4 hours after the fourth dose of CA4P; 72h 4- 72 hours after the fourth dose of CA4P; 6# RT- 1 hour after sixth fraction of radiotherapy; CA4P3 – 4 hours after the third dose of CA4P.

Table 7.5

DCE-CT derived median permeability surface area product (PS) values (ml/100ml/min) and percentage change from previous time point for patients with SCC Head & Neck receiving weekly CA4P, cetuximab and RT (UKR104 cohort 6).

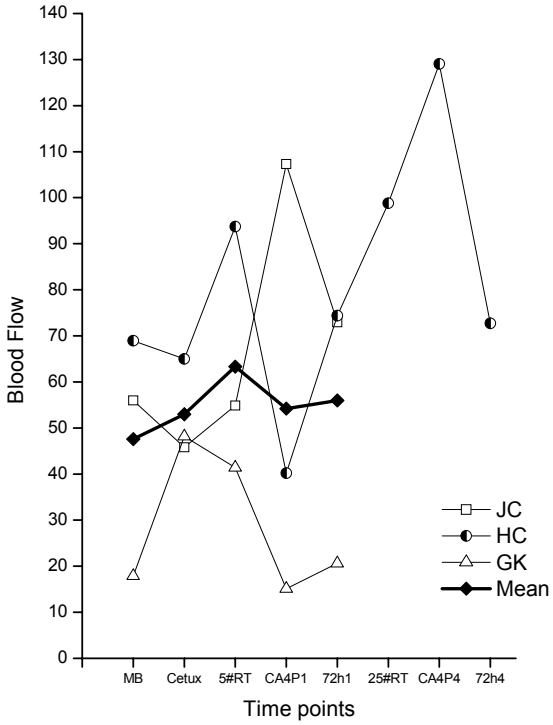

Figure 7.4

Graph of median single level tumour blood flow for HNSCC patients receiving weekly CA4P, weekly cetuximab and RT (Cohort 6), plotted at the following time points: MB- mean baseline; 2# RT- 1 hour after second fraction of radiotherapy; CA4P1 – 4 hours after the first dose of CA4P; 72h 4 – 72 hours after the first dose of CA4P; 25# RT- 1 hour after twenty fifth fraction of radiotherapy; CA4P4 – 4 hours after the fourth dose of CA4P; 72h 4 – 72 hours after the fourth dose of CA4P.

	MB	Cet	*change (%)*	5#RT	*change (%)*	CA4P1	*change (%)*	72h 1	*change (%)*
JC36	55.98	**45.80**[a]	*-18.18*	54.90	*-1.92*	**107.30**[a]	*91.69*	**72.95**[a]	*30.33*
HC38	68.93	64.97	*-5.75*	**93.73**[a]	*35.98*	**40.20**[a]	*-41.68*	74.37	*7.88*
GK39	17.90	**48.2**[a]	*169.27*	**41.4**[a]	*131.28*	15.1	*-15.64*	20.6	*15.08*
Mean	47.60	52.99	*48.45*	**63.34**[b]	*55.11*	54.20	*11.46*	55.97	*17.76*

	25#RT	*change (%)*	CA4P4	*change (%)*	72h 4	*change (%)*
HC38	**98.80**[a]	*43.33*	**129.05**[a]	*87.21*	72.70	*5.46*

[a]***Individual change in BF >2x mean difference between 2 baseline scans***

[b]***Group change in BF >2x mean difference between 2 baseline scans***

MB- mean baseline; Cet- 4 to 6 days after first dose of cetuximab and prior to the first fraction of radiotherapy; 5# RT- 1 hour after fifth fraction of radiotherapy; CA4P1 – 4 hours after the first dose of CA4P; 72h 1- 72 hours after the first dose of CA4P; 25# RT- 1 hour after twenty fifth fraction of radiotherapy; CA4P4 – 4 hours after the fourth dose of CA4P; 72h 4- 72 hours after the fourth dose of CA4P; 6# RT- 1 hour after sixth fraction of radiotherapy; CA4P3 – 4 hours after the third dose of CA4P.

Table 7.6

DCE-CT derived median Blood Flow (BF) values (ml/100ml/min) and percentage change from mean baseline for patients with SCC Head & Neck receiving weekly CA4P, cetuximab and RT (UKR104 cohort 6).

	MB	Cet	*change (%)*	5#RT	*change (%)*	CA4P1	*change (%)*	72h 1	*change (%)*
JC36	55.98	**45.80**[a]	*-18.18*	54.90	*19.87*	**107.30**[a]	*95.45*	**72.95**[a]	*-32.01*
HC38	68.93	64.97	*-5.75*	93.73	*44.28*	**40.20**[a]	*-57.11*	**74.37**[a]	*84.99*
GK39	17.90	**48.2**[a]	*169.27*	41.4	*-14.11*	**15.10**[a]	*-63.53*	20.60	*36.42*
Mean	47.60	52.99	*48.45*	63.34	*16.68*	54.20	*-8.40*	55.97	*29.80*

	25#RT	*change (%)*	CA4P4	*change (%)*	72h 4	*change (%)*
HC38	**98.80**[a]	*32.86*	**129.05**[a]	*30.62*	**72.70**[a]	*-43.67*

[a]***Individual change in BF >2x mean difference between 2 baseline scans***

[b]***Group change in BF >2x mean difference between 2 baseline scans***

MB- mean baseline Cet- 4 to 6 days after first dose of cetuximab and prior to the first fraction of radiotherapy; 5# RT- 1 hour after fifth fraction of radiotherapy; CA4P1 – 4 hours after the first dose of CA4P; 72h 1- 72 hours after the first dose of CA4P; 25# RT- 1 hour after twenty fifth fraction of radiotherapy; CA4P4 – 4 hours after the fourth dose of CA4P; 72h 4- 72 hours after the fourth dose of CA4P; 6# RT- 1 hour after sixth fraction of radiotherapy; CA4P3 – 4 hours after the third dose of CA4P.

Table 7.7

DCE-CT derived median Blood Flow (BF) values (ml/100ml/min) and percentage change from previous time point for patients with SCC Head & Neck receiving weekly CA4P, cetuximab and RT (UKR104 cohort 6).

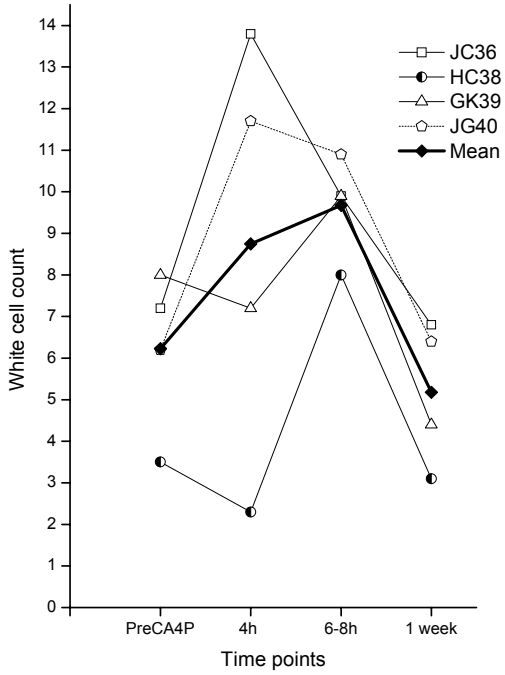

Figure 7.5

Graph of individual and group mean changes in white cell count for HNSCC patients receiving weekly CA4P, weekly cetuximab and RT (Cohort 6), plotted at the following time points: PreCA4P- after third or fourth fraction of radiotherapy in week of sampling, after second dose of cetuximab and prior to CA4P; 4h- 4 hours after CA4P; 6- 8h- 6 to 8 hours after CA4P; 1 week- 7 days after CA4P.

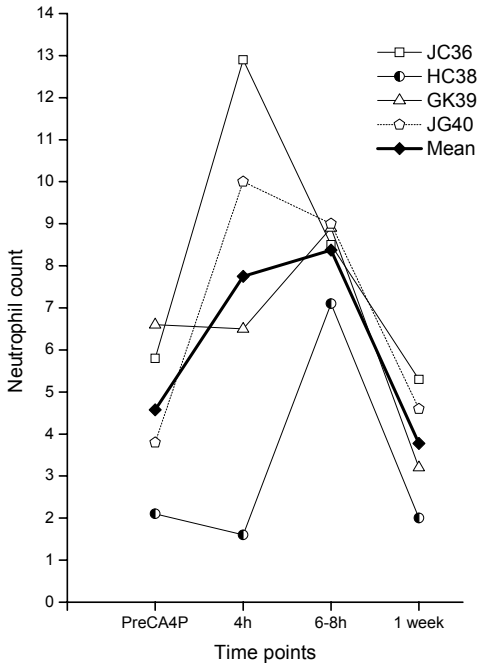

Figure 7.6

Graph of individual and group mean changes in neutrophil count for HNSCC patients receiving weekly CA4P, weekly cetuximab and RT (Cohort 6), plotted at the following time points: PreCA4P- after third or fourth fraction of radiotherapy in week of sampling, after second dose of cetuximab and prior to CA4P; 4h- 4 hours after CA4P; 6- 8h- 6 to 8 hours after CA4P; 1 week- 7 days after CA4P.

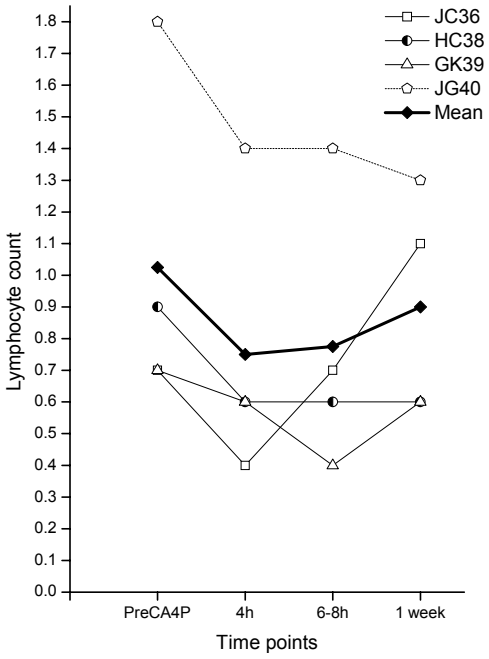

Figure 7.7

Graph of individual and group mean changes in lymphocyte count for HNSCC patients receiving weekly CA4P, weekly cetuximab and RT (Cohort 6), plotted at the following time points: PreCA4P- after third or fourth fraction of radiotherapy in week of sampling, after second dose of cetuximab and prior to CA4P; 4h- 4 hours after CA4P; 6- 8h- 6 to 8 hours after CA4P; 1 week- 7 days after CA4P.

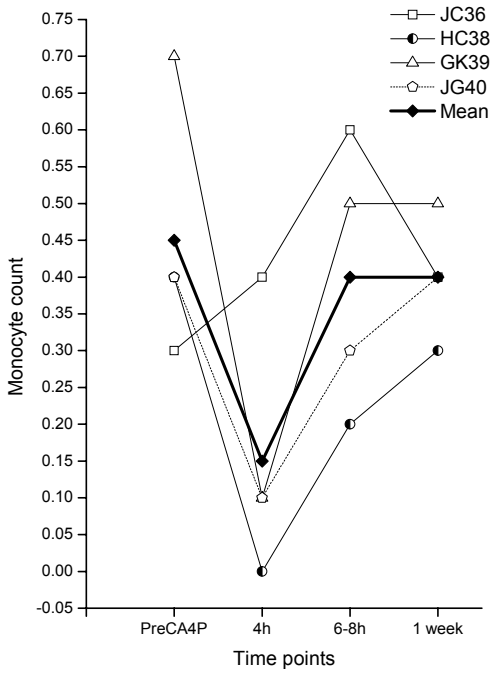

Figure 7.8

Graph of individual and group mean changes in monocyte count for HNSCC patients receiving weekly CA4P, weekly cetuximab and RT (Cohort 6), plotted at the following time points: PreCA4P- after third or fourth fraction of radiotherapy in week of sampling, after second dose of cetuximab and prior to CA4P; 4h- 4 hours after CA4P; 6- 8h- 6 to 8 hours after CA4P; 1 week- 7 days after CA4P.

JC36	PreCA4P	4h	6-8h	1 week
Hb	135	137	140	124
Plt	502	490	473	387
WBC	7.2	13.8	9.9	6.8
Neu	5.8	12.9	8.5	5.3
Lym	0.7	0.4	0.7	1.1
Mon	0.3	0.4	0.6	0.4

HC38	PreCA4P	4h	6-8h	1 week
Hb	131	125	138	129
Plt	168	138	145	145
WBC	3.5	2.3	8	3.1
Neu	2.1	1.6	7.1	2
Lym	0.9	0.6	0.6	0.6
Mon	0.4	0	0.2	0.3

GK39	PreCA4P	4h	6-8h	1 week
Hb	134	136	131	138
Plt	254	237	248	323
WBC	8	7.2	9.9	4.4
Neu	6.6	6.5	8.9	3.2
Lym	0.7	0.6	0.4	0.6
Mon	0.7	0.1	0.5	0.5

JG40	PreCA4P	4h	6-8h	1 week
Hb	119	127	132	117
Plt	333	334	346	297
WBC	6.2	11.7	10.9	6.4
Neu	3.8	10	9	4.6
Lym	1.8	1.4	1.4	1.3
Mon	0.4	0.1	0.3	0.4

Table 7.8

Full blood count results for head and neck cancer patients receiving CA4P, cetuximab and radical radiotherapy (UKR104 cohort 6).

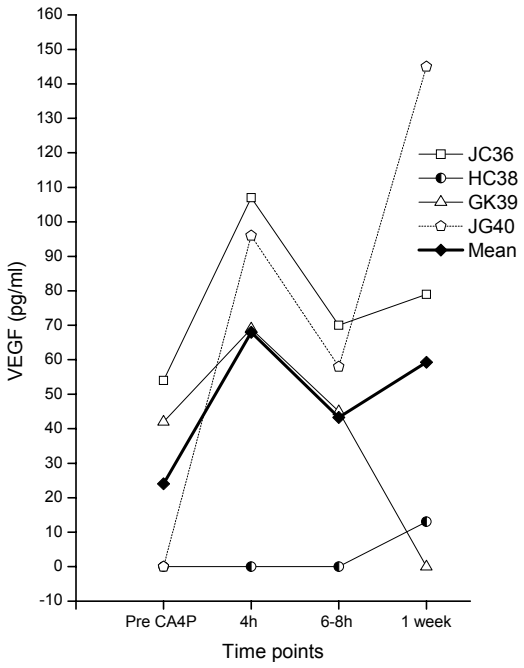

Figure 7.9

Graph of individual and group mean changes in plasma VEGF concentration for HNSCC patients receiving weekly CA4P, weekly cetuximab and RT (Cohort 6), plotted at the following time points: PreCA4P- after third or fourth fraction of radiotherapy in week of sampling, after second dose of cetuximab and prior to CA4P; 4h- 4 hours after CA4P; 6- 8h- 6 to 8 hours after CA4P; 1 week- 7 days after CA4P.

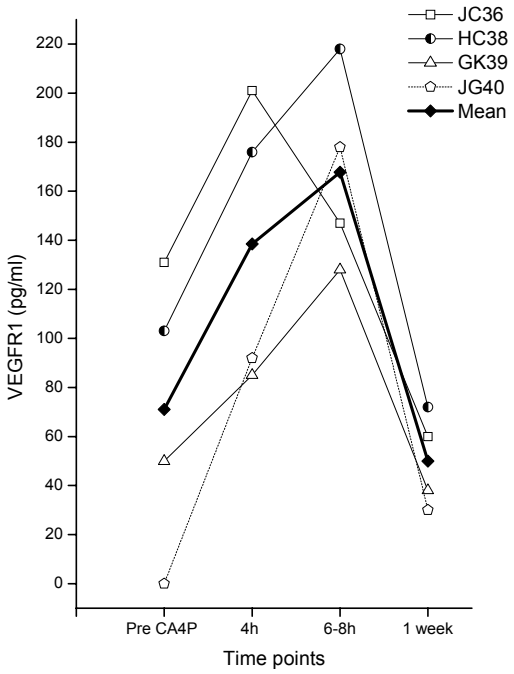

Figure 7.10

Graph of individual and group mean changes in plasma VEGFR1 concentration for HNSCC patients receiving weekly CA4P, weekly cetuximab and RT (Cohort 6), plotted at the following time points: PreCA4P- after third or fourth fraction of radiotherapy in week of sampling, after second dose of cetuximab and prior to CA4P; 4h- 4 hours after CA4P; 6- 8h- 6 to 8 hours after CA4P; 1 week- 7 days after CA4P.

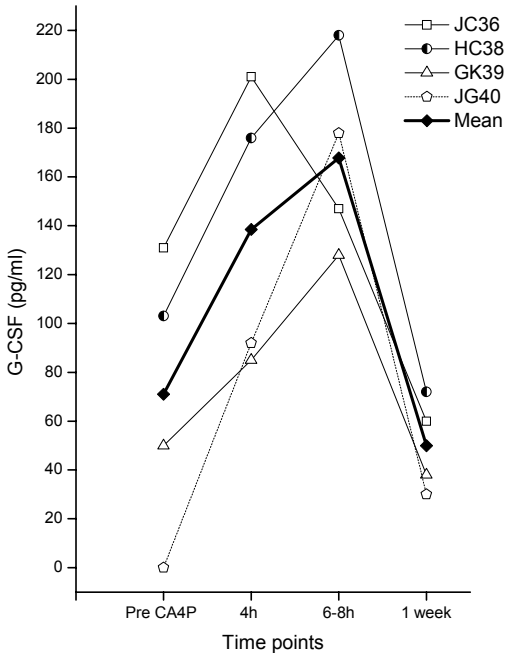

Figure 7.11

Graph of individual and group mean changes in plasma G-CSF concentration for HNSCC patients receiving weekly CA4P, weekly cetuximab and RT (Cohort 6), plotted at the following time points: PreCA4P- after third or fourth fraction of radiotherapy in week of sampling, after second dose of cetuximab and prior to CA4P; 4h- 4 hours after CA4P; 6- 8h- 6 to 8 hours after CA4P; 1 week- 7 days after CA4P.

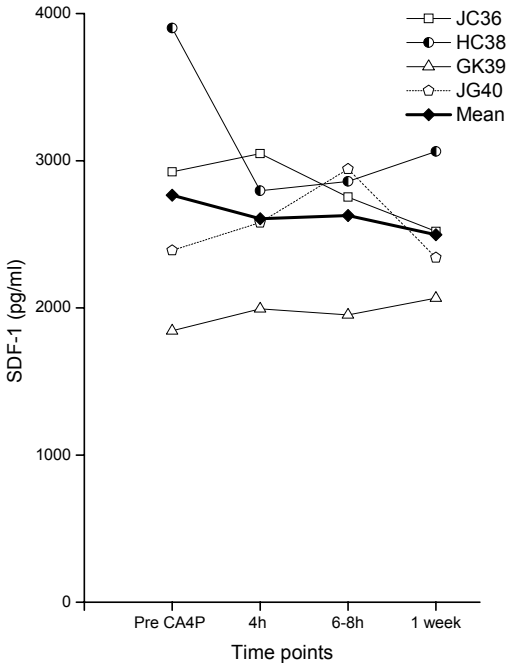

Figure 7.12

Graph of individual and group mean changes in plasma SDF-1 concentration for HNSCC patients receiving weekly CA4P, weekly cetuximab and RT (Cohort 6), plotted at the following time points: PreCA4P- after 3 to 4 fractions of radiotherapy, after second dose of cetuximab and prior to CA4P; 4h- 4 hours after CA4P; 6- 8h- 6 to 8 hours after CA4P; 1 week- 7 days after CA4P.

A VEGF (pg/ml)

	Pre CA4P	4h	6-8h	1 week
JC36	54	107	70	79
HC38	0	0	0	13
GK39	42	69	45	0
JG40	0	96	58	145

B VEGF R1 (pg/ml)

	Pre CA4P	4h	6-8h	1 week
JC36	131	201	147	60
HC38	103	176	218	72
GK39	50	85	128	38
JG40	0	92	178	30

C G-CSF (pg/ml)

	Pre CA4P	4h	6-8h	1 week
JC36	81	77	53	80
HC38	20	39	91	29
GK39	83	147	194	50
JG40	21	54	56	27

D SDF-1 (pg/ml)

	Pre CA4P	4h	6-8h	1 week
JC36	2924	3048	2753	2520
HC38	3092	2796	2859	3063
GK39	1845	1994	1953	2067
JG40	2390	2580	2944	2341

Table 7.9

ELISA results for head and neck cancer patients receiving CA4P, cetuximab and radical radiotherapy (UKR104 cohort 6).

CHAPTER 8

Concluding discussion

After preliminary *in vitro* testing of new anti-cancer therapies, or combinations of therapies, simple assays such as tumour growth delay provide some measure of the potential *in vivo* anti-tumour effects. They also enable a comparison of the effects produced by multiple different combinations. The preclinical experiments described in this thesis have explored the anti-tumour and vascular effects of concurrent CA4P and radiotherapy, and the impact of adding the nitric oxide synthase inhibitor, L-NNA, or the anti-EGFR monoclonal antibody, cetuximab, to this combination.

The non-isotope specific inhibitor of NOS, L-NNA, is a promising novel vascular directed therapy (Ng et al., 2007c). NOS inhibition has been shown to suppress the NO-dependent angiogenesis produced as a consequence of fractionated radiotherapy (Sonveaux et al., 2003). The experiments in this thesis have confirmed that LNNA can be effectively delivered by, either, chronic oral or daily i.p. administration, although chronic oral dosing of L-NNA is the most effective single agent schedule in this model. Crucially, for the first time in either the clinical or preclinical settings, the pharmacokinetic analysis revealed that L-NNA is concentrated and retained in tumours. Similar to the effects observed with L-NNA and tubulin-binding vascular disruptive agents in previous studies, our findings with L-NNA and CA4P were consistent with increased intratumoural vascular damage ([Tozer et al., 2009], [Wachsberger et al., 2005]). This beneficial effect was independent of the schedule of CA4P used, as it was seen with both weekly CA4P (100mg/ kg) and daily CA4P (50mg/kg).

When combined with radiotherapy, none of the three single agent schedules of L-NNA examined consistently enhanced its anti-tumour effects. Weekly CA4P 100mg/kg i.p. did enhance the effects of radiotherapy, although this beneficial anti-tumour effect was schedule dependent and was lost with the daily dosing regime. No consistent improvement in tumour growth delay was produced by the addition of chronic oral LNNA to radiotherapy, combined with either weekly or daily CA4P.

We have postulated that the scheduling of the treatments contributed to these findings, with daily CA4P, chronic oral and daily i.p. L-NNA, all increasing tumour hypoxia. Alternatively, the loss of NO (a potent radiosensitiser in hypoxic conditions) secondary to L-NNA may have increased radioresistance ([De Ridder et al., 2008], [Mitchell et al., 1998]). To fully elucidate the complex interactions of radiotherapy with these vascular directed therapies, further study is required, taking into account their different modes of action, consequent changes in tumour microenvironment and radiation cell kill mechanisms. This may be undertaken through examining alternative scheduling for L-NNA in combination with radiotherapy, including adjuvant administration following completion of radiotherapy, or with increased dose intensity administering 3 daily doses between weeks of radiotherapy (Friday, Saturday and Sunday). Ideally this would use different human xenograft models and include investigations to determine whether other tumour factors such as expression of eNOS or iNOS, hypoxic fraction, growth fraction or relative vascular area contribute to the responsiveness of tumours.

The preclinical work in this thesis demonstrated an enhanced anti-tumour effect, through adding cetuximab to the combination of CA4P and radiotherapy in the poorly differentiated hypopharyngeal SCC xenograft model, FaDu. Cetuximab, a monoclonal antibody that competitively inhibits EGFR, is known to produce tumour vascular effects and is an indirect inhibitor of angiogenesis ([Petit et al., 1997],

[Perrotte et al., 1999]). This triple combination therapy consistently produced the longest time to tumour regrowth and in the series of experiments described, was also the only treatment to produce a significant tumour growth delay compared to radiation alone. Despite the significant enhancement in tumour growth delay effects, seen in the CaNT model with the combination of weekly CA4P and radiotherapy, no additional benefit was seen in the FaDU tumour model, compared to radiotherapy alone. This confirms that some tumours have greater sensitivity to the vascular disruptive effects of CA4P.

Consistent with the known anti-tumour effects of cetuximab, described in other tumour models, a significant reduction in the ability of the primary tumours to metastasise to local lymph nodes was observed in the cohorts receiving cetuximab and radiotherapy (Perrotte et al., 1999). This effect was unaltered with the addition of CA4P. The development of lymph node metastases was, however, a significant confounding factor in this series of experiments, which were primarily concerned with the growth of the primary tumour. In the highest dose cohorts, the effect from the burden of disease as a result of lymphatic spread was most profound. Only 2 mice in the radiotherapy alone arm, receiving 24Gy, reached the defined endpoint of the study and were able to be included in the statistical comparison, thus limiting the use of this cohort as a control arm for comparison.

In conclusion, the combination of cetuximab, CA4P and fractionated radiotherapy has displayed promising anti-tumour effects in the work presented in this thesis. Further investigation of the interaction between these treatments is warranted, including investigation of the mechanisms behind the observed enhanced tumour growth delay effects produced. Extending this work to include other HNSCC xenografts and tumour types, where cetuximab has shown to be effective, would

help determine if there are molecular or genetic predictors of response to this combination and whether these findings are specific to HNSCC or can be applied to other malignancies.

As new targeted anticancer treatments become available it is important that testing strategies evolve to accurately determine their efficacy and potential role in the management of malignancies. The clinical component of this thesis described a series of experiments, utilising DCE-CT imaging to assess tumour vascularity and the changes resulting from the combination of vascular directed therapies and radiotherapy in non small cell lung cancer (NSCLC) and head and neck squamous cell carcinoma (HNSCC). Functional imaging techniques, such as DCE-CT and FDG-PET, provide non-invasive biomarkers, which can be harnessed to aid diagnosis, determine response to treatment and also offer prognostic information. However, prior to being widely adopted, these imaging techniques should, preferably, be validated by comparison with immunohistochemistry in resected tumours; as was undertaken in Chapter 5.

Hypoxia selects tumour cells resistant to apoptosis, as well as those that are more genetically unstable and of increased malignant, invasive and metastatic potential (Fukumura and Jain, 2007). It is also an important factor in determining tumour response to treatment, as it reduces both radiosensitivity and the sensitivity to some chemotherapeutic agents ([Gray et al., 1953], [Koch et al. 2003]). This study is the first to demonstrate significant correlations between DCE-CT parameters and immunohistochemical staining of intra-tumoural hypoxia ([Newbold et al., 2009], [De Schutter et al., 2005]).

The significant inverse correlation, between the pimonidazole fraction (pHF) and DCE-CT derived BV demonstrated, is consistent with the expected reduction in the functional vessel volume in tumour regions with increased chronic hypoxia (Rijken et al., 2000). No correlation was observed between the endogenous marker of hypoxia, Glut-1, and DCE-CT derived BV, although a negative correlation was seen between Glut-1 and PS. The observed mismatch of staining and lack of correlation between Glut-1 and pimonidazole in these NSCLC tumours may be a result of aerobic glycolysis, and also upregulation PI3K/ Akt pathway by HER2 or EGFR signalling producing increases in HIF1α synthesis, even in nonhypoxic conditions ([Warburg et al., 1927], [Laughner et al., 2001]). It may also be due to a variation in Glut-1 expression between different tumour types, as greater expression of Glut-1 was observed in SCCs whereas increased pimonidazole staining was seen in the adenocarcinomas.

A surprising finding was the lack of direct correlation between relative vascular area (as defined by CD34) and any of the DCE-CT parameters. However, significant negative correlations were demonstrated between relative vascular area and pimonidazole fraction (pHF), confirming the known inverse relationship between microvessel density and hypoxia in tumours. The dependence of the FDG-PET parameter, SUVmax, on both the expression of the glucose transporter, Glut-1, and reduced tumour permeability (PS) was also shown.

Correlating whole tumour immunohistochemical and volumetric DCE-CT parameters provides challenges, and therefore the results produced have to be considered alongside the inherent inaccuracies of the technique. The comparison of 4μm thick histological sections with 5mm CT sections, the shrinkage and distortion of resected tissue, difficulties in selection of corresponding CT slice and potential normal lung vasculature inclusion in DCE CT analysis, are all potential confounding factors.

The findings in this thesis suggested an ability to quantify whole tumour hypoxia in NSCLC using volumetric DCE-CT. To fully realise the potential of volumetric CT as a biomarker of intratumoural hypoxia in NSCLC, further work is required to establish whether the same correlations are observed in smaller subvolumes, potentially as small as 5mm^3. This would enable its use in dose painting techniques in the planning of complex radiotherapy treatments. The identification of hypoxia may also be of benefit in assessing tumour response to anti-cancer therapies, in particular vascular directed therapies. By providing accurate functional data on NSCLC, volumetric DCE-CT also has the potential to be implemented as a tool to aid the prognostic stratification of patients and selection for treatment.

In the final 2 chapters of this thesis, DCE-CT was used to assess changes in tumour vascularity as part of the UKR-104 phase 1b study, examining the safety and toxicity of combining CA4P and radiotherapy. In Chapter 6, patients with advanced NSCLC were treated with palliative radiotherapy in combination with daily, weekly or twice weekly CA4P. Volumetric DCE-CT detected significant treatment-induced changes in both whole tumour blood volume and permeability surface area product. Through inclusion of DCE-CT data from 24 patients, we accurately determined the reproducibility of the volumetric technique at our centre and used this to assess the significance of changes in these parameters resulting from the different components of the treatment.

From the DCE-CT analysis of these NSCLC tumours, significant increases in tumour blood volume (BV) were observed at 1 hour following radiotherapy, with no reduction in this effect when a dose of CA4P was given 72 hours previously. This may reflect greater blood flow in the remaining functional larger tumour vessels, following damage and disruption to the smaller and more immature blood vessels of the tumour by CA4P (Tozer et al., 2001). Reductions in BV were observed in the

majority of patients after the administration of CA4P, which is in keeping with its described vascular disruptive action (Dark et al., 1997). However, significant decreases only occurred in patients where significant individual increases in blood volume had been previously observed following the commencement of radiotherapy. This may represent sensitisation of the tumour vasculature to the effects of CA4P by radiotherapy, with a more pronounced effect in tumours sensitive to the effects of CA4P. Due to the small numbers of patients in each cohort of this study, it is not possible to gauge whether a true difference exists between the weekly and twice weekly scheduling of CA4P, although a significant group effect was only observed in the cohort receiving twice weekly CA4P.

Significant group increases in PS after the second fraction of radiotherapy, were seen in all of the NSCLC cohorts receiving CA4P, but were not seen following the fourth fraction in the cohort receiving twice weekly doses of CA4P or after the sixth fraction in those receiving weekly CA4P. The first dose of concurrent CA4P seems to have the greatest effect on tumour permeability (PS), and a reduction in the magnitude of this effect occurs with further doses of CA4P. This may reflect the loss of small blood vessels within the tumour, due to the CA4P-induced disruption of interphase microtubules in endothelial cells, with the remaining larger blood vessels less sensitive to vascular disruptive effects of CA4P (Tozer et al., 2001).

The data from this thesis supports the hypothesis that enhanced endothelial cell damage results from the combination of radiotherapy and the concurrent administration of CA4P in advanced NSCLC, without any significant overlapping or enhanced acute toxicity. This is of particular relevance given that radiation-induced damage to the tumour vasculature is known to be an important determinant of tumour cell survival (Garcia-Barros et al., 2003). No significant dose limiting toxicities were observed in any of the NSCLC patients in this study. However, to fully

establish the role for this combination therapy in NSCLC, further phase 2 studies are required. These should be undertaken using weekly CA4P at a dose of 50mg/m^2 for conventional daily radiotherapy fractionations (5 days per week). If using a twice weekly radiotherapy fractionation, either weekly or twice weekly CA4P (at the same dose of 50mg/m^2) may be used. Given the lack of overlapping toxicities seen in this study, CA4P also lends itself to potential combinations with concurrent chemoradiation schedules, which would need to be further assessed as part of future phase 1 studies.

The final component to the clinical work in this thesis examined radical radiotherapy in combination with CA4P and cetuximab. Following the publication of a large randomised phase 3 study, showing improved overall survival compared to radiotherapy alone, cetuximab is now widely given concurrently with radical radiotherapy (Bonner et al., 2006). In the UK, the National Institute for Health and Clinical Excellence has now recommended it for the treatment of locally advanced HNSCC, in patients of good performance status where the use of platinum-based concurrent chemotherapy is contraindicated (NICE, 2008). In parallel with the work described in Chapter 4, this clinical study attempted to fully evaluate the impact of combining radiotherapy with CA4P and cetuximab, with single level DCE-CT, full blood count and cytokine testing performed, in addition to the assessment of acute toxicity.

The experiments in chapter 7 have demonstrated that single level DCE-CT parameters can be used to detect acute changes in the tumour vasculature in HNSCCs undergoing treatment with radiotherapy, cetuximab and CA4P. However, due to significant dose limiting toxicities of myocardial ischaemia in 2 patients, the study was discontinued after the fourth patient was treated and only 3 patients underwent DCE-CT scanning. The expected reduction in blood flow 4 hours after

CA4P was observed, in 2 of the 3 assessable patients, but otherwise a marked heterogeneity in the DCE-CT parameters was seen, which may represent the inherent heterogeneity of the tumours.

In this chapter, specific circulatory biomarkers were also studied and significant vasculogenic responses to CA4P-induced vascular damage were demonstrated. Despite having samples from only 4 patients, significant acute rises in neutrophil count and VEGFR1 were produced. Similar rises were also seen with VEGF and GCSF, although these did not reach statistical significance. These parameters returned to baseline at 1 week after receiving CA4P. This indicates that the indirect antiangiogenic action of cetuximab does not prevent this vasculogenic response in patients with HNSCC who are receiving radical radiotherapy, cetuximab and CA4P.

The presence of pre-existing hypertension produces a greater blood pressure rise following CA4P associated with increased cardiac strain, demonstrable by a rise in cardiac enzymes (Ke Q et al., 2007). In this preclinical study these blood pressure and cardiac effects were prevented by treatment with anti-hypertensive agents, using either calcium-channel antagonists or nitrates. Prior to examining the combination of cetuximab, CA4P and radiotherapy again in the clinical setting, further preclinical testing is required. Anti-hypertensive therapies or other agents must demonstrate the ability to modulate the detrimental normal tissue cardiovascular effects produced by the combination of CA4P and cetuximab, without the loss of the combined antitumour effects.

In summary, through the translational research described in this thesis, the potential for utilising the vascular disruptive effects of CA4P with fractionated radiotherapy has been explored. This work has encompassed preclinical and clinical studies, examining the anti-tumour effects of adding other vascular directed therapies to this combination. It has used both DCE-CT imaging and circulatory biomarkers to assess treatment induced changes in tumour vascularity. In addition, it has validated volumetric DCE-CT as a biomarker of hypoxia in NSCLC. The results from this thesis, add to the body of work defining the role of vascular disruptive therapies, in combination with radiotherapy. They provide further information to guide future studies in this field, highlighting the role of DCE-CT and functional imaging in such work.

APPENDIX A

Matching of histology with Dynamic Contrast Enhanced CT

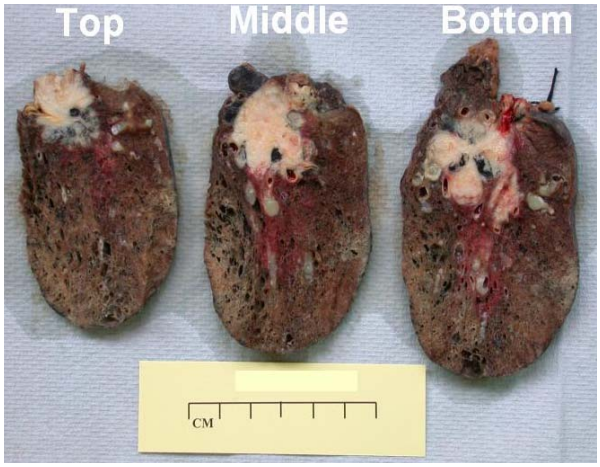

Figure A1

Specimen pictures from time of cut-up are shown, with 3 sections taken from the top, middle and bottom of the NSCLC tumour. For each section obtained, measurements were taken of the distance from the top, middle and bottom of tumour.

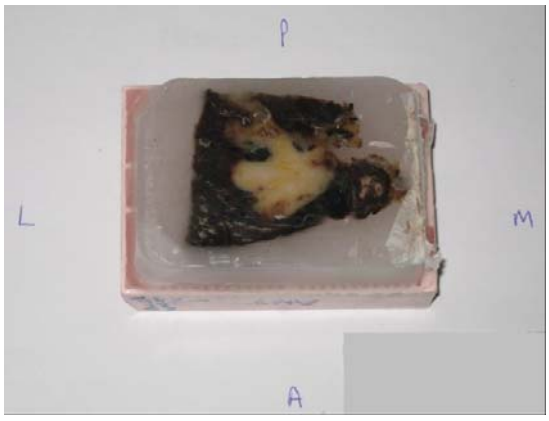

Figure A2

Tissue block picture: section from middle of the tumour. The trimmed section had been embedded in paraffin wax, within a cassette. The orientation of the tumour within the lung, at the time of cut-up, was labelled on the cassette and surrounding paper: **L** lateral, **P** posterior, **M** medial, and **A** anterior.

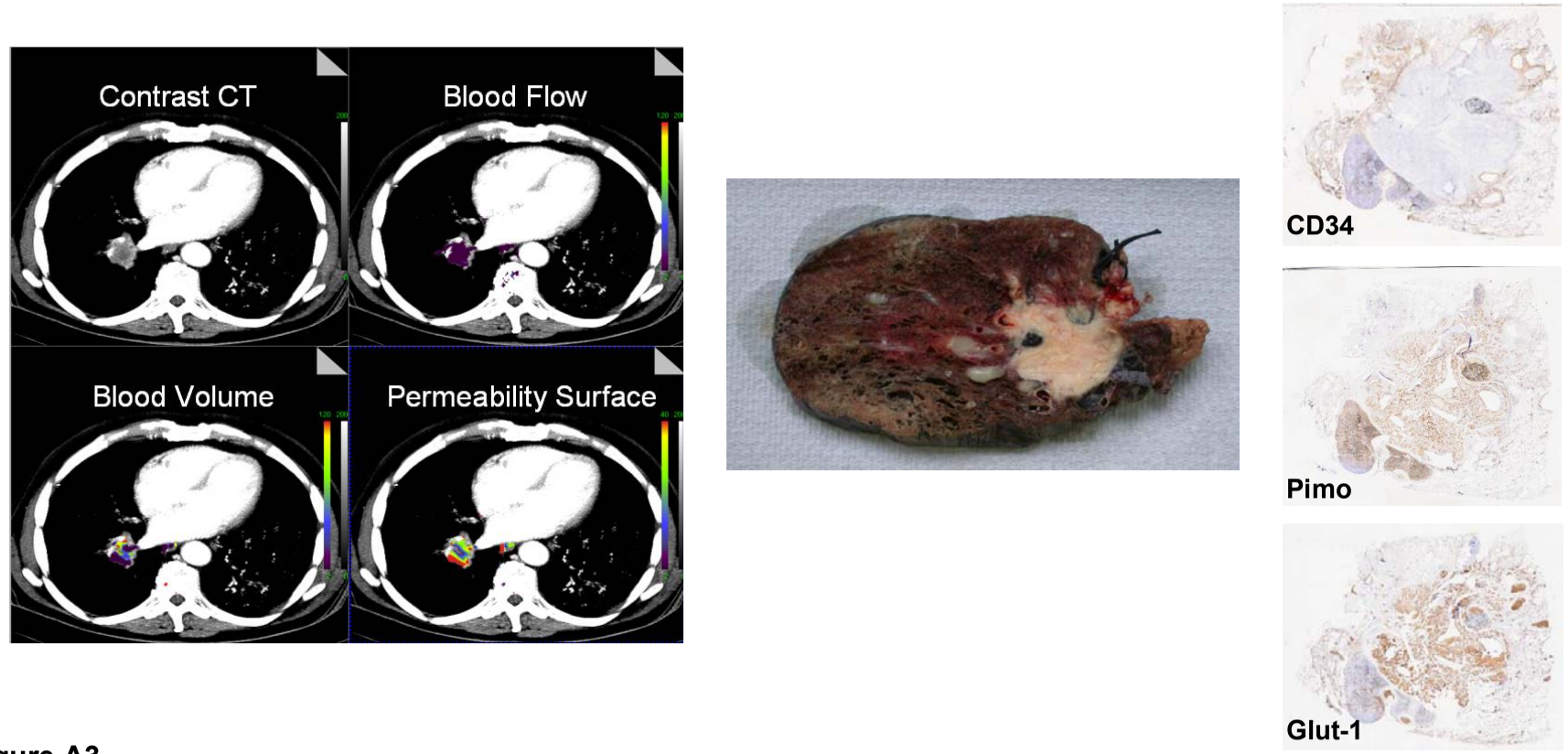

Figure A3

Specimen picture and immunohistochemical staining for CD34, pimonidazole (Pimo) and Glut-1, of section obtained from middle of tumour. Corresponding DCE-CT parametric maps for blood volume (BV), permeability surface area product (PS) and blood flow (BF), from middle slice of tumour.

APPENDIX B

UKR-104 study inclusion and exclusion criteria

Inclusion Criteria:

Patients had to meet the following criteria to be eligible for the study:

1) A minimum four-week interval from the time a patient last received chemotherapy, immunotherapy or radiotherapy prior to the first dose of study drugs (six weeks for therapy known to be associated with delayed toxicity such as nitrosoureas or mitomycin-C).
2) Histopathologically or cytologically confirmed non-small cell lung cancer (NSCLC), squamous head and neck cancer or prostatic adenocarcinoma.
3) Patients with NSCLC will have inoperable disease unsuitable for radical radiotherapy, patients with head and neck cancer will have locally advanced tumours stage III or IV and patients with prostate cancer will have locally advanced tumours with PSA >20, Gleason score ≥7 or stage T3 or T4.
4) Measurable or non-measurable disease.
5) Age 18 years or older.
6) ECOG PS < 2.
7) Life expectancy > 12 weeks.
8) Adequate bone marrow function:
9) Absolute granulocyte count (neutrophils and bands) > 1500 cells/mm^3
10) Platelet count > 100,000 cells/mm^3
11) PT/PTT within the institution ULN or INR <1.1
12) Adequate hepatic function:
13) Total bilirubin <1.5 mg/dL
14) Alanine and aspartate aminotransferase (ALT/AST) < 2.5 times the institutional upper normal limit unless clearly related to hepatic metastases, in which case ALT/AST must be < 5 times upper normal limit.

15) Adequate renal function: serum creatinine < 2.0 mg/dL or CrCl >60 mL/min.
16) Patients must provide written and voluntary informed consent and be available for periodic follow-up.
17) Fertile patients must abstain from sexual intercourse or use effective birth control.
18) All women of childbearing potential (WOCBP) must have a negative serum or urine pregnancy test documented within 72 hours prior to study enrolment.

WOCBP include any female who has experienced menarche and who has not undergone successful surgical sterilization (hysterectomy, etc.) or is not postmenopausal; or women on hormone replacement therapy. Even women who are using oral, implanted or, injectable contraceptive hormones or mechanical products such as an intrauterine device or barrier methods (IUD, diaphragm) to prevent pregnancy or practicing abstinence or where partner is sterile (e.g. vasectomy), should be considered to be of child bearing potential.

Exclusion Criteria:

Patients displaying any of the following criteria were not eligible for this study:

1) Serious intercurrent infections or other nonmalignant medical illnesses that are uncontrolled or whose control may be jeopardized by the complications of this therapy.
2) Grade 2 (CTC v.2.0) or greater pre-existing peripheral neuropathy (motor or sensory).
3) Active brain metastasis, including symptomatic involvement, evidence of cerebral oedema by CT or MRI, radiographic evidence of progression since definitive therapy, or continued requirement for corticosteroids.
4) Major surgery within the preceding four weeks.
5) Symptomatic peripheral vascular disease or cerebrovascular disease.

6) Psychiatric disorders or other conditions rendering patients incapable of complying with the requirements of the protocol.
7) Pregnant or breast-feeding women.
8) History of angina (stable or more severe, even if controlled with medications), myocardial infarction, CHF, non-controlled atrial arrhythmias or clinically significant arrhythmias including conduction abnormality, nodal junctional arrhythmias and dysrhythmias, sinus bradycardia or tachycardia, supraventricular arrhythmias, atrial fibrillation or flutter, syncope or vasovagal episodes.
9) Uncontrolled hypertension (defined as blood pressure consistently greater than 150/100 irrespective of medication).
10) Uncontrolled hypokalemia and/or hypomagnesemia.
11) ECG with evidence of prior myocardial infarction (e.g., significant Q waves), QTc > 450 msec or other clinically significant abnormalities.
12) Patients taking any drug(s) known to prolong the QTc interval, which cannot be interrupted for at least four days during each 21-day treatment cycle. Patients with conditions associated with QTc prolongation.
13) Concurrent investigational therapy.
14) Concurrent antineoplastic therapy (radiation therapy to a site apart from that in study, cytotoxic or biologic therapy, other than Cetuximab given as stated in the protocol).
15) Concurrent hormonal therapy with the exception of GnRH agonists in patients with prostate cancer, HRT, oral contraceptives, and megestrol acetate used for anorexia/cachexia.

REFERENCES

Aboagye EO, Price P M 2003. Use of positron emission tomography in anticancer drug development. Invest New Drugs 21(2):169-81.

Aebersold D M, Burri P, Beer K T, Laissue J, Djonov V, Greiner R H, Semenza G L (2001). Expression of hypoxia-inducible factor-1alpha: a novel predictive and prognostic parameter in the radiotherapy of oropharyngeal cancer. Cancer Res 61(7):2911-6.

Ahmed B, Landuyt W, Griffioen A W, Van Oosterom A, Van den Bogaert W, Lambin P (2006). In vivo antitumour effect of combretastatin A-4 phosphate added to fractionated irradiation. Anticancer Res 26(1A):307-10.

Ah-See M L, Makris A, Taylor N J, Harrison M, Richman P I, Burcombe R J, Stirling J J, d'Arcy J A, Collins D J, Pittam M R, Ravichandran D, Padhani A R (2008). Early changes in functional dynamic magnetic resonance imaging predict for pathologic response to neoadjuvant chemotherapy in primary breast cancer. Clin Cancer Res 14(20):6580-9.

Airley R, Loncaster J, Davidson S, Bromley M, Roberts S, Patterson A, Hunter R, Stratford I, West C (2001). Glucose transporter glut-1 expression correlates with tumor hypoxia and predicts metastasis-free survival in advanced carcinoma of the cervix. Clin Cancer Res 7(4):928-34.

Airley R E, Loncaster J, Raleigh J A, Harris A L, Davidson S E, Hunter R D, West C M, Stratford I J (2003). GLUT-1 and CAIX as intrinsic markers of hypoxia in carcinoma of the cervix: relationship to pimonidazole binding. Int J Cancer 104(1):85-91.

Anderson H L, Yap J T, Miller M P, Robbins A, Jones T, Price P M (2003a). Assessment of pharmacodynamic vascular response in a phase I trial of combretastatin A4 phosphate. J Clin Oncol 21:2823-30.

Anderson H, Yap J T, Wells P, Miller M P, Propper D, Price P, Harris A L (2003b).Measurement of renal tumour and normal tissue perfusion using positron emission tomography in a phase II clinical trial of razoxane. Br J Cancer 89(2):262-7.

Allalunis-Turner M J, Franko A J, Parliament M B (1999). Modulation of oxygen consumption rate and vascular endothelial growth factor mRNA expression in human malignant glioma cells by hypoxia. Br J Cancer 80(1-2):104-9.

Avontuur J A, Buijk S L, Bruining H A (1998). Distribution and metabolism of N(G)-nitro-L-arginine methyl ester in patients with septic shock. Eur J Clin Pharmacol 54(8):627-31.

Axel L (1980). Cerebral blood flow determination by rapid-sequence computed tomography: theoretical analysis. Radiology 137(3):679-86.

Azuma C, Raleigh J A, Thrall D E (1997). Longevity of pimonidazole adducts in spontaneous canine tumors as an estimate of hypoxic cell lifetime. Radiat Res 148(1):35-42.

Baguley B C (2003). Antivascular therapy of cancer: DMXAA. Lancet Oncol 4(3):141-8.

Balza E, Carnemolla B, Mortara L, Castellani P, Soncini D, Accolla R S, Borsi L (2010).Therapy-induced antitumor vaccination in neuroblastomas by the combined targeting of IL-2 and TNFalpha. Int J Cancer 127(1):101-10.

Balza E, Mortara L, Sassi F, Monteghirfo S, Carnemolla B, Castellani P, Neri D, Accolla R S, Zardi L, Borsi L (2006). Targeted delivery of tumor necrosis factor-alpha to tumor vessels induces a therapeutic T cell-mediated immune response that protects the host against syngeneic tumors of different histologic origin. Clin Cancer Res. Apr 15;12(8):2575-82.

Beresford M J, Harris A L, Ah-See M, Daley F, Padhani A R, Makris A (2006). The relationship of the neo-angiogenic marker, endoglin, with response to neoadjuvant chemotherapy in breast cancer. Br J Cancer 95(12):1683-8.

Beauregard D A, Hill S A, Chaplin D J, Brindle K M (2001). The susceptibility of tumors to the antivascular drug combretastatin A4 phosphate correlates with vascular permeability. Cancer Res 61(18):6811-5.

Belotti D, Vergani V, Drudis T, Borsotti P, Pitelli M R, Viale G, Giavazzi R, Taraboletti G. (1996). The microtubule-affecting drug paclitaxel has anti-angiogenic activity. Clin. Cancer Res. 2, 1843–1849.

Bergers, G, Brekken R, McMahon G, Vu T H, Itoh T, Tamaki K, Tanzawa K, Thorpe P, Itohara S, Werb Z, Hanahan D (2000). Matrix metalloproteinase-9 triggers the angiogenic switch during carcinogenesis. Nature Cell Biol 2(10):737-44.

Bertolini F, Shaked Y, Mancuso P, Kerbel R S (2006). The multifaceted circulating endothelial cell in cancer: towards marker and target identification. Nat Rev Cancer 6(11):835-45.

Bhattacharya A, Tóth K, Mazurchuk R, Spernyak J A, Slocum H K, Pendyala L, Azrak R, Cao S, Durrani F A, Rustum Y M (2004).Lack of microvessels in well-differentiated regions of human head and neck squamous cell carcinoma A253 associated with functional magnetic resonance imaging detectable hypoxia, limited drug delivery, and resistance to irinotecan therapy. Clin Cancer Res 10(23):8005-17.

Bianco C, Giovannetti E, Ciardiello F, Mey V, Nannizzi S, Tortora G, Troiani T, Pasqualetti F, Eckhardt G, de Liguoro M, Ricciardi S, Del Tacca M, Raben D, Cionini L, Danesi R (2006). Synergistic antitumor activity of ZD6474, an inhibitor of vascular endothelial growth factor receptor and epidermal growth factor receptor signaling, with gemcitabine and ionizing radiation against pancreatic cancer. Clin Cancer Res 12(23):7099-107.

Bibby M C, Double J A (1993). Flavone acetic acid--from laboratory to clinic and back. Anticancer Drugs 4(1):3-17.

Bilenker J H, Flaherty K T, Rosen M, Davis L, Gallagher M, Stevenson J P, Sun W, Vaughn D, Giantonio B, Zimmer R, Schnall M, O'Dwyer P J (2005). Phase 1 trial of combretastatin a-4 phosphate with carboplatin. Clin Cancer Res 11(4):1527-33.

Blakey D C, Westwood F R, Walker M, Hughes G D, Davis P D, Ashton S E, Ryan A J (2002). Antitumor activity of the novel vascular targeting agent ZD6126 in a panel of tumor models. Clin Cancer Res 8(6):1974-83.

Bland J M, Altman D G (1996a). Measurement error proportional to the mean. BMJ 313(7049):106.

Bland J M, Altman D G (1996b). Measurement error and correlation coefficients. BMJ 313(7048):41-2.

Bland J M, Altman D G (1996c). Measurement error. BMJ 313(7059):744.

Boehle A S, Sipos B, Kliche U, Kalthoff H, Dohrmann P (2001). Combretastatin A-4 prodrug inhibits growth of human non-small cell lung cancer in a murine xenotransplant model. Ann Thorac Surg 71(5):1657-65.

Boehm T, Folkman J, Browder T, O'Reilly M S (1997). Anti-angiogenic therapy of experimental cancer does not induce acquired drug resistance. Nature 390:404-7.

Bonner J A, Harari P M, Giralt J, Azarnia N, Shin D M, Cohen R B, Jones C U, Sur R, Raben D, Jassem J, Ove R, Kies M S, Baselga J, Youssoufian H, Amellal N, Rowinsky E K, Ang K K (2006). Radiotherapy plus cetuximab for squamous-cell carcinoma of the head and neck. N Engl J Med. Feb 9;354(6):567-78.

Borre M, Offersen B V, Nerstrøm B, Overgaard J (1998). Microvessel density predicts survival in prostate cancer patients subjected to watchful waiting. Br J Cancer 78(7):940-4.

Bouck N (1990). Tumor angiogenesis: the role of oncogenes and tumor suppressor genes. Cancer Cells 2:179-185.

Boyland E, Boyland M E (1937). Studies in tissue metabolism: The action of colchicines and B. typhus extract. Biochem J 31(3):454-60.

Bozec A, Lassalle S, Gugenheim J, Fischel J L, Formento P, Hofman P, Milano G (2006). Enhanced tumour antiangiogenic effects when combining gefitinib with the antivascular agent ZD6126. Br J Cancer 95(6):722-8.

Bozec A, Sudaka A, Fischel J L, Brunstein M C, Etienne-Grimaldi M C, Milano G (2008). Combined effects of bevacizumab with erlotinib and irradiation: a preclinical study on a head and neck cancer orthotopic model. Br J Cancer 99(1):93-9.

Bozec A, Sudaka A, Toussan N, Fischel J L, Etienne-Grimaldi M C, Milano G (2009). Combination of sunitinib, cetuximab and irradiation in an orthotopic head and neck cancer model. Ann Oncol 20(10):1703-7.

Brazelle W D, Shi W, Siemann D W (2006). VEGF-associated tyrosine kinase inhibition increases the tumor response to single and fractionated dose radiotherapy. Int J Radiat Oncol Biol Phys 65(3):836-41.

Brooks A C, Kanthou C, Cook I H, Tozer G M, Barber P R, Vojnovic B, Nash G B, Parkins C S (2003). The vascular-targeting agent combretastatin A-4-phosphate induces neutrophil recruitment to endothelial cells in vitro. Anticancer Res 23:3199-206.

Broumas A R, Pollard R E, Bloch S H, Wisner E R, Griffey S, Ferrara K W (2005). Contrast-enhanced computed tomography and ultrasound for the evaluation of tumor blood flow. Invest Radiol 40(3):134-47.

Brouty-Boyé D, Zetter B R (1980). Inhibition of cell motility by interferon. Science 208(4443):516-8.

Browder T, Butterfield C E, Kräling B M, Shi B, Marshall B, O'Reilly M S, Folkman J (2000). Antiangiogenic scheduling of chemotherapy improves efficacy against experimental drug-resistant cancer. Cancer Res 60(7):1878-86.

Brown J M, Giaccia A J (1998). The unique physiology of solid tumours: opportunities (and problems) for cancer therapy. Cancer Res 58(7):1408-16.

Brown R S, Leung J Y, Kison P V, Zasadny K R, Flint A, Wahl R L (1999). Glucose transporters and FDG uptake in untreated primary human non-small cell lung cancer. J Nucl Med 40(4):556-65.

Buckley DL. Uncertainty in the analysis of tracer kinetics using dynamic contrast-enhanced T1-weighted MRI. Magn Reson Med. 2002 Mar;47(3):601-6.

Burger J A, Kipps T J (2006). CXCR4: a key receptor in the crosstalk between tumor cells and their microenvironment. Blood 107(5):1761-7.

Camp E R, Yang A, Liu W, Fan F, Somcio R, Hicklin D J, Ellis L M (2006). Roles of nitric oxide synthase inhibition and vascular endothelial growth factor receptor-2 inhibition on vascular morphology and function in an in vivo model of pancreatic cancer. Clin Cancer Res 12(8):2628-33.

Camphausen K, Moses M A, Beecken W D, Khan M K, Folkman J, O'Reilly M S. Radiation therapy to a primary tumor accelerates metastatic growth in mice (2001). Cancer Res 61(5):2207-11.

Cao Y, Li C Y, Moeller B J, Yu D, Zhao Y, Dreher M R, Shan S, Dewhirst M W (2005). Observation of incipient tumour angiogenesis that is independent of hypoxia and hypoxia inducible factor-1 activation. Cancer Res 65(13):5498-505.

Ceradini D J, Kulkarni A R, Callaghan M J, Tepper O M, Bastidas N, Kleinman M E, Capla J M, Galiano R D, Levine J P, Gurtner G C (2004). Progenitor cell trafficking is regulated by hypoxic gradients through HIF-1 induction of SDF-1. Nat Med 10(8):858-64.

Chalkley H W (1943). Method for the quantitative morphological analysis of tissues. J Natl Cancer Inst 4:47-53.

Chang Y S, di Tomaso E, McDonald D M, Jones R, Jain R K, Munn L L. (2000). Mosaic blood vessels in tumors: frequency of cancer cells in contact with flowing blood. Proc Natl Acad Asci USA 97(26):14608-13.

Chantrain C F, DeClerck Y A, Groshen S, McNamara G (2003). Computerized quantification of tissue vascularization using high-resolution slide scanning of whole tumor sections. J Histochem Cytochem 51(2):151-8.

Chaplin D J, Pettit G R, Hill S A (1999). Anti-vascular approaches to solid tumour therapy: evaluation of combretastatin A4 phosphate. Anticancer Res 19(1A):189-95.

Chapman J D (1991).Measurement of tumor hypoxia by invasive and non-invasive procedures: a review of recent clinical studies. Radiother Oncol 20 Suppl 1:13-9.

Chapman J D, Baer K, Lee J (1983). Characteristics of the metabolism-induced binding of misonidazole to hypoxic mammalian cells. Cancer Res 43(4):1523-8.

Chen T W, Yang Z G, Wang Q L, Li Y, Qian L L, Chen H J (2010). Whole tumour quantitative measurement of first-pass perfusion of oesophageal squamous cell carcinoma using 64-row multidetector computed tomography: Correlation with microvessel density. Eur J Radiol [Epub ahead of print].

Chen Y, Zhang J, Dai J, Feng X, Lu H, Zhou C (2009). Angiogenesis of renal cell carcinoma: perfusion CT findings. Abdom Imaging 35(5):622-628.

Ching L M, Cao Z, Kieda C, Zwain S, Jameson M B, Baguley B C (2002). Induction of endothelial cell apoptosis by the antivascular agent 5,6-Dimethylxanthenone-4-acetic acid. Br J Cancer 86:1937-42.

Ciardiello F, Caputo R, Bianco R, Damiano V, Fontanini G, Cuccato S, De Placido S, Bianco A R, Tortora G (2001). Inhibition of growth factor production and angiogenesis in human cancer cells by ZD1839 (Iressa), a selective epidermal growth factor receptor tyrosine kinase inhibitor. Clin Cancer Res 7(5):1459-65.

Corner C, Simonds H, Rojas A M, Dickson J (2007). A Unique High Dose Palliative Radiotherapy Regime used in the Treatment of Lung Cancer. Clin Oncol (R Coll Radiol) 19(3 Suppl):S27.

Coulter J A, McCarthy H O, Worthington J, Robson T, Scott S, Hirst D G (2008). The radiation-inducible pE9 promoter driving inducible nitric oxide synthase radiosensitizes hypoxic tumour cells to radiation. Gene Ther 15(7):495-503.

Cullis E R, Kalber T L, Ashton S E, Cartwright J E, Griffiths J R, Ryan A J, Robinson S P (2006). Tumour overexpression of inducible nitric oxide synthase (iNOS) increases angiogenesis and may modulate the anti-tumour effects of the vascular disrupting agent ZD6126. Microvasc Res 71(2):76-84.

Dachs G U, Steele A J, Coralli C, Kanthou C, Brooks A C, Gunningham S P, Currie M J, Watson A I, Robinson B A, Tozer G M (2006). Anti-vascular agent Combretastatin A-4-P modulates hypoxia inducible factor-1 and gene expression. BMC Cancer 6:280.

D'Amato R J, Loughnan M S, Flynn E, Folkman J (1994). Thalidomide is an inhibitor of angiogenesis. Proc Natl Acad Sci U S A 91(9):4082-5.

Dark G G, Hill S A, Prise V E, Tozer G M, Pettit G R, Chaplin D J (1997). Combretastatin A-4, an agent that displays potent and selective toxicity toward tumor vasculature. Cancer Res 57(10):1829-34.

Davis P D, Dougherty G J, Blakey D C, Galbraith S M, Tozer G M, Holder A L, Naylor M A, Nolan J, Stratford M R, Chaplin D J, Hill S A (2002). ZD6126: a novel vascular-targeting agent that causes selective destruction of tumor vasculature. Cancer Res 62(24):7247-53.

Davis P D, Tozer G M, Naylor M A, Thomson P, Lewis G, Hill S A (2002). Enhancement of vascular targeting by inhibitors of nitric oxide synthase. Int J Radiat Oncol Biol Phys 54(5):1532-6.

Dean P, Mascio L, Ow D, Sudar D, Mullikin J (1990). Proposed standard for image cytometry data files. Cytometry 11(5):561-9.

Denekamp J (1982). Endothelial cell proliferation as a novel approach to targeting tumour therapy. Br J Cancer 46: 711-20.

Denekamp J, Hill S A, Hobson B (1983). Vascular occlusion and tumour cell death. Eur J Cancer Clin Oncol 19:271-5.

Denekamp J, Hobson B (1982). Endothelial cell proliferation in experimental tumours. Br J Cancer 46:711-20.

de Jong J S, van Diest P J, Baak J P (2000). Hot spot microvessel density and the mitotic activity index are strong additional prognostic indicators in invasive breast cancer. Histopathology 36(4):306-12.

de Langen AJ, van den Boogaart VE, Marcus JT, Lubberink M (2008). Use of H2(15)O-PET and DCE-MRI to measure tumor blood flow. Oncologist 13(6):631-44.

De Neve W, Evelhoch J, Everett C, Simpson N, Bissery M C, Corbett T, Valeriote F (1990). Interaction between flavone acetic acid (LM-975, NSC 349512) and radiation in Glasgow's osteogenic sarcoma in vivo. Int J Radiat Oncol Biol Phys 18(6):1359-65.

De Ridder M, Verellen D, Verovski V, Storme G (2008). Hypoxic tumor cell radiosensitization through nitric oxide. Nitric Oxide 19:164-9.

De Schutter H, Landuyt W, Verbeken E, Goethals L, Hermans R, Nuyts S (2005).The prognostic value of the hypoxia markers CA IX and GLUT 1 and the cytokines VEGF and IL 6 in head and neck squamous cell carcinoma treated by radiotherapy +/- chemotherapy. BMC Cancer 5:42.

Devries A F, Griebel J, Kremser C, Judmaier W, Gneiting T, Kreczy A, Ofner D, Pfeiffer K P, Brix G, Lukas P (2001). Tumor microcirculation evaluated by dynamic magnetic resonance imaging predicts therapy outcome for primary rectal carcinoma. Cancer Res 61(6):2513-6.

Dewhirst M W (1998). Concepts of oxygen transport at the microcirculatory level. Semin Radiat Oncol 8(3):143-50.

Dewhirst M W, Ong E T, Braun R D, Smith B, Klitzman B, Evans S M, Wilson D (1999). Quantification of longitudinal tissue pO2 gradients in window chamber tumours: impact on tumour hypoxia. Br J Cancer 79(11-12):1717-22.

Dewhirst M W, Cao Y, Moeller B (2008). Cycling hypoxia and free radicals regulate angiogenesis and radiotherapy response. Nat Rev Cancer 8(6):425-37.

di Tomaso E, Capen D, Haskell A, Hart J, Logie J J, Jain R K, McDonald D M, Jones R, Munn L L (2005). Mosaic tumor vessels: cellular basis and ultrastructure of focal regions lacking endothelial cell markers. Cancer Res 65(13):5740-9.
Dougherty G J, Dougherty S T (2009). Exploiting the tumor microenvironment in the development of targeted cancer gene therapy. Cancer Gene Ther 16(3):279-90.

Dowlati A, Robertson K, Cooney M, Petros W P, Stratford M, Jesberger J, Rafie N, Overmoyer B, Makkar V, Stambler B, Taylor A, Waas J, Lewin J S, McCrae K R, Remick S C (2002). A phase 1 pharmacokinetic and translational study of the novel vascular targeting agent combretastatin a-4 phosphate on a single dose intravenous schedule in patients with advanced cancer. Cancer Res 62(12):3408-16.

Drevs J, Siegert P, Medinger M, Mross K, Strecker R, Zirrgiebel U, Harder J, Blum H, Robertson J, Jürgensmeier J M, Puchalski T A, Young H, Saunders O, Unger C (2007). Phase I clinical study of AZD2171, an oral vascular endothelial growth factor signaling inhibitor, in patients with advanced solid tumors. J Clin Oncol 25(21):3045-54.

Duan Y, Yu L J, Lu P O, Wang W Z (2008). Correlation between SUV of (18)F-FDG PET-CT and the expression of GLUT1, MVD and Ki67 in non-small cell lung cancer. Zhonghua Zhong Liu Za Zhi 30(10):764-7.

Ebhard A, Kahlert S, Goede V, Hemmerlein B, Plate K H, Augustin H G (2000). Heterogeneity of angiogenesis and blood vessel maturation in human tumors: implications for antiangiogenic tumor therapies. Cancer Res 60:1388-93.

Eder J P Jr, Supko J G, Clark J W, Puchalski T A, Garcia-Carbonero R, Ryan D P, Shulman L N, Proper J, Kirvan M, Rattner B, Connors S, Keogan M T, Janicek M J, Fogler W E, Schnipper L, Kinchla N, Sidor C, Phillips E, Folkman J, Kufe D W (2002). Phase I clinical trial of recombinant human endostatin administered as a short intravenous infusion repeated daily. J Clin Oncol 20(18):3772-84.

Eisenhauer E A, Therasse P, Bogaerts J, Schwartz L H, Sargent D, Ford R, Dancey J, Arbuck S, Gwyther S, Mooney M, Rubinstein L, Shankar L, Dodd L, Kaplan R, Lacombe D, Verweij J (2009). New response evaluation criteria in solid tumours: revised RECIST guideline (version 1.1). Eur J Cancer 45(2):228-47.

Escudier B, Eisen T, Stadler W M, Szczylik C, Oudard S, Siebels M, Negrier S, Chevreau C, Solska E, Desai A A, Rolland F, Demkow T, Hutson T E, Gore M, Freeman S, Schwartz B, Shan M, Simantov R, Bukowski R M; TARGET Study Group (2007). Sorafenib in advanced clear-cell renal-cell carcinoma. N Engl J Med 356(2):125-34.

Evelhoch J L, LoRusso P M, He Z, DelProposto Z, Polin L, Corbett T H, Langmuir P, Wheeler C, Stone A, Leadbetter J, Ryan A J, Blakey D C, Waterton J C (2004). Magnetic resonance imaging measurements of the response of murine and human tumors to the vascular-targeting agent ZD6126. Clin Cancer Res 10(11):3650-7.

Ferrara N, Kerbel R S (2005). Angiogenesis as a therapeutic target. Nature 438(7070):967-74.

Folkes L K, Christlieb M, Madej E, Stratford M R, Wardman P (2007). Oxidative metabolism of combretastatin A-1 produces quinone intermediates with the potential to bind to nucleophiles and to enhance oxidative stress via free radicals. Chem Res Toxicol 20(12):1885-94.

Folkins C, Shaked Y, Man S, Tang T, Lee C R, Zhu Z, Hoffman R M, Kerbel R S (2009). Glioma tumor stem-like cells promote tumor angiogenesis and vasculogenesis via vascular endothelial growth factor and stromal-derived factor 1. Cancer Res 69(18):7243-51.

Folkman J (1971). Tumor angiogenesis: Therapeutic implications. N Engl J Med 285:1182-6.

Folkman J (1990). What is the evidence that tumors are angiogenesis dependent? J Natl Cancer Inst 82(1):4-6.

Folkman J (1995). Angiogenesis in cancer, vascular, rheumatoid and other disease. Nat Med 1(1):27-31.
Folkman J (2006). Antiangiogenesis in cancer therapy--endostatin and its mechanisms of action. Exp Cell Res 312(5):594-607.

Folkman J, Cole P, Zimmerman S (1966). Tumor behaviour in isolated perfused organs: In vitro growth and metastasis of biopsy material in rabbit thyroid and canine intestinal segment. Ann Surg 164:491-502.

Fong G H, Rossant J, Gersenstein M, Breiman M L (1995). Role of the Flt-1 receptor tyrosine kinase in regulating the assembly of vascular endothelium. Nature 376:62-6.

Forsythe J A, Jiang B H, Iyer N V, Agani F, Leung S W, Koos R D, Semanza G L (1996). Activation of vascular endothelial growth factor gene transcription by hypoxia-inducible factor 1. Mol Cell Biol 16(9):4604-13.

Fukumura D, Gohongi T, Kadambi A, Izumi Y, Ang J, Yun C O, Buerk D G, Huang P L, Jain R K (2001). Predominant role of endothelial nitric oxide synthase in vascular endothelial growth factor-induced angiogenesis and vascular permeability. Proc Natl Acad Sci USA 98(5):2604-9.

Fukumura D, Jain R K (2008). Imaging angiogenesis and the microenvironment. APMIS 116(7-8):695-715.

Fukumura D, Kashiwagi S, Jain R K (2006). The role of nitric oxide in tumour progression. Nat Rev Cancer 6(7):521-34.

Fukumura D, Xu L, Chen Y, Gohongi T, Seed B, Jain R K (2001). Hypoxia and acidosis independently up-regulate vascular endothelial growth factor transcription in brain tumors in vivo. Cancer Res 61(16):6020-4.

Gabra H, Jameson M, AS1404–202 Study Group Investigators (2007). Update of phase II study of DMXAA (AS1404) combined with carboplatin and paclitaxel in recurrent ovarian cancer. Eur J Cancer Suppl 5(4):319, abstract 5028.

Gabryś D, Greco O, Patel G, Prise K M, Tozer G M, Kanthou C (2007). Radiation effects on the cytoskeleton of endothelial cells and endothelial monolayer permeability. Int J Radiat Oncol Biol Phys 69(5):1553-62.

Gafner V, Trachsel E, Neri D (2006). An engineered antibody-interleukin-12 fusion protein with enhanced tumor vascular targeting properties. Int J Cancer 119(9):2205-12.

Galbraith S M, Lodge M A, Taylor N J, Rustin G J, Bentzen S, Stirling J J, Padhani A R (2002). Reproducibility of dynamic contrast-enhanced MRI in human muscle and tumours: comparison of quantitative and semi-quantitative analysis. NMR Biomed. Apr;15(2):132-42.

Galbraith S M, Maxwell R J, Lodge M A, Tozer G M, Wilson J, Taylor N J, Stirling J J, Sena L, Padhani A R, Rustin G J (2003). Combretastatin A4 phosphate has tumor antivascular activity in rat and man as demonstrated by dynamic magnetic resonance imaging. J Clin Oncol 21(15):2831-42.

Galbraith S M, Rustin G J, Lodge M A, Taylor N J, Stirling J J, Jameson M, Thompson P, Hough D, Gumbrell L, Padhani A R (2002). Effects of 5,6-dimethylxanthenone-4-acetic acid on human tumor microcirculation assessed by dynamic contrast-enhanced magnetic resonance imaging. J Clin Oncol 20(18):3826-40.

Garcia-Barros M, Paris F, Cordon-Cardo C, Lyden D, Rafii S, Haimovitz-Friedman A, Fuks Z, Kolesnick R (2003). Tumor response to radiotherapy regulated by endothelial cell apoptosis. Science 300(5622):1155-9.

Gasparini G, Longo R, Fanelli M, Taylor B A (2005). Combination of antiangiogenic therapy with other anticancer therapies: results, challenges and open questions. J Clin Oncol 23(6):1295-1311

Giatromanolaki A, Koukourakis M I, Kakolyris S, Turley H, O'Byrne K, Scott P A, Pezzella F, Georgoulias V, Harris A L, Gatter K C (1998). Vascular endothelial growth factor, wild-type p53, and angiogenesis in early operable non-small cell lung cancer. Clin Cancer Res 4(12):3017-24.

Ginns L C, Roberts D H, Mark E J, Brusch J L, Marler J J (2003). Pulmonary capillary hemangiomatosis with atypical endotheliomatosis: successful antiangiogenic therapy with doxycycline. Chest 124:2017–2022.

Goh V, Halligan S, Daley F, Wellsted D M, Guenther T, Bartram C I (2008). Colorectal tumor vascularity: quantitative assessment with multidetector CT--do tumor perfusion measurements reflect angiogenesis? Radiology 249(2):510-7.

Goldman E (1907). The growth of malignant disease in man and the lower animals with special reference to the vascular system. Lancet North Am Ed 2:1236-40.

Gonzalez J, Kumar A J, Conrad C A, Levin V A (2007). Effect of bevacizumab on radiation necrosis of the brain. Int J Radiat Oncol Biol Phys 67(2):323-6.

Gorski D H, Beckett M A, Jaskowiak N T, Calvin D P, Mauceri H J, Salloum R M, Seetharam S, Koons A, Hari D M, Kufe D W, Weichselbaum R R (1999). Blockage of the vascular endothelial growth factor stress response increases the antitumor effects of ionizing radiation. Cancer Res 59(14):3374-8.

Gould S, Westwood F R, Curwen J O, Ashton S E, Roberts D W, Lovick S C, Ryan A J (2007). Effect of pretreatment with atenolol and nifedipine on ZD6126-induced cardiac toxicity in rats J Natl Cancer Inst. 99(22):1724-8.

Grau C, Horsman M R, Overgaard J (1992). Improving the radiation response in a C3H mouse mammary carcinoma by normobaric oxygen or carbogen breathing. Int J Radiat Oncol Biol Phys 22(3):415-9.

Gray L H, Conger A D, Ebert M, Hornsey S, Scott O C (1953). The concentration of oxygen dissolved in tissues at the time of irradiation as a factor in radiotherapy. Br J Radiol 26(312):638-48.

Gray L H, Green F O, Hawes C A (1958). Effect of nitric oxide on the radiosensitivity of tumour cells. Nature 182(4640):952-3.

Grosios K, Loadman P M, Swaine D J, Pettit G R, Bibby M C (2000). Combination chemotherapy with combretastatin A-4 phosphate and 5-fluorouracil in an experimental murine colon adenocarcinoma. Anticancer Res 20:229-34.

Gustafson D L, Frederick B, Merz A L, Raben D (2008). Dose scheduling of the dual VEGFR and EGFR tyrosine kinase inhibitor vandetanib (ZD6474, Zactima) in combination with radiotherapy in EGFR-positive and EGFR-null human head and neck tumor xenografts. Cancer Chemother Pharmacol 61(2):179-88

Haber R S, Rathan A, Weiser K R, Pritsker A, Itzkowitz S H, Bodian C, Slater G, Weiss A, Burstein D E (1998). GLUT1 glucose transporter expression in colorectal carcinoma: a marker for poor prognosis. Cancer 83(1):34-40.

Hanahan D, Folkman J (1996). Patterns and emerging mechanisms of the angiogenic switch during tumorigenesis. Cell 86(3):353-64.

Harris A L (2002). Hypoxia: a key regulatory factor in tumour growth. Nat Rev Cancer 2(1):38-47.

Harris S R, Schoeffner D J, Yoshiji H, Thorgeirsson U P (2002). Tumor growth enhancing effects of vascular endothelial growth factor are associated with increased nitric oxide synthase activity and inhibition of apoptosis in human breast cancer xenografts. Cancer Lett 179(1):95-101.

Hartford A C, Gohongi T, Fukumura D, Jain R K (2000). Irradiation of a primary tumor, unlike surgical removal, enhances angiogenesis suppression at a distal site: potential role of host-tumor interaction. Cancer Res 60(8):2128-31.

Hast J, Schiffer I B, Neugebauer B, Teichman E, Schreiber W, Brieger J, Kim D W, Gebhard S, Born C J, Strugala M, Sagemüller J, Brenner W, Mann W J, Oesch F, Thelen M, Hengstler J G (2002). Angiogenesis and fibroblast proliferation precede formation of recurrent tumors after radiation therapy in nude mice. Anticancer Res 22(2A):677-88.

Hattori K, Dias S, Hessig B, Hackett N R, Lyden D, Tateno M, Hicklin D J, Zhu Z, Witte L, Crystal R G, Moore M A, Rafii S (2001). Vascular endothelial growth factor and angiopoietin-1 stimulate postnatal haematopoiesis by recruitment of vasculogenic and haematopoietic stem cells. J Exp Med 193(9):1005-14.

Heinrich M C, Maki R G, Corless C L, Antonescu C R, Harlow A, Griffin D, Town A, McKinley A, Ou W B, Fletcher J A, Fletcher C D, Huang X, Cohen D P, Baum C M, Demetri G D (2008). Primary and secondary kinase genotypes correlate with the biological and clinical activity of sunitinib in imatinib-resistant gastrointestinal stromal tumor. J Clin Oncol 26(33):5352-9

Helmlinger G, Yuan F, Dellian M, Jain R K (1997). Interstitial pH and pO2 gradients in solid tumors in vivo: high-resolution measurements reveal a lack of correlation. Nat Med 3(2):177-82.

Herbst R S, Mullani N A, Davis D W, Hess K R, McConkey D J, Charnsangavej C, O'Reilly M S, Kim H W, Baker C, Roach J, Ellis L M, Rashid A, Pluda J, Bucana C, Madden T L, Tran H T, Abbruzzese J L (2002). Development of biologic markers of response and assessment of antiangiogenic activity in a clinical trial of human recombinant endostatin. J Clin Oncol 20(18):3804-14.

Heymach J V, Johnson B E, Prager D, Csada E, Roubec J, Pesek M, Spásová I, Belani C P, Bodrogi I, Gadgeel S, Kennedy S J, Hou J, Herbst R S (2007). Randomized, placebo-controlled phase II study of vandetanib plus docetaxel in previously treated non small-cell lung cancer. J Clin Oncol 25(27):4270-7.

Higashi K, Ueda Y, Sakurai A, Wang X M, Xu L, Murakami M, Seki H, Oguchi M, Taki S, Nambu Y, Tonami H, Katsuda S, Yamamoto I (2000). Correlation of Glut-1 glucose transporter expression with. Eur J Nucl Med 27(12):1778-85.

Hill S A, Lonergan S J, Denekamp J, Chaplin D J (1993). Vinca alkaloids: anti-vascular effects in a murine tumour. Eur J Cancer 9:1320-4.

Hill S A, Tozer G M, Pettit G R, Chaplin D J (2002). Preclinical evaluation of the antitumour activity of the novel vascular targeting agent Oxi 4503. Anticancer Res 22:1453-8.

Hill S A, Williams K B, Denekamp J (1989). Vascular collapse after flavone acetic acid: a possible mechanism of its anti-tumour action. Eur J Cancer Clin Oncol 25:1419-24.

Hlatky L, Hahnfeldt P, Folkman J (2002). Clinical application of antiangiogenic therapy: microvessel density, what it does and doesn't tell us. J Natl Cancer Inst 94(12):883-93.

Hoang T, Huang S, Armstrong E, Eickhoff J C, Harari P M (2006). Augmentation of radiation response with the vascular targeting agent ZD6126. Int J Radiat Oncol Biol Phys 64(5):1458-65.

Hobbs A J, Higgs A, Moncada S (1999). Inhibition of nitric oxide synthase as a potential therapeutic target. Annu Rev Pharmacol Toxicol 39:191-220.

Höckel M, Vaupel P (2001).Tumor hypoxia: definitions and current clinical, biologic, and molecular aspects. J Natl Cancer Inst. Feb 21;93(4):266-76.

Hokland S L, Horsman M R (2007). The new vascular disrupting agent combretastatin-A1-disodium-phosphate (OXi4503) enhances tumour response to mild hyperthermia and thermoradiosensitization. Int J Hyperthermia 23(7):599-606.

Honess D J, Hu D E, Bleehen N M (1991). A study of the mechanism of hydralazine enhancement of thermal damage in the KHT tumour. Int J Hyperthermia 7(4):667-79.

Hori K, Furumoto S, Kubota K (2008). Tumor blood flow interruption after radiotherapy strongly inhibits tumor regrowth. Cancer Sci 99(7):1485-91.

Hori K, Saito S (2003). Microvascular mechanisms by which the combretastatin A-4 derivative AC7700 (AVE8062) induces tumour blood flow stasis. Br J Cancer 89(7):1334-44.

Hori K, Saito S, Nihei Y, Suzuki M, Sato Y (1999). Antitumor effects due to irreversible stoppage of tumor tissue blood flow: evaluation of a novel combretastatin A-4 derivative, AC7700. Jpn J Cancer Res 90(9):1026-38.

Horsman M R, Christensen K L, Overgaard J (1989). Hydralazine-induced enhancement of hyperthermic damage in a C3H mammary carcinoma in vivo. Int J Hyperthermia 5(2):123-36.

Horsman M R, Murata R (2002). Combination of vascular targeting agents with thermal or radiation therapy. Int J Radiat Oncol Biol Phys 54(5):1518-23.

Horsman M R, Murata R, Breidahl T, Nielsen F U, Maxwell R J, Stødkiled-Jørgensen H, Overgaard J (2000). Combretastatins novel vascular targeting drugs for improving anti-cancer therapy. Adv Exp Med Biol 476:311-23.

Horsman M R, Murata R, Overgaard J (2001). Improving local tumour control by combing vascular targeting drugs, mild hyperthermia, and radiation. Acta Oncol 40(4):497-503.

Horsman M R, Murata R, Overgaard J (2002). Combination studies with combretastatin radiation: effects in early and late responding tissues. Radiother Oncol 64:S50.

Horsman M R, Overgaard J (2007). Hyperthermia: a potent enhancer of radiotherapy. Clin Oncol (R Coll Radiol) 19(6):418-26.

Horsman MR, Siemann DW (2006). Pathophysiologic effects of vascular-targeting agents and the implications for combination with conventional therapies. Cancer Res 66(24):11520-39.

Hoskin P J, Carnell D M, Taylor N J, Smith R E, Stirling J J, Daley F M, Saunders M I, Bentzen S M, Collins D J, d'Arcy J A, Padhani A P (2007). Hypoxia in prostate cancer: correlation of BOLD-MRI with pimonidazole immunohistochemistry-initial observations. Int J Radiat Oncol Biol Phys 68(4):1065-71.

Hua J, Sheng Y, Pinney K G, Garner C M, Kane R R, Prezioso J A, Pettit G R, Chaplin D J, Edvardsen K (2003). Oxi4503, a novel vascular targeting agent: effects on blood flow and antitumour activity in comparison to combretastatin A-4 phosphate. Anticancer Res 23(2B):1433-40.

Hudes G, Carducci M, Tomczak P, Dutcher J, Figlin R, Kapoor A, Staroslawska E, Sosman J, McDermott D, Bodrogi I, Kovacevic Z, Lesovoy V, Schmidt-Wolf I G, Barbarash O, Gokmen E, O'Toole T, Lustgarten S, Moore L, Motzer RJ; Global ARCC Trial (2007). Temsirolimus, interferon alfa, or both for advanced renal-cell carcinoma. NEngl Jmed 356:2271-81.

Hurwitz H, Fehrenbacher L, Novotny W, Cartwright T, Hainsworth J, Heim W, Berlin J, Baron A, Griffing S, Holmgren E, Ferrara N, Fyfe G, Rogers B, Ross R, Kabbinavar F (2004). Bevacizumab plus irinotecan, fluorouracil, and leucovorin for metastatic colorectal cancer. N Engl J Med 350(23):2335-42.

Hutchison G J, Valentine H R, Loncaster J A, Davidson S E, Hunter R D, Roberts SA, Harris A L, Stratford I J, Price P M, West C M (2004). Hypoxia-inducible factor 1alpha expression as an intrinsic marker of hypoxia: correlation with tumor oxygen, pimonidazole measurements, and outcome in locally advanced carcinoma of the cervix. Clin Cancer Res 10(24):8405-12.

Ide A G, Baker N H, Warren S L (1939). Vascularization of the Brown Pearce rabbit epithelioma transplant as seen in the transparent ear chamber. Am J Roentgenol 42:891–899.

Ignarro L J (2002). Nitric oxide as a unique signalling molecule in the vascular system: a historical overview. J Physiol Pharmacol 53:503–514.

Irion L C, Prolla J C, Hartmann A A, da Silva V D (2003). [Morphometric intratumoral microvessel area evaluation could be a useful indicator for coadjuvant therapy in ressected NSCLC]. Rev Port Pneumol 9(1):19-32.

Irion L C, Prolla J C, Hartmann A A, Irion K L, Da Silva V D (2008). Angiogenesis in non-small cell lung cancer: microvessel area in needle biopsy in vascular tumor density. Anal Quant Cytol Histol 30(2):83-91.

Ivanov S, Liao S Y, Ivanova A, Danilkovitch-Miagkova A, Tarasova N, Weirich G, Merrill M J, Proescholdt M A, Oldfield E H, Lee J, Zavada J, Waheed A, Sly W, Lerman M I, Stanbridge E J (2001). Expression of hypoxia-inducible cell-surface transmembrane carbonic anhydrases in human cancer. Am J Pathol 158(3):905-19.

Izumi Y, Xu L, di Tomaso E, Fukumura D, Jain R K (2002). Tumour biology: herceptin acts as an anti-angiogenic cocktail. Nature 416(6878):279-80.

Jain R K (1987). Transport of molecules across tumor vasculature. Cancer Metastasis Rev 6(4):559-93.

Jain R K (1988). Determinants of tumour blood flow: a review. Cancer Res 48(10):2641-58.

Jain R K (2003). Molecular regulation of vessel maturation. Nat Med 9(6):685-93.

Jain R K (2005). Normalisation of tumor vasculature: an emerging concept in antiangiogenic therapy. Science 307(5706):58-62.

Janssen H L, Haustermans K M, Sprong D, Blommestijn G, Hofland I, Hoebers F J, Blijweert E, Raleigh J A, Semenza G L, Varia M A, Balm A J, van Velthuysen M L, Delaere P, Sciot R, Begg A C (2002). HIF-1A, pimonidazole, and iododeoxyuridine to estimate hypoxia and perfusion in human head-and-neck tumors. Int J Radiat Oncol Biol Phys 54(5):1537-49.

Jaschke W, Sievers R S, Lipton M J, Cogan M G (1990). Cine-computed tomographic assessment of regional renal blood flow. Acta Radiol 31(1):77-81.

Jinzaki M, Tanimoto A, Mukai M, Ikeda E, Kobayashi S, Yuasa Y, Narimatsu Y, Murai M (2000). Double-phase helical CT of small renal parenchymal neoplasms: correlation with pathologic findings and tumor angiogenesis. J Comput Assist Tomogr 24(6):835-42.

Jordan B F, Runquist M, Raghunand N, Baker A, Williams R, Kirkpatrick L, Powis G, Gillies R J (2005). Dynamic contrast-enhanced and diffusion MRI show rapid and dramatic changes in tumor microenvironment in response to inhibition of HIF-1alpha using PX-478. Neoplasia 7(5):475-85.

Kalas W, Gilpin S, Yu J L, May L, Krchnakova H, Bornstein P, Rak J (2003). Restoration of thrombospondin 1 expression in tumor cells harbouring mutant ras oncogene by treatment with low doses of doxycycline, Biochem Biophys Res Commun 310:109–114.

Kanthou C, Tozer G M (2002). The tumor vascular targeting agent combretastatin A-4-phosphate induces reorganization of the actin cytoskeleton and early membrane blebbing in human endothelial cells. Blood 99(6):2060-9.

Karkkainen M J, Mäkinen T, Alitalo K (2002). Lymphatic endothelium: a new frontier of metastasis research. Nat Cell Biol 4(1):E2-5.

Kashiwagi S, Izumi Y, Gohongi T, Demou Z N, Xu L, Huang P L, Buerk D G, Munn L L, Jain R K, Fukumura D (2005). NO mediates mural cell recruitment and vessel morphogenesis in murine melanomas and tissue-engineered blood vessels. J Clin Invest 115(7):1816-27.

Kashiwagi S, Tsukada K, Xu L, Miyazaki J, Kozin S V, Tyrrell J A, Sessa W C, Gerweck L E, Jain R K, Fukumura D (2008). Perivascular nitric oxide gradients normalize tumor vasculature. Nat Med 14(3):255-7.

Ke Q, Bodylak N, Rigor D L, Hurst N W, Chaplin D, Kang P M (2007). International Conference on Vascular Targeted Therapies in Oncology.

Kerbel R, Folkman J (2002). Clinical translation of angiogenesis inhibitors. Nat Rev Cancer 2(10):727-39.

Kim K J, Li B, Winer J, Armanini M, Gillett N, Phillips H S, Ferrara N (1993). Inhibition of vascular endothelial growth factor-induced angiogenesis suppresses tumour growth in vivo. Nature 362(6423):841-4.

Kim T J, Ravoori M, Landen C N, Kamat A A, Han L Y, Lu C, Lin Y G, Merritt W M, Jennings N, Spannuth W A, Langley R, Gershenson D M, Coleman R L, Kundra V, Sood A K (2007). Antitumor and antivascular effects of AVE8062 in ovarian carcinoma. Cancer Res 7(19):9337-45.

King A, Selak M A, Gottlieb E (2006). Succinate dehydrogenase and fumarate hydratase: linking mitochondrial dysfunction and cancer. Oncogene. 25(34):4675-82.

Kirwan I G, Loadman P M, Swaine D J, Anthoney D A, Pettit G R, Lippert J W 3rd, Shnyder S D, Cooper P A, Bibby M C (2004). Comparative preclinical pharmacokinetic and metabolic studies of the combretastatin prodrugs combretastatin A4v phosphate and A1 phosphate. Clin Cancer Res 10:1446-53.

Kiura K, Nakagawa K, Shinkai T, Eguchi K, Ohe Y, Yamamoto N, Tsuboi M, Yokota S, Seto T, Jiang H, Nishio K, Saijo N, Fukuoka M (2008). A randomized, double-blind, phase IIa dose-finding study of Vandetanib (ZD6474) in Japanese patients with non-small cell lung cancer. J Thorac Oncol 3(4):386-93.

Koch S, Mayer F, Honecker F, Schittenhelm M, Bokemeyer C (2003). Efficacy of cytotoxic agents used in the treatment of testicular germ cell tumours under normoxic and hypoxic conditions in vitro. Br J Cancer 89:2133–2139.

Krause M, Ostermann G, Petersen C, Yaromina A, Hessel F, Harstrick A, van der Kogel A J, Thames H D, Baumann M (2005). Decreased repopulation as well as increased reoxygenation contribute to the improvement in local control after targeting of the EGFR by C225 during fractionated irradiation. Radiother Oncol 76(2):162-7.

Krogh A (1922). The Anatomy and Physiology of Capillaries, Yale University Press, New York.

Konerding M A, Malkush W, Klapthor B, van Ackern C, Fait E, Hill S A, Parkins C, Chaplin D J, Presta M, Denekamp J (1999). Evidence for characteristic vascular patterns in solid tumours: quantitative studies using corrosion casts. Br J Cancer 80(5-6):724-32.

Koppenol W H, Bounds P L, Dang C V (2011). Otto Warburg's contributions to current concepts of cancer metabolism. Nat Rev Cancer 11(5):325-37.

Kucia M, Reca R, Miekus K, Wanzeck J, Wojakowski W, Janowska-Wieczorek A, Ratajczak J, Ratajczak M Z (2005). Trafficking of normal stem cells and metastasis of cancer stem cells involve similar mechanisms: pivotal role of the SDF-1-CXCR4 axis. Stem Cells 23(7):879-94.

Kurup A, Lin C W, Murry D J, Dobrolecki L, Estes D, Yiannoutsos C T, Mariano L, Sidor C, Hickey R, Hanna N (2006). Recombinant human angiostatin (rhAngiostatin) in combination with paclitaxel and carboplatin in patients with advanced non-small-cell lung cancer: a phase II study from Indiana University. Ann Oncol 17(1):97-103.

Lal A, Peters H, St Croix B, Haroon Z A, Dewhirst M W, Strausberg R L, Kaanders J H, van der Kogel A J, Riggins G J (2001). Transcriptional response to hypoxia in human tumors. J Natl Cancer Inst 93(17):1337-43.

Lamuraglia M, Escudier B, Chami L, Schwartz B, Leclère J, Roche A, Lassau N (2006). To predict progression-free survival and overall survival in metastatic renal cancer treated with sorafenib: pilot study using dynamic contrast-enhanced Doppler ultrasound. Eur J Cancer 42(15):2472-9.

Landuyt W, Ahmed B, Nuyts S, Theys J, Op de Beeck M, Rijnders A, Anné J, van Oosterom A, van den Bogaert W, Lambin P (2001). In vivo antitumor effect of vascular targeting combined with either ionizing radiation or anti-angiogenesis treatment. Int J Radiat Oncol Biol Phys 49(2):443-50.

Lankester K J, Taylor N J, Stirling J J, Boxall J, D'Arcy J A, Leach M O, Rustin G J, Padhani A R (2005). Effects of platinum/taxane based chemotherapy on acute perfusion in human pelvic tumours measured by dynamic MRI. Br J Cancer. Oct 31;93(9):979-85.

Lash C J, Li A E, Rutland M, Bagueley B C, Zwi L J, Wilson W R (1998). Enhancement of the anti-tumour effects of the antivascular agent 5,6-dimethylxanthenone-4-acetic acid (DMXAA) by combining with 5-hydroxytryptamine and bioreductive drugs. Br J Cancer 78(4):439-45.

Lassau N, Chami L, Benatsou B, Peronneau P, Roche A (2007). Dynamic contrast-enhanced ultrasonography (DCE-US) with quantification of tumor perfusion: a new diagnostic tool to evaluate the early effects of antiangiogenic treatment. Eur Radiol 17 Suppl 6:F89-98.

Laughner E, Taghavi P, Chiles K, Mahon P C, Semenza G L (2001). HER2 (neu) signaling increases the rate of hypoxia-inducible factor 1alpha (HIF-1alpha) synthesis: novel mechanism for HIF-1-mediated vascular endothelial growth factor expression. Mol Cell Biol 21(12):3995-4004.

Lee T Y, Tjin Tham Sjin R M, Movahedi S, Ahmed B, Pravda E A, Lo K M, Gillies S D, Folkman J, Javaherian K (2008). Linking antibody Fc domain to endostatin significantly improves endostatin half-life and efficacy. Clin Cancer Res 14(5):1487-93.

Leith J T, Padfield G, Quaranto L, Michelson S (1992). Effect of preirradiation of transplantation site on growth characteristics and hypoxic fractions in human colon tumor xenografts. Cancer Res 52(8):2162-6.

Lester J F, Macbeth F R, Toy E, Coles B (2006). Palliative radiotherapy regimens for non-small cell lung cancer. Cochrane Database Syst Rev, CD002143.

Lewis W H (1927). The vascular pattern of tumors. Johns Hopkins Hosp. Bull. 41, 156–162.

Ley C D, Horsman M R, Kristjansen P E (2007). Early effects of combretastatin-A4 disodium phosphate on tumor perfusion and interstitial fluid pressure. Neoplasia 9(2):108-12.

Li C Y, Shan S, Huang O, Braun R D, Lanzen J, Hu K, Lin P, Dewhirst M W (2000). Initial stages of tumor cell-induced angiogenesis: evaluation via skin window chambers in rodent models. J Natl Cancer Inst 92(2):143-7.
Li L, Rojiani A, Siemann D W (1998). Targeting the tumor vasculature with combretastatin A-4 disodium phosphate: effects on radiation therapy. Int J Radiat Oncol Biol Phys 42(4):899-903.

Li H, Fan X, Houghton J (2007). Tumour microenvironment: The role of the tumour stroma in cancer. J Cell Biochem 101:805-15.

Lin PS, Ho KC, Tsai S (1996). Tumor necrosis factor-alpha suppresses the regrowth of fractionated irradiated endothelial cells in vitro. Cancer Biother Radiopharm 11(4):251-7.

Lin C M, Singh S B, Chu P S, Dempcy R O, Schmidt J M, Pettit G R, Hamel E (1988). Interactions of tubulin with potent natural and synthetic analogs of the antimitotic agent combretastatin: a structure-activity study. Mol Pharmacol 34(2):200-8.

Liu G, Rugo H S, Wilding G, McShane T M, Evelhoch J L, Ng C, Jackson E, Kelcz F, Yeh B M, Lee F T Jr, Charnsangavej C, Park J W, Ashton E A, Steinfeldt H M, Pithavala Y K, Reich S D, Herbst R S (2005). Dynamic contrast-enhanced magnetic resonance imaging as a pharmacodynamic measure of response after acute dosing of AG-013736, an oral angiogenesis inhibitor, in patients with advanced solid tumors: results from a phase I study. J Clin Oncol 23(24):5464-73.

Llovet J M, Ricci S, Mazzaferro V, Hilgard P, Gane E, Blanc JF, de Oliveira AC, Santoro A, Raoul JL, Forner A, Schwartz M, Porta C, Zeuzem S, Bolondi L, Greten TF, Galle PR, Seitz JF, Borbath I, Häussinger D, Giannaris T, Shan M, Moscovici M, Voliotis D, Bruix J; SHARP Investigators Study Group (2008). Sorafenib in advanced hepatocellular carcinoma. N Engl J Med 359:378-390.

López A, Lorente J A, Steingrub J, Bakker J, McLuckie A, Willatts S, Brockway M, Anzueto A, Holzapfel L, Breen D, Silverman M S, Takala J, Donaldson J, Arneson C, Grove G, Grossman S, Grover R (2004). Multiple-center, randomized, placebo-controlled, double-blind study of the nitric oxide synthase inhibitor 546C88: effect on survival in patients with septic shock. Crit Care Med 32(1):21-30.

Loncaster J A, Harris A L, Davidson S E, Logue J P, Hunter R D, Wycoff C C, Pastorek J, Ratcliffe P J, Stratford I J, West C M (2001). Carbonic anhydrase (CA IX) expression, a potential new intrinsic marker of hypoxia: correlations with tumor oxygen measurements and prognosis in locally advanced carcinoma of the cervix. Cancer Res 61(17):6394-9.

Lowndes S A, Adams A, Timms A, Fisher N, Smythe J, Watt S M, Joel S, Donate F, Hayward C, Reich S, Middleton M, Mazar A, Harris A L (2008). Phase I study of copper-binding agent ATN-224 in patients with advanced solid tumors. Clin Cancer Res 14(22):7526-34.

Ma S H, Le H B, Jia B H, Wang Z X, Xiao Z W, Cheng X L, Mei W, Wu M, Hu Z G, Li Y G (2008). Peripheral pulmonary nodules: relationship between multi-slice spiral CT perfusion imaging and tumor angiogenesis and VEGF expression. BMC Cancer 8:186.

Maglione D, Guerriero V, Viglietto G, Delli-Bovi P, Persico M G (1991). Isolation of a human placenta cDNA coding for a protein related to the vascular permeability factor. Proc Natl Acad Sci USA 88:9267-71.

Maher E J, Timothy A, Squire C J, Goodman A, Karp S J, Paine C H, Ryall R, Read G (1993). Audit: the use of radiotherapy for NSCLC in the UK. Clin Oncol (R Coll Radiol), 5, 72-9.

Marletta M A (1993). Nitric Oxide synthase structure and mechanism. J Biol Chem 268(17):12231-4.

Masferrer J L, Leahy K M, Koki A T, Zweifel B S, Settle S L, Woerner B M, Edwards D A, Flickinger A G, Moore R J, Seibert K (2000). Antiangiogenic and antitumor activities of cyclooxygenase-2 inhibitors. Cancer Res 60(5):1306-11.

Mayr N A, Yuh W T, Arnholt J C, Ehrhardt J C, Sorosky J I, Magnotta V A, Berbaum K S, Zhen W, Paulino A C, Oberley L W, Sood A K, Buatti J M (2000). Pixel analysis of MR perfusion imaging in predicting radiation therapy outcome in cervical cancer. J Magn Reson Imaging 12(6):1027-33.

Mazzucchelli R, Montironi R, Santinelli A, Lucarini G, Pugnaloni A, Biagini G (2000). Vascular endothelial growth factor expression and capillary architecture in high-grade PIN and prostate cancer in untreated and androgen-ablated patients. Prostate 45(1):72-9.

McCarville M B, Streck C J, Dickson P V, Li C S, Nathwani A C, Davidoff A M (2006). Angiogenesis inhibitors in a murine neuroblastoma model: quantitative assessment of intratumoral blood flow with contrast-enhanced gray-scale US. Radiology 240(1):73-81.

McDonald D M and Choyke P L (2003). Imaging of angiogenesis: from microscope to clinic. Nat Med 9(6):713-25.

McKeage M J, Jameson M B, AS1404–201 Study Group Investigators (2008). Comparison of safety and efficacy between squamous and non-squamous non-small cell lung cancer (NSCLC) patients in phase II studies of DMXAA (ASA404). J Clin Oncol 26(15S):8072

McNeel D G, Eickhoff J, Lee F T, King D M, Alberti D, Thomas J P, Friedl A, Kolesar J, Marnocha R, Volkman J, Zhang J, Hammershaimb L, Zwiebel J A, Wilding G (2005). Phase I trial of a monoclonal antibody specific for alphavbeta3 integrin (MEDI-522) in patients with advanced malignancies, including an assessment of effect on tumor perfusion. Clin Cancer Res 11(21):7851-60.

Meert A P, Paesmans M, Martin B, Delmotte P, Berghmans T, Verdebout J M, Lafitte J J, Mascaux C, Sculier J P (2002).The role of microvessel density on the survival of patients with lung cancer: a systematic review of the literature with meta-analysis. Br J Cancer 87(7):694-701.

Meijerink M R, van Cruijsen H, Hoekman K, Kater M, van Schaik C, van Waesberghe J H, Giaccone G, Manoliu R A (2007). The use of perfusion CT for the evaluation of therapy combining AZD2171 with gefitinib in cancer patients. Eur Radiol 17(7):1700-13.

Meyer T, Gaya A M, Dancey G, Stratford M R, Othman S, Sharma S K, Wellsted D, Taylor N J, Stirling J J, Poupard L, Folkes L K, Chan P S, Pedley R B, Chester K A, Owen K, Violet J A, Malaroda A, Green A J, Buscombe J, Padhani A R, Rustin G J, Begent R H (2009). A phase I trial of radioimmunotherapy with 131I-A5B7 anti-CEA antibody in combination with combretastatin-A4-phosphate in advanced gastrointestinal carcinomas. Clin Cancer Res 15(13):4484-92.

Miles K A, Hayball M, Dixon A K (1991). Colour perfusion imaging: a new application of computed tomography. Lancet 337(8742):643-5.

Millauer B, Wizigmann-Voos S, Schnürch H, Martinez R, Møller N P, Risau W, Ullrich A (1993). High affinity VEGF binding and developmental expression suggest Flk-1 as a major regulator of vasculogenesis and angiogenesis. Cell 72(6):835-46.

Miller K, Wang M, Gralow J, Dickler M, Cobleigh M, Perez E A, Shenkier T, Cella D, Davidson N E (2007). Paclitaxel plus bevacizumab versus paclitaxel alone for metastatic breast carcinoma. N Engl J Med 357(26):2666-76.

Mitchell J B, DeGraff W, Kim S, Cook J A, Gamson J, Christodoulou D, Feelisch M, Wink D A (1998). Redox generation of nitric oxide to radiosensitize hypoxic cells. Int J Radiat Oncol Biol Phys 42:795-8.

Mohamedali K A, Kedar D, Sweeney P, Kamat A, Davis D W, Eve B Y, Huang S, Thorpe P E, Dinney C P, Rosenblum M G (2005). The vascular-targeting fusion toxin VEGF121/rGel inhibits the growth of orthotopic human bladder carcinoma tumors. Neoplasia 7(10):912-20.

Mohamedali K A, Poblenz A T, Sikes C R, Navone N M, Thorpe P E, Darnay B G, Rosenblum M G (2006). Inhibition of prostate tumor growth and bone remodeling by the vascular targeting agent VEGF121/rGel. Cancer Res 66(22):10919-28.

Morgan B, Thomas A L, Drevs J, Hennig J, Buchert M, Jivan A, Horsfield M A, Mross K, Ball H A, Lee L, Mietlowski W, Fuxuis S, Unger C, O'Byrne K, Henry A, Cherryman G R, Laurent D, Dugan M, Marmé D, Steward W P (2003). Dynamic contrast-enhanced magnetic resonance imaging as a biomarker for the pharmacological response of PTK787/ZK 222584, an inhibitor of the vascular endothelial growth factor receptor tyrosine kinases, in patients with advanced colorectal cancer and liver metastases: results from two phase I studies. J Clin Oncol 21(21):3955-64.

Motzer R J, Hutson T E, Tomczak P, Michaelson M D, Bukowski R M, Rixe O, Oudard S, Negrier S, Szczylik C, Kim S T, Chen I, Bycott P W, Baum C M, Figlin R A (2007). Sunitinib versus interferon alfa in metastatic renal-cell carcinoma. N Engl J Med 356(2):115-24.

Mullani N A, Gould K L (1983). First-pass measurements of regional blood flow with external detectors. J Nucl Med. Jul;24(7):577-81.

Murata R, Horsman M R (2004). Tumour-specific enhancement of thermoradiotherapy at mild temperatures by the vascular targeting agent 5,6-dimethylxanthenone-4-acetic acid. Int J Hyperthermia 20(4):393-404.

Murata R, Overgaard J, Horsman M R (2000). Combining combretastatin A-4 disodium phosphate and radiation in a fractionated schedule to improve local control in mice. Radiother Oncol 56:S98.

Murata R, Overgaard J, Horsman M R (2001c).Combretastatin A-4 disodium phosphate: a vascular targeting agent that improves that improves the anti-tumor effects of hyperthermia, radiation, and mild thermoradiotherapy. Int J Radiat Oncol Biol Phys 51(4):1018-24.

Murata R, Siemann D W, Overgaard J, Horsman M R (2001a). Interaction between combretastatin A-4 disodium phosphate and radiation in murine tumors. Radiother Oncol 60(2):155-61.

Murata R, Siemann D W, Overgaard J, Horsman M R (2001b). Improved tumor response by combining radiation and the vascular-damaging drug 5,6-dimethylxanthenone-4-acetic acid. Radiat Res 156(5 Pt 1):503-9.

Murohara T, Asahara T, Silver M, Bauters C, Masuda H, Kalka C, Kearney M, Chen D, Symes J F, Fishman M C, Huang P L, Isner, J M (1998). Nitric oxide synthase modulates angiogenesis in response to tissue ischemia. J Clin Invest 101(11):2567-78.

Nathan C, Xie Q W (1994). Nitric oxide synthases: roles, tolls, and controls. Cell 78(6):915-8.

Nathan P D, Judson I, Padhani A, Harris A, Carden C P, Smythe J, Collins D, Leach M, Walicke P, Rustin G J (2008). A phase I study of combretastatin A4 phosphate (CA4P) and bevacizumab in subjects with advanced solid tumors. J Clin Oncol 26(15S):3550.

Nelkin B D, Ball D W (2001). Combretastatin A-4 and doxorubicin combination treatment is effective in a preclinical model of medullary thyroid carcinoma. Oncol Rep 8(1):157-60.

Newbold K, Castellano I, Charles-Edwards E, Mears D, Sohaib A, Leach M, Rhys-Evans P, Clarke P, Fisher C, Harrington K, Nutting C (2009). An exploratory study into the role of dynamic contrast-enhanced magnetic resonance imaging or perfusion computed tomography for detection of intratumoral hypoxia in head-and-neck cancer. Int J Radiat Oncol Biol Phys 74(1):29-37.

Ng Q S, Goh V, Klotz E, Fichte H, Saunders M I, Hoskin P J, Padhani A R (2006). Quantitative assessment of lung cancer perfusion using MDCT: does measurement reproducibility improve with greater tumor volume coverage? AJR Am J Roentgenol 187(4):1079-84.

Ng Q S, Goh V, Carnell D, Meer K, Padhani A R, Saunders M I, Hoskin P J (2007a). Tumor antivascular effects of radiotherapy combined with combretastatin a4 phosphate in human non-small-cell lung cancer. Int J Radiat Oncol Biol Phys 67(5):1375-80.

Ng Q S, Goh V, Milner J, Padhani A R, Saunders M I, Hoskin P J (2007b). Acute tumor vascular effects following fractionated radiotherapy in human lung cancer: In vivo whole tumor assessment using volumetric perfusion computed tomography. Int J Radiat Oncol Biol Phys. Feb 1;67(2):417-24.

Ng Q S, Goh V, Milner J, Stratford M R, Folkes L K, Tozer G M, Saunders M I, Hoskin, P J (2007c). Effect of nitric-oxide synthesis on tumour blood volume and vascular activity: a phase I study. Lancet Oncol 8(2):111-8.

NICE (2008). Cetuximab for the treatment of locally advanced squamous cell cancer of the head and neck (TA145). www.nice.org.uk

Nordsmark M, Loncaster J, Aquino-Parsons C, Chou S C, Ladekarl M, Havsteen H, Lindegaard J C, Davidson S E, Varia M, West C, Hunter R, Overgaard J, Raleigh J A (2003). Measurements of hypoxia using pimonidazole and polarographic oxygen-sensitive electrodes in human cervix carcinomas. Radiother Oncol 67(1):35-44.

Olive P L, Durand R E, Raleigh J A, Luo C, Aquino-Parsons C (2000). Comparison between the comet assay and pimonidazole binding for measuring tumour hypoxia. Br J Cancer 83(11):1525-31.

Olofsson B, Pajusola K, Kaipainen A, von Euler G, Joukov V, Saksela O, Orpana A, Pettersson R F, Alitalo K, Eriksson U (1996). Vascular endothelial growth factor B, a novel growth factor for endothelial cells. Proc Natl Acad Sci USA 93(6):2576-81.

O'Reilly M S (2006). Radiation combined with antiangiogenic and antivascular agents. Semin Radiat Oncol 16(1):45-50.

Padera T P, Stoll B R, Tooredman J B, Capen D, di Tomaso E, Jain R K (2004). Pathology: cancer cells compress intratumour vessels. Nature 427(6976):695.

Panigrahy D, Singer S, Shen L Q, Butterfield C E, Freedman D A, Chen E J, Moses M A, Kilroy S, Duensing S, Fletcher C, Fletcher J A, Hlatky L, Hahnfeldt P, Folkman J, Kaipainen A (2002). PPARgamma ligands inhibit primary tumor growth and metastasis by inhibiting angiogenesis. J Clin Invest 110(7):923-32.

Patlak CS, Blasberg RG, Fenstermacher JD (1983). Graphical evaluation of blood-to-brain transfer constants from multiple-time uptake data. J Cereb Blood Flow Metab 3(1):1-7.

Patlak CS, Blasberg RG (1985). Graphical evaluation of blood-to-brain transfer constants from multiple-time uptake data. Generalizations. J Cereb Blood Flow Metab 5(4):584-90.

Paris F, Fuks Z, Kang A, Capodieci P, Juan G, Ehleiter D, Haimovitz-Friedman A, Cordon-Cardo C, Kolesnick R (2001). Endothelial apoptosis as the primary lesion initiating intestinal radiation damage in mice. Science 293(5528):293-7.

Park C M, Goo J M, Lee H J, Kim M A, Kim H C, Kim K G, Lee C H, Im J G (2009). FN13762 murine breast cancer: region-by-region correlation of first-pass perfusion CT indexes with histologic vascular parameters. Radiology 251(3):721-30.

Parkins C S, Holder A L, Hill S A, Chaplin D J, Tozer G M (2000). Determinants of anti-vascular action by combretastatin A-4 phosphate: role of nitric oxide. Br J Cancer 83(6):811-6.

Pattillo CB, Sari-Sarraf F, Nallamothu R, Moore BM, Wood GC, Kiani MF (2005).Targeting of the antivascular drug combretastatin to irradiated tumors results in tumor growth delay. Pharm Res 22(7):1117-20.

Pattillo CB, Venegas B, Donelson FJ, Del Valle L, Knight LC, Chong PL, Kiani MF (2009). Radiation-guided targeting of combretastatin encapsulated immunoliposomes to mammary tumors. Pharm Res 26(5):1093-100.

Pedley R B, Hill S A, Boxer G M, Flynn A A, Boden R, Watson R, Dearling J, Chaplin D J, Begent R H (2001). Eradication of colorectal xenografts by combined radioimmunotherapy and combretastatin a-4 3-O-phosphate. Cancer Res 61(12):4716-22.

Peichev M, Naiyer A J, Pereira D, Zhu Z, Lane W J, Williams M, Oz M C, Hicklin D J, Witte L, Moore M A, Rafii S (2000). Expression of VEGFR-2 and AC133 by circulating human CD34(+) cells identifies a population of functional endothelial precursors. Blood 95(3):952-8.

Pelus L M, Bian H, Fukuda S, Wong D, Merzouk A, Salari H (2005). The CXCR4 agonist peptide, CTCE-0021, rapidly mobilizes polymorphonuclear neutrophils and hematopoietic progenitor cells into peripheral blood and synergizes with granulocyte colony-stimulating factor. Exp Hematol 33(3):295-307.

Perez L A, Dombkowski D, Efird J, Preffer F, Suit H D (1995). Cell proliferation kinetics in human tumor xenografts measured with iododeoxyuridine labeling and flow cytometry: a study of heterogeneity and a comparison between different methods of calculation and other proliferation measurements. Cancer Res 55(2):392-8.

Perrotte P, Matsumoto T, Inoue K, Kuniyasu H, Eve B Y, Hicklin D J, Radinsky R, Dinney C P (1999). Anti-epidermal growth factor receptor antibody C225 inhibits angiogenesis in human transitional cell carcinoma growing orthotopically in nude mice. Clin Cancer Res 5(2):257-65.

Petit A M, Rak J, Hung M C, Rockwell P, Goldstein N, Fendly B, Kerbel R S (1997). Neutralizing antibodies against epidermal growth factor and ErbB-2/neu receptor tyrosine kinases down-regulate vascular endothelial growth factor production by tumor cells in vitro and in vivo: angiogenic implications for signal transduction therapy of solid tumors. Am J Pathol 151(6):1523-30.

Pignon J P, le Maître A, Maillard E, Bourhis J; MACH-NC Collaborative Group (2009). Meta-analysis of chemotherapy in head and neck cancer (MACH-NC): an update on 93 randomised trials and 17,346 patients. Radiother Oncol 92(1):4-14.

Pili R, Rosenthal M, AS1404-203 study group investigators (2008). Addition of DMXAA (ASA404) to docetaxel in patients with hormone-refractory metastatic prostate cancer (HRMPC): update from a randomized, phase II study. J Clin Oncol 26(15S):5007

Plowman J, Narayanan V L, Dykes D, Szarvasi E, Briet P, Yoder O C, Paull K D (1986). Flavone acetic acid: a novel agent with preclinical tumor activity against colon adenocarcinoma 38 in mice. Cancer Treat Rep 70:631-5.

Prise V E, Honess D J, Stratford M R L, Wilson J, Tozer G M (2002). The vascular response of tumor and normal tissues in the rat to the vascular targeting agent, combretastatin A-4-phosphate, at clinically relevant doses. Int J Oncol 21:717-26.

Puhakka A, Kinnula V, Näpänkangas U, Säily M, Koistinen P, Pääkkö P, Soini Y (2003). High expression of nitric oxide synthases is a favorable prognostic sign in non-small cell lung carcinoma. APMIS 111(12):1137-46.

Quintero M, Brennan P A, Thomas G J, Moncada S (2006). Nitric oxide is a factor in the stabilization of hypoxia-inducible factor-1alpha in cancer: role of free radical formation. Cancer Res 66(2):770-4.

Raben D, Bianco C, Damiano V, Bianco R, Melisi D, Mignogna C, D'Armiento F P, Cionini L, Bianco A R, Tortora G, Ciardiello F, Bunn P (2004). Antitumor activity of ZD6126, a novel vascular-targeting agent, is enhanced when combined with ZD1839, an epidermal growth factor receptor tyrosine kinase inhibitor, and potentiates the effects of radiation in a human non-small cell lung cancer xenograft model. Mol Cancer Ther 3(8):977-83.

Raleigh J A, Chou S C, Arteel G E, Horsman M R (1999). Comparisons among pimonidazole binding, oxygen electrode measurements, and radiation response in C3H mouse tumors. Radiat Res 151(5):580-9.

Ran S, Mohamedali K A, Luster T A, Thorpe P E, Rosenblum M G (2005). The vascular-ablative agent VEGF(121)/rGel inhibits pulmonary metastases of MDA-MB-231 breast tumors. Neoplasia 7(5):486-96.

Ravi R, MookerjeeB, Bhujwalla Z M, Sutter C H, Artemov D, Zeng Q, Dillehay L E, Madan A, Semanza G L, Bedi A (2000). Regulation of tumor angiogenesis by p53-induced degradation of hypoxia-inducible factor 1alpha. Genes Dev 14(1):34-44.

Relf M, LeJeune S, Scott P A, Fox S, Smith K, Leek R, Moghaddam A, Whitehouse R, Bicknell R, Harris A L (1997). Expression of the angiogenic factors vascular endothelial cell growth factor, tumor growth factor beta-1, platelet-derived endothelial cell growth factor, placenta growth factor and pleiotrophin in human primary breast cancer and its relation to angiogenesis. Cancer Res 57(5):963-9.

Ribatti D, Vacca A, Dammacco F (2003). New non-angiogenesis dependent pathways for tumor growth. Eur J Cancer 39:1835–1841.

Rijken P F, Bernsen H J, Peters J P, Hodgkiss R J, Raleigh J A, van der Kogel A J (2000). Spatial relationship between hypoxia and the (perfused) vascular network in a human glioma xenograft: a quantitative multi-parameter analysis. Int J Radiat Oncol Biol Phys 48(2):571-82.

Rini B I, Halabi S, Rosenberg J E, Stadler W M, Vaena D A, Ou S S, Archer L, Atkins J N, Picus J, Czaykowski P, Dutcher J, Small E J (2008). Bevacizumab plus interferon alpha monotherapy in patients with metastatic renal cell carcinoma: CALGB 90206. J Clin Oncol 26(33):5422-8.

Roberts J T, Bleehen N M, Workman P, Walton M I (1984). A phase I study of the hypoxic cell radiosensitizer Ro-03-8799. Int J Radiat Oncol Biol Phys 10(9):1755-8.

Rofstad E K, Gaustad J V, Egeland T A, Mathiesen B, Galappathi K (2010). Tumors exposed to acute cyclic hypoxic stress show enhanced angiogenesis, perfusion and metastatic dissemination. Int J Cancer 127(7):1535-46.

Rojas A, Carl U, Reghebi K (1990). Effect of normobaric oxygen on tumor radiosensitivity: fractionated studies. Int J Radiat Oncol Biol Phys 18(3):547-53.

Rojas A, Stratford M R, Bentzen S M, Denekamp J (2004). Is sensitization with nicotinamide and carbogen dependent on nicotinamide concentration at the time of irradiation? Int J Radiat Biol 80(7):499-506.

Roose T P, Netti A, Munn, Boucher Y, Jain R K (2003). Solid stress generated by spheroid growth estimated using a linear poroelasticity model small star, filled. Microvasc Res 66(3):204-12.

Rustin G J, Galbraith S M, Anderson H, Stratford M, Folkes L K, Sena L, Gumbrell L, Price P M (2003). Phase I clinical trial of weekly combretastatin A4 phosphate: clinical and pharmacokinetic results. J Clin Oncol 21(15):2815-22.

Rustin G J, Nathan P D, Boxall J, Saunders L, Ganesan T S, Shreeves G E (2005). A phase 1b trial of weekly combretastatin A- 4 phosphate (CA4P) in combination with carboplatin or paclitaxel in patients with advanced cancer. J Clin Oncol 23(16S):3103

Salz L B, Clarke S, Diaz-Rubio E, Scheithauer W, Figer A, Wong R, Koski S, Lichinister M, Yang T S, Rivera F, Couture F, Sirzén F, Cassidy J (2008). Bevacizumab in combination with oxaliplatin-based chemotherapy as first-line therapy in metastatic colorectal carcinoma. J Clin Oncol 26(12):2013-9.

Sandison J C (1928). Observations on growth of blood vessels as seen in transparent chamber introduced into rabbit' s ear. Am. J. Anat. 41, 475–496.

Sandler A, Gray R, Perry M C, Brahmer J, Schiller J H, Dowlati A, Lilenbaum R, Johnson D H (2006). Paclitaxel-carboplatin alone or with bevacizumab for non-small-cell lung cancer. N Engl J Med 355(24):2542-50.

Sandström M, Johansson M, Bergström P, Bergenheim AT, Henriksson R (2008). Effects of the VEGFR inhibitor ZD6474 in combination with radiotherapy and temozolomide in an orthotopic glioma model. J Neurooncol 88(1):1-9.

Santimaria M, Moscatelli G, Viale G L, Giovannoni L, Neri G, Viti F, Leprini A, Borsi L, Castellani P, Zardi L, Neri D, Riva P (2003).Immunoscintigraphic detection of the ED-B domain of fibronectin, a marker of angiogenesis, in patients with cancer. Clin Cancer Res 9(2):571-9.

Saunders M I, Anderson P J, Bennett M H, Dische S, Minchinton A, Stratford M R, Tothill M (1984). The clinical testing of Ro 03-8799--pharmacokinetics, toxicology, tissue and tumor concentrations. Int J Radiat Oncol Biol Phys 10(9):1759-63.

Schaefer J F, Schneider V, Vollmar J, Wehrmann M, Aebert H, Friedel G, Vonthein R, Schick F, Claussen C D (2006). Solitary pulmonary nodules: association between signal characteristics in dynamic contrast enhanced MRI and tumor angiogenesis. Lung Cancer 53(1):39-49.

Seed L, Slaughter D P, Limarzi L R (1940). Effect of colchicine on human cancer. Surgery 7:696-709.

Semenza G L (2003). Targeting HIF-1 for cancer therapy. Nat Rev Cancer 3(10):721-32.

Senger D R, Galli S J, Dvorak A M, Perruzzi C A, Harvey V S, Dvorak H F (1983). Tumor cells secrete a vascular permeability factor that promotes accumulation of ascites fluid. Science 219(4587):983-5.

Seshadri M, Mazurchuk R, Spernyak J A, Bhattacharya A, Rustum Y M, Bellnier D A (2006). Activity of the vascular-disrupting agent 5,6-dimethylxanthenone-4-acetic acid against human head and neck carcinoma xenografts. Neoplasia 8(7):534-42.

Sessa C, Lorusso P, Tolcher A, Braghetti A, Besenval M, Terrot T, De Naro S, Daglish B, Veyrat-Follet C, Fontaine H, Marsoni S (2005). A pharmacokinetic and DCE-MRI-dynamic phase I study of the antivascular combretastatin analogue AVE8062A, administered every 3 weeks. Proc Amer Assoc Cancer Res 46 (abstract 5827).

Shaked Y, Ciarrocchi A, Franco M, Lee C R, Man S, Cheung A M, Hicklin D J, Chaplin D, Foster F S, Benezra R, Kerbel R S (2006). Therapy-induced acute recruitment of circulating endothelial progenitor cells to tumors. Science 313(5794):1785-7.

Shaked Y, Tang T, Woloszynek J, Daenen L G, Man S, Xu P, Cai S , Arbeit J M, Voest E E, Chaplin D J, Smythe J, Harris A, Nathan P, Judson I, Rustin G, Bertolini F, Link D C, Kerbel R S (2009). Contribution of granulocyte colony-stimulating factor to the acute mobilization of endothelial precursor cells by vascular disrupting agents. Cancer Res 69(19):7524-8.

Shi W, Siemann D W (2005). Targeting the tumor vasculature: enhancing antitumor efficacy through combination treatment with ZD6126 and ZD6474. In Vivo 19(6):1045-50.

Shnyder S D, Cooper P A, Pettit G R, Lippert J W 3rd, Bibby M C (2003). Combretastatin A-1 phosphate potentiates the antitumour activity of cisplatin in a murine adenocarcinoma model. Antcancer Res 23(2B0:1619-23.

Siemann D W, Mercer E, Lepler S, Rojani A M (2002). Vascular targeting agents enhance chemotherapeutic agent activities in solid tumour therapy. Int J Cancer 99:1-6

Siemann D W, Rojiani A M (2002). Enhancement of radiation therapy by the novel vascular targeting agent ZD6126. Int J Radiat Oncol Biol Phys 53(1):164-71.

Siemann D W, Rojiani A M (2005).The vascular disrupting agent ZD6126 shows increased antitumor efficacy and enhanced radiation response in large, advanced tumors. Int J Radiat Oncol Biol Phys 62(3):846-53.

Siemann D W, Shi W (2004). Efficacy of combined antiangiogenic and vascular disrupting agents in treatment of solid tumors. Int J Radiat Oncol Biol Phys 60(4):1233-40.

Siemann D W, Shi W (2008). Dual targeting of tumor vasculature: combining Avastin and vascular disrupting agents (CA4P or OXi4503). Anticancer Res 28(4B):2027-31.

Simon G H, Fu Y, Berejnoi K, Fournier L S, Lucidi V, Yeh B, Shames D M, Brasch R C (2005).Initial computed tomography imaging experience using a new macromolecular iodinated contrast medium in experimental breast cancer. Invest Radiol 40(9):614-20.

Singh R K, Gutman M, Bucana C D, Sanchez R, Llansa N, Fidler I J (1995). Interferons alpha and beta down-regulate the expression of basic fibroblast growth factor in human carcinomas. Proc Natl Acad Sci U S A 92(10):4562-6.

Singhal S, Mehta J, Desikan R, Ayers D, Roberson P, Eddlemon P, Munshi N, Anaissie E, Wilson C, Dhodapkar M, Zeddis J, Barlogie B (1999). Antitumor activity of thalidomide in refractory multiple myeloma. N Engl J Med 341(21):1565-71.

Smith G P, Calveley S B, Smith M J, Baguley B C (1987). Flavone acetic acid (NSC 347512) induces haemorrhagic necrosis of mouse colon 26 and 38 tumours. Eur J Cancer Clin Oncol 23:1209-11.

Sonveaux P, Brouet A, Havaux X, Grégoire V, Dessy C, Balligand J L, Feron O (2003). Irradiation-induced angiogenesis through the up-regulation of the nitric oxide pathway: implications for tumor radiotherapy. Cancer Res 63(5):1012-9.

Soria J C, Sessa C, Perotti A, Massard C, Armand J P, Lassau N, Farace F, Borghi E, Gianni L. A comprehensive study of translational research and safety exploration of the vascular disrupting agent (VDA) AVE8062 in combination with cisplatin administered every 3 weeks to patients with advanced solid tumors. Proc Amer Assoc Cancer Res 49 (abstract LB-302).

Staflin K, Järnum S, Hua J, Honeth G, Kannisto P, Lindvall M (2006). Combretastatin A-1 phosphate potentiates the antitumour activity of carboplatin and paclitaxel in a severe combined immunodeficiency disease (SCID) mouse model of human ovarian carcinoma. Int J Gynecol Cancer 16(4):1557-64.

Steel G G (1979). Terminology in the description of drug-radiation interactions. Int J Radiat Oncol Biol Phys 5(8):1145-50.

Steel G G, Peckham M J (1979). Exploitable mechanisms in combined radiotherapy-chemotherapy: the concept of additivity. Int J Radiat Oncol Biol Phys 5(1):85-91.

Steel G G (2002). Basic clinical radiobiology for radiation oncologists, 3rd edn.: Edward Arnold, London.

Stratford M R (2008). Enhanced fluorescence detection of cis-combretastatins by post-column photolysis. J Chromatogr A 1181(1-2):162-5.

Stratford M R, Dennis M F (1999). Determination of combretastatin A-4 and its phosphate ester pro-drug in plasma by high-performance liquid chromatography. J Chromatogr B Biomed Sci Appl 721(1):77-85.

Stevenson J P, Rosen M, Sun W, Gallagher M, Haller D G, Vaughn D, Giantonio B, Zimmer R, Petros W P, Stratford M, Chaplin D, Young S L, Schnall M, O'Dwyer P J(2003). Phase I trial of the antivascular agent combretastatin A4 phosphate on a 5-day schedule to patients with cancer: magnetic resonance imaging evidence for altered tumor blood flow. J Clin Oncol 21(23):4428-38.

Sullivan C A, Ghosh S, Ocal I T, Camp R L, Rimm D L, Chung GG (2009). Microvessel area using automated image analysis is reproducible and is associated with prognosis in breast cancer. Hum Pathol. 40(2):156-65.

Tabrizi-Fard M A, Fung H L (1996). Reversed-phase high-performance liquid chromatography method for the analysis of nitro-arginine in rat plasma and urine. J Chromatogr B Biomed Appl 679(1-2):7-12.

Tanaka F, Otake Y, Yanagihara K, Kawano Y, Miyahara R, Li M, Yamada T, Hanaoka N, Inui K, Wada H (2001). Evaluation of angiogenesis in non-small cell lung cancer: comparison between anti-CD34 antibody and anti-CD105 antibody. Clin Cancer Res. Nov;7(11):3410-5.

Tannock I F (1968). The relationship between cell proliferation and the vascular system in a transplanted mouse mammary tumour. Br J Cancer 22:258-73.

Tateishi U, Kusumoto M, Nishihara H, Nagashima K, Morikawa T, Moriyama N (2002). Contrast-enhanced dynamic computed tomography for the evaluation of tumor angiogenesis in patients with lung carcinoma. Cancer 95(4):835-42.

Teifke A, Behr O, Schmidt M, Victor A, Vomweg T W, Thelen M, Lehr H A (2006). Dynamic MR imaging of breast lesions: correlation with microvessel distribution pattern and histologic characteristics of prognosis. Radiology 239(2):351-60.

Therasse P, Arbuck S G, Eisenhauer E A, Wanders J, Kaplan R S, Rubinstein L, Verweij J, Van Glabbeke M, van Oosterom A T, Christian M C, Gwyther S G (2000). New guidelines to evaluate the response to treatment in solid tumors. European Organization for Research and Treatment of Cancer, National Cancer Institute of the United States, National Cancer Institute of Canada. J Natl Cancer Inst 92(3):205-16.

Thomas J P, Arzoomanian R Z, Alberti D, Marnocha R, Lee F, Friedl A, Tutsch K, Dresen A, Geiger P, Pluda J, Fogler W, Schiller J H, Wilding G (2003). Phase I pharmacokinetic and pharmacodynamic study of recombinant human endostatin in patients with advanced solid tumors. J Clin Oncol 21(2):223-31.

Thomlinson R H, Gray L H (1955). The histological structure of some human lung cancers and the possible implications for radiotherapy. Br J Cancer 9(4):539-49.

Thorpe PE (2004).Vascular targeting agents as cancer therapeutics. Clin Cancer Res. 10(2):415-27.

Trivella M, Pezzella F, Pastorino U, Harris A L, Altman DG; Prognosis In Lung Cancer (PILC) Collaborative Study Group (2007). Microvessel density as a prognostic factor in non-small-cell lung carcinoma: a meta-analysis of individual patient data. Lancet Oncol 8(6):488-99.

Tofts P S, Brix G, Buckley D L, Evelhoch J L, Henderson E, Knopp M V, Larsson H B, Lee T Y, Mayr N A, Parker G J, Port R E, Taylor J, Weisskoff R M (1999). Estimating kinetic parameters from dynamic contrast-enhanced T(1)-weighted MRI of a diffusable tracer: standardized quantities and symbols. J Magn Reson Imaging 10(3):223-32.

Tofts P S (1997). Modeling tracer kinetics in dynamic Gd-DTPA MR imaging. J Magn Reson Imaging 7(1):91-101.

Tong R T, Boucher Y, Kozin S V, Winkler F, Hicklin D J, Jain R K (2004). Vascular normalization by vascular endothelial growth factor receptor 2 blockade induces a pressure gradient across the vasculature and improves drug penetration in tumors. Cancer Res 64(11):3731-6.

Tozer G M, Kanthou C, Baguely B C (2005). Disrupting tumour blood vessels. Nat Rev Cancer 5:423-435.

Tozer G M, Kanthou C, Lewis G, Prise V E, Vojnovic B, Hill S A (2008). Tumour vascular disrupting agents: combating treatment resistance. Br J Radiol 81 Spec No 1:S12-20.

Tozer G M, Prise V E, Bell K M (1995). The influence of nitric oxide on tumour vascular tone. Acta Oncol 34(3):373-7.

Tozer G M, Prise V E, Chaplin D J (1997). Inhibition of nitric oxide synthase induces a selective reduction in tumor blood flow that is reversible with L-arginine. Cancer Res 57(5):948-55.

Tozer G M, Prise V E, Lewis G, Xie S, Wilson I, Hill S A (2009). Nitric oxide synthase inhibition enhances the tumor vascular-damaging effects of combretastatin a-4 3-o-phosphate at clinically relevant doses. Clin Cancer Res 15(11):3781-90.

Tozer G M, Prise V E, Wilson J, Locke R J, Vojnovic B, Stratford M R, Denis M F, Chaplin D J (1999). Combretastatin A-4 phosphate as a tumor vascular-targeting agent: early effects in tumors and normal tissues. Cancer Res 59(7):1626-34.

Tozer G M, Prise V E, Wilson J, Cemazar M, Shan S, Dewhirst M W, Barber P R, Vojnovic B Chaplin D J (2001). Mechanisms associated with tumor vascular shut-down induced by combretastatin A-4 phosphate: intravital microscopy and measurement of vascular permeability. Cancer Res 61(17):6413-22.

Unetsubo T, Konouchi H, Yanagi Y, Murakami J, Fujii M, Matsuzaki H, Hisatomi M, Nagatsuka H, Asaumi J (2009). Dynamic contrast-enhanced magnetic resonance imaging for estimating tumor proliferation and microvessel density of oral squamous cell carcinomas. Oral Oncol 45(7):621-6.

Urtasun R C, Chapman J D, Raleigh J A, Franko A J, Koch C J (1986). Binding of 3H-misonidazole to solid human tumors as a measure of tumor hypoxia. Int J Radiat Oncol Biol Phys 12(7):1263-7.

van Baardwijk A, Dooms C, van Suylen R J, Verbeken E, Hochstenbag M, Dehing-Oberije C, Rupa D, Pastorekova S, Stroobants S, Buell U, Lambin P, Vansteenkiste J, De Ruysscher D (2007).The maximum uptake of (18)F-deoxyglucose on positron emission tomography scan correlates with survival, hypoxia inducible factor-1alpha and GLUT-1 in non-small cell lung cancer. Eur J Cancer 43(9):1392-8.

van den Beucken T, Koritzinsky M, Niessen H, Dubois L, Savelkouls K, Mujcic H, Jutten B, Kopacek J, Pastorekova S, van der Kogel A J, Lambin P, Voncken W, Rouschop K M, Wouters B G (2009). Hypoxia-induced expression of carbonic anhydrase 9 is dependent on the unfolded protein response. J Biol Chem 92(3):437-42.

van Laarhoven H W, Kaanders J H, Lok J, Peeters W J, Rijken P F, Wiering B, Ruers T J, Punt C J, Heerschap A, van der Kogel A J (2006). Hypoxia in relation to vasculature and proliferation in liver metastases in patients with colorectal cancer. Int J Radiat Oncol Biol Phys 64(2):473-82.

Varghese A J, Gulyas S, Mohindra J K (1976). Hypoxia-dependent Reduction of I -(2Nitro1 -imidazolyl)-3-methoxy-2-propanol by Chinese Hamster Ovary Cells and KHT Tumor Cells in Vitro and in Vivo. Cancer Res 36(10):3761-65.

Vaupel P, Harrison L (2004). Tumor hypoxia: causative factors, compensatory mechanisms, and cellular response. Oncologist 9 Suppl 5:4-9.

Vermeulen P B, Gasparini G, Fox S B, Colpaert C, Marson L P, Gion M, Beliën J A, de Waal R M, Van Marck E, Magnani E, Weidner N, Harris A L, Dirix L Y (2002). Second international consensus on the methodology and criteria of evaluation of angiogenesis quantification in solid human tumours. Eur J Cancer 38(12):1564-79.

Vincent L, Kermani P, Young L M, Cheng J, Zhang F, Shido K, Lam G, Bompais-Vincent H, Zhu Z, Hicklin D J, Bohlen P, Chaplin D J, May C, Rafii S (2005). Combretastatin A4 phosphate induces rapid regression of tumor neovessels and growth through interference with vascular endothelial-cadherin signalling. J Clin Investigation 115:2992-3006.

Vukovic V, Haugland H K, Nicklee T, Morrison A J, Hedley D W (2001). Hypoxia-inducible factor-1alpha is an intrinsic marker for hypoxia in cervical cancer xenografts. Cancer Res 61(20):7394-8.

Vukovic V, Tannock I F (1997). Influence of low pH on cytotoxicity of paclitaxel, mitoxantrone and topotecan. Br J Cancer 75:1167-72.

Wachsberger P R, Burd R, Marero N, Daskalakis C, Ryan A, McCue P, Dicker A P (2005). Effect of the tumour vascular-damaging agent, ZD6126, on the radioresponse of U87 glioblastoma. Clin Cancer Res 11(2 Pt 1):835-42.

Walenta S, Snyder S, Haroon Z A, Braun R D, Amin K, Brizel D, Mueller-Klieser W, Chance B, Dewhirst M W (2001). Tissue gradients of energy metabolites mirror oxygen tension gradients in a rat mammary carcinoma model. Int J Radiat Oncol Biol Phys 51(3):840-8.

Walsh W H (1844). The anatomy, physiology, pathology and treatment of cancer. Boston: Ticknor and Co.

Wang J H, Min P Q, Wang P J, Cheng W X, Zhang X H, Wang Y, Zhao X H, Mao X Q (2006).Dynamic CT Evaluation of Tumor Vascularity in Renal Cell Carcinoma. AJR Am J Roentgenol 186(5):1423-30.

Warburg O, Wind F, Negelein E (1927). The metabolism of tumors in the body. J Gen Physiol 8(6):519-30.

Wedam S B, Low J A, Yang S X, Chow C K, Choyke P, Danforth D, Hewitt S M, Berman A, Steinberg S M, Liewehr D J, Plehn J, Doshi A, Thomasson D, McCarthy N, Koeppen H, Sherman M, Zujewski J, Camphausen K, Chen H, Swain S M (2006). Antiangiogenic and antitumor effects of bevacizumab in patients with inflammatory and locally advanced breast cancer. J Clin Oncol 24(5):769-77.

Wester K, Ranefall P, Bengtsson E, Busch C, Malmström P U (1999). Automatic quantification of microvessel density in urinary bladder carcinoma. Br J Cancer. Dec;81(8):1363-70.

Wildiers H, Ahmed B, Guetens G, De Boeck G, de Bruijn E A, Landuyt W, van Oosterom A T (2004). Combretastatin A-4 phosphate enhances CPT-11 activity independently of the administration sequence. Eur J Cancer 40(2):284-90.

Willam C, Masson N, Tian Y M, Mahmood S A, Wilson M I, Bicknell R, Eckhardt K U, Maxwell P H, Ratcliffe P J, Pugh C W (2002). Peptide blockade of HIFalpha degradation modulates cellular metabolism and angiogenesis. Proc Natl Acad Sci USA 99(16):10423-8.

Willett C G, Boucher Y, di Tomaso E, Duda D G, Munn L L, Tong R T, Chung D C, Sahani D V, Kalva S P, Kozin S V, Mino M, Cohen K S, Scadden D T, Hartford A C, Fischman A J, Clark J W, Ryan D P, Zhu A X, Blaszkowsky L S, Chen H X, Shellito P C, Lauwers GY, Jain R K (2004). Direct evidence that the VEGF-specific antibody bevacizumab has antivascular effects in human rectal cancer. Nat Med 10(2):145-7.

Williams K J, Telfer B A, Brave S, Kendrew J, Whittaker L, Stratford I J, Wedge S R (2004). ZD6474, a potent inhibitor of vascular endothelial growth factor signaling, combined with radiotherapy: schedule-dependent enhancement of antitumor activity. Clin Cancer Res 10(24):8587-93.

Wilson W R, Li A E, Cowan D S, Siim B G (1998). Enhancement of tumor radiation response by the antivascular agent 5,6-dimethylxanthenone-4-acetic acid. Int J Radiat Oncol Biol Phys 42(4):905-8.

Winkler F, Kozin S V, Tong R T, Chae S S, Booth M F, Garkavtsev I, Xu L, Hicklin D J, Fukumura D, di Tomaso E, Munn L L, Jain R K (2004). Kinetics of vascular normalization by VEGFR2 blockade governs brain tumor response to radiation: role of oxygenation, angiopoietin-1, and matrix metalloproteinases. Cancer Cell 6(6):553-63.

Wolfkiel C J, Ferguson J L, Chomka E V, Law W R, Labin I N, Tenzer M L, Booker M, Brundage B H (1987). Measurement of myocardial blood flow by ultrafast computed tomography. Circulation 76(6):1262-73.

Wood J, Bonjean K, Ruetz S, Bellahcene A, Devy L, Foidart J M, Castronovo V, Green J R (2002). Novel antiangiogenic effects of the bisphosphonate compound zoledronic acid. J Pharmacol Exp Ther 302:1055–1061.
Worthington J, McCarthy H O, Barrett E, Adams C, Robson T, Hirst D G (2004). Use of the radiation-inducible WAF1 promoter to drive iNOS gene therapy as a novel anti-cancer treatment. J Gene Med 6(6):673-80.

Xiong H Q, Herbst R, Faria S C, Scholz C, Davis D, Jackson E F, Madden T, McConkey D, Hicks M, Hess K, Charnsangavej C A, Abbruzzese J L (2004). A phase I surrogate endpoint study of SU6668 in patients with solid tumors. Invest New Drugs 22(4):459-66.

Xu L, Fukumura D, Jain R K (2002). Acidic extracellular pH induces vascular endothelial growth factor (VEGF) in human glioblastoma cells via ERK1/2 MAPK pathway-Mechanism of low pH induced VEGF. J Biol Chem 277:11368-11374.

Yankeelov T E, Niermann K J, Huamani J, Kim D W, Quarles C C, Fleischer A C, Hallahan D E, Price R R, Gore J C (2006). Correlation between estimates of tumor perfusion from microbubble contrast-enhanced sonography and dynamic contrast-enhanced magnetic resonance imaging. J Ultrasound Med 25(4):487-97.

Yao J, Yang Z G, Chen H J, Chen T W, Huang J (2010).Gastric adenocarcinoma: can perfusion CT help to noninvasively evaluate tumor angiogenesis? Abdom Imaging [Epub ahead of print].

Yeung S C, She M, Yang H, Pan J, Sun L, Chaplin D (2007). Combination chemotherapy including combretastatin A4 phosphate and paclitaxel is effective against anaplastic thyroid cancer in a nude mouse xenograft model. J Clin Endocrinol Metab 92(8):2902-9

Yi C A, Lee K S, Kim E A, Han J, Kim H, Kwon O J, Jeong Y J, Kim S (2004). Solitary pulmonary nodules: dynamic enhanced multi-detector row CT study and comparison with vascular endothelial growth factor and microvessel density. Radiology 233(1):191-9.

Yonenaga Y, Mori A, Onodera H, Yasuda S, Oe H, Fujimoto A, Tachibana T, Imamura M (2005). Absence of smooth muscle actin-positive pericyte coverage of tumor vessels correlates with hematogenous metastasis and prognosis of colorectal cancer patients. Oncology 69(2):159-66.

Younes M, Brown R W, Stephenson M, Gondo M, Cagle P T (1997). Overexpression of Glut1 and Glut3 in stage I nonsmall cell lung carcinoma is associated with poor survival. Cancer 80(6):1046-51.

Younes M, Juarez D, Lechago L V, Lerner S P (2001). Glut 1 expression in transitional cell carcinoma of the urinary bladder is associated with poor patient survival. Anticancer Res 21(1B):575-8.

Young H, Baum R, Cremerius U, Herholz K, Hoekstra O, Lammertsma A A, Pruim J, Price P (1999).Measurement of clinical and subclinical tumour response using [18F]-fluorodeoxyglucose and positron emission tomography: review and 1999 EORTC recommendations. European Organization for Research and Treatment of Cancer (EORTC) PET Study Group. Eur J Cancer 35(13):1773-82.

Yu J, deMuinck E D, Zhuang Z, Drinane M, Kauser K, Rubanyi G M, Qian H S, Murata T, Escalante B, Sessa W C (2005). Endothelial nitric oxide synthase is critical for ischemic remodeling, mural cell recruitment, and blood flow reserve. Proc Natl Acad Sci USA 102(31):10999-1004.

Yuan F, Chen Y, Dellian M, Safabakhsh N, Ferrara N, Jain R K (1996). Time-dependent vascular regression and permeability changes in established human tumor xenografts induced by an anti-vascular endothelial growth factor/vascular permeability factor antibody. Proc Natl Acad Sci U S A 93(25):14765-70.

Zhang S C, Hironaka S, Ohtsu A, Yoshida S, Hasebe T, Fukayama M, Ochiai A (2006). Computer-assisted analysis of biopsy specimen microvessels predicts the outcome of esophageal cancers treated with chemoradiotherapy. Clin Cancer Res 12(6):1735-42.

Zhang X M, Yu D, Zhang H L, Dai Y, Bi D, Liu Z, Prince M R, Li C (2008). 3D dynamic contrast-enhanced MRI of rectal carcinoma at 3T: correlation with microvascular density and vascular endothelial growth factor markers of tumor angiogenesis. J Magn Reson Imaging 27(6):1309-16.

Zhong H, De Marzo A M, Laughner E, Lim M, Hilton D A, Zagzag D, Buechler P, Isaacs W B, Semenza G L, Simons J W (1999). Overexpression of hypoxia-inducible factor 1alpha in common human cancers and their metastases. Cancer Res 59(22):5830-5.

Zhu A X, Sahani D V, Duda D G, di Tomaso E, Ancukiewicz M, Catalano O A, Sindhwani V, Blaszkowsky L S, Yoon S S, Lahdenranta J, Bhargava P, Meyerhardt J, Clark J W, Kwak E L, Hezel A F, Miksad R, Abrams T A, Enzinger P C, Fuchs C S, Ryan D P, Jain R K (2009). Efficacy, safety, and potential biomarkers of sunitinib monotherapy in advanced hepatocellular carcinoma: a phase II study. J Clin Oncol 27(18):3027-35.

Ziche M, Morbidelli L, Choudhuri R, Zhang H T, Donnini S, Granger H J, Bicknell R (1997). Nitric oxide synthase lies downstream from vascular endothelial growth factor-induced but not basic fibroblast growth factor-induced angiogenesis. J Clin Invest 99(11):2625-34.

Zips D, Eicheler W, Geyer P, Hessel F, Dörfler A, Thames H D, Haberey M, Baumann M (2005). Enhanced susceptibility of irradiated tumor vessels to vascular endothelial growth factor receptor tyrosine kinase inhibition. Cancer Res 65(12):5374-9.

Zwi L J, Baguley B C, Gavin J B, Wilson W R (1989). Blood flow as a major determinant in the antitumor action of flavone acetic acid. J Natl Cancer Inst 81:1005-13.